IN VITRO ASSESSMENT OF THE CORROSION PROTECTION OF BIOMIMETIC CALCIUM PHOSPHATE COATINGS ON MAGNESIUM

A thesis
submitted in partial fulfilment
of the requirements for the Degree of

DOCTOR OF PHILOSOPHY IN MECHANICAL ENGINEERING
IN THE
UNIVERSITY OF CANTERBURY

BY

JAY WATERMAN

University of Canterbury

2012

Preface

This thesis is submitted as a partial requirement for the degree of Doctor of Philosophy in Mechanical Engineering. This research was conducted under the supervision of Dr. Mark P. Staiger in the Mechanical Engineering Department, University of Canterbury, between October 2008 and July 2012.

Abstract

The use of magnesium for degradable implants can fill the need for temporary, load bearing, metallic orthopaedic implants without the risks and expense of further surgeries once the bone has healed. Mg is non toxic and biocompatible, but the corrosion rate in the body is too high. The rate will need to be moderated if these implants are to be made clinically useful.

A review of common orthopaedic coatings found that the biomimetic calcium phosphate coating process meets the criteria for a good coating. This process was designed for permanent implants, and its corrosion protection properties were unknown on Mg. The research presented here evaluates and optimizes aspects of the corrosion protection of biomimetic coatings *in vitro*.

To accurately identify the corrosion mechanisms of such coatings, the *in vitro* behaviour of several common simulated body fluids and buffer systems was evaluated.

The deposition of biomimetic coatings on Mg was compared to Ti. The effect of common surface treatments on the deposition, composition, and ultimate corrosion protection was identified in order to understand the corrosion properties of these coatings. Following the results, the biomimetic method was modified to optimize the protection by reducing the defects. The corrosion properties of these modified coatings were assessed *in vitro*.

The limitation of the biomimetic coatings was found to be in all cases sensitive to the defects present in the coating. While these could be minimized, they were not eliminated. This led to unfavourable corrosion properties. To solve this problem, a novel treatment was developed to give the biomimetic coatings self-healing properties. This treatment promoted local repair in the coating at the defects, greatly improving the corrosion properties.

The *in vitro* model was increased in complexity by adding first amino acids, then proteins. The corrosion behaviour of the coatings was compared in these solutions to understand the effects of these molecules. The data gathered will help to build a better model of *in vivo* corrosion, and allow better prediction of the performance of biomimetic coatings for corrosion resistance.

Acknowledgements

I would like to thank all of the many individuals and organizations that supported and assisted this work.

First and foremost I would like to thank my supervisors Dr. Mark Staiger, Dr. Nick Birbilis, Dr. Timothy Woodfield, and Dr. George Dias for their guidance, support and encouragement over the entire course of my studies.

Additionally, I would like to thank the associated collaborators, researcher, and technicians that supported, helped and trained me throughout, including Kevin Stobbs, Mike Flaws, Julian Philips, Paul Southward, Damian Walls, Dr. Takanori Sato, Dr. Milo Kral, Dr. Nicholas Kirkland, Dr. Thanh Nguyen, Karl Buchanan, Jemimah Walker, Shaylin Shadanbaz, Xuan Li as well as many others.

I would like to thank the New Zealand Ministry of Science and Innovation as well as the University of Canterbury for supporting this work financially.

I would like to specially thank Michael Rendl Snowdon Marshall, Christopher and Josephine Marshall for all of the support and encouragement during my stay in New Zealand. I would also like to thank all of my family for all of their support throughout.

Publications

Waterman, J., A. Pietak, N. Birbilis, T. Woodfield, G. Dias, and M.P. Staiger, *Corrosion resistance of biomimetic calcium phosphate coatings on magnesium due to varying pretreatment time.* Materials Science and Engineering: B, 2011. **176**(20): p. 1756-1760.

Waterman, J. and M.P. Staiger, *Coating Systems for Magnesium-Based Biomaterials - State of the Art*, in *Magnesium Technology 2011*. 2011, John Wiley & Sons, Inc. p. 403-408.

Kirkland, N., J. Waterman, N. Birbilis, G. Dias, T. Woodfield, R. Hartshorn, and M. Staiger, *Buffer-regulated biocorrosion of pure magnesium.* Journal of Materials Science: Materials in Medicine, 2012. **23**(2): p. 283-291.

Waterman, J., *Improving in vitro corrosion resistance of biomimetic calcium phosphate coatings for Mg substrates using calcium hydroxide layer.* Corrosion Engineering, Science and Technology, 2012. **47**(5): p. 340-345.

Nguyen, T., J. Waterman, M. Staiger, and T. Woodfield, *Controlling in vitro corrosion rate of pure Mg with rough surface texture via biomimetic coating systems.* Corrosion Engineering, Science and Technology, 2012. **47**(5): p. 358-364.

Presentations

Waterman, J., Staiger, M. P, Pietak, A., Mahoney, T., Dias, G. and Woodfield, T., *Biomimetic Calcium Phosphate Coatings for Improved Magnesium Metal Based Orthopaedic Implants*, 19th Annual Conference of the ASBTE, Sydney, 21-23 January 2009, *presentation*.

Waterman, J., Staiger, M. P, Pietak, A., Shadanbaz, S., Dias, G., Woodfield, T., *Effects of Magnesium Alloy Composition on Biomimetic Calcium Phosphate Coatings for Orthopaedic Implants*, 2nd International Symposium on Surface and Interface of Biomaterials (ISSIB-II), Hong Kong, 4-6 January 2010, *presentation*.

Waterman, J., Staiger, M. P, Dias, G., Woodfield, T., *Corrosion Protection of Biomimetic Calcium Phosphate Coatings on Magnesium*, 2nd Symposium on Biodegradable Metals, Maratea, Italy, 1-3 September 2010, *poster*.

Waterman, J. and M.P. Staiger, *Coating Systems for Magnesium-Based Biomaterials - State of the Art*, TMS 2011, San Diego, 27 February – 3 March, 2011, *presentation*.

Waterman, J., Kirkland, N., Hartshorn, R., Birbilis, N., Woodfield, T., Dias, G., Staiger, M.P., *NMR Studies on the Complex Behavior of Magnesium and HEPES for In Vitro Testing*, 21st Annual Conference of the ASBTE, Queenstown, New Zealand, 27-29 April, 2011, *poster*.

Waterman, J., Markwitz, A., Birbilis, N., Staiger, M.P., *Controlling the Corrosion of Mg using Ion Implantation for Biomedical Implants*, 3rd Symposium on Biodegradable Metals, Quebec City, Canada, 1-5 August 2011, *poster*.

Waterman, J. ., Birbilis, N., Woodfield, T., Dias, G., Staiger, M.P., *Self Healing Corrosion Resistant Coatings for Biodegradable Mg*, 9th World Biomaterials Congress, Chengdu, China, 1-5 June, 2012, *presentation*.

Contents

Table of Figures

Table of Tables

Equations

List of Abbreviations

Abbreviation	Meaning
ACP	Amorphous calcium phosphate
BSA	Bovine Serum Albumin
CaP	Calcium phosphate
CDA	Calcium deficient apatite
CPE	Constant phase element
DCPA	Dicalcium phosphate anhydrous (monetite)
DCPD	Dicalcium phosphate dihydrate (brushite)
ECAD	Electrochemical assisted deposition
E_{Corr}	Corrosion potential
EDL	Electrolytic double layer
EDS	Energy dispersive X-ray spectroscopy
EIS	Electrochemical impedance spectroscopy
FBS	Foetal bovine serum
FTIR	Fourier transform infrared spectroscopy
GA-XRD	Glancing angle X-ray diffraction
HA	Hydroxyapatite
HSA	Human serum albumin
HBSS	Hanks' balanced salt solution
HCO3	Bicarbonate buffer system
HCO_3^-	Bicarbonate ion
HEPES	4-(2-hydroxyethyl)-1-piperazineethanesulfonic acid
i_{Corr}	Corrosion current density
MCPA	Monocalcium phosphate anhydrous
MCPM	Monocalcium phosphate monohydrate
MEM	Minimum essential medium
MEM+BSA	Minimum essential medium with bovine serum albumin
MES	2-(N-morpholino)ethanesulfonic acid
OCaP	Octacalcium phosphate
OCP	Open circuit potential
PDP	Potentiodynamic polarization
PIPES	piperazine-N,N′-bis(2-ethanesulfonic acid)
RP	Polarization resistance
SBF	Simulated body fluid
Tricine	N-(2-Hydroxy-1,1-bis(hydroxymethyl)ethyl)glycine
TRIS	2-Amino-2hydroxymethyl-propane-1,2-diol
XRD	X-ray diffraction

CHAPTER 1: Introduction

1.1. Overview of the Problems

Magnesium (Mg) is a promising material for a new class of biodegradable orthopedic implants [1]. The use of Mg for biomedical applications has been examined for over a century [2]. As a metal, Mg is attractive for biomaterials because it is lightweight, has good mechanical properties for load bearing implants. The elastic modulus of Mg is lower than that of other available implant metals such as stainless steels and titanium alloys, much closer to that of bone. This property can reduce the effect of stress shielding. These properties, while appreciated, are secondary compared to the *in vivo* degradability of Mg. Unlike other metals, Mg has the potential to degrade in the body. This allows it to be used for temporary implants. This would allow the implant to remain in the body only while needed, degrading and dissolving away without the need for surgical retrieval. This eliminates the cost and associated tissue damage necessary for removal and it decreases the likelihood of long term complications associated with permanent implants [3].

Mg is uniquely suitable for the role of biodegradable implants due to its corrosion properties and biocompatibility. Mg is the fourth most abundant metal ion found in the body, is vital for physiological processes and found in every cell [1, 4, 5]. The requirement of Mg in the body means there are homeostatic mechanisms to control the amounts in the body [6, 7]. Excess Mg can be easily removed by the kidneys [8, 9]. The result of this is that although an upper limit exists [10], large amounts of Mg can be safely excreted by the body. The implant can therefore degrade during and after the healing of the original bone it was designed to support. Moreover, most (50-60%) Mg in the body exists in bone tissue, and Mg is necessary for bone growth [8, 11]. These properties make Mg ideal for orthopedic use.

The fact that Mg will degrade *in vivo* is what allows it to be used. Unfortunately, this also presents the biggest challenge. Mg is very active, and Mg corrodes too quickly in the body for it to be effectively used [2, 12, 13]. If the implant corrodes too quickly, the mechanical strength of the implant will decrease at a rate that is faster than the new bone growth that is required to take up the load. Too much Mg^{2+} released all at once can create hypermagnesemia [10, 14]. Furthermore, Mg^{2+} ions are not the only by-product of the

corrosion reaction. The corrosion is accompanied by the generation of hydrogen gas and an increase in the pH. Rapid hydrogen evolution leads to hydrogen gas collecting in the tissue [15]. The rapid corrosion rate of Mg is what has kept this material from being widely used as an implant to date [2]. To keep these effects from becoming problems, the rate at which the corrosion reactions take place must be carefully controlled. The control must slow the corrosion rate enough to allow the body time to mitigate the corrosion products, yet it must degrade eventually to retain the benefits of a degradable implant.

Some method is therefore needed to control the corrosion rate of the Mg *in vivo*. Changing the bulk properties of the Mg through alloying or protecting the Mg with a coating are methods of overcoming the corrosion rate problem [16]. Alloying is attractive because it changes the properties of the entire structure, and is thus an area of active research [17, 18]. The protection thus far provided by alloying is limited by the elements that can be used. In a degradable alloy, every constituent ultimately ends up free in the body, so the toxicity limits must be observed [10]. Of the alloying elements available, there are further limits to the benefits to corrosion resistance. The formation of secondary phases and galvanic corrosion limits the protection provided [15]. Likewise, any coating must also follow the criteria for biocompatibility. Many industrial coating systems for Mg are very corrosion resistant, e.g. chromate conversion coatings, but also very toxic [19]. The coating system also has another requirement not found for many other applications, it is not to stop corrosion completely, but degrade and allow the Mg to degrade in a controlled manner.

The ideal coating should therefore be something that slows corrosion rate in physiological solutions, contains no elements that are not biologically safe, and enhances the biocompatibility. Calcium phosphate (CaP) coatings are already well known for their properties improving the biocompatibility of orthopaedic implants [20]. These coatings have been used on stainless steel and titanium to improve the biological response. As calcium phosphates are the major mineral component of bone, the coating is highly suitable for orthopaedic applications. Coatings that mimic the structure of natural bone, i.e. biomimetic coatings will be composed of atoms and phases that are present in the body already. Bone tissue is by necessity insoluble under normal physiological fluids, so CaP can protect from corrosion. However, depending on the phase, these coatings have also been observed to be susceptible to biodegradation [21]. Therefore, these coatings are perfect for a degradable implant. The calcium phosphate coating can in theory be optimized to protect the Mg

implant from corrosion for a period of time before degrading without leaving any toxic by-products.

While biomimetic CaP coatings have been shown to be biocompatible on permanent implants, there is a lack of data on their corrosion protection properties and optimization on Mg. Biomimetic coatings have known problems with adhesion and defects that may diminish the corrosion protection that can be provided [20]. As such, optimization of the deposition and corrosion mechanisms of these coatings needs to be determined before they can be used clinically. Corrosion rates and tests must be performed in order to understand the effect of the biological solutions on the ultimate corrosion properties of these coatings on Mg.

The *in vivo* environment is complicated. Many ion, organic molecules, and cells exist in a physiological solution which can affect the corrosion rate of the implant. In order to understand the corrosion properties of each individual component, they will need to be studied individually *in vitro*. This will require isolating the factors that influence the corrosion of Mg *in vivo*, and representing them effectively in an artificial environment. Much of the *in vitro* corrosion work done to date makes assumptions about the relevance of the *in vitro* environment which may or may not be correct. While simplifications must be made, it is important to validate the mechanism and rate changes that accompany the *in vitro* approximations. For the measurement obtained to be useful, it must be an accurate measurement of the effect that will be present *in vivo*. This is especially true when comparing samples that may have very different corrosion properties, such as uncoated and coated samples.

The following work will evaluate the corrosion resistance of biomimetic coatings. These parameters and creation of these coatings will be studied and attempted to be optimized for corrosion protection *in vitro*. To understand the individual effects of the corrosion environment on these coatings, the *in vitro* solutions will be studied for pH changes, buffer capacity and performance, and ionic and organic composition to identify and compare the effect of each molecule. The results will elucidate the important aspects of *in vitro* corrosion studies of coated samples, as well as advance the technology of biomimetic coating on Mg for corrosion resistance.

1.2. Outline of the Thesis

The chapters of the thesis are summarized as follows:

Chapter 2 provides an overview of the state of the art of reducing the corrosion rate of Mg for biomaterials via surface treatments and coatings. The processes and coating types are described in terms of the benefits and shortcomings of the coatings based on recent publications. The *in vitro* corrosion solutions used in these studies is also discussed, as well as the techniques for measuring the corrosion rate. The variation in coating type, *in vitro* conditions, and ultimate corrosion protection factors of different coatings on Mg are compared.

Chapter 3 investigates the use of buffer type on the measured corrosion rate and electrochemical behaviour of uncoated Mg in different simulated body fluids (SBFs). The interaction between the buffer and the Mg ions in solution is measured to validate the choice of the buffer. The buffer properties investigated here determine the proper *in vitro* solutions to be used for further investigations into the corrosion behaviour of the coatings.

Chapter 4 begins the investigation of the biomimetic coating formation properties on the corrosion protection these coatings provide. The deposition of the Mg is compared to the deposition on Ti. The effect of the surface treatment on the final coating and the later corrosion rate in SBFs are measured. The effect of the different solutions and buffers on the measured protection are investigated. The limits of protection and failure mode of the coatings is examined. The formation of the coatings based on pretreatment is discussed and the usefulness of the pretreatments is determined.

Chapter 5 continues the investigation of the biomimetic coatings by modifying the coating deposition process based on the data obtained in Chapter 4. The additional modification was designed to improve the corrosion properties of the coatings given the deposition properties on Mg. The effect of the modification of the coating process on composition and corrosion rate are determined. The mechanisms for increased protection of the modified coatings are discussed.

Chapter 6 presents a novel method for improving the properties of the biomimetic coatings by introducing a self-healing mechanism. This mechanism overcomes the limitation of the biomimetic coating corrosion protection. The behaviour *in vitro* and the mechanisms of the increased protection were determined.

Chapter 7 takes all of the coating types prepared earlier and investigates the individual effects of a more complicated *in vitro* environment. The corrosion behaviour with the addition of amino acids, and then proteins to the solution was measured. The effect of each was documented, as well as the effects of the buffer choices as determined in Chapter 3.

Chapter 8 presents the overall conclusions of the research and the direction future work will need to take to bring these coatings and Mg implants to clinical applications.

1.3. References

1. Staiger, M.P., A.M. Pietak, J. Huadmai, and G. Dias, *Magnesium and its alloys as orthopedic biomaterials: A review.* Biomaterials, 2006. **27**(9): p. 1728-1734.
2. Witte, F., *The History of Biodegradable Magnesium Implants: A Review.* Acta Biomaterialia, 2010. **6**(5): p. 1680-1692.
3. Virtanen, S., *Corrosion of Biomedical Implant Materials.* Corrosion Reviews, 2008. **26**(2): p. 147-172.
4. Saris, N.-E.L., E. Mervaala, H. Karppanen, J.A. Khawaja, and A. Lewenstam, *Magnesium: An update on physiological, clinical and analytical aspects.* Clinica Chimica Acta, 2000. **294**(1-2): p. 1-26.
5. Seiler, H.G. and H. Sigel, *Handbook of Toxicity of Inorganic Compounds*. 1988, New York, USA: Marcel Dekker Inc.
6. Vormann, J., *Magnesium: Nutrition and Metabolism.* Molecular Aspects of Medicine, 2003. **24**: p. 27-37.
7. Sojka, J.E. and C.M. Weaver, *Magnesium Supplementation and Osteopososis.* Nutrition Review, 1995. **53**(3): p. 71-74.
8. Okuma, T., *Magnesium and bone strength.* Nutrition, 2001. **17**: p. 679-680.
9. Wolf, F.I., Cittadini, A., *Chemistry and biochemistry of magnesium.* Molecular Aspects of Medicine, 2003. **24**: p. 3-9.
10. Yuen, C.K. and W.Y. Ip, *Theoretical risk assessment of magnesium alloys as degradable biomedical implants.* Acta Biomaterialia, 2010. **6**(5): p. 1808-1812.
11. Zreiqat, H., C.R. Howlett, A. Zannettino, P. Evans, G. Schulze-Tanzil, C. Knabe, and M. Shakibaei, *Mechanisms of Magnesium-Stimulated Adhesion of Osteoblastic Cells*

to Commonly Used Orthopaedic Implants. Journal of Biomedical Materials Research, 2002. **62**(2): p. 175-184.
12. Song, G., *Control of biodegradation of biocompatable magnesium alloys.* Corrosion Science, 2007. **49**(4): p. 1696-1701.
13. Witte, F., N. Hort, C. Vogt, S. Cohen, K.U. Kainer, R. Willumeit, and F. Feyerabend, *Degradable biomaterials based on magnesium corrosion.* Current Opinion in Solid State and Materials Science, 2008. **12**(5-6): p. 63-72.
14. Dorland, *Dorland's Illustrated Medical Dictionary, 32e*. 2011: Saunders.
15. Song, G.L. and A. Atrens, *Corrosion Mechanisms of Magnesium Alloys.* Advanced Engineering Materials, 1999.
16. Zeng, R., W. Dietzel, F. Witte, N. Hort, and C. Blawert, *Progress and Challenge for Magnesium Alloys as Biomaterials.* Advanced Engineering Materials, 2008. **10**(8): p. B3-B14.
17. Gu, X., Y. Zheng, Y. Cheng, S. Zhong, and T. Xi, *In vitro corrosion and biocompatibility of binary magnesium alloys.* Biomaterials, 2009. **30**(4): p. 484-498.
18. Kirkland, N.T., N. Birbilis, J. Walker, T. Woodfield, G.J. Dias, and M.P. Staiger, *In-vitro dissolution of magnesium–calcium binary alloys: Clarifying the unique role of calcium additions in bioresorbable magnesium implant alloys.* Journal of Biomedical Materials Research Part B: Applied Biomaterials, 2010: p. n/a-n/a.
19. Gray, J.E. and B. Luan, *Protective coatings on magnesium and its alloys -- a critical review.* Journal of Alloys and Compounds, 2002. **336**(1-2): p. 88-113.
20. León, B. and J.A. Jansen, *Thin Calcium Phosphate Coatings for Medical Implants*. 2008: Springer.
21. Buser, D., R.K. Schenk, S. Steinemann, J.P. Fiorellini, C.H. Fox, and H. Stich, *Influence of surface characteristics on bone integration of titanium implants. A histomorphometric study in miniature pigs.* Journal of Biomedical Materials Research, 1991. **25**(7): p. 889-902.

CHAPTER 2: Literature Review

2.1. Introduction

Magnesium (Mg) and magnesium alloys have the potential to be useful in creating better orthopedic implants [1]. Magnesium alloys can offer the strength and toughness required for load bearing implants where ceramics and polymers fall short. Other metals currently used for implants, such as stainless steels and titanium alloys, have elastic moduli that are much higher than natural bone, leading to unwanted stress shielding. The elastic modulus of magnesium and many magnesium alloys are much closer to bone [2]. Also, a second surgery is required to remove current metallic implants. Magnesium shows promise as the material for biodegradable implants that degrade in the body without requiring removal. It is found in abundance in the body, and the degradation by-product Mg^{2+} ions have been shown to be non toxic to cells [3]. In addition, magnesium may actually serve to stimulate new bone growth [1]. With all of these favourable properties magnesium looks very promising for this application. However, there are some challenges to be overcome.

Magnesium and its alloys in general have low corrosion resistance, which is important for metal implants given the very aggressive environment in the physiological system [4]. Toxic degradation products and loss of mechanical properties are the major concerns [5]. The low corrosion resistance of magnesium leads to loss of mechanical properties too quickly. It also leads to rapid hydrogen gas evolution within the body. For these reasons, pure unaltered magnesium metal is not an ideal implant material. Furthermore, it is desirable to optimize the biological response to these implants to maximize recovery. The biological response to the surface of the implant is important for compatibility of the implant with surrounding tissue [6]. Since corrosion and biocompatibility are ultimately surface phenomena, surface modification through treatments or coating systems will be needed to optimize implant properties.

A good coating or surface treatment will be one that will control corrosion of the implant, maintaining mechanical integrity for the duration the implant is required. To be effective on many types of implants, it will be ideal for the coating to cover complex surfaces completely to ensure corrosion does not occur too quickly. Also, the coating must have good adhesion to the metal substrate, and have acceptable wear resistance to protect the implant during the insertion operation and throughout the load cycles of the implant life. It is also of great concern that the implant be non-toxic and fully degradable itself after the duration required. Additionally, good cellular response and attachment is desirable allow the implant to become fully integrated with the biological system. A suitable coating that meets these criteria will allow biodegradable magnesium implants to become a feasible alternative to current metallic orthopaedic implants. What follows is a discussion of the various approaches taken to overcome the problems facing magnesium implants.

2.1.1. The Corrosion of Magnesium

In order to determine how best to control the corrosion of magnesium, it is important to understand the mechanism of corrosion, especially in physiological environments. In general, magnesium metal corrodes in aqueous environments to form magnesium hydroxide and hydrogen gas [7]. The overall corrosion reaction of magnesium is given in Equation 2-1.

$$Mg + 2H_2O \rightarrow Mg(OH)_2 + H_{2(g)} \qquad \text{Equation 2-1}$$

In general, corrosion will form a surface coating of $Mg(OH)_2$ and/or MgO [7]. This forms a passivation layer that will generally slow the corrosion rate. The passive layer protects the substrate until the oxide layer is penetrated, exposing unoxidized metal to solution. The corrosion is accelerated locally when this occurs. However, the corrosion degradation products re-passivate the surface, slowing further corrosion [8]. Galvanic corrosion will occur when Mg is put into contact with other metals. This can be due to

either external metals or internal secondary or impurity phases. Metals that have a low hydrogen overvoltage can cause severe galvanic corrosion. Examples are Ni, Fe, and Cu. The severity of galvanic corrosion is not as high for metals with lower hydrogen overvoltage such as Al, Zn, Cd, and Sn [7].

Physiological environments are typically very aggressive environments for metals. Corrosion tests carried out in simulated body fluids (SBF), which are fluids that contain many of the ions commonly found in the body, give some indication of how a metal will perform in an actual environment. In simulated body fluid, the rapid corrosion of magnesium can mainly be attributed to the presence of chloride ions. The Cl^- replaces OH^- into the $Mg(OH)_2$ at the surface and $MgCl_2$ is formed. $MgCl_2$ is quite soluble, and thus increases the rate of corrosion by destroying the passivation layer of magnesium hydroxide [9]. The effect of the Cl^- can be seen when corrosion is compared to a sample in a similar solution with a minimal amount of Cl^-. Pitting and surface cracking is the major mechanism of corrosion in SBF due to Cl^- ions [10, 11]. Because of the aggressive nature of physiological fluids on Mg corrosion, the use of Mg as a biodegradable implant material will need modification to slow the corrosion rate [1, 2].

2.1.2. Biocompatibility

Increasing the biocompatibility of the implant is also important. The response of the cells and tissue to a foreign-body implant is critical to the performance of the implant and the recovery of the patient [12]. Toxicity is crucial for the purposes of a biodegradable implant. If the implant is to degrade in vivo, then the inclusion of toxic elements or compounds must be minimized or eliminated from the implants [5]. This condition eliminates many of the common techniques used for corrosion resistance of magnesium in other applications. For example, heavy metals and chromate conversion coatings that have been used for magnesium corrosion resistance should not be used [13]. In addition to toxicity, cellular response while the implant is in place is of great importance. The biocompatibility of titanium implants has been investigated fairly extensively for

orthopaedic implants [14-18]. A magnesium implant will also need to exhibit good biocompatibility if it is to be effective.

2.2. Magnesium Alloys as Substrates

2.2.1. Alloying

Alloying the magnesium with appropriate elements to overcome problems of corrosion and biocompatibility has been the focus of much research, and will be important to perfecting magnesium implants [2, 19, 20]. Alloying elements that modify the corrosion layers to increase the stability of the $Mg(OH)_2$ can slow down corrosion, but often alloys with multiple phases exhibit microgalvanic corrosion [7].

The scope of alloying elements and concentrations for orthopaedic magnesium is severely limited [21]. For biocompatibility, alloying is limited to element that will not cause acute toxicity or long term damage, e.g. carcinogenic metals [5, 22]. For corrosion protection, the elements are limited to those that are not electrochemically too far apart and thus promote corrosion. The amount of alloying is also limited by the solubility limit of the alloying elements, as secondary phases that form will have a different electrochemical potential. This leads to galvanic corrosion [7]. For most Mg alloys, the alpha magnesium phase is anodic to the other phases that form [23]. The rapid corrosion rates in multiphase alloys limit the total amounts of alloying that can be used.

Given these constraints, the number of alloys suitable for biomedical Mg is limited. Of these, which ones can be used for magnesium is further limited by the corrosion protection. Unfortunately, many of the best performing elements for enhancing corrosion resistance are toxic or non-biological elements, e.g. aluminium and titanium. Recently, Kirkland et al. surveyed a number of biocompatible alloys in the range for biocorrosion [19]. The results of the study showed that most safe elements offer only limited

corrosion protection to Mg. A number of rare earth elements have also been suggested as possible candidates for biodegradable alloys [24-27]. While some of these rare earth elements have been tested for acute toxicity, the lack of data on the long term health effects of these elements means that further study will be required before they can be used clinically [5].

For the corrosion testing of coated samples, many alloys have been used as substrates. Figure 2-1 shows the distribution of alloys used to test corrosion protective coatings in the reviewed literature (See Appendix A). The most popular substrate for *in vitro* tests is pure Mg, although with varying levels of purity [28-49]. The small changes to the purity of the Mg can have large effects on the corrosion rate, which must be accounted for when comparing across studies [50, 51].

Various Mg-Al alloys have been used as well. The commercial aluminium alloys possess good corrosion resistance by themselves, compared to pure Mg. AZ31 [31, 48, 52-64], AZ91 [29, 47-49, 65-71] and other AZ alloys [72-74] are readily available and easy to use for corrosion tests, but may perhaps not be the most suitable for biomedical alloys due to the concentrations of Al, which may cause problems once introduced to the body [75-77].

Calcium as an alloying element has been used due to the compatibility of calcium with the body, since it is naturally regulated and removed similar to Mg. Thus, Ca containing alloys have also been used [57, 78-80]. Calcium does have the disadvantage of accelerating the corrosion rates of pure Mg due to it being an even more active metal [81, 82].

Zinc is also a non toxic element, if used in low concentrations [5], that has been used [20, 78, 83, 84]. Zinc can change the corrosion properties slightly although microgalvanic cells may form above the solubility limit in Mg, and higher Zn content is restricted by toxicity issues.

Ternary alloys of calcium and zinc have also been studied for implant materials [85-87]. Additionally a number of other assorted alloys have been chosen as substrates for biocorrosion research with other elements such as manganese [88], rare earth alloys [89], and others.

The choice of the alloy for a biodegradable implant is something that will be dependent on the desired mechanical and corrosion properties. The substrate may or may not be critical to the coating, depending on the type of coating used and how it is applied.

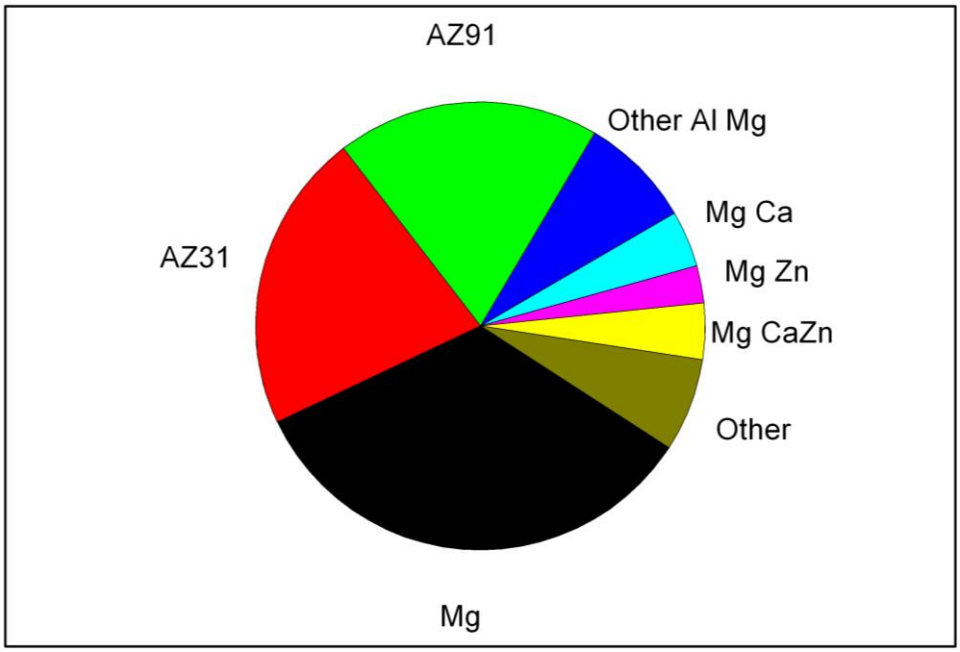

Figure 2-1: Mg alloys used in the surveyed literature for coating evaluation with protective coatings.

2.2.2. Bulk Metallic Glasses

The galvanic corrosion that forms between different phases is a limitation to the amount of alloying that can be used in a magnesium metal implant device. Overcoming the galvanic corrosion would open up a wide range of compositions for tailoring the metal properties. The formation of amorphous bulk metallic glass (BMG) is one approach to

completely remove corrosion potential difference due to the crystal structure in the metal. Casting metallic glasses requires specific alloy compositions and extremely high cooling rates to freeze the liquid metal without the formation of crystalline grains [90]. This presents a problem in creating fully amorphous structures of dimensions larger than a few millimetres. Alloy compositions can be optimized to form BMGs. Recently MgZnCa alloys at compositions with good glass forming ability have been of interest for biomedical and other applications [91-95]. These ternary alloys do not contain highly toxic elements, enabling them to be used in degradable implants.

Amorphous MgZnCa alloys have been tested *in vivo* to show reduced hydrogen evolution [95]. Amorphous alloys above 28 at. % Zn showed particularly good passivation properties, due to the formation of a zinc oxide layer. However, the BMG samples created were sheets only 0.5mm thick, so again, dimensional constraints due to the formation of BMGs may limit the use of fully glassy materials for larger implants. Gu et al. reported similar results for 2mm thick MgZnCa BMG samples, including reduced corrosion rate and increased response in cell culture tests [91]. Again, with larger implant materials, the total amount of elements such as Zn need to be controlled, and therefore these high Zn ternary alloys may pose biocompatibility issues.

2.2.3. Ion Implantation

An alternative to forming bulk metallic glasses for the substrate is to make the surface amorphous on a crystalline material using a surface treatment technique. Ion implantation provides a possible route of creating a modified surface like this. Accelerating ions to high velocities and implanting them into the surface of the substrate can cause a collision cascade that destroys the long range order of crystals in the metal, leaving a glassy surface. Chatterjee et al. has demonstrated such phase formation in aluminium substrates by ion implantation [96]. Glassy surfaces can also be formed after ion beam mixing a coated surface layer with the substrate [97].

This method of surface modification could be used to increase corrosion resistance. Advantages of ion implantation include modification of the existing substrate surface, often creating a gradual transition between the modified surface and the bulk of the material. This generally tends to make strong, adherent treatments that do not have the problems of adhesion, thermal stresses, and cracking that separate secondary coating phases tend to have. Plasma immersion ion implantation (PIII or PI^3) of Al, Zr, and Ti has been used to create corrosion resistance on AZ91. The mechanism of corrosion protection is due to the introduction of elements near the surface to increases the density of the corresponding oxide during corrosion, resulting in a more protective passivation layer [98]. However, additional elements may not be desirable if they are linked to toxicity like Al, or do not degrade such as Ti [99]. Using a thin implanted layer at the surface as opposed to bulk alloying can decrease the amount of introduced toxic ions.

Wan et al. used Zn ions due to their biocompatibility, but found Zn ion implantation in MgCa alloys increased the corrosion rate rather than decrease it [100]. Oxygen ion implantation has also been attempted but with little success against chloride solutions [101]. Nitrogen ion implantation has been used to improve corrosion resistance of magnesium. Nakatsugawa et al. reported nitrogen ion implantation reducing the corrosion rate of AZ91D to 15% of the untreated metal in 5% NaCl [102]. Similarly, Tian et al. used PIII to improve the corrosion resistance of AZ31B [103]. With ion implantation, the implant energy and dosage are critical to maximizing the implant performance. Ion implantation has the drawbacks of requiring line of sight to the target. Also, the total depth of ion penetration is limited, thus only allowing the very initial surface of substrate to be protected.

Numerous attempts to improve the *in vitro* corrosion resistance of Mg via alloying or phase modification have been done, although there exists no single solution to meets all of the implant design criteria as of yet. While there are many promising areas, the alloying method is limited fundamentally. The type and kind of alloying element is limited to those that are biocompatible. Even the compatible elements have upper limits on the amount that can be safely excreted by the body [5]. Of those that remain, there are

limits on traditional alloying to help with the corrosion rate [19], and although rare earth elements may seem promising, they will need to be vetted for long term biocompatibility. Thus, alloying of Mg does not appear to be a complete strategy for solving the corrosion rate problems of biodegradable Mg. The corrosion rates will have to be mitigated by an additional surface treatment or coating to meet the design criteria.

2.3. Coatings

A simple but effective method to reduce corrosion is to coat the metal so as to provide a barrier between the metal and the environment. Corrosion resistant coatings are commonly used for metals in many applications. For biodegradable Mg, the coating is required to keep the corrosive ions in the physiological system (especially Cl^-) away from the Mg until sufficient time has passed and the bone has healed. Once this has occurred, it is desirable that the coating eventually yields to the environment and degrades along with the magnesium, leaving no harmful traces. Numerous corrosion resistant coating types and application methods have been studied for Mg (Figure 2-2). The search for a biocompatible biodegradable coating that will provide the right amount of protection for orthopaedic purposes has covered many of these areas.

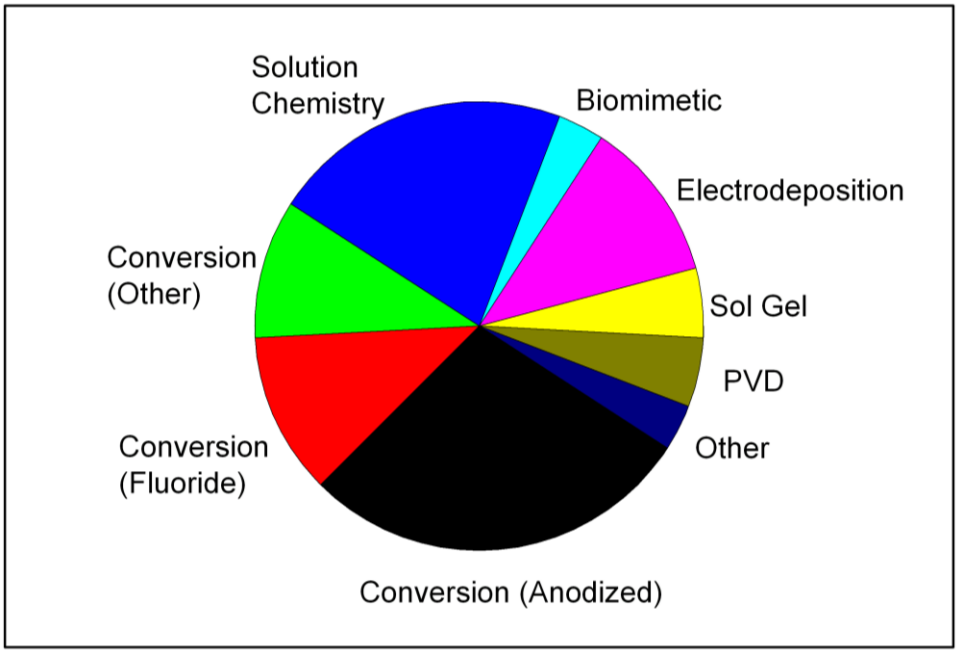

Figure 2-2: Reviewed corrosion protection studies for biodegradable Mg by coating type.

2.3.1. Conversion Coatings

Conversion coatings are produced by directly converting the outer surface of a metal into a different form to provide a protective coating [104]. This uses an electrical and/or chemical process to convert the metal matrix into an oxidized form that is not susceptible to corrosion. For magnesium, the conversion of the magnesium alloy surface into a dense magnesium oxide layer in an anodization process can be considered a type of conversion coating, as well as chemical conversion coatings including chromate, phosphate/permanganate, fluoride and others [13, 104]. These coatings convert the surface, thus creating a dense adherent coating that can often be made with few defects. These coatings have a proven track record in industrial corrosion protection, but many of them use dangerous elements, e.g. chromium, that are unsuitable for biomaterials. Properties of these coatings also will depend to some extent on the substrate chemistry as it is converted. Thus, these coatings can vary in properties as the alloy itself changes, which might present difficulties if it is desirable to modify the substrate alloy for mechanical properties and leave the corrosion protection intact. Overall, a significant

amount of research into coatings for biomedical implants has taken place using conversion coatings (Figure 2-2).

2.3.1.1. Oxide coatings/Anodization

A common practice is to use anodization to form a protective corrosion resistant layer on metals. This process represents the largest segment of the researched conversion coatings presented here (Figure 2-2). Anodization uses and electrical current to form a thick, dense oxide layer that is more protective than the natural layer that develops. Magnesium oxide layers can be formed by anodizing Mg which slow short term corrosion rate in SBFs such as Hanks balanced salt solution (HBSS) [29, 32, 33, 43, 47, 54, 55, 65, 67, 69, 70, 72, 74, 78, 85, 89, 105].

Furthermore, qualities of the coating like density can be optimized by controlling the voltage profiles during anodization [106]. The corrosion protection of the oxide layer can be increased by performing the anodization in a silicate solution, creating Mg_2SiO_4 on the surface as well as MgO [47]. These additions can change the density of the layer by modifying the Pilling-Bedworth ratio, leading to additional corrosion protection [107]. However, magnesium oxide layers will convert to magnesium hydroxide in aqueous solutions, and magnesium hydroxide is soluble in chloride solutions such as body fluid [108]. Further, greater anodization does not always improve the corrosion resistance. For example, Xue et al. found anodization greatly increased polarization resistance in a NaCl solution, but after longer (2 hours) treatment time the resistance decreased by a factor of 2 [47]. Because these films are not stable in biological solutions, anodization alone is unlikely to produce the protective coating required for many bioapplications. Instead, anodization can be used as a pretreatment to another coating system. For example, anodized layers can be used to control the amount and rate of calcium phosphate compounds precipitated on the surface in SBFs [33].

2.3.1.2. Fluoride Conversion Coatings

Fluoride conversion coatings solve the MgO solubility problem of anodized coatings by converting the magnesium not to an oxide like MgO but rather into MgF_2. MgF_2 has greater chemical stability due to the high electronegativity of the fluorine atom, which makes the ionic compound more difficult to separate. Because of this, MgF_2 is more stable in water than $MgCl_2$, and negates the effect of Cl^- attack. Consequently, the MgF_2 conversion coatings on commercial Mg alloys exhibit improved corrosion resistance [104]. Conversion coatings can be created by reacting the Mg substrate with hydrofluoric acid until a passive MgF_2 coating forms on the surface [31, 35, 54, 56, 70]. Because HF is highly corrosive and dangerous to work with, research into conversion coatings using other fluorides such as KF has been attempted as well [46].

Like other chemical conversion coatings this process can coat complex shapes and form uniform, dense coatings. The coverage and corrosion protection of the coatings increases with HF concentration up to 40% HF[54]. The formation of the conversion coatings will involve the creation of MgF_2 and $Mg(OH)_2$ with the amount of MgF_2 dependant on fluoride concentration [109]. This affects the created coating and thus the corrosion resistance [56]. Fluoride conversion coatings significantly increase the corrosion resistance in SBFs [31, 35, 54] as well as *in vivo* [25]. Fluoride coatings are not completely passive [70] and will dissolve with time causing attack to the substrate [25]. Despite this, these coatings have been used to slow down *in vivo* corrosion in order to extend the life of the mechanical strength of the implants [110]. The release of fluorine ions is not cytotoxic [111] so the main challenge for fluoride conversion coatings is optimizing the corrosion rate.

Conversion coatings of other types exist, but as stated before, are limited to those that are biocompatible. Phosphate conversion coatings can be used but are poorly protective without additional species [104]. Rare earth (RE) conversion coatings have been attempted for biomedical magnesium alloys, specifically cerium is of interest [53, 74]. Cerium does not interact much with the body, so can be safe for implants [112]. Cui et al. demonstrated that the corrosion resistance of AZ31 increased the polarization

resistance by a factor of ~7.5 in SBF after 10 minutes of immersion [53]. However, since the stability of Cerium coatings is so contingent on local environment and can degrade after several hours [113] these coatings will need more research to determine if they will be viable for biomedical use.

2.3.2. Calcium Phosphates

One of the most biocompatible coating options for orthopedics is calcium phosphate (CaP) coatings. Coatings of different CaPs have been researched extensively for use in biomedical applications [114, 115]. Several biologically important types of apatite are hydroxyapatite (HA), octocalcium phosphate (OCP), tricalcium phosphate (TCP), dicalcium phosphate dihydrate (DCPD) and amorphous calcium phosphates, often containing other secondary ion substitutions.

The mineral component of bone itself is an apatite, but also contains other ions such as carbonate and phosphate groups. This mineral structure is built upon a collagen matrix. The similarity of calcium phosphate coatings to bone minerals gives them good biocompatibility [115]. Calcium phosphate coatings have been used to increase the integration of the implant to the bone [116, 117]. HA coated titanium implants have been found to increase cell proliferation and bone formation [118]. CaPs are perfect candidates for protective coatings for Mg implants because they can be fairly insoluble in physiological conditions and are very biocompatible. However, the coating must be complete and adherent to the substrate to provide adequate corrosion protection. The quality of the coating created is dependent on the process and process parameters used for formation [115]. Calcium phosphate coatings have been of interest for corrosion reduction with researchers reporting corrosion resistance of CaP coatings *in vitro* [34, 36-42, 48, 57-59, 61-64, 66, 68, 71, 72, 79, 84, 86-88].

2.4. Coating Techniques

2.4.1. Plasma Spray

The most popular commercial procedure to attach calcium phosphate coatings to a metallic implant is the plasma spray method. This entails using a jet of neutral gas, inserting the material or precursors for the material to be coated into the jet and plasmatizing by some means, for example *via* a DC arc. The plasma spray is directed onto the substrate where the coating forms. The process makes precise control of the composition by control of the feed powders and the thickness of the coating [119]. Plasma sprayed hydroxyapatite has been used to coat implants to increase biocompatibility of implants [120, 121]. However, the high temperatures required for this process means care must be taken to avoid the presence of unwanted phases, as well as decomposition of the coating and/or substrate [119]. For Mg and its biocompatible alloys, the temperatures reached with plasma spray will be great enough to melt or change the substrate, making this technology difficult to apply to Mg. Plasma spray is also limited by the line of sight to the substrate, making complex shapes and porous structures difficult to coat uniformly. Other techniques to apply calcium phosphate coatings to metallic substrates have been attempted to overcome problems related to plasma spray such as poor integrity and adhesion, low crystallinity, and mechanical failure of the coating [122]. Some of these methods might be more appropriate for magnesium based materials.

2.4.2. Solution Chemistry Coatings

Solution chemistry methods for coating metals with calcium phosphates have a number of advantages. Simple and low cost setup, the ability to coat complex and porous materials, and the ability to use low temperatures make these coatings attractive for Mg substrates. For biomaterials, calcium phosphate coatings make up the majority of these types of coating due to their biocompatibility. The oxidation of Mg creates a local pH rise

which promotes calcium phosphate deposition in solutions containing calcium and phosphate ions [63]. This can be leveraged to easily create coatings in simple solutions.

However, this method also has its drawbacks, as magnesium is highly reactive in aqueous environments it tends to corrode during the coating process. Furthermore, for calcium phosphate compounds, substitutions by Mg^{2+} ion in the crystal lattice of compounds like HA are known to promote defects, limit crystallization [123], and decrease the stability of the created compound [124]. Hiromoto and Yamamoto reported HA coatings created on Mg and alloys in single step solution treatments [48]. The ionic concentration and pH of the coating solution affect the coating deposited. They reported reduction in corrosion current density of 10^3 to 10^4 times lower in 3.5% NaCl than uncoated Mg using potentiodynamic polarization (PDP). Hu et al. reported creation of a DCPD coating in solution on AZ91 alloy by titrating K_2HPO_4 into a $Ca(NO_3)_2$ solution [68]. The DCPD coating was transformed into HA over time in SBF, and the corrosion resistance of the coating increased to 4210 ohms from 331 on uncoated Mg. By PDP tests, corrosion current density dropped from 70 to 2.6 $\mu A/cm^2$. Tomozawa reported solution chemistry techniques to form HA on pure Mg in solution [39]. Increasing temperature to 333K or higher increased HA formation and $Mg(OH)_2$ formation. However, by increasing Ca concentration HA formation could be increased without affecting $Mg(OH)_2$ formation, which may be undesirable to have underneath the coating, due to its high solubility. Xu et al. reported in vivo studies using calcium phosphate coatings prepared by solution methods on Mg Mn Zn alloys [88]. The surface properties of the coated samples supported cell growth and exhibit higher overall osteoconductivity compared to uncoated samples. Because these solution coatings can avoid using any toxic elements, the biocompatibility is good. However creating a dense and adherent enough coating to remain crack free and fully protective in solution for the required amount of time remains an issue.

2.4.3. Biomimetic Coatings

One particularly interesting subset of these calcium phosphate solution coatings is the biomimetic coating process. The biomimetic process uses solutions similar in ionic composition to physiological fluids with the aim of creating a coating that is similar in properties to the layer that would form *in vivo* [125]. The similarity of a biomimetic coating to natural bone mineral can increase bioactivity of the surface [126]. The bone-like layer created is intended to enhance the activity of bone cells that come into contact with it, thus promoting faster integration of the implant [127]. The difference here is the change in composition and crystal structure of the biomimetic coatings compared to pure crystalline calcium phosphate coatings like stoichiometric hydroxyapatite. Substitution of other ions into the apatite lattice decreases the Ca/P atomic ratio from that of synthetic apatite closer to natural bone [128]. Common substituting ions include CO_3^{2-}, HPO_4^{2-}, Mg^{2+}, and others [129]. The crystallinity of the apatite decreases as well due to these substitutions [114, 123]. It is these changes that give the biomimetic coatings their unique properties.

Biomimetic coatings were originally developed to increase the bioactivity of calcium phosphate coatings for titanium implants [116, 118, 130, 131]. While corrosion protection is not a role of these coatings on Ti, the fact that these coatings are created stable in simulated body fluids suggests they can be useful for protecting corrosion of Mg substrates, as well as incorporating the biological properties. Some initial studies of biomimetic calcium phosphate coatings for corrosion protection have been shown to reduce corrosion on Mg [34, 42] and AZ91D [68].

Biomimetic coatings offer some key advantages for coating implants. These include high biocompatibility [42] both *in vitro* and *in vivo* [88], osteogenicity [127], and bone bonding ability [132]. Other advantages include possible coating of complex shaped and porous implants, low temperature deposition (and thus can coat low melting temperature substrates), simplicity of the process and low cost [133, 134].

Disadvantages to such coatings include the coating time. The literature reports up to 48 hours [34, 129] or as long as 5 days [42]. The deposition of a biomimetic layer is actually easier on Mg than on Ti due to the pH rise that comes from the corrosion of the Mg substrate [63]. The Mg^{2+} ions from the corrosion reaction also affect the nucleation of the calcium phosphate coating on the crystal structure. Because of this, the Mg ion concentration has been found to be critical to the formation and attachment of these coatings [135].

Another problem for corrosion is the method often creates cracks and other defects in the coating [34, 42, 136]. Sealing the coatings with NaOH is only moderately effective while hydrothermal treatment does not seem to help at all [42]. Defects in the coatings will allow the corrosion reactions to proceed on the underlying Mg substrate. Thus, elimination of the defects is required if these coatings are to be used for corrosion protection.

2.4.4. Electrochemical Assisted Deposition (ECAD) Coatings

Calcium phosphate coating formation can be assisted by the application of external potentials and currents. These processes are collectively referred to as electrodeposition. The setup for these methods is inexpensive and relatively simple, and the process can be carried out at low temperatures. The processing parameters can be easily controlled to optimize the coating created.

ECAD uses the reduction of water in an aqueous solution to promote the precipitation of calcium phosphates on the surface of a metallic substrate. Reduction of H_2O generates H_2 gas and leaves behind OH^- at the cathode. This leads to a local rise in pH at the surface of the substrate. An increase in pH decreases the solubility of calcium phosphates in solution, leading to precipitation at the surface.

The ECAD process for calcium phosphate can be controlled using a number of methods [115]. A constant potential can be held between the working electrode (the surface to be coated) and the counter electrode, typically made of an inert material such as platinum or graphite. Constant potential between the working and counter electrodes means the potential between the solution and the electrode is not directly controlled. Potential and current are therefore related to aspects of the coatings such as cell geometry, solution composition, counter electrode material, etc. This method has been used to form coatings of HA on AZ91D and have been shown to reduce corrosion currents as measured by electrochemical methods (PDP and electrochemical impedance spectroscopy (EIS)) [137].

Alternately, the coating process can be performed potentiostatically, where the working electrode is held at a constant voltage relative to a reference electrode. The reference electrode is placed near the working substrate in order to maintain a constant potential difference between the solution and the coating. This is useful for keeping the potential at a desired level to cause reduction of H_2O, without rising to levels that can reduce other metal ions in the solution. In this setup, the current will decrease as the substrate becomes coated and the exposed area of the electrode drops. Lower OH production at the cathode leads to a pH drop near the working electrode, and therefore a drop in deposition rate. DCPD coatings have been created on Mg alloys using the potentiostatic method, and while the resulting coatings do reduce corrosion rates, total coverage from thick, dense coatings that completely protect the substrates remains an issue [57].

To keep the hydroxide ion production constant, fixed current, or galvanostatic methods have been used to coat magnesium with this method. The standard three electrode cell is used, but the controls are set to keep current applied between the working and counter electrodes constant. Provided H_2O is the only molecule undergoing oxidation and reduction in solution, then the rate of OH^- production near the surface remains constant, keeping the pH profile roughly equal during the process. The voltage can spike during the process, especially after the substrate is partially coated. Song found the galvanostatic method of coating to form a calcium phosphate coating that was protective in SBFs,

dropping the measured corrosion current significantly over a 48 hour test [137]. Wen used the galvanostatic method to coat AZ31 with HA. PDP results show protective effects. Corrosion potential (E_{corr}) was increased and corrosion current density (I_{corr}) decreased. Post treatment in an alkali solution can result in greater stability of the coating, resulting in a lower rate of mass loss over 30 days [138]. Calcium phosphate and chitosan composite coatings have also been reported on Mg alloys by Wu et al. [71]. By performing the deposition in a solution containing a HA suspension as well as chitosan, composite coatings could be formed during the deposition process.

Finally, the voltage profile can be controlled to optimize the coatings created. Aside from galvanostatic and potentiostatic control, other voltage profiles used in this process include pulsed profiles. Ion diffusion in the coating solution can limit the rate of coating, needing longer than the current can source. Additionally, the reduction of water at the cathode produces hydrogen gas when the voltage is high. The net result of these factors can be loose, porous coatings [139]. Pulse duration can be modified to change properties of the coatings. This includes crystal size, with longer durations leading to larger crystals [124]. Pulsed current deposition on MgZnCa alloys has been studied, the coatings show improved protection and exhibit increased E_{corr} and decreased I_{corr} [139].

One downside of ECAD methods is the lack of complete dense adhesive coatings [57]. Hydrogen evolution at the surface of the metallic substrate creates gas bubbles that block chemical formation of the ceramic at the interface, resulting in volcano-like interfaces as reported by Kumar et al. [140]. Unfortunately the evolution of hydrogen gas is unavoidable for these type of ECAD coatings in aqueous solutions, and is indeed necessary to raise the pH at the surface and drive the coating process.

For electrodeposition processes that are not based around pH solubility, it is possible to avoid the reduction of water by performing the reactions in non-aqueous solutions. Due to the need for an electrically conductive fluid, ionic liquids present themselves as an alternative plating medium. Bakkar and Neubert have reported successful plating of Mg substrates with metallic Zn to increase corrosion resistance [49]. Ionic liquid composition, applied current density, and substrate alloy composition was found to affect

the coating created. While these types of coatings avoid the gas bubble problem, they rely on the reduction of a metal ion. Therefore they share the weaknesses of any metallic coating. Since any metal coating that will corrode slower than Mg will have a higher corrosion potential, any exposed Mg will form a galvanic cell and experience accelerated corrosion.

2.4.5. Sol-Gel Coatings

The Sol-gel process is a technique for the synthesis of metal oxides and other ceramic materials from colloidal solutions of organic precursor molecules [141]. Sol-gel coating processes can create coatings on complex shapes, use low temperatures and coatings can be created very thin. The process can require precise controls, and the raw materials are sometimes expensive [134]. The sol-gel coating process can be used for many biomaterial applications [142]. Hydroxyapatite can be formed by sol-gel methods [143], and this method has been used to improve the osteoconductivity on Ti implants [144].

For biomedical Mg, a sol-gel coating process has been used to create titania coatings that slow the corrosion rate in HBSS and Kokubo's solution [60, 80]. Reported protection has been 200 [60] to 2000 times more protective [80] on AZ31 and MgCa alloys than bare substrates, respectively. Although Ti is not directly cytotoxic [145], The long term protection and biodegradation of the titania coatings may be a problem since Ti does not have a biological excretion pathway like Mg, and the residual titania coating after the degradation of the implant may become an issue [99]. Sol gel coatings of silica have also been tested on Mg alloy ZE41 [146]. The coatings were found to slow the corrosion rate in a 3.5% NaCl solution at room temperature over 168 hours by a factor of 3. However, the performance *in vivo* is impossible to predict as the tests were performed in an unbuffered, non-physiological corrosion medium. These coatings also needed to be sintered at 400° C, which is high enough to modify the grain structure of the underlying Mg alloys.

2.4.6. Chemical Vapour Deposition

Coatings can be created by chemical reactions of gaseous chemicals near a heated substrate. This technique is known as chemical vapour deposition. Coating with this method allows the production of multilayer and composite coatings as well as complex shapes without line of sight. [147] For example, CVD has been used as an alternative to plasma spray to create a stable, crystalline, bioactive hydroxyapatite coating on 316 L stainless steels [148]. Most CVD processes are fairly high temperature, often requiring the substrate to be stable at temperatures above 600° C. These temperatures are therefore unsuitable for the coating of Mg. However, there are lower temperature processes being explored to limit temperatures to around 180° C [13].

2.4.7. Physical Vapour Deposition

Physical vapour deposition (PVD) is a method of forming thin film coatings. It can produce dense uniform coatings on flat surface, precise control over composition. It covers a variety of methods of processing where a vaporized form of the coating is produced in a vacuum environment and deposited onto the substrate. PDV techniques are necessarily line of sight. Additionally, the equipment can be expensive, the coating process can be time consuming, and it often produces amorphous coatings [134].

2.4.7.1. Metal Coatings Under PVD

Metal coatings have been used to prevent degradation of magnesium. Pure magnesium coating on a magnesium alloy particularly susceptible to corrosion has been show to decrease the corrosion. If alloying elements increase the corrosion potential, then a high purity deposition coating of pure magnesium on the surface will slow the corrosion [149]. Coatings of other metals may be achieved as well. Physical vapour deposition coating of aluminium has been successfully applied to magnesium AZ31 alloy [150]. The coating

did corrode in a NaCl solution, however, and aluminium is not the best choice for biocompatibility. Still, a metal coating for corrosion resistance is a viable option for protection, provided the coating metal has a low toxicity. Zirconium [151] and zinc [49] are possible candidates in this respect. The unfortunate downside to metallic coatings on magnesium is galvanic corrosion when any defect in the coating is present. If the coating metal is more noble than the substrate, the substrate will corrode preferentially [10]. A gap in the coating will lead to severe localized galvanic corrosion of the substrate underneath, and loss of mechanical properties will follow. Since magnesium has a lower corrosion potential than all other engineering metals the applications of metallic coatings is limited.

2.4.7.2. Pulsed Laser Deposition (PLD)

PLD uses a laser to vaporize a target and allow the vapor to condense on the surface of the substrate. This method allows for greater control of the crystallinity and composition and thickness of the coating [115]. Pulsed laser deposition has been studied on other implant materials, notably titanium [122, 152-154], however their protectiveness in corrosive solutions on magnesium is not widely reported.

2.4.7.3. Ion Beam Assisted Deposition (IBAD)

IBAD can produce coatings with good adhesion and allows precise control of the coating chemistry, including the Ca:P ratio. Yang et al reported using IBAD to coat AZ31 [59]. Calcium phosphate coatings created were heat treated to transform them into HA. Annealing improved the mechanical properties. Coatings were tested in a 3% NaCl solution for corrosion properties. Coated samples were more protective, although pitting did occur through cracks in the coating.

2.4.8. Composite Coatings

Multiple coating types, processes and compositions can be combined to form composite coatings. For example, microarc oxidation (MAO) can be used as a precursor to other coating types such as electrodeposition [72], or polymer coatings such as PLGA [73], or PLLA [89]. The first process or coating seeks to supplement the corrosion resistance by enhancing the adhesion/deposition of the first layer and/or providing a secondary barrier to corrosion. The use of alkali treatments on Ti is quite common to form a layer that supports the deposition of a subsequent CaP coating [15-17, 126, 155]. Two stage biomimetic coatings that provide better coverage of the initial CaP coating has also been used on Ti with success [129].

MgF_2 conversion coating and subsequent HA deposition have been reported by Jo et al. to slow the corrosion rate of Mg by a factor of 3.5, as measured by ion release in SBF over 70 hours [44]. PLGA on MAO layers have reduced the corrosion current 10x in Hanks, and had the benefit of allowing the coating to perform slow drug release as well [73]. Lu et al. used a secondary coating of PLLA on a MAO layer to improve the corrosion resistance by sealing the microcracks and micropores in the as created coating [89]. The use of a composite coating to resolve the problems and shortcomings of a single coating process can improve the overall performance of the system.

2.5. *In Vitro* Corrosion Evaluation

2.5.1. In Vitro Corrosion Solutions

As noted above, the corrosion of a Mg implant will be dependent on the surrounding environment. The *in vivo* environment is a complex place with a great many individual biological components, chemicals, cells and processes in play. It is a difficult environment to take analytical corrosion measurements in, and can be expensive to do trials in, thus making it undesirable for quick screening and optimization of the coatings. Salunke et al. have reported coatings tested *in vivo* but were unable to report precise

corrosion rates occurring *in vivo*, simply that the films remained intact after 48 hours of implantation [28]. Similarly, Wang et al. reported better biocompatibility of CaP coated Mg but direct corrosion measurements were performed *in vitro* [64].

Also, large numbers of tests are often needed to establish statistical significance *in vivo* due to variability between animals. Therefore, corrosion measurements *in vitro* can be used to systematically analyze coatings and corrosion rates. *In vivo*, the expected dominant corrosion reaction will be with H_2O and Cl^-. These will be the direct participants in the corrosion reaction. In addition to these, other ions, organic molecules (amino acids and proteins), and cells will be present, and may also influence the corrosion reaction. The immune response may encapsulate the Mg in proteins and prevent corrosion [156-159], although some data has shown that proteins can increase the corrosion rate [160]. The effect of proteins on the ultimate corrosion rate is complicated, and affected by the environmental conditions [161, 162]. The exact effect and importance on any coating will need to be investigated *in vitro* in order to predict and understand the ultimate *in vivo* behaviour.

The design of an *in vitro* test for corrosion assessment of coatings should not aim to perfectly replicate the *in vivo* environment. It should accurately provide a standard, invariant system in which the conditions that dominate the corrosion behaviour *in vivo* are built into the test design. In the aqueous solutions, chloride ions are the most responsible for breaking down the passive layer [10, 11]. To measure this effect, one of the most common corrosion solutions for *in vitro* is a simple NaCl solution. The Cl^- ion concentration in human blood plasma is around 103 mM [156], or around 0.6% NaCl by weight. The Na^+ ions act as spectators without affecting the overall corrosion reaction. Accelerated corrosion tests for coatings are sometimes carried out in higher concentrations of NaCl, such as 3.5% [37, 41, 48, 52, 61, 146] or even 5% [29]. For more biological significance, tests on these coatings is done in lower concentrations of NaCl, either near blood plasma levels of Cl- or at the slightly higher levels popular in cell culture SBFs such as Hanks Balanced Salt Solution near 0.9% [46, 47, 64, 67]. The ability of a coating to prevent the corrosion due to Cl- is easy to measure in these SBFs.

As the simplest and most mechanistically relevant test, NaCl solutions account for almost one third of reported *in vitro* corrosion tests on coated Mg substrates reviewed (Figure 2-3).

Although Cl^- concentration is a significant factor for the corrosion of pure Mg, and none of the other common ions in human blood plasma play a direct role in the corrosion mechanism of Mg, a simple NaCl solution might miss some important effects on corrosion behavior that may be relevent *in vivo*. Thus, a more complicated solution that better approximates the physiological fluids may be desirable for coating corrosion tests. Calcium, carbonate and phosphate ions by themselves do not interact with the layers directly, but the corrosion of Mg in solution can lead to deposition of calcium phosphates on the surface that retards further corrosion [2, 163]. SBFs that contain the ions present in blood plasma are therefore useful corrosion test solutions. Different SBFs exists with varying amounts of each salt depending on the intended use (*e.g.* cell culture) [14, 156], although typically differences from physiological fluids is small. Some popular corrosion test solutions reported for coating evaluation are HBSS [32, 34, 35, 53-55, 57, 60, 62, 64, 73, 79, 85, 87, 89], and other SBFs with very similar or slightly modified compositions [38, 43, 47, 64, 66, 68, 83, 86]. Because some of these cell culture solutions contain higher Cl^- concentrations than found in blood plasma, and other ions are perhaps less important, modified formulas such as those proposed by Kokubo et al. [14] are being used for *in vitro* corrosion experiments as well[36, 45, 72, 80, 84]. Solutions containing the ionic salts with none of the organic components of the physiological system have the advantages of including the other ions found in the blood to more closely resemble the actual target environment. Moreover, they do not contain the cells, proteins and other organic material. This negates the requirment of conducting tests in a sterile, controlled environment to avoid culturing bacteria and other organisms that can change the properties of the solution.

The next step up in complexity from ionic solutions is the addition of organic molecules such as amino acids. Standard SBFs containing amino acids for cell culture and other biological work can be used for corrosion tests, such as Eagle's Minimum Essential

Medium (MEM) [40], Dulbecco's Modified MEM (DMEM) [28, 31, 42], and similar solutions. Amino acids can affect the properties of the solution such as buffer capacity [164] and may chelate with different ions [156]. Amino acids can also adsorb onto the surface of Mg alloys and create an additional barrier to corrosion [165].

Proteins add another level of complexity of the *in vitro* solution to more closely represent the physiological fluids. Protein interaction with the surface of implants is very important to the biocompatibility of the implant [166]. The interaction of these molecules with the surfaces can influence the corrosion rates as well [28, 42]. In the surveyed literature, ionic solutions of simple NaCl, slightly more complicated ionic SBFs or both are very common. SBFs that also contain organic molecules are much less widely reported (Figure 2-3). While the simple SBFs are very useful for corrosion measurements, other organic molecules can affect the ultimate corrosion behaviour, so these tests will need to be done to validate the results before transitioning from an *in vitro* to and *in vivo* model.

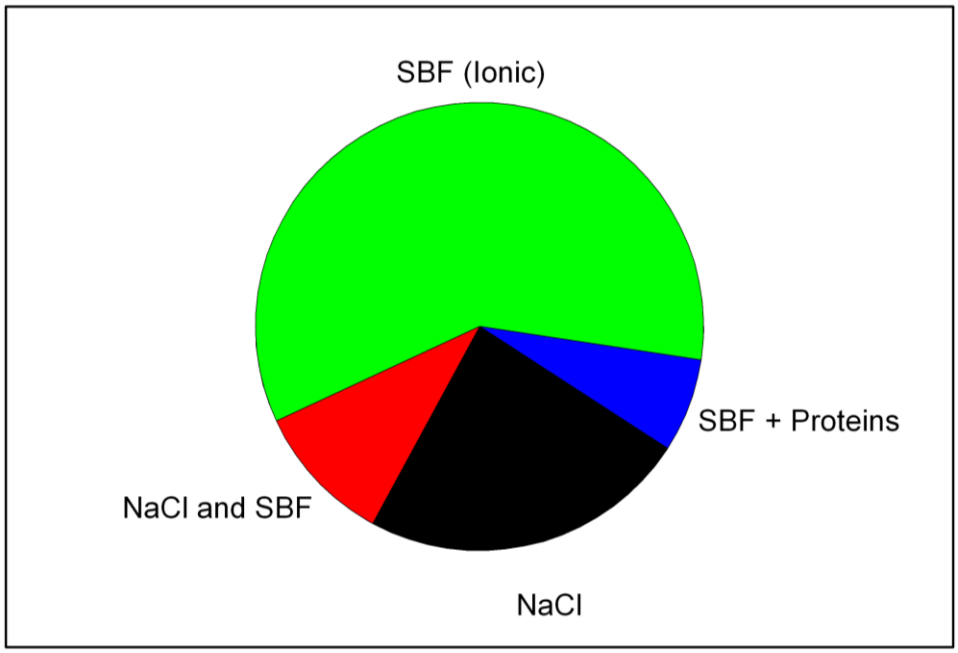

Figure 2-3: Proportion of SBFs used to evaluate corrosion properties of protective coatings and surface treatments *in vitro* in the surveyed literature.

2.5.2. Buffer Systems

pH is a critical element to the corrosion and passivation behaviour of Mg and small changes in pH greatly affect the corrosion rate [167]. In vivo, this is closely maintained at a constant range of 7.4-7.6 by the carbon dioxide/bicarbonate buffer in the blood. Thus, the corrosion behaviour and coating performance should be measured within this range. The passivation behaviour and corrosion kinetics change drastically with pH [168] as the changes in pH affect the $Mg(OH)_2$ layer that forms on the surface. The pH may also affect the chemical stability of the coating applied to the layer, and further change the corrosion properties. An example would be calcium phosphate coatings that experience a change in stability and morphology with varying pH [134].

The problem with corrosion being pH dependant is that the corrosion reaction itself changes the acidity of the solution. The process reduces water to H_2 gas and OH^- ions that will increase the pH. The problem affects the results *in vitro* when this is not maintained at a constant level by an active mechanism such as the body's carbonate buffer system. Therefore, care must be taken when setting up an *in vitro* corrosion test to minimize the effect the pH rise has on the system. The appropriate use of a buffer will help minimize the pH changes that occur during corrosion. While many buffering agents can be used, the ideal buffer candidates are ones that follow these criteria: (a) able to maintain pH close to the physiological range; (b) should not affect the corrosion reactions; (c) should not interfere or change the solubility of the corrosion layer or any coating; and (d) should not react with, bind with, or otherwise alter the constituents of the *in vitro* solution other than the hydroxide ions to control the pH [169].

A practical choice for a buffer *in vitro* is to use the HCO_3/CO_2 buffer, such as the one used in the body [170]. This buffer requires the test to be conducted in an atmosphere of CO_2, usually 5%, to maintain a physiological pH [156]. Interestingly, the CO_2 buffer system is not as widely used as other buffer systems in the testing of coated samples *in vitro* (Figure 2-4) [28, 31, 40, 42, 88]. However, *in vitro* this buffer requires a high availability of carbonate ions. The influence of the carbonate rich buffer has been shown to slow the corrosion rates of Mg [156]. The carbonate ions have been found to deposit

in the corrosion layers of the Mg, thus affecting the rate [162, 169]. It is therefore of concern that the corrosion mechanism of the implant is not changed by using this buffer.

An important requirement of a CO_2/HCO_3 buffer system is that the testing atmosphere must be controlled. In order to perform *in vitro* tests more easily, many researchers have used other chemical buffers that do not require a controlled atmosphere. Chemical buffers like borate, phosphate, and citric acid can be used but these do not have good physiological relevance [51, 168, 171]. The ideal buffers are ones that have a pKa near 7.4 for good buffer capacity at the physiological pH and do not interact with the other constituents of the media [172]. Tris-(hydroxymethyl)aminomethane (TRIS) has been used for testing the corrosion protection of coating on Mg [32, 38, 43, 83, 86]. TRIS has a poor buffering capacity above pH of around 7.5, and has also been known to react with proteins, making it a poor choice for *in vitro* solutions that contain proteins.

Zwitterionic buffers have been developed for cell cultures to meet the requirements of good pH control and low interaction with the media. The most popular of these currently were first developed by Good et al. in 1966 [172]. These buffers include MES, PIPES, and HEPES, all zwitterions that have good buffer capacity in the physiological range and low interaction with the rest of the media. Of these, the most popular in Mg biocorrosion studies is HEPES (Figure 2-4). HEPES has been used as a pH control for a number of coating performance evaluations for biodegradable implants [34, 45, 66, 84]. HEPES, with a pKa of 7.55, high solubility and negligible complex interaction with the other biological salts is a good choice for an *in vitro* buffer.

All of these chemical buffers can help resist changes in pH due to corrosion over time. However, these only address the problem up to the buffer capacity of the solution. For Mg, which corrodes very quickly, the ratio of solution to corrosion surface area, the frequency the solution is replaced, and the total duration of the test must be limited to keep the test relevant. The corrosion behaviour changes with pH rise, and corrosion measurements no longer mimic the physiological environment. For immediate electrochemical tests a rise in local pH as the test is conducted may affect the measured result, and the effect can become significant over time. An appropriate buffer is helpful

in mitigating the pH rise, and extending validity to the results. Disturbingly, a large number of studies on the corrosion protection of coatings did not use or did not report using a buffer (Figure 2-4). The corrosion mechanism and measured rates of corrosion will be different if the pH is allowed to rise too much, and if it goes above 11 [47, 64] it will passivate the Mg [7]. When the pH is not monitored, no buffer is used, and/or the solution to sample ratio is low/not specified, it is difficult to have confidence that the reported corrosion rates will remain valid *in vivo*, which is the entire purpose of the *in vitro* approximation. It is important to realize that the buffer resists pH change, but does not hold it constant. A buffer will extend the time the pH stays in the desired range. pH can be returned to the desired level by adding an acid to the solution to neutralize the OH^- released. Of course, the addition of the acid will affect the ionic composition of the solution, and certain acids are more appropriate than others. The use of HCl to adjust the pH as is sometimes the case [32, 38, 43] is discouraged due to the strong relationship between Cl^- ion concentration and corrosion rate of Mg. These studies are then simply trading an unphysiological pH for an unphysiological amount of Cl^- in the corrosion medium.

Alternatively, pH and ionic concentrations can be maintained by refreshing the solution. In addition to causing a pH change, the amount of dissolved magnesium ions in solution changes the solution and corrosion reaction slightly as well [23]. Therefore, changing the solution can restore the solution back to the bodily concentrations of Mg^{2+}. In the body, there are a number of mechanisms for maintaining concentration of salts at appropriate levels. Allowing the Mg to build up significantly *in vitro* will not be representative of the environment *in vivo*. The solution to sample surface area ratio, the duration of testing, and the rate of corrosion will determine how often the solution must be refreshed. The solution refresh will restore the pH regardless of the buffer type used, if any.

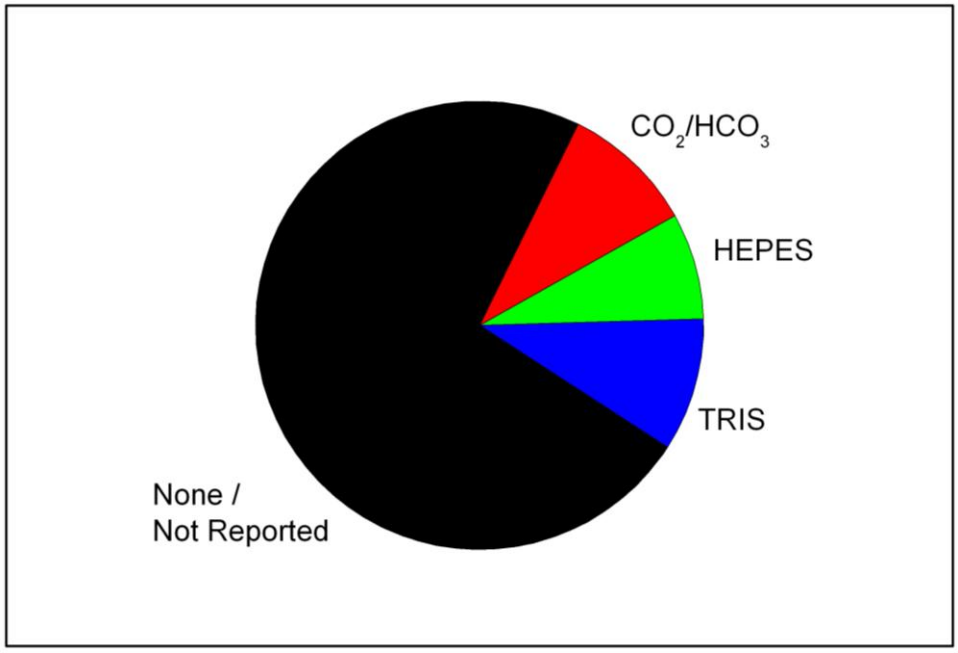

Figure 2-4: Relative usage of buffer systems used in the *in vitro* corrosion tests of coatings on Mg in the reviewed literature.

2.6. Corrosion tests

2.6.1. Cumulative: Mass Loss and Ion Release

The corrosion testing falls within two categories: cumulative corrosion tests and instantaneous electrochemical tests. Cumulative tests show the amount of corrosion that has occurred by measuring the cumulative physical changes created by the corrosion reaction. The loss in mass from the magnesium substrate is one method. Collecting and measuring the volume of hydrogen gas evolved allows you to indirectly measure the corrosion rate by the H_2 by-product of the reaction. Additionally, monitoring the concentration of Mg^{2+} ions in solution will indicate how much of the substrate has corroded. Measuring the pH of the solution can also indicate the level of corrosion that has taken place overall, but is not desirable because of the effect this has on the corrosion rate. These cumulative tests show quantitatively how much corrosion has occurred since the beginning of the test but do not tell you anything about the mechanism or nature of the corrosion. For evaluating coatings in an *in vitro* environment cumulative tests are

effective for measuring the change in corrosion resistance compared with uncoated samples. As with all tests, the corrosion response will vary due to the quality of coating, substrate alloy, SBF used, and the duration of the immersion test. Chen et al. reported a reduction in corrosion by ~67 times for a hydroxyapatite coating after 48 hours [40]. Zhang et al. reported the mass loss on a DCPD coating on Mg 1% Ca alloy over 3 days to be 4 times greater on the control than the coated sample [79]. Chiu et al. reported a protection factor of ~3.4 over 18 days for a fluoride conversion coating [35], and Zhu et al. measured a $Mg(OH)_2$ conversion coating with a protection factor of 1.17 after 31 days [55].

Mass loss is not necessarily the best choice for the corrosion measurement of coated Mg in SBF because the corrosion of Mg in SBF is known to precipitate additional calcium phosphates on the substrate [63], thus making the mass measurements difficult to do precisely unless the coating is removed completely. Chromic acid is useful for calcium phosphate coatings as it can dissolve these ceramic coatings while leaving the substrate relatively uncorroded [23]. The cleaning methods will depend on the alloy, the coating, and the corrosion solution, so the chemistry of the coating and the underlying substrate must be considered before using acid removal techniques such as this. As Zhu et al. found over 31 days of corrosion testing, the corrosion rate for the coated and control samples varied considerably [55]. This illustrates the importance of monitoring the corrosion rate over time for these coated samples.

Selective ion measurement has been used to calculate the total Mg^{2+} ions released to solution [156]. However, this omits the Mg incorporated into the corrosion layers of magnesium hydroxides, carbonates or phosphates. Also, the increase in Mg^{2+} ions if the solution is not periodically refreshed and allowed to remove these ions, will affect the corrosion potential with the solution according to the Nernst equation [173]. Mg ion measurement also measures the total amount of corrosion, but does not reveal details about the mechanisms.

2.6.2. Cumulative Corrosion tests: Hydrogen Evolution

The next most common cumulative corrosion test is the measurement of hydrogen gas evolved, commonly referred to as hydrogen evolution tests [174]. H_2 evolution tests capture the gas evolved from the cathodic half of the corrosion reaction. Because stoichometrically the amounts of H_2 generated is linked to the amount of oxidized Mg, this is an indirect method for measuring the total amount of corrosion. This measurement can be monitored continuously, without the need for removing the sample from the solution. To perform the test, the sample is immersed in the corrosion solution. A funnel and burette are filled with solution, then inverted over the immersed Mg to collect the gas evolved. As long as the gas is completely captured and no other sources or sinks of H_2 gas are present other than the measurement apparatus, this method can be an accurate corrosion measurement. Also, since the volume of H_2 generated is of concern to the surrounding tissue when implanted *in vivo* [1, 2], this method provides direct measurement of the hydrogen generation rates, something that will be necessary to optimize if these degradable implants are to be used in vivo . H_2 generation tests have the same limitations as other cumulative tests such as mass loss, which is they do not provide mechanistic data, or any information regarding where the corrosion is occurring. Thus, cumulative tests must be supplemented with electrochemical methods.

2.6.3. Electrochemical corrosion tests

Electrochemical tests can be used to examine the instantaneous rates of reaction electrochemically. Methods such as potentiodynamic polarization (PDP) and electrochemical impedance spectroscopy (EIS) are used to estimate the electrochemical properties, as these are difficult to measure directly.

2.6.3.1. Potentiodynamic Polarization:

PDP works by polarizing the sample and measuring the current of the half reactions at various potentials, then extrapolating to estimate the corrosion current density. A PDP scan starts at a potential below the open circuit potential (OCP), forcing the cathodic half reaction to dominate, and scans at increasing potential until some point higher than the OCP. The corrosion current density can be estimated by extrapolating from the Tafel slopes of each line [175]. Since the potential will be held at voltages much higher than OCP, the anodic reaction will be forced to occur at high currents during the test, which for active metals such as magnesium means the surface can become severely corroded. This can change the corrosion layer, surface roughness, and surrounding solution pH over the test. The test is therefore considered to be destructive to the sample.

PDP is quite popular, showing up in many of the reviewed papers on coating corrosion measurements (Figure 2-5). PDP has the disadvantages of being a destructive test, since the test can change the substrate significantly. PDP is also an extrapolation, and obtaining a corrosion current density relies on the fit of linear Tafel slopes. If the behaviour is nonlinear, it is possible the estimated current density will have a great degree of variability. As an example, if the literature surveyed here is limited to the studies using pure Mg substrates, and PDP tests in some type of SBF, we can see large variations across the control samples. Measured pure Mg corrosion rates can vary from 0.1 to 1430 $\mu A/cm^2$. This is a very large variation for similar materials in SBFs. Purity, SBF composition and measurement parameters are responsible for the variations. However, some consistency should be expected if these *in vitro* tests are designed to identify corrosion rates by accurately simulating the *in vivo* environment. Since testing parameters vary so widely, the coatings will be presented here by comparing the ratio of the corrosion rate of the uncoated control sample of a given alloy over the coated sample. This will allow a somewhat direct comparison of the quality and integrity of the coatings across the various tests and substrates in the literature.

2.6.3.2. Electrochemical Impedance Spectroscopy:

EIS is a technique particularly suited to measuring the performance of coatings [175]. The technique uses the same three electrode setup as PDP. A small AC signal (on the order of 10mV) is used to polarize the surface and the resulting impedance of the system is measured. The signal frequency is varied to obtain a frequency response curve that is representative of the coatings and corrosion layers of the sample. The resulting curves shed light on to the behaviour of the corrosion layer, and the resistance to corrosion provided by the coating. This can be related to the thickness, coverage, and porosity of coatings, making it very useful to identify the relative effect and mechanism of corrosion protection provided by different coatings and surface treatments. EIS is also a non-destructive technique, or more precisely minimally destructive technique. Due to the small potentials applied, the impressed currents and thus the imposed oxidation of the substrate is much smaller than a typical PDP scan. As such, multiple EIS scans can be taken on the same sample with minimal change to the sample due to the measurement. Therefore, multiple scans taken over intervals can be used to monitor the changes in the corrosion behaviour over time. The benefits of the EIS methods for coated samples make it quite a useful test, which is gaining popularity for coatings aimed at Mg implants (Figure 2-5).

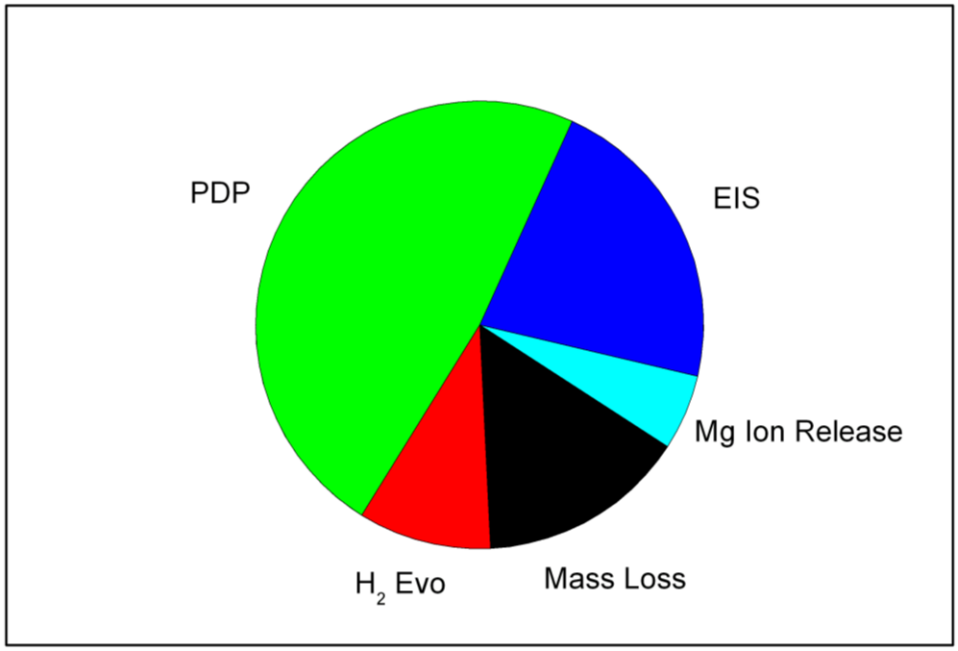

Figure 2-5: Relative usage of corrosion test type to evaluate coating performance in the literature.

2.7. Review of Corrosion Protection Properties of Coatings Assessed in the Literature

Many different coating systems have been studied to show corrosion protection in the literature. These use different coating types, performed with different application techniques, on different substrates, tested in different corrosion solutions. With the great variety of experimental techniques, it is unsurprising that the reported results vary to such a great extent. To show some of the variation present amongst the experimental results the substrates of those using some type of pure Mg and the AZ31 alloy across the literature were compared. Of these tests that used PDP as a corrosion rate measurement technique the measured corrosion rates of the uncoated control samples are shown in Figure 2-6 A. These tests were all performed in simulated body fluids, attempting to simulate the body, with the same alloys. The results across the literature span two orders of magnitude, highlighting the variation the test parameters can create. A similar trend of the resistance of pure Mg using EIS was observed (Figure 2-6 B). The fact that even similar substrates across *in vitro* studies are so different makes comparing the provided

protection by the coatings quite difficult across samples. It should not be surprising therefore that *in vitro* tests corrosion rates are so different than the rates *in vivo* [156, 162, 176]. Clearly identifying the relative corrosion rates *in vitro* will require more understanding of the environment than using a standard SBF and hoping for the best.

In spite of these variations, the comparisons can at least be estimated as a corrosion protection factor (CPF). Substrates and test solutions that lead to lower corrosion rates will generate coating results with lower corrosion rates than those with high corrosion rates to begin with. The assessment of the properties of the coating should thus be normalized to the control sample used. Therefore, the protection factor is defined as the rate of the uncoated substrate divided by the coated sample. Higher coating protection factors should in theory indicate more protective coatings, *i.e.* a corrosion protection factor of 1 indicates the coating provide no more protection than a bare sample, and a corrosion protection factor of 100 says the rate of corrosion is 100 times slower when the coating is applied. This also solves the problem of directly comparing different test types by converting them numerically to a unitless value. This is a rough comparator, as the effect of corrosion solutions, test types, and buffers will provide sources of error and inconsistency, but the CPF will indicate something about the landscape of the literature.

Figure 2-7 shows the CPF of different coating types reported in the literature at the latest timepoint measured. The majority of the tests are performed immediately or within a few hours, with fewer tests reported over longer durations. The highest protection factors are shown initially, whereas longer timepoints show decreased CPFs. The decrease will be important in identifying a coating that can last over time. For example, anodized coatings have been tested with high initial CPFs, but there are few long term tests. For an oxide coating, which is not stable in SBF, making sure the coating protects for the required amount of time will be crucial. Fluoride conversion coatings, as well as composite coatings of multiple types have been shown to exhibit long term corrosion protection. Again, these ratings can be somewhat suspicious depending on test type. The corrosion solutions, buffer systems, and experimental methods vary greatly across the literature, making it difficult to say with confidence how relevant and related these reported factors

are. Other factors will be at work as well. In order to fully understand the protection mechanisms of the coating, and predict its performance *in vivo*, understanding the parameters of the *in vitro* tests will be critical to obtaining valid corrosion data *in vitro*.

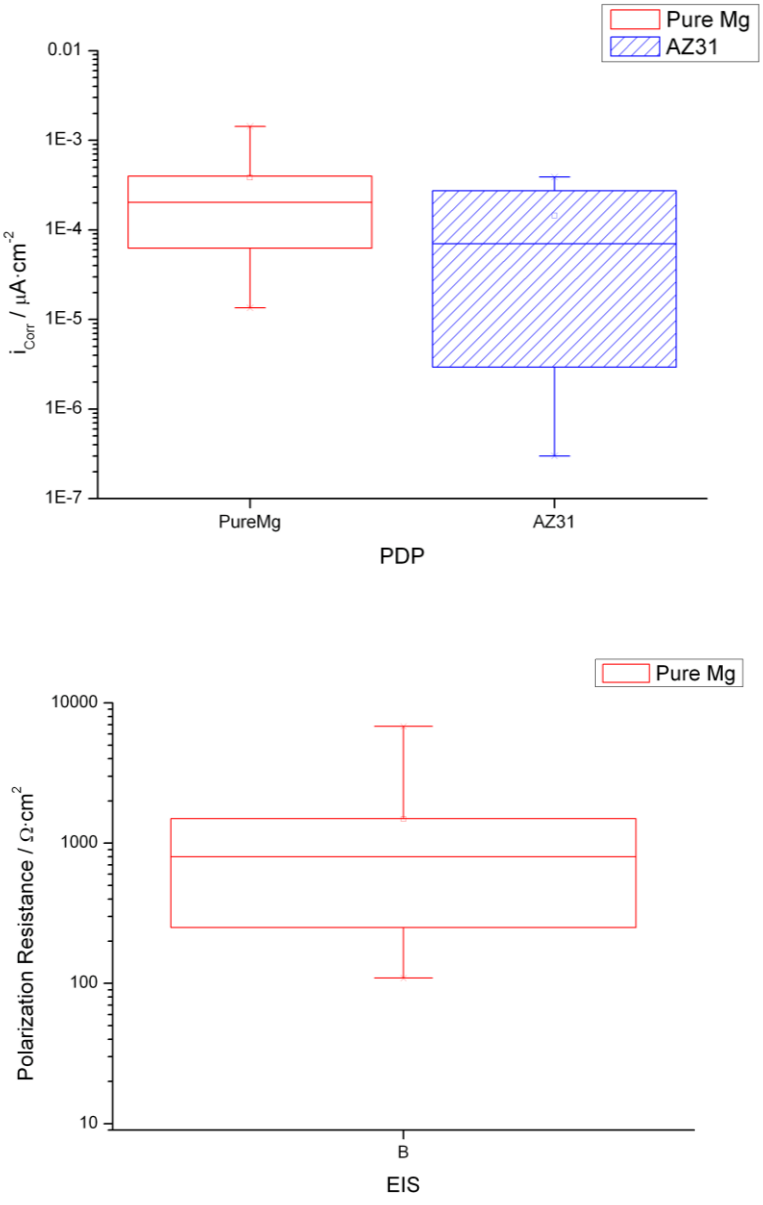

Figure 2-6: Box plots of available control samples for in vitro evaluation of coatings by PDP (A) and EIS (B).

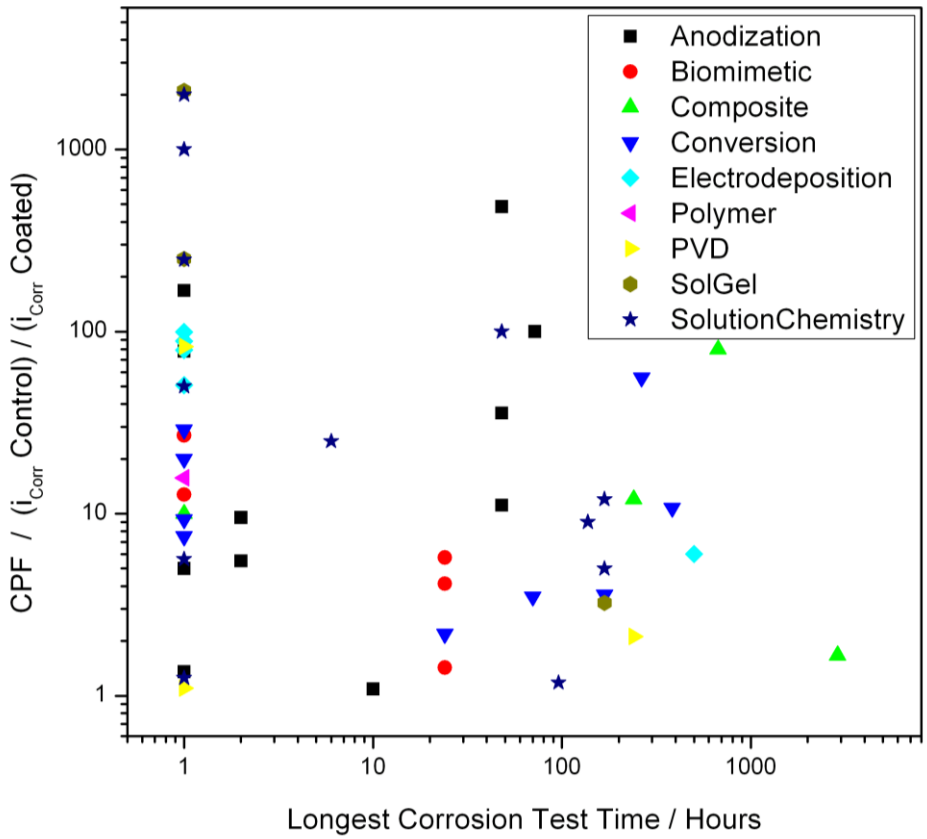

Figure 2-7: Coating protection factors calculated at the longest reported immersion time for different types of coatings.

2.8. Research Aims

The above review of the literature highlights some significant gaps in the knowledge and design process of corrosion resistant coatings and surface treatments for biomedical Mg. A multitude of coating types and processes has been examined by a number of different methods. However, the corrosion behaviour is highly dependent on the test environment, which must be carefully controlled if meaningful data about the corrosion mechanisms *in vivo* is to be collected. This means the coating protection must be studied in solutions where the pH, buffer system, ionic composition, and organic inclusions of amino acids and proteins. These components should be looked at individually in order to understand the complex system as a whole. The in vitro test environments must be kept consistent in

assessing the corrosion performance across multiple coating systems, alloys, and immersion times. This is necessary in order to properly understand the behaviour of the corrosion protection of the coating. The variation in *in vitro* tests reported across the literature is large. This is true even when using the same alloys. With the control samples differing by orders of magnitude, the comparison and ultimate predictions of in vivo behaviour is not possible. Hence, the first step is to construct and identify the parameters important *in vitro* for testing the corrosion resistance of the coatings.

The corrosion protection system for Mg biomaterials must meet a number of criteria for biomaterials applications. The amount of corrosion protection provided will be the key to optimizing Mg implants. The coating must provide corrosion protection, but also be able to degrade after the implant has performed its function. Completely or extremely insoluble coating products like titania or hydroxyapatite may cause problems if they persist after the underlying substrate has degraded. The degradation products must also be fully biocompatible, as they will end up inside the bloodstream of the patient. The biocompatibility and bone growth onto the implant is also important, and should be optimized if at all possible. Thus, corrosion inhibitors that have not been shown to be biocompatible are suspect, such as aluminium, or rare earth elements that have not been thoroughly investigated in the longer term following implantation.

The coating system is also important, as the properties of Mg and the implant shape will limit the choices of deposition. The ideal coating must be processed at low temperatures and suitable environments due to the melting temperature and reactivity of Mg. The final implant shape may need to be a porous or complex-shaped structure, which cannot be coated completely or uniformly by techniques requiring line of sight. The use of toxic or non-biocompatible precursors and intermediate chemicals during the coating process is not inconceivable, but these must be completely removed before the device is implanted. If the coating process can avoid this concern it will be beneficial.

A coating system in the literature that meets the desired criteria is the biomimetic coating. This coating type has been well documented recently for its biocompatible properties on titanium implants, but has received little attention for Mg. It is biocompatible, imitates

natural bone structure, and contains no elements or structures not found in the body anyway. The process is done at body temperature, and is coated in simple solutions that contain no elements that are not found in physiological fluids. The solubility of the phases is similar to natural bone, and thus more insoluble than Mg, and thus can be protective under corrosion conditions, yet less insoluble than the HA used on permanent Ti implants. The biocompatibility and osteogenic properties of biomimetic coatings have already been proven by numerous tests on Ti, which gives us confidence that it will be just as useful in promoting bone growth on degradable implants. The gap in the knowledge is the corrosion properties, as the corrosion protection of Ti has not been a design requirement of the coatings.

The work that follows will investigate the formation mechanisms of these coatings on Mg substrates, and examine the effects of surface conditions, process parameters and conditions effect on the corrosion protection properties of these coatings. The corrosion performance and protection in multiple in vitro solutions will be examined to determine what, how and why the coatings corrode and protect Mg substrates.

2.9. References

1. Staiger, M.P., A.M. Pietak, J. Huadmai, and G. Dias, *Magnesium and its alloys as orthopedic biomaterials: A review.* Biomaterials, 2006. **27**(9): p. 1728-1734.
2. Witte, F., N. Hort, C. Vogt, S. Cohen, K.U. Kainer, R. Willumeit, and F. Feyerabend, *Degradable biomaterials based on magnesium corrosion.* Current Opinion in Solid State and Materials Science, 2008. **12**(5-6): p. 63-72.
3. Li, L., J. Gao, and Y. Wang, *Evaluation of cyto-toxicity and corrosion behavior of alkali-heat-treated magnesium in simulated body fluid.* Surface and Coatings Technology, 2004. **185**(1): p. 92-98.
4. Park, J.B. and J.D. Bronzino, eds. *Biomaterials Principles and Applications*. 2003, CRC Press: Boca Raton. 250.
5. Yuen, C.K. and W.Y. Ip, *Theoretical risk assessment of magnesium alloys as degradable biomedical implants.* Acta Biomaterialia, 2010. **6**(5): p. 1808-1812.
6. Williams, D.F., *On the mechanisms of biocompatibility.* Biomaterials, 2008. **29**(20): p. 2941-2953.
7. Song, G.L. and A. Atrens, *Corrosion Mechanisms of Magnesium Alloys.* Advanced Engineering Materials, 1999.

8. Hänzi, A.C., P. Gunde, M. Schinhammer, and P.J. Uggowitzer, *On the biodegradation performance of an Mg-Y-RE alloy with various surface conditions in simulated body fluid.* Acta Biomaterialia, 2009. **5**(1): p. 162-171.
9. Wang, Y., M. Wei, J. Gao, J. Hu, and Y. Zhang, *Corrosion process of pure magnesium in simulated body fluid.* Materials Letters, 2008. **62**(14): p. 2181-2184.
10. Song, G. and A. Atrens, *Understanding Magnesium Corrosion - A Framework for Improved Alloy Performance.* Advanced Engineering Materials, 2003. **5**(12): p. 837-858.
11. Xin, Y., K. Huo, H. Tao, G. Tang, and P.K. Chu, *Influence of aggressive ions on the degradation behavior of biomedical magnesium alloy in physiological environment.* Acta Biomaterialia, 2008. **4**(6): p. 2008-2015.
12. Ramaswamy, Y., C. Wu, and H. Zreiqat. *Orthopedic coating materials: considerations and applications*. 2009.
13. Gray, J.E. and B. Luan, *Protective coatings on magnesium and its alloys -- a critical review.* Journal of Alloys and Compounds, 2002. **336**(1-2): p. 88-113.
14. Kokubo, T. and H. Takadama, *How useful is SBF in predicting in vivo bone bioactivity?* Biomaterials, 2006. **27**(15): p. 2907-2915.
15. Nishiguchi, S., T. Nakamura, M. Kobayashi, H.-M. Kim, F. Miyaji, and T. Kokubo, *The effect of heat treatment on bone-bonding ability of alkali-treated titanium.* Biomaterials, 1999. **20**(5): p. 491-500.
16. Kim, H.M., F. Miyaji, T. Kokubo, and T. Nakamura, *Effect of heat treatment on apatite-forming ability of Ti metal induced by alkali treatment.* Journal of Materials Science: Materials in Medicine, 1997. **8**(6): p. 341-347.
17. Kim, H.M., F. Miyaji, T. Kokubo, S. Nishiguchi, and T. Nakamura, *Graded surface structure of bioactive titanium prepared by chemical treatment.* Journal of Biomedical Materials Research, 1999. **45**(2): p. 100-107.
18. Kim, H.-M., F. Miyaji, T. Kokubo, and T. Nakamura, *Preparation of bioactive Ti and its alloys via simple chemical surface treatment.* Journal of Biomedical Materials Research, 1996. **32**(3): p. 409-417.
19. Kirkland, N.T., J. Lespagnol, N. Birbilis, and M.P. Staiger, *A survey of bio-corrosion rates of magnesium alloys.* Corrosion Science, 2010. **52**(2): p. 287-291.
20. Gu, X., Y. Zheng, Y. Cheng, S. Zhong, and T. Xi, *In vitro corrosion and biocompatibility of binary magnesium alloys.* Biomaterials, 2009. **30**(4): p. 484-498.
21. Willliams, D., *New Interests in Magnesium.* Medical Device Technology, 2006. **17**(3): p. 9-10.
22. Purnama, A., H. Hermawan, J. Couet, and D. Mantovani, *Assessing the biocompatibility of degradable metallic materials: State of the art and focus on the genetic regulation potential.* Acta Biomaterialia, 2010. **6**(5): p. 1800-1807.
23. Friedrich, H.E., *Magnesium Technology : Metallurgy, Design Data, Applications*, ed. H.E. Friedrich and B.L. Mordike. 2006, Heidelberg: Springer.
24. Rettig, R. and S. Virtanen, *Composition of corrosion layers on a magnesium rare-earth alloy in simulated body fluids.* Journal of Biomedical Materials Research - Part A, 2009. **88**(2): p. 359-369.

25. Witte, F., J. Fischer, J. Nellesen, C. Vogt, J. Vogt, T. Donath, and F. Beckmann, *In vivo corrosion and corrosion protection of magnesium alloy LAE442.* Acta Biomaterialia, 2010. **6**(5): p. 1792-9.
26. Hänzi, A.C., M.M. Weder, B. Gerold, and P.J. Uggowitzer. *New Bio-absorbable Magnesium Alloys for Medical Applications*. in *Light Metals Technology Conference*. 2007. Canada.
27. Gruhl, S., F. Witte, J. Vogt, and C. Vogt, *Determination of concentration gradients in bone tissue generated by a biologically degradable magnesium implant.* Journal of Analytical Atomic Spectrometry, 2009. **24**(2): p. 181-188.
28. Salunke, P., V. Shanov, and F. Witte, *High purity biodegradable magnesium coating for implant application.* Materials Science and Engineering: B, 2011. **176**(20): p. 1711-1717.
29. Shi, Z., G. Song, and A. Atrens, *The corrosion performance of anodised magnesium alloys.* Corrosion Science, 2006. **48**(11): p. 3531-3546.
30. Durdu, S., A. Aytac, and M. Usta, *Characterization and corrosion behavior of ceramic coating on magnesium by micro-arc oxidation.* Journal of Alloys and Compounds, 2011. **509**(34): p. 8601-8606.
31. Carboneras, M., M.C. GarcÃ-a-Alonso, and M.L. Escudero, *Biodegradation kinetics of modified magnesium-based materials in cell culture medium.* Corrosion Science, 2011. **53**(4): p. 1433-1439.
32. Shi, P., W.F. Ng, M.H. Wong, and F.T. Cheng, *Improvement of corrosion resistance of pure magnesium in Hanks' solution by microarc oxidation with sol-gel TiO2 sealing.* Journal of Alloys and Compounds, 2009. **469**(1-2): p. 286-292.
33. Hiromoto, S., T. Shishido, A. Yamamoto, N. Maruyama, H. Somekawa, and T. Mukai, *Precipitation control of calcium phosphate on pure magnesium by anodization.* Corrosion Science, 2008. **50**(10): p. 2906-2913.
34. Waterman, J., A. Pietak, N. Birbilis, T. Woodfield, G. Dias, and M.P. Staiger, *Corrosion resistance of biomimetic calcium phosphate coatings on magnesium due to varying pretreatment time.* Materials Science and Engineering: B, 2011. **176**(20): p. 1756-1760.
35. Chiu, K.Y., M.H. Wong, F.T. Cheng, and H.C. Man, *Characterization and corrosion studies of fluoride conversion coating on degradable Mg implants.* Surface & Coatings Technology, 2007(202): p. 590-598.
36. Hiromoto, S. and M. Tomozawa, *Corrosion behavior of magnesium with hydroxyapatite coatings formed by hydrothermal treatment.* Materials Transactions, 2010. **51**(11): p. 2080-2087.
37. Tomozawa, M. and S. Hiromoto, *Microstructure of hydroxyapatite- and octacalcium phosphate-coatings formed on magnesium by a hydrothermal treatment at various pH values.* Acta Materialia, 2011. **59**(1): p. 355-363.
38. Liu, G.Y., J. Hu, Z.K. Ding, and C. Wang, *Bioactive calcium phosphate coating formed on micro-arc oxidized magnesium by chemical deposition.* Applied Surface Science, 2011. **257**(6): p. 2051-7.
39. Tomozawa, M., S. Hiromoto, and Y. Harada, *Microstructure of hydroxyapatite-coated magnesium prepared in aqueous solution.* Surface and Coatings Technology. **204**(20): p. 3243-3247.

40. Chen, X.B., N. Birbilis, and T.B. Abbott, *A simple route towards a hydroxyapatite-Mg(OH)2 conversion coating for magnesium.* Corrosion Science, 2011. **53**(6): p. 2263-2268.
41. Tomozawa, M. and S. Hiromoto, *Growth mechanism of hydroxyapatite-coatings formed on pure magnesium and corrosion behavior of the coated magnesium.* Applied Surface Science, 2011. **257**(19): p. 8253-8257.
42. Keim, S., J.G. Brunner, B. Fabry, and S. Virtanen, *Control of magnesium corrosion and biocompatibility with biomimetic coatings.* Journal of Biomedical Materials Research - Part B Applied Biomaterials, 2011. **96 B**(1): p. 84-90.
43. Zhao, L., C. Cui, Q. Wang, and S. Bu, *Growth characteristics and corrosion resistance of micro-arc oxidation coating on pure magnesium for biomedical applications.* Corrosion Science, 2010. **52**(7): p. 2228-2234.
44. Jo, J.-H., B.-G. Kang, K.-S. Shin, H.-E. Kim, B.-D. Hahn, D.-S. Park, and Y.-H. Koh, *Hydroxyapatite coating on magnesium with MgF2 interlayer for enhanced corrosion resistance and biocompatibility.* Journal of Materials Science: Materials in Medicine, 2011. **22**: p. 2437-2447.
45. Chen, Y., Y. Song, S. Zhang, J. Li, C. Zhao, and X. Zhang, *Interaction between a high purity magnesium surface and PCL and PLA coatings during dynamic degradation.* Biomedical Materials, 2011. **6**: p. 025005-025005.
46. Pereda, M.D., C. Alonso, M. Gamero, J.A. del Valle, and M. Fernandez Lorenzo de Mele, *Comparative study of fluoride conversion coatings formed on biodegradable powder metallurgy Mg: the effect of chlorides at physiological level.* Materials Science & Engineering: C (Materials for Biological Applications), 2011. **31**(5): p. 858-65.
47. Xue, D., Y. Yun, M.J. Schulz, and V. Shanov, *Corrosion protection of biodegradable magnesium implants using anodization.* Materials Science and Engineering: C, 2010. **31**(2): p. 215-223.
48. Hiromoto, S. and A. Yamamoto, *High corrosion resistance of magnesium coated with hydroxyapatite directly synthesized in an aqueous solution.* Electrochimica Acta, 2009. **54**(27): p. 7085-7093.
49. Bakkar, A. and V. Neubert, *Electrodeposition onto magnesium in air and water stable ionic liquids: From corrosion to successful plating.* Electrochemistry Communications, 2007. **9**(9): p. 2428-2435.
50. Polmear, I.J., *Magnesium and Magnesium Alloys*, in *ASM Specialty Handbook*, A. International, Editor. 1999, The Materials Information Society: USA. p. 3-84.
51. Inoue, H., K. Sugahara, A. Yamamoto, and H. Tsubakino, *Corrosion rate of magnesium and its alloys in buffered chloride solutions.* Corrosion Science, 2002. **44**(3): p. 603-610.
52. Han, X.G., X.P. Zhu, and M.K. Lei, *Electrochemical properties of microarc oxidation films on a magnesium alloy modified by high-intensity pulsed ion beam.* 2011.
53. Cui, X., Y. Yang, E. Liu, G. Jin, J. Zhong, and Q. Li, *Corrosion behaviors in physiological solution of cerium conversion coatings on AZ31 magnesium alloy.* Applied Surface Science, 2011. **257**(23): p. 9703-9709.

54. Zhang, C.Y., J.C. Gao, and C.L. Liu. *Effect of fluoride treatment on corrosion property of AZ31 magnesium alloy in Hank's solution*. 2011. Changsha, China: Trans Tech Publications.
55. Zhu, Y., G. Wu, Y.-H. Zhang, and Q. Zhao, *Growth and characterization of Mg(OH)2 film on magnesium alloy AZ31.* Applied Surface Science, 2011.
56. da Conceicao, T.F., N. Scharnagl, C. Blawert, W. Dietzel, and K.U. Kainer, *Surface modification of magnesium alloy AZ31 by hydrofluoric acid treatment and its effect on the corrosion behaviour.* Thin Solid Films, 2010. **518**(18): p. 5209-5218.
57. Chun-Yan, Z., Z. Rong-Chang, L. Cheng-Long, and G. Jia-Cheng, *Comparison of calcium phosphate coatings on Mg-Al and Mg-Ca alloys and their corrosion behavior in Hank's solution.* Surface and Coatings Technology, 2008. **204**(21-22): p. 3636-3640.
58. Hahn, B.-D., D.-S. Park, J.-J. Choi, J. Ryu, W.-H. Yoon, J.-H. Choi, H.-E. Kim, and S.-G. Kim, *Aerosol deposition of hydroxyapatiteâ€“chitosan composite coatings on biodegradable magnesium alloy.* Surface and Coatings Technology, 2011. **205**(8-9): p. 3112-3118.
59. Yang, J.X., Y.P. Jiao, F.Z. Cui, I.-S. Lee, Q.S. Yin, and Y. Zhang, *Modification of degradation behavior of magnesium alloy by IBAD coating of calcium phosphate.* Surface and Coatings Technology, 2008. **202**(22-23): p. 5733-5736.
60. Hu, J., C. Zhang, B. Cui, K. Bai, S. Guan, L. Wang, and S. Zhu, *In vitro degradation of AZ31 magnesium alloy coated with nano TiO 2 film by sol-gel method.* Applied Surface Science, 2011. **257**(21): p. 8772-8777.
61. Hiromoto, S. and M. Tomozawa, *Hydroxyapatite coating of AZ31 magnesium alloy by a solution treatment and its corrosion behavior in NaCl solution.* Surface and Coatings Technology, 2011. **205**(19): p. 4711-4719.
62. Li-li, T., W. Qiang, G. Fang, X. Xiao-song, Q. Jian-hong, and Y. Ke, *Preparation and characterization of Ca-P coating on AZ31 magnesium alloy.* TRANSACTIONS OF NONFERROUS METALS SOCIETY OF CHINA, 2010. **20**(Suppl. 2): p. S648-S654-S648-S654.
63. Gray-Munro, J.E. and M. Strong, *The mechanism of deposition of calcium phosphate coatings from solution onto magnesium alloy AZ31.* Journal of Biomedical Materials Research Part A, 2009. **90A**(2): p. 339-350.
64. Wang, Q., L. Tan, W. Xu, B. Zhang, and K. Yang, *Dynamic behaviors of a CaP coated AZ31B magnesium alloy during in vitro and in vivo degradations.* Materials Science and Engineering: B, 2011. **176**(20): p. 1718-1726.
65. Peixoto Barbosa, D. and G. Knörnschild, *Anodization of Mg-alloy AZ91 in NaOH solutions.* Surface and Coatings Technology, 2009. **203**(12): p. 1629-1636.
66. Kannan, M.B. and L. Orr, *In Vitro mechanical integrity of hydroxyapatite coated magnesium alloy.* Biomedical Materials, 2011. **6**(4): p. 045003 (11 pp.)-045003 (11 pp.).
67. Yao, Z.P., L.L. Li, X.R. Liu, and Z.H. Jiang, *Preparation of ceramic conversion layers containing Ca and P on AZ91D Mg alloys by plasma electrolytic oxidation.* Surface Engineering, 2010. **26**(5): p. 317-320.
68. Hu, J., C. Wang, W.C. Ren, S. Zhang, and F. Liu, *Microstructure evolution and corrosion mechanism of dicalcium phosphate dihydrate coating on magnesium*

alloy in simulated body fluid. Materials Chemistry and Physics, 2010. **119**(1-2): p. 294-298.
69. Jianrui, L., G. Yina, and H. Weidong, *Study on the corrosion resistance of phytic acid conversion coating for magnesium alloys.* Surface and Coatings Technology, 2006. **201**(3-4): p. 1536-1541.
70. Li, J.-z., J.-g. Huang, Y.-w. Tian, and C.-s. Liu, *Corrosion action and passivation mechanism of magnesium alloy in fluoride solution.* TRANSACTIONS OF NONFERROUS METALS SOCIETY OF CHINA, 2009. **19**(1): p. 50-54.
71. Wu, C., Z. Wen, C. Dai, Y. Lu, and F. Yang, *Fabrication of calcium phosphate/chitosan coatings on AZ91D magnesium alloy with a novel method.* Surface and Coatings Technology, 2010. **204**(20): p. 3336-3347.
72. Shi, Y., M. Qi, Y. Chen, and P. Shi, *MAO-DCPD composite coating on Mg alloy for degradable implant applications.* 2011. **65**(14): p. 2201-2204.
73. Ping, L., L. Yin, G. Meiqing, F. Haidong, and X. Xinhua, *Corrosion and drug release properties of EN-plating/PLGA composite coating on MAO film.* Materials Science & Engineering: C (Materials for Biological Applications), 2011. **31**(7): p. 1285-9.
74. Shengxue, Y., L. Qiaoyan, H. Jing, Z. Zhanwei, and Z. Qianyun, *Preparation and Performance of Rare Earths Chemical Conversion Film on Magnesium Alloy.* Journal of Rare Earths, 2006. **24**(1, Supplement 1): p. 397-400.
75. Ferreira, P.C., K.d.A. Piai, A.M.M. Takayanagui, and S.I. Segura-Muñoz, *Aluminum as a risk factor for Alzheimer's disease.* Revista Latino-Americana De Enfermagem, 2008. **16**(1): p. 151-157.
76. Flaten, T.P., *Aluminium as a risk factor in Alzheimer's disease, with emphasis on drinking water.* Brain Research Bulletin, 2001. **55**(2): p. 187-196.
77. Jose L, D., *Reproductive and developmental toxicity of aluminum: A review.* Neurotoxicology and Teratology, 1995. **17**(4): p. 515-521.
78. Lei, T., C. Ouyang, W. Tang, L.-F. Li, and L.-S. Zhou, *Preparation of MgO coatings on magnesium alloys for corrosion protection.* Surface and Coatings Technology, 2010. **204**(23): p. 3798-3803.
79. Zhang, C.-y., R.-c. Zeng, R.-s. Chen, C.-l. Liu, and J.-c. Gao, *Preparation of calcium phosphate coatings on Mg-1.0Ca alloy.* TRANSACTIONS OF NONFERROUS METALS SOCIETY OF CHINA, 2010. **20, Supplement 2**(0): p. s655-s659-s655-s659.
80. Meiheng, L., C. Qian, Z. Wenjin, H. Wangyu, and S. Yong, *Corrosion behavior in SBF for titania coatings on Mg-Ca alloy.* Journal of Materials Science, 2011. **46**(7): p. 2365-9.
81. Li, Z., X. Gu, S. Lou, and Y. Zheng, *The development of binary Mg-Ca alloys for use as biodegradable materials within bone.* Biomaterials, 2008. **29**(10): p. 1329-1344.
82. Kim, W.-C., J.-G. Kim, J.-Y. Lee, and H.-K. Seok, *Influence of Ca on the corrosion properties of magnesium for biomaterials.* Materials Letters, 2008. **62**(25): p. 4146-4148.
83. Chen, S., S. Guan, B. Chen, W. Li, J. Wang, L. Wang, S. Zhu, and J. Hu, *Corrosion behavior of TiO2 films on Mg–Zn alloy in simulated body fluid.* Applied Surface Science, 2011. **257**(9): p. 4464-4467.

84. Song, Y., S. Zhang, J. Li, C. Zhao, and X. Zhang, *Electrodeposition of Ca-P coatings on biodegradable Mg alloy: In vitro biomineralization behavior.* Acta Biomaterialia, 2010. **6**(5): p. 1736-1742.
85. Lei, T., C. Ouyang, W. Tang, L.-F. Li, and L.-S. Zhou, *Enhanced corrosion protection of MgO coatings on magnesium alloy deposited by an anodic electrodeposition process.* Corrosion Science. **52**(10): p. 3504-3508.
86. Meng, E.C., S.K. Guan, H.X. Wang, L.G. Wang, S.J. Zhu, J.H. Hu, C.X. Ren, J.H. Gao, and Y.S. Feng, *Effect of electrodeposition modes on surface characteristics and corrosion properties of fluorine-doped hydroxyapatite coatings on Mg-Zn-Ca alloy.* Applied Surface Science, 2011. **257**(11): p. 4811-4816.
87. Wei, Z., H. Du, and E. Zhang, *The formation mechanism and biocorrosion property of CaSiO3/CaHPO4 · 2H2O composite conversion coating on the extruded Mg-Zn-Ca alloy for bone implant application·.* Surface and Interface Analysis, 2011. **43**: p. 791-794.
88. Xu, L., F. Pan, G. Yu, L. Yang, E. Zhang, and K. Yang, *In vitro and in vivo evaluation of the surface bioactivity of a calcium phosphate coated magnesium alloy.* Biomaterials, 2009. **30**(8): p. 1512-1523.
89. Lu, P., L. Cao, Y. Liu, X. Xu, and X. Wu, *Evaluation of magnesium ions release, biocorrosion, and hemocompatibility of MAO/PLLA-modified magnesium alloy WE42.* Journal of Biomedical Materials Research - Part B Applied Biomaterials, 2011. **96 B**(1): p. 101-109.
90. Greer, A.L., *Metallic glasses...on the threshold.* Materials Today, 2009. **12**(1-2): p. 14-22.
91. Gu, X., Y. Zheng, S. Zhong, T. Xi, J. Wang, and W. Wang, *Corrosion of, and cellular responses to Mg-Zn-Ca bulk metallic glasses.* Biomaterials, 2010. **31**(6): p. 1093 - 1103.
92. Li, Q.-F., H.-R. Weng, Z.-Y. Suo, Y.-L. Ren, X.-G. Yuan, and K.-Q. Qiu, *Microstructure and mechanical properties of bulk Mg-Zn-Ca amorphous alloys and amorphous matrix composites.* Materials Science and Engineering: A, 2008. **487**(1-2): p. 301-308.
93. Senkov, O.N. and J.M. Scott, *Formation and thermal stability of Ca-Mg-Zn and Ca-Mg-Zn-Cu bulk metallic glasses.* Materials Letters, 2004. **58**(7-8): p. 1375-1378.
94. Senkov, O.N. and J.M. Scott, *Glass forming ability and thermal stability of ternary Ca-Mg-Zn bulk metallic glasses.* Journal of Non-Crystalline Solids, 2005. **351**(37-39): p. 3087-3094.
95. Zberg, B., P.J. Uggowitzer, and J.F. Loffler, *MgZnCa glasses without clinically observable hydrogen evolution for biodegradable implants.* Nat Mater, 2009. **8**(11): p. 887-891.
96. Chatterjee, P. and A.K. Batabyal, *Metallic glass formation by CH4+ ion implantation into Al, Fe and Ni thin films.* Journal of Non-Crystalline Solids, 1990. **124**(2-3): p. 131-138.
97. Liu, B.X., W.S. Lai, and Q. Zhang, *Irradiation induced amorphization in metallic multilayers and calculation of glass-forming ability from atomistic potential in the*

binary metal systems. Materials Science and Engineering: R: Reports, 2000. **29**(1-2): p. 1-48.
98. Liu, C., Y. Xin, X. Tian, and P.K. Chu, *Corrosion behavior of AZ91 magnesium alloy treated by plasma immersion ion implantation and deposition in artificial physiological fluids.* Thin Solid Films, 2007. **516**(2-4): p. 422-427.
99. Nordberg, G., *Handbook on the Toxicology of Metals*. 2007: Academic Press.
100. Wan, Y.Z., G.Y. Xiong, H.L. Luo, F. He, Y. Huang, and Y.L. Wang, *Influence of zinc ion implantation on surface nanomechanical performance and corrosion resistance of biomedical magnesium-calcium alloys.* Applied Surface Science, 2008. **254**(17): p. 5514-5516.
101. Wan, G.J., M.F. Maitz, H. Sun, P.P. Li, and N. Huang, *Corrosion properties of oxygen plasma immersion ion implantation treated magnesium.* Surface and Coatings Technology, 2007. **201**(19-20): p. 8267-8272.
102. Nakatsugawa, I., R. Martin, and E.J. Knystautas, *Improving Corrosion Resistance of AZ91D Magnesium Alloy by Nitrogen Ion Implantation.* Corrosion, 1996. **52**(12): p. 921-926.
103. Tian, X.B., C.B. Wei, S.Q. Yang, R.K.Y. Fu, and P.K. Chu, *Corrosion resistance improvement of magnesium alloy using nitrogen plasma ion implantation.* Surface and Coatings Technology, 2005. **198**(1-3): p. 454-458.
104. Chen, X.B., N. Birbilis, and T.B. Abbot, *Review of Corrosion-Resistant Conversion Coatings for Magnesium and Its Alloys.* Corrosion (Houston), 2011. **67**(3): p. D1-D16-D1-D16.
105. Yong, Z., J. Zhu, C. Qiu, and Y. Liu, *Molybdate/phosphate composite conversion coating on magnesium alloy surface for corrosion protection.* Applied Surface Science, 2008. **255**(5, Part 1): p. 1672-1680.
106. Liu, X., T. Zhang, Y. Shao, G. Meng, and F. Wang, *Effect of alternating voltage treatment on the corrosion resistance of pure magnesium.* Corrosion Science, 2009. **51**(8): p. 1772-1779.
107. Vermilyea, D.A., *On the mechanism of the oxidation of metals.* Acta Metallurgica, 1957. **5**(9): p. 492-495.
108. Friedrich, H.E. and B.L. Mordike, *Magnesium technology : metallurgy, design data, applications*. 2006, Berlin ; New York: Springer. xxii, 677 p.
109. Verdier, S., N. van der Laak, S. Delalande, J. Metson, and F. Dalard, *The surface reactivity of a magnesium–aluminium alloy in acidic fluoride solutions studied by electrochemical techniques and XPS.* Applied Surface Science, 2004. **235**(4): p. 513-524.
110. Thomann, M., C. Krause, N. Angrisani, D. Bormann, T. Hassel, H. Windhagen, and A. Meyer-Lindenberg, *Influence of a magnesium-fluoride coating of magnesium-based implants (MgCa0.8) on degradation in a rabbit model.* Journal of Biomedical Materials Research Part A, 2010. **93A**(4): p. 1609-1619.
111. Grillo, C.A., F. Alvarez, and M.A. Fernández Lorenzo de Mele, *Biological effects of magnesium particles degradation on UMR-106 cell line: Influence of fluoride treatments.* Colloids and Surfaces. B, Biointerfaces, 2011. **88**(1): p. 471-476.
112. Nakamura, Y., Y. Tsumura, Y. Tonogai, T. Shibata, and Y. Ito, *Differences in Behavior among the Chlorides of Seven Rare Earth Elements Administered*

Intravenously to Rats. Fundamental and Applied Toxicology, 1997. **37**(2): p. 106-116.
113. Rudd, A.L., C.B. Breslin, and F. Mansfeld, *The corrosion protection afforded by rare earth conversion coatings applied to magnesium.* Corrosion Science, 2000. **42**(2): p. 275-288.
114. Barrere, F., *Biomimetic Calcium Phosphate Coatings: Physicochemistry and Biological Activity*. 2002, University of Twente: Enschede.
115. León, B. and J.A. Jansen, *Thin Calcium Phosphate Coatings for Medical Implants*. 2008: Springer.
116. Barrere, F. and C.M.v.d. Valk, *Osteogenecity of octacalcium phosphate coatings applied on porous metal implants.* Journal of Biomedical Materials Research Part A, 2003. **66A**(4): p. 779-788.
117. Barrere, F., C.M. van der Valk, G. Meiger, R.A.J. Dalmeijer, K. De Groot, and P. Layrolle, *Osteointegration of biomimetic apatite coating applied onto dense and porous metal implants in femurs of goats.* Journal of Biomedical Materials Research Part B: Applied Biomaterials, 2003. **67B**(1): p. 655-665.
118. Zhu, L., X. Ye, G. Tang, N. Zhao, Y. Gong, Y. Zhao, J. Zhao, and X. Zhang, *Biomimetic coating of compound titania and hydroxyapatite on titanium.* Journal of Biomedical Materials Research Part A, 2007. **83A**(4): p. 1165-1175.
119. Kou, M., T. Toda, and O. Fukumasa, *Production of fine hydroxyapatite films using the well-controlled thermal plasma.* Surface and Coatings Technology, 2008. **202**(22-23): p. 5753-5756.
120. Chen, D., E.H. Jordan, M. Gell, and M. Wei, *Apatite formation on alkaline-treated dense TiO2 coatings deposited using the solution precursor plasma spray process.* Acta Biomaterialia, 2008. **4**(3): p. 553-559.
121. Gross, K.A. and C.C. Berndt, *Thermal processing of hydroxyapatite for coating production.* Journal of Biomedical Materials Research, 1998. **39**(4): p. 580-587.
122. Koch, C.F., S. Johnson, D. Kumar, M. Jelinek, D.B. Chrisey, A. Doraiswamy, C. Jin, R.J. Narayan, and I.N. Mihailescu, *Pulsed laser deposition of hydroxyapatite thin films.* Materials Science and Engineering: C, 2007. **27**(3): p. 484-494.
123. Bigi, A., G. Falini, E. Foresti, A. Ripamonti, M. Gazzano, and N. Roveri, *Magnesium influence on hydroxyapatite crystallization.* Journal of Inorganic Biochemistry, 1993. **49**(1): p. 69-78.
124. Lin, S., R.Z. LeGeros, and J.P. LeGeros, *Adherent octacalciumphosphate coating on titanium alloy using modulated electrochemical deposition method.* Journal of Biomedical Materials Research, 2003. **66A**(4): p. 819-828.
125. Barrère, F., *Biomimetic Calcium Phosphate Coatings: Physicochemistry and Biological Activity*. 2002, University of Twente.
126. Baker, K.C., M.A. Anderson, S.A. Oehlke, A.I. Astashkina, D.C. Haikio, J. Drelich, and S.W. Donahue, *Growth, characterization and biocompatibility of bone-like calcium phosphate layers biomimetically deposited on metallic substrata.* Materials Science and Engineering: C, 2006. **26**(8): p. 1351-1360.
127. Barrère, F., *Osteogenecity of octacalcium phosphate coatings applied on porous metal implants.* Journal of Biomedical Materials Research Part A, 2003. **66A**(4): p. 779-788.

128. Landi, E., A. Tampieri, M. Mattioli-Belmonte, G. Celotti, M. Sandri, A. Gigante, P. Fava, and G. Biagini, *Biomimetic Mg- and Mg,CO3-substituted hydroxyapatites: synthesis characterization and in vitro behaviour.* Journal of the European Ceramic Society, 2006. **26**(13): p. 2593-2601.
129. Habibovic, P., F. Barrere, C.A. van Blitterswijk, K. de Groot, and P. Layrolle, *Biomimetic hydroxyapatite coating on metal implants.* Journal of the American Ceramic Society, 2002. **85**(3): p. 517-22.
130. Kokubo, T., *Formation of biologically active bone-like apatite on metals and polymers by a biomimetic process.* Thermochimica Acta, 1996. **280-281**: p. 479-490.
131. Lin, C.-M. and S.-K. Yen, *Biomimetic growth of apatite on electrolytic TiO2 coatings in simulated body fluid.* Materials Science and Engineering: C, 2006. **26**(1): p. 54-64.
132. Barrère, C.M.v.d.V.F., *Osteointegration of biomimetic apatite coating applied onto dense and porous metal implants in femurs of goats.* Journal of Biomedical Materials Research Part B: Applied Biomaterials, 2003. **67B**(1): p. 655-665.
133. Wen, H.B., J.G.C. Wolke, J.R. de Wijn, Q. Liu, F.Z. Cui, and K. de Groot, *Fast precipitation of calcium phosphate layers on titanium induced by simple chemical treatments.* Biomaterials, 1997. **18**(22): p. 1471-1478.
134. Leon, B. and J.A. Jansen, eds. *ERROR Thin Calcium Phosphate Coatings for Medical Implants*. ed. B. Leon. 2009, Springer: New York.
135. Barrere, F., C.A. van Blitterswijk, K. de Groot, and P. Layrolle, *Nucleation of biomimetic Ca-P coatings on Ti6Al4V from a SBF×5 solution: influence of magnesium.* Biomaterials, 2002. **23**(10): p. 2211-2220.
136. Lorenz, C., J.G. Brunner, P. Kollmannsberger, L. Jaafar, B. Fabry, and S. Virtanen, *Effect of surface pre-treatments on biocompatibility of magnesium.* Acta Biomaterialia, 2009. **5**(7): p. 2783-2789.
137. Song, Y.W., D.Y. Shan, and E.H. Han, *Electrodeposition of hydroxyapatite coating on AZ91D magnesium alloy for biomaterial application.* Materials Letters, 2008. **62**(17-18): p. 3276-3279.
138. Wen, C., S. Guan, L. Peng, C. Ren, X. Wang, and Z. Hu, *Characterization and degradation behavior of AZ31 alloy surface modified by bone-like hydroxyapatite for implant applications.* Applied Surface Science, 2009. **255**(13-14): p. 6433-6438.
139. Wang, H.X., S.K. Guan, X. Wang, C.X. Ren, and L.G. Wang, *In vitro degradation and mechanical integrity of Mg-Zn-Ca alloy coated with Ca-deficient hydroxyapatite by the pulse electrodeposition process.* Acta Biomaterialia, 2010. **6**(5): p. 1743-1748.
140. Kumar, M., H. Dasarathy, and C. Riley, *Electrodeposition of brushite coatings and their transformation to hydroxyapatite in aqueous solutions.* Journal of Biomedical Materials Research, 1999. **45**(4): p. 302-310.
141. Livage, J., *Sol-gel processes.* Current Opinion in Solid State and Materials Science, 1997. **2**(2): p. 132-138.
142. Hench, L.L., *Sol-gel materials for bioceramic applications.* Current Opinion in Solid State and Materials Science, 1997. **2**(5): p. 604-610.

143. Stoica, T.F., C. Morosanu, A. Slav, T. Stoica, P. Osiceanu, C. Anastasescu, M. Gartner, and M. Zaharescu, *Hydroxyapatite films obtained by sol-gel and sputtering.* Thin Solid Films, 2008. **516**(22): p. 8112-8116.
144. Nguyen, H.Q., D.A. Deporter, R.M. Pilliar, N. Valiquette, and R. Yakubovich, *The effect of sol–gel-formed calcium phosphate coatings on bone ingrowth and osteoconductivity of porous-surfaced Ti alloy implants.* Biomaterials, 2004. **25**(5): p. 865-876.
145. Giavaresi, G., R. Giardino, L. Ambrosio, G. Battiston, R. Gerbasi, M. Fini, L. Rimondini, and P. Torricelli, *In vitro biocompatibility of titanium oxide for prosthetic devices nanostructured by low pressure metal-organic chemical vapor deposition.* The International journal of artificial organs, 2003. **26**(8): p. 774-780.
146. Lopez, A.J., E. Otero, and J. Rams, *Sol-gel silica coatings on ZE41 magnesium alloy for corrosion protection.* Surface & Coatings Technology, 2010. **205**(7): p. 2375-85.
147. Choy, K.L., *Chemical vapour deposition of coatings.* Progress in Materials Science, 2003. **48**(2): p. 57-170.
148. Trommer, R.M., L.A. Santos, and C.P. Bergmann, *Alternative technique for hydroxyapatite coatings.* Surface and Coatings Technology, 2007. **201**(24): p. 9587-9593.
149. Yamamoto, A., A. Watanabe, K. Sugahara, H. Tsubakino, and S. Fukumoto, *Improvement of corrosion resistance of magnesium alloys by vapor deposition.* Scripta Materialia, 2001. **44**(7): p. 1039-1042.
150. Wu, G., X. Zeng, and G. Yuan, *Growth and corrosion of aluminum PVD-coating on AZ31 magnesium alloy.* Materials Letters, 2008. **62**(28): p. 4325-4327.
151. Xin, Y., C. Liu, K. Huo, G. Tang, X. Tian, and P.K. Chu, *Corrosion behavior of ZrN/Zr coated biomedical AZ91 magnesium alloy.* Surface and Coatings Technology, 2009. **203**(17-18): p. 2554-2557.
152. Mróz, W., M. Jedynski, A. Prokopiuk, A. Ślósarczyk, and Z. Paszkiewicz, *Characterization of calcium phosphate coatings doped with Mg, deposited by pulsed laser deposition technique using ArF excimer laser.* Micron, 2009. **40**(1): p. 140-142.
153. Sygnatowicz, M. and A. Tiwari, *Controlled synthesis of hydroxyapatite-based coatings for biomedical application.* Materials Science and Engineering: C, 2008. **29**(3): p. 1071-1076.
154. Zeng, H. and W.R. Lacefield, *The study of surface transformation of pulsed laser deposited hydroxyapatite coatings.* Journal of Biomedical Materials Research, 2000. **50**(2): p. 239-247.
155. Kokubo, T., F. Miyaji, H.M. Kim, and T. Nakamura, *Spontaneous Formation of Bonelike Apatite Layer on Chemically Treated Titanium Metals.* Journal of the American Ceramic Society, 1996. **79**(4): p. 1127-1129.
156. Yamamoto, A. and S. Hiromoto, *Effect of inorganic salts, amino acids and proteins on the degradation of pure magnesium in vitro.* Materials Science and Engineering: C, 2009. **29**(5): p. 1559-1568.
157. Liu, C., Y. Xin, X. Tian, and P.K. Chu, *Degradation Susceptibility of Surgical Magnesium Alloy in Artificial Biological Fluid Containing Albumin.* Journal of Materials Research, 2007. **22**(7): p. 1806-1814.

158. Liu, C.L., Y.J. Wang, R.C. Zeng, X.M. Zhang, W.J. Huang, and P.K. Chu, *In vitro corrosion degradation behaviour of Mg–Ca alloy in the presence of albumin.* Corrosion Science, 2010. **52**(10): p. 3341-3347.
159. Yang, L., N. Hort, R. Willumeit, and F. Feyerabend, *Effects of corrosion environment and proteins on magnesium corrosion.* Corrosion Engineering, Science and Technology, 2012.
160. Clark, G.C.F. and D.F. Williams, *The effects of proteins on metallic corrosion.* Journal of Biomedical Materials Research, 1982. **16**(2): p. 125-134.
161. Mueller, W.-D., M. Lucia Nascimento, and M.F. Lorenzo de Mele, *Critical discussion of the results from different corrosion studies of Mg and Mg alloys for biomaterial applications.* Acta Biomaterialia, 2010. **6**(5): p. 1749-1755.
162. Willumeit, R., J. Fischer, F. Feyerabend, N. Hort, U. Bismayer, S. Heidrich, and B. Mihailova, *Chemical surface alteration of biodegradable magnesium exposed to corrosion media.* Acta Biomaterialia, 2011. **7**(6): p. 2704-2715.
163. Rettig, R. and S. Virtanen, *Time-dependent electrochemical characterization of the corrosion of a magnesium rare-earth alloy in simulated body fluids.* Journal of Biomedical Materials Research Part A, 2008. **85A**(1): p. 167-175.
164. Malda, J., T.B.F. Woodfield, M. Radisic, S. Levenberg, C. Oomens, F.P. Baaijens, P. Svalander, and G. Vunjak-Novakovic, *Cell Nutrition : In Vitro and In Vivo.* Tissue Engineering : A Textbook, 2008(1): p. 327-362.
165. Gu, X.N., Y.F. Zheng, and L.J. Chen, *Influence of artificial biological fluid composition on the biocorrosion of potential orthopedic Mg-Ca, AZ31, AZ91 alloys.* Biomedical Materials, 2009. **4**(6): p. 8.
166. Latour, R., *Biomaterials: Protein-Surface Interactions*.
167. Ralston, K.D., G. Williams, and N. Birbilis, *Effect of pH on the Grain Size Dependence of Magnesium Corrosion.* Corrosion, 2012. **68**(6): p. 507-517.
168. Ng, W.F., K.Y. Chiu, and F.T. Cheng, *Effect of pH on the in vitro corrosion rate of magnesium degradable implant material.* Materials Science and Engineering: C, 2010. **30**(6): p. 898-903.
169. Kirkland, N., J. Waterman, N. Birbilis, G. Dias, T. Woodfield, R. Hartshorn, and M. Staiger, *Buffer-regulated biocorrosion of pure magnesium.* Journal of Materials Science: Materials in Medicine, 2012. **23**(2): p. 283-291.
170. Boron, W.F. and E.L. Boulpaep, eds. *Medical Physiology*. 2nd ed. 2008, Saunders: New York.
171. Hiromoto, S., A. Yamamoto, N. Maruyama, H. Somekawa, and T. Mukai, *Influence of pH and flow on the polarisation behaviour of pure magnesium in borate buffer solutions.* Corrosion Science, 2008. **50**(12): p. 3561-3568.
172. Good, N.E., G.D. Winget, W. Winter, T.N. Connolly, S. Izawa, and M.M. Singh, *Hydrogen Ion Buffers for Biological Research.* Biochemistry, 1966. **5**(2): p. 467-477.
173. Jones, D.A., *Principles and Prevention of Corrosion*. 1992, Englewood Cliffs, NJ: Prentice-Hall.
174. Song, G., A. Atrens, and D.H. St. John, *An hydrogen evolution method for the estimation of the corrosion rate of magnesium alloys*, in *Magnesium Technology 2001 Symposium*, J.N. Hyrn, Editor. 2001, Minerals, Metals & Materials Society: New Orleans. p. 255–262.

175. Tait, W.S., *An Introduction to Electrochemical Corrosion Testing for Practicing Engineers and Scientists*. 1994: PairODocs Publications.
176. Witte, F., J. Nellesen, H.-A. Crostack, V. Kaese, A. Pisch, F. Beckmann, and H. Windhagen, *In vitro and in vivo corrosion measurements of magnesium alloys.* Biomaterials, 2006. **27**(7): p. 1013-1018.

CHAPTER 3: Buffering *in vitro* Solutions for Corrosion Testing

3.1. *In vitro* Corrosion Measurement of Mg

Magnesium and its alloys in general have low corrosion resistance, which is important for metal implants given the very aggressive environment in the physiological system [1]. Because it is difficult to measure corrosion rates precisely *in vivo*, *in vitro* methods for researching corrosion rates and corrosion protection methods will be required. The challenge with creating an *in vitro* test will be to accurately simulate the relevant corrosion environment found *in vivo*. A good *in vitro* approximation will be one that correctly models the mechanism of corrosion that will be expected *in vivo* as well as the rate. The mechanism and the corrosion layers that form need to be able to be assessed accurately and consistently. Ultimately, the aim of developing an *in vitro* model is also to reduce the cost of screening new alloy and coating systems, so ideally this should be accomplished simply and easily.

The pH is a critical factor in the corrosion and passivation mechanisms of Mg [2]. Therefore pH control is essential for the design of an *in vitro* corrosion model. As discussed in Chapter 2, many studies that evaluate coatings in the literature for corrosion resistance fail to control the pH. The resulting corrosion data is therefore only valid for an unknown pH, which is not necessarily biologically relevant. In order to accurately test some of the corrosion properties and resistances *in vitro*, the *in vitro* pH must be controlled. A buffer will provide a pH moderator to keep these tests in the appropriate range. While various buffer systems are reported for *in vitro* biocorrosion tests [3], it is not clear which buffers are the most appropriate, and what the effect of the buffer is on the corrosion rate of Mg in SBF. Thus, a detailed investigation into some of the most relevant buffer systems for *in vitro* tests was conducted with the intent of elucidating the effect of the buffer properties on the corrosion reactions of Mg.

3.1.1. The Corrosion of Mg

The corrosion rate of any metal is dependent on the environment to which it is in contact. While the corrosion reaction of metallic Mg is thermodynamically favourable in body fluids, the corrosion rate is dependent on a number of factors. One important aspect is the pH [2, 4, 5]. The corrosion reactions of Mg in aqueous solutions are very dependent on pH, and are given in Equation 3-1 to Equation 3-3.

$$Mg_{(s)} \rightarrow Mg^{2+}_{(aq)} + 2\ e^- \qquad \text{Equation 3-1}$$

$$2\ H_2O_{(l)} + 2\ e^- \rightarrow H_{2(g)} + 2\ OH^-_{(aq)} \qquad \text{Equation 3-2}$$

$$Mg^{2+}_{(aq)} + 2\ OH^-_{(aq)} \rightarrow Mg(OH)_{2(s)} \qquad \text{Equation 3-3}$$

The dissolution of Mg must be accompanied by the reduction of either H^+ (which actually exists as H_3O^+ in solution) or H_2O to produce H_2 gas. Reducing H^+ takes less energy than reducing H_2O so the pH, or total concentration of H^+ with respect to H_2O directly impacts the kinetics of the net corrosion reaction. The oxidized Mg can form the relatively insoluble (in water) precipitate $Mg(OH)_2$. The layer that forms protects the substrate from further oxidation and reduces the corrosion rate. However, this layer is attacked by Cl^- ions, thus preventing Mg from fully passivating in Cl^- solutions [6]. With the high Cl^- content of physiological fluids, the $Mg(OH)_2$ layer does not fully protect Mg *in vivo*, and corrosion takes place. The formation and solubility of $Mg(OH)_2$ depends on the concentration of OH^- in solution. Therefore, when measuring the corrosion rate for estimating corrosion performance, the pH must be known. If the corrosion mechanism is to be studied, the pH must be kept at the conditions to be investigated, otherwise the mechanism can change due to the relative passivation [7] or deposition of insoluble coating products [8]. If absolute corrosion rates are to be compared, in the instance of alloys or coatings designed to slow the corrosion rate, the pH must be uniform across the tests. The measurement and control of pH will therefore be critical to measuring corrosion rates of Mg in *in vitro* solutions with accuracy and reproducibility.

The pH in physiological systems is dynamically regulated, with pH in most body fluids kept in the range of 7.4-7.6. Due to the chemical interactions required *in vivo*, it critical that the pH does not stray too far from these ranges. As such, the regulatory mechanisms of the body

actively compensate for this [9]. This is done with the carbonic acid/bicarbonate buffer. The generation of bicarbonate ions from metabolism is regulated and compensated by releasing this as CO_2 gas in the lungs [10]. The net reaction is given in Equation 3-4:

$$CO_2 + H_2O \rightleftharpoons H_2CO_3 \rightleftharpoons HCO_3^- + H^+ \qquad \text{Equation 3-4}$$

By Le Chatelier's principle, the removal of CO_2 gas increases the pH as the equilibrium is restored through the removal of carbonic acid. When CO_2 is retained by the body, the equilibrium is shifted the other way, producing more H^+ and lowering the pH. This mechanism reacts to keep the pH fairly constant. Thus, *in vivo* it is expected that the pH of the surrounding fluids will be within this range, and the corrosion will reflect this. The pH directly at the surface of the substrate will depend on the diffusion rates of solution in the body. But overall, the environment for biodegradable implants is expected to be pH regulated.

Biodegradable Mg devices are intended to be used *in vivo*. One may assume therefore, that corrosion tests should simply be carried out *in vivo*. But there are a number of problems with this specific to Mg corrosion and coatings that arise.

- Expense: It is very expensive to perform surgeries necessary to implant devices. Maintaining the housing and care needed for animal studies is a large cost.
- Variability: Every animal will have unique properties, and slightly different chemistry, depending on genetic and environmental factors. While these can be minimized by using genetically similar animals and doing trials over a large number of statistical samples, this increases the costs.
- Environment: Even when the proper care is taken to prevent variation from affecting the results, the environmental variables cannot usually be separated from one another. It is not possible *in vivo* to study the effect of individual components, rather the system as a whole must be used.
- Absolute measurements: Corrosion rate can be compared after device removal by mass loss. But this gives only a bulk measurement of corrosion. In general, monitoring the rate over time becomes problematic. Electrochemical tests are difficult to perform *in vivo*.

- Ethics: If a new coating fails to perform, the resulting corrosion can cause discomfort to the animal. Therefore, a method of screening these before hand is required.

Consequently, corrosion and mechanistic studies are performed *in vitro* [3]. This allows the simplification of the environment such that effects of individual components may be measured. Unfortunately, this removes the active buffer control system that is present *in vivo*. As Mg corrodes in a finite volume of solution, this results in the generation of H_2 gas and the production of OH^-. Therefore, the pH will increase [7]. The electrochemical behaviour of Mg is highly sensitive to alterations in pH [5]. If the pH increases outside of the range 7.4-7.6 the reaction kinetics and mechanisms will no longer be physiologically relevant. Steps that can be taken to mitigate this may include: (i) short immersion times; (ii) large solution volume to sample surface area ratio; (iii) frequent solution refreshment; (iv) the use of buffering agents.

Limiting tests to short immersion times can help reduce the corrosion reaction that takes place, and thus the pH change that occurs, but corrosion tests should in practice have some time to allow the surface layers to settle and the reactions to take place [11]. Electrochemical tests can be done relatively quickly for Mg. It has been reported that Mg in SBF needs 15 minutes for the electrochemical double layer (EDL) to settle [12]. A potentiodynamic polarization (PDP) scan can be done in a matter of minutes, as can electrochemical impedance spectroscopy (EIS). For bulk corrosion tests such as mass loss and H_2 evolution, it is necessary that corrosion take place to an extent that it can be measured. Thus, some corrosion will have to occur. The limitation of time before the pH is out of the range 7.4-7.6 is dependent on corrosion rate.

The rate of pH rise will also be dependent on the ratio of sample area to solution volume. In general, larger volume of solution will mean a greater amount of OH^- from the corrosion reaction can be generated before the pH moves outside of the range. Apparatus geometry is often a limiting factor for solution volume. Alternatively, replacing the solution with new solution is a possible method to combat pH rise. This also can be used to replenish salts that have deposited due to the corrosion reactions. However, although these methods are valuable for corrosion testing, a buffer system that can resist changes in pH, providing some active control similar to that found in the body, will be necessary as well.

The obvious choice to replace the control mechanism of the body's buffer is to use a buffer system *in vitro* as well. A chemically similar CO_2/HCO_3 buffer has been used for *in vitro* tests [13-15] as well as a number of chemical buffers [16-18]. Many of the chemical buffers used for this type of work use or are based on the 12 Good's buffers formulated to have properties ideal for *in vitro* solutions [19]. These buffers are designed for use in biological work, and thus possess suitable properties for biological solutions. However, use of a chemical buffer system *in vitro* is quite different to the environment *in vivo*. Thus, if these buffers are to be used for corrosion measurement, the effect of the buffer on the corrosion reaction must be understood. The effect the buffer has on the local pH level, the relative formation/dissociation of $Mg(OH)_2$ in a Cl^- environment, and the interaction with other salts in the in vitro solution must be known. To compare the performance of these buffers over time for analytical corrosion tests *in vitro*, the changes to corrosion kinetics of pure Mg exposed to various buffers was assessed under *in vitro* conditions.

3.2. Buffer Assessment:

Six different buffers were chosen in this study to examine the effect that different buffers might have. In the reviewed literature, the most commonly reported buffers for the corrosion testing of coated Mg *in vitro* were 2-Amino-2hydroxymethyl-propane-1,2-diol (TRIS) [17, 20-23], carbon dioxide and bicarbonate (hereafter referred to as bicarbonate or HCO_3) [15, 24-27], and 4-(2-hydroxyethyl)-1-piperazineethanesulfonic acid (HEPES) [16, 18, 28, 29]. As HEPES is one of the 12 Good's buffer designed for cell culture work, other Good's buffers 2-(N-morpholino)ethanesulfonic acid (MES), piperazine-N,N′-bis(2-ethanesulfonic acid) (PIPES), and N-(2-Hydroxy-1,1-bis(hydroxymethyl)ethyl)glycine (Tricine) were investigated as well [19]. The structure of the buffers is shown in Figure 3-1 and some relevant physical properties in Table 3-2.

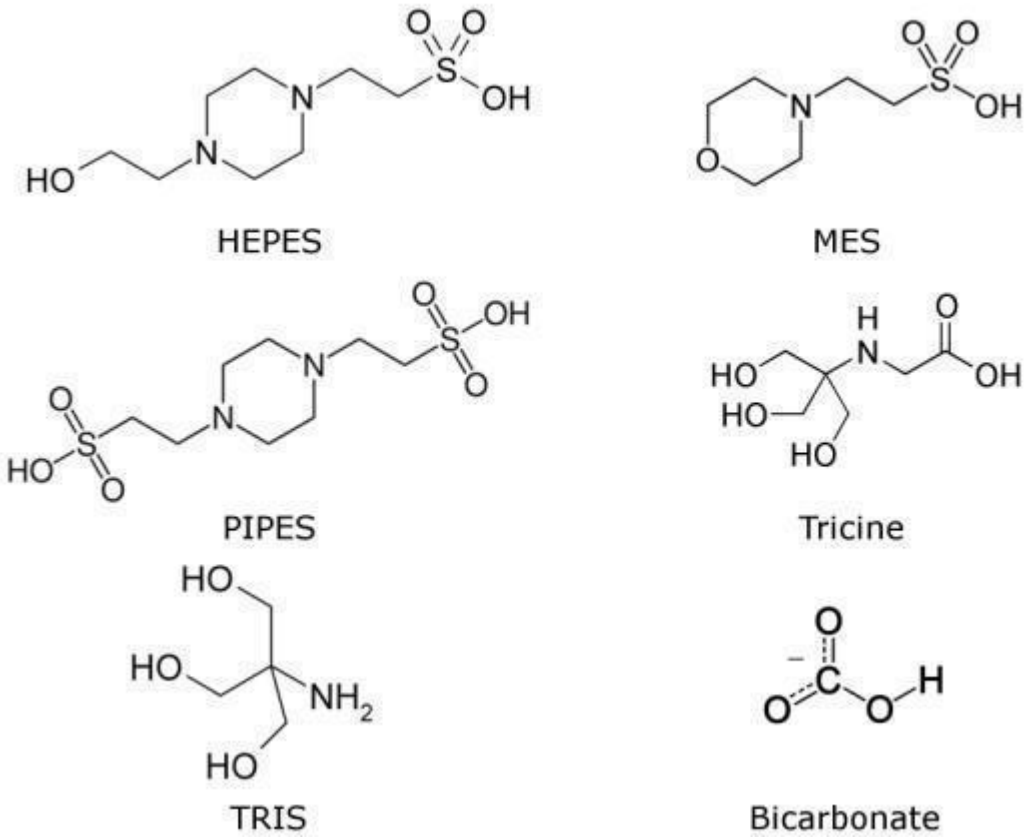

Figure 3-1: Chemical structures of the buffers used in this study.

3.2.1. CO_2/HCO_3^-

The CO_2/bicarbonate buffer is commonly used for *in vitro* cell culture work to control pH [13]. The buffer is prepared by adding sodium bicarbonate to the SBF and keeping it in an atmosphere of CO_2, typically between 5 and 10%. The carbon dioxide in the atmosphere affects the equilibrium reaction between carbonic acid and bicarbonate to balance the pH near physiological conditions according to Equation 3-4.

This buffer system is the system that controls the pH of the blood, through controlling the production of carbonates through metabolism and the gas exchange through the lungs. As it is chemically equivalent it provides a good choice for replicating the *in vivo* conditions *in vitro*. The buffer does require the CO_2 atmosphere to be controlled, necessitating the use of an incubator or similar equipment. *In vitro* evaluation of Mg and Mg coatings often makes use of this system [15, 25-27]. Setting the pH of this buffer to the desired starting level (7.40) is done by tuning the CO_2 gas level to the appropriate amount to reach the desired

equilibrium. In this study ~5% CO_2 was used, adjusted to reach a starting pH of 7.40 ± 0.01 for each solution.

3.2.2. TRIS

TRIS is a compound that has been widely used in biology and cell culture work due to its effectiveness near physiological pH. The useful buffer range of TRIS is 7-9. It is a primary amine, and will thus undergo reactions as such, for example condensation with aldehydes. The use of TRIS for in vitro Mg corrosion is fairly common in the literature [17, 20-23]. Unfortunately, in these studies the acid form TRIS-HCl is often used, or the base form with added HCl to bring the pH down to the appropriate level (7.4). Due to the sensitivity of Mg corrosion to Cl^-, the addition of HCl to the SBF is not desirable. For the purposes of this study, HNO_3 was chosen to bring the pH down from the initial pH of about 10 to 7.4. As a monoprotic strong acid, nitric acid will not introduce an additional pKa and change the buffering capacity of the solution. Although the nitrate ion is not present in large amounts in biological solutions, it is a spectator ion that is not expected to interact with the corrosion reactions or the salts of the SBFs used here.

Although popular for biological tests, TRIS is known to inhibit some enzymes and should be used with care if proteins are to be present in the SBF [30]. TRIS is reported to cause problems with silver chloride electrodes due to Ag precipitates clogging the junction [31]. Thus, for this study, saturated calomel electrodes (SCE) were used.

3.2.3. Good's Buffers

The zwitterionic buffers that Good et al. presented in 1966 were designed specifically to overcome some of the problems with existing biological buffers. Among the criteria used for these was to have pKa's at values where the buffering capacity is high at physiological ranges (i.e. between 6 and 8), should be highly soluble in water, should not cross biological membranes, should not interfere with, or bind to, metal ions, and should be stable under the conditions used. Because zwitterions fit the criteria well, Good designed an array of zwitterionic buffers for biological use. Of the 12 Good's buffers, HEPES seems to be the one most used for Mg corrosion protection evaluation [16, 18, 28, 29]. The pKa of HEPES leads it to be used commonly for solutions at a pH of 7.4. In this work, HEPES and selected other

buffers with chemical structures similar to HEPES and TRIS were selected with slightly different properties in order to examine the effect of these differences on the corrosion reactions of pure Mg in vitro.

3.3. Materials and Methods

3.3.1. Substrate Material

Pure Mg (99.98%, Timminco, Canada) was used for all tests. The Mg was ground with 600 grit SiC paper, rinsed with ethanol (96%) and allowed to dry in air.

3.3.2. Electrochemical Tests

Electrochemical tests performed included potentiodynamic polarization (PDP) and electrochemical impedance spectroscopy (EIS). A three electrode setup was used with a Pt counter electrode and a saturated calomel reference electrode (SCE). 300 mL of solution was used for each test, and the area of the working electrode was 1 cm^2. The solutions, cell and electrodes were heated to 37° C prior to the start of each test, and held at that temperature for the entirety of the test.

PDP was used to examine the corrosion kinetics. PDP scans for all samples were carried out from -150 mV vs. OCP to +200mV with a current limitation of 1 mA/cm^2. The scan rate during PDP was 1mV/s. Samples were allowed 30 min of stabilization in solution at open circuit for the first round of PDP tests, and allowed to freely corrode for 8 hours for the second round. For each solution and time point, 5 samples were tested with PDP to identify the range of uncertainty associated with the solutions and the Tafel fit approximations.

EIS was tested at a rate of once per hour starting after 2 hours of stabilization to up to 8 hours. A sinusoidal 10mV peak to peak signal across a frequency range from 50 kHz to 20 mHz was used.

3.3.3. Buffered Solutions

Two solutions were used for electrochemical tests. 103 mM NaCl was used as a simple SBF to test only the effect of the Cl^- at physiological levels and the buffering agent on the corrosion rate of pure Mg. The second solution was a standard formulation of Hank's Balanced Salt Solution (HBSS) (Sigma-Aldrich). The total concentration of Cl^- in this solution is higher than physiological solutions (Table 3-1). However, this is used quite commonly in the literature for corrosion measurements, and is therefore a solution of interest [32-37]. This solution contains other inorganic salts such as found in the body, without proteins or cells. In this way, only the interactions of the corroding Mg with the buffer in question are studied, without complications of proteins and other organic molecules which may affect the outcome. For more complicated *in vitro* tests, such interactions should not be overlooked. However, for this study these are eliminated.

Each solution had the buffer added to the correct molar concentration, and was then balanced to pH of 7.40 ± 0.01 at 37° C. For HCO_3 buffered solutions this was done by calibrating the CO_2 atmosphere (5%) to reach pH = 7.40. The remaining buffers were titrated using additions of either 1M NaOH (HEPES, MES, PIPES, TRICINE) or 1M HNO_3 (TRIS). HNO_3 was chosen because it is a monoprotic strong acid, and will therefore not add an additional pKa to interfere with the buffer capacity.

The zwitterionic buffers are not expected to contribute to the ionic strength and conductivity of the solutions by themselves [38], but once protonated/deprotonated, they carry a charge and can affect the solution resistance. The concentration deprotonated will be equal to the concentration of dissociation at the pH of 7.4 for each buffer. Solution conductivity was tested with a conductivity meter at 37° C for each buffer solution.

Table 3-1: Composition of simulated body fluids used in this test compared to Human Plasma

Component	Human plasma (HP)	NaCl Solution	Hank's balanced salt solution (HBSS)
Na^+	142	103	145
Cl^-	103	103	144.6
K^+	5.0	-	5.8
Ca^{2+}	2.5	-	1.3
Mg2+	1.5	-	0.4
HPO_4^{2-}	1.0	-	0.8
SO_4^{2-}	0.5	-	0.4
HCO_3^-	22-30	-	-
D-Glucose	5	-	5.5
Phenol red	-	0.03	0.03

All concentrations in mM
Concentrations of inorganic blood plasma given as in Ref [39].

3.4. Results and Discussion

3.4.1. Theoretical Buffer Capacity

The buffer capacity was estimated and plotted for each buffer at concentrations specified at pH of 7 to 8 (Figure 3-2). A HCO_3 concentration of 26.2 mM under 5% CO_2 atmosphere was used as this is standard for cell culture work [13]. HEPES is generally used at concentrations of 25mM to provide a balance between pH for cell culture work without harmful effects to the cells. 25mM was chosen as the concentration for all other buffers for consistency. While all of these buffers are used for biological conditions, the differences in pKa will result in different buffer capacities, which will be important for the amount of pH control over time. The buffer capacity is a representation of the change in pH for a given addition of strong acid or base and is calculated using Equation 3-5 where K_w is the dissociation constant of water, K_a is the acid dissociation constant of the buffer at 37° C, and C_{buf} is the concentration of the buffer in solution. The physical properties and concentrations of these buffers that were used in the calculation are listed in Table 3-2.

$$Buffer\ Capacity = \beta = 2.303\left(\frac{K_w}{[H^+]} + [H^+] + \sum \frac{C_{buf} K_a [H^+]}{(K_a + [H^+])^2}\right) \qquad \text{Equation 3-5}$$

Table 3-2: Physical properties and concentrations of buffers

Buffer	Mmass (g/mol)	Conc. (mM)	pKa_1 @ 37° C	pKa_2
HEPES	238.3	25	3	7.31
MES	195.2	25	5.97	
Tricine	179.17	25	2.3	7.8
PIPES	302.37	25	6.7	
TRIS	121.14	25	7.9	
HCO_3	84.01	26.2	6.3	10.3

Buffer capacity, β, is greatest when the pH of the solution equals the pKa of the buffering agent. HEPES has the highest buffer capacity at pH of 7.4. HCO_3 overcomes only MES as the weakest buffer, due to the pKa_1 at 6.3. The HCO_3^- ion, while important for the body as a buffering agent, is not the only mechanism that comes into play. Within the body is an active regulation system that can alter the partial pressure of CO_2 gas through the lungs, and can vary the amount of HCO_3^- released through metabolism of organic molecules [9, 10]. Thus, the total carbonate at a specific body location is not static. However, the buffer under a CO_2 atmosphere will have a mechanism for exchanging carbonate external to the corrosion cell *in vitro* as well. Thus the total concentration of HCO_3^- will be affected by the gas exchange with the atmosphere, altering the buffer capacity and pH.

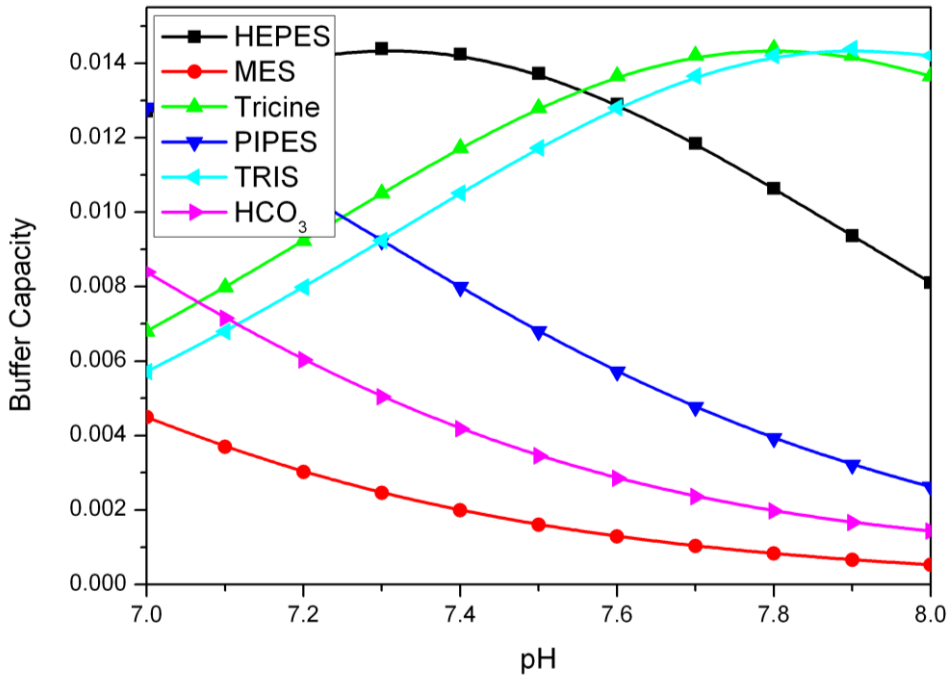

Figure 3-2: Theoretical buffer capacity, β, from pH 7 to 8 of each buffer used in this study at the given concentrations in Table 3-2.

3.4.2. Solution Resistance

Figure 3-3 tabulates the solution resistance of each buffer once buffered to capacity. The solution resistance varied with buffer choice. This was due to the additional ions added to bring the pH of the solution to 7.40 at 37° C. The solution conductivity in HBSS was higher than NaCl in every case due to the additional ions present in the solution. . The total current between the working and counter electrodes will be affected by the solution resistance due to these differences in solution conductivity. This opens the possibility that the measured current densities, and therefore the extrapolated i_{Corr} calculations will have some error introduced when comparing across different solutions [11]. From Figure 3-3, it was determined that the conductivity difference between buffers was smaller than the difference between HBSS and NaCl. Therefore the effect on the corrosion rate, especially with the large surface area for the counter electrode, should be minimal. Therefore the differences here are ignored. This is fairly good assumption as the EIS later will show that the uncompensated solution resistance for each buffer is small compared to the charge transfer resistance of the metal-solution interface.

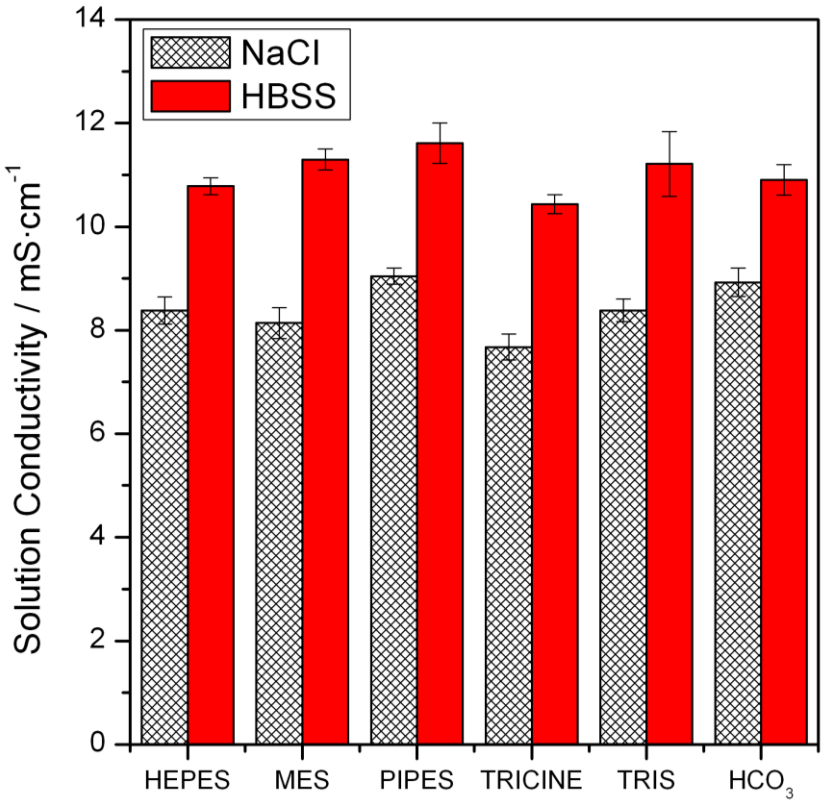

Figure 3-3: Solution conductivity of buffered solutions in NaCl and HBSS at 37° C.

3.5. Electrochemical Response

3.5.1. Bicarbonate Buffer

The measured corrosion potentials (E_{Corr}) of pure Mg with the bicarbonate buffer were lower in NaCl than HBSS as seen in Figure 3-4A. The amount of the salts, particularly the Mg^{2+}, increases the potential in HBSS from that of a simple NaCl solution. For both solutions, E_{Corr} rises over the 8 hours, in part due to the release of additional Mg^{2+} from the corrosion. The bicarbonate itself has a certain buffer capacity, thus as corrosion occurs the pH will rise and the corrosion will slow. The corrosion current density (i_{Corr}) of the HCO_3 (Figure 3-4B) drops dramatically with time in NaCl. This is due to the passive layer that forms as pH increases [40]. The corrosion rate compared to other buffer systems remains quite high. HCO_3 buffered systems in NaCl have higher anodic kinetics than all other buffers at both 30 minutes (Figure 3-5) and 8 hours (Figure 3-6).

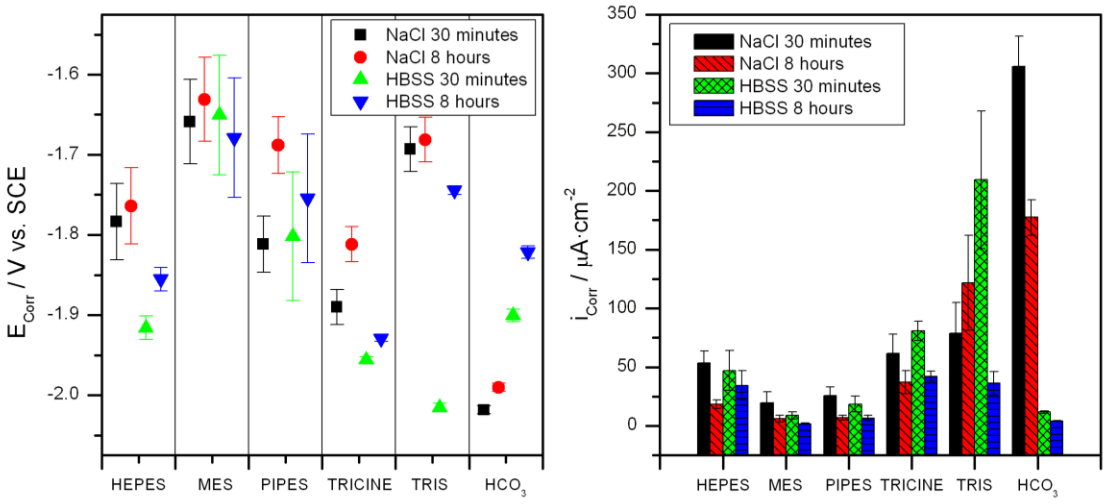

Figure 3-4: Electrochemical PDP results A) E_{Corr} and B) i_{Corr} for all buffered systems of NaCl and HBSS at 30 minutes and 8 hours.

Figure 3-9F shows that in NaCl, from 30 min to 8 hours the cathodic kinetics are very similar, as the thin, nonconductive $Mg(OH)_2$ and $MgCO_3$ layer does not impede the charge transfer to form hydrogen gas. There is also a small decrease in anodic kinetics, that is responsible for the decrease in i_{Corr}. The behaviour in HBSS showed a slight cathodic decrease and a large anodic decrease. Due to the nature of the solution, the protection layer was much more effective. The coating impedance in NaCl shows a small two time constant impedance curve characteristic of a semi-protective hydroxide layer that formed after 30 minutes (Figure 3-10A) that grew but remained similar in composition after 8 hours of corrosion (Figure 3-10B). The impedance in HBSS was quite different (Figure 3-11). Here the secondary time constant is very large, indicative of a highly protective coating layer. Rather than the semi-soluble $Mg(OH)_2$ and $MgCO_3$ layers formed in NaCl, the layer is near complete, severely limiting the diffusion of corrosive solution to the Mg metal, and reducing the anodic dissolution. The pH of the solution is just high enough that with Mg corrosion, the calcium in solution can form a protective layer of $CaCO_3$ and/or $CaHPO_4$ that further protected the substrate. This accounts for the great disparity in corrosion properties between these two SBFs. This greater protection in HBSS is in spite of the increased Cl^- content of the HBSS over the simple NaCl solution.

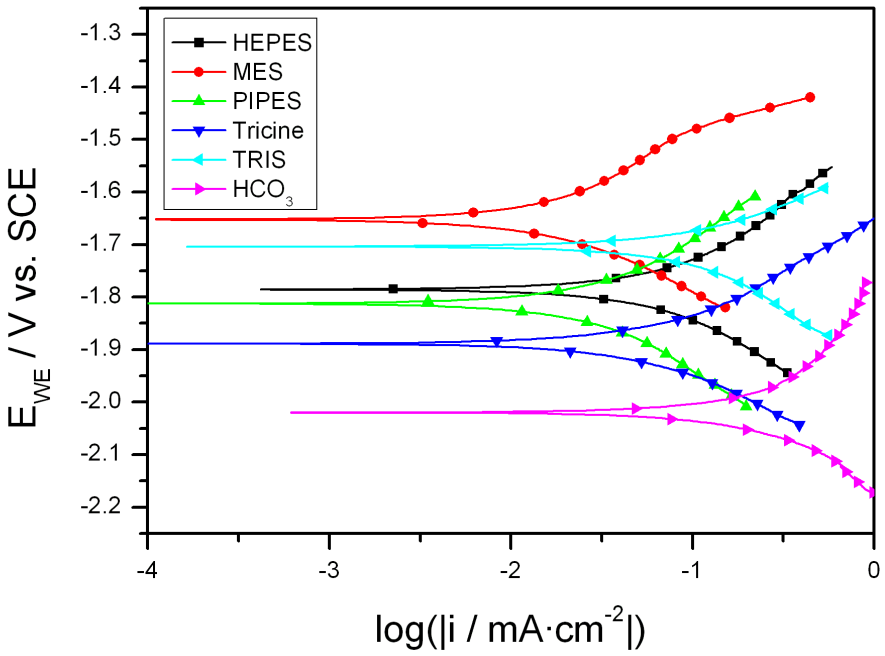

Figure 3-5: Polarization of Mg in buffered NaCl solutions after 30 minutes immersion.

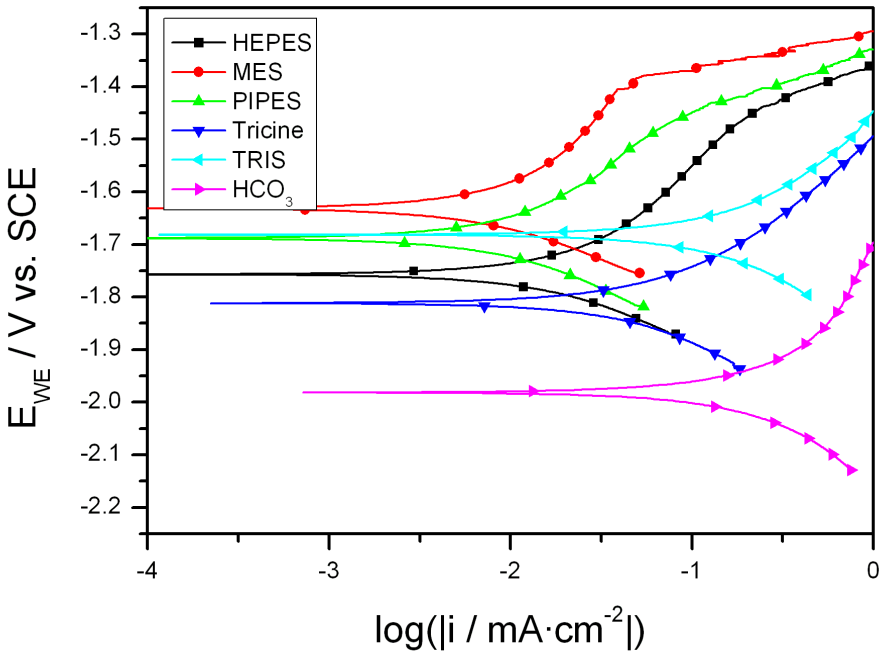

Figure 3-6: Polarization of Mg in buffered NaCl solutions after 8 hours immersion.

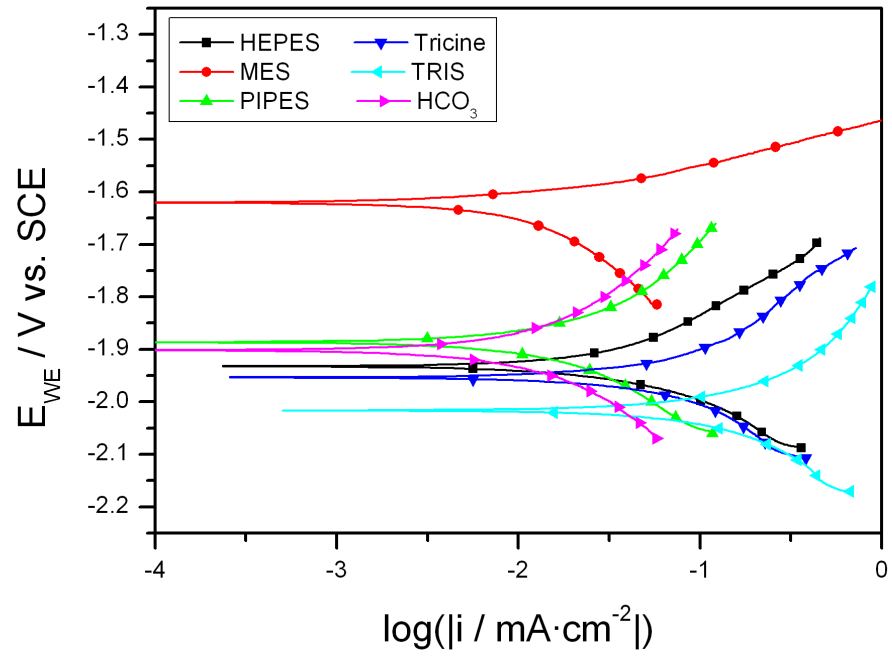

Figure 3-7: Polarization of Mg in buffered HBSS solutions after 30 minutes.

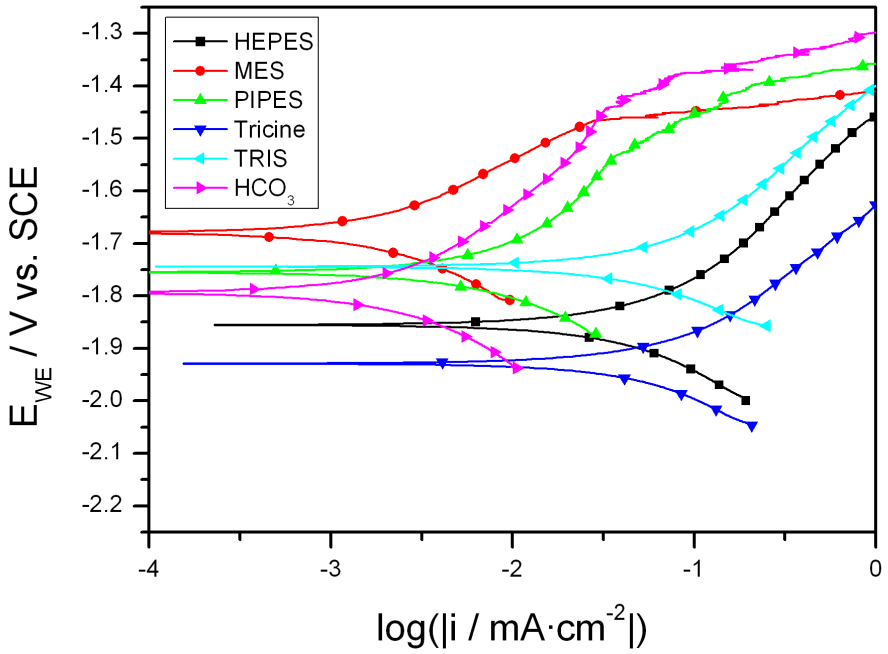

Figure 3-8: Polarization of Mg in buffered HBSS solutions after 8 hours.

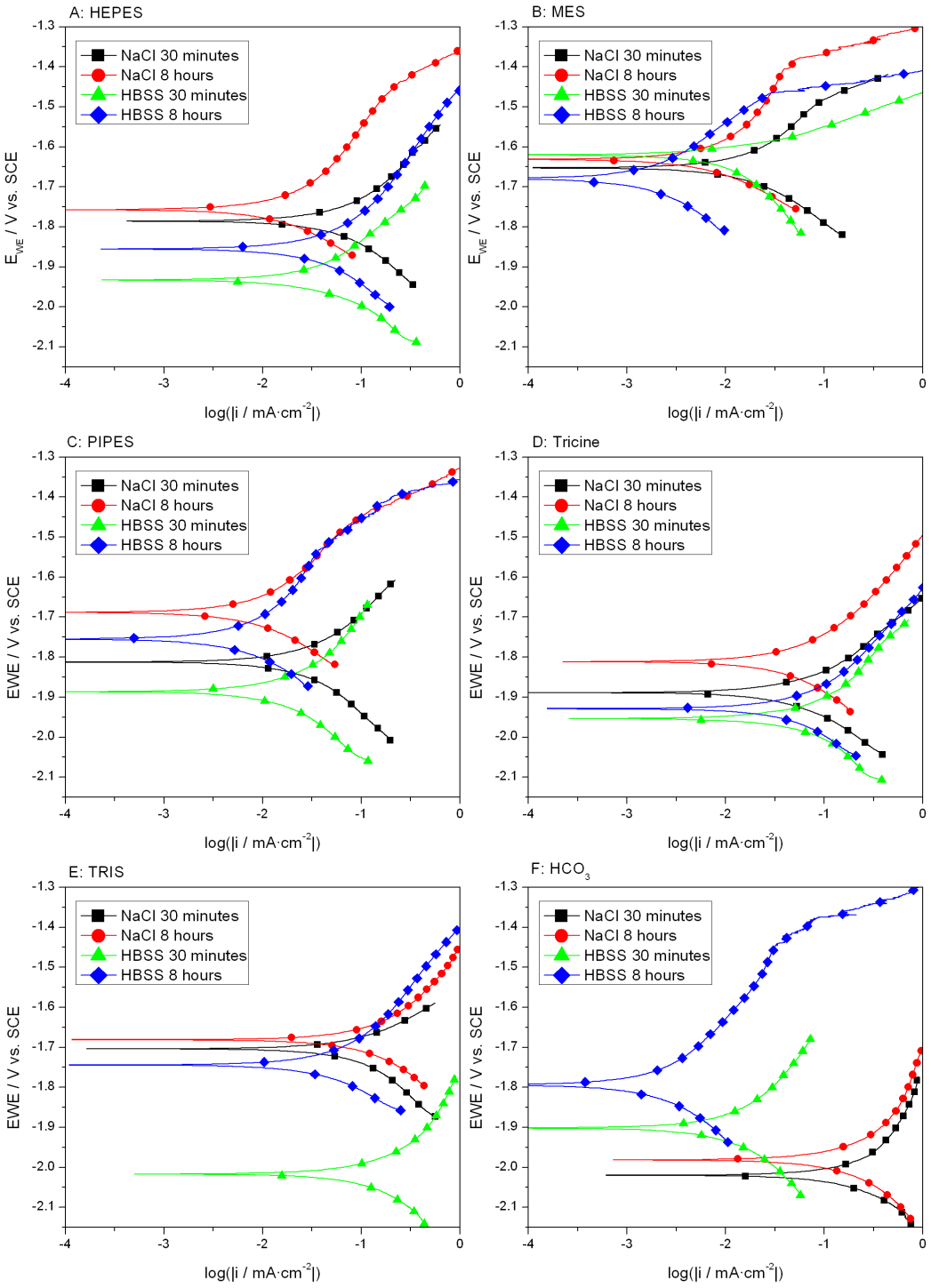

Figure 3-9: PDP over time of Mg in buffered solutions of both NaCl and HBSS with A) HEPES, B) MES, C) PIPES, D) Tricine, E) Tris, and F) HCO_3.

3.5.2. TRIS Buffer

The next common buffer agent TRIS displayed a relatively high potential in NaCl that increased slightly over the 8 hour test, staying well within the error. The initial corrosion current density increased from 78.7 ± 26 to 121 ± 40 $\mu A \cdot cm^{-2}$. The rise was due to the increase in surface area from pitting as corrosion occurred. TRIS had one of the largest cathodic kinetics of any buffer in NaCl at both 30 minutes (Figure 3-5) and 8 hours (Figure 3-6). Similarly high cathodic kinetics were seen in HBSS (Figure 3-7, Figure 3-8). In HBSS, E_{Corr} and i_{Corr} both changed significantly from 30 min to 8 hours. This suggests that perhaps the corrosion layer has not fully settled after 30 minutes in this solution despite the open circuit potential (OCP) settling to a constant value. The shift in corrosion potential was not accompanied by major shifts in kinetics of either reaction (Figure 3-9E). The corrosion over time in the solutions is therefore not varying due to large changes in the type of reaction or passivation layer. The changing surface area and pH, as held by the buffer, are the cause of the change in potential.

EIS results confirmed this as the resistance of the layers in the Nyquist plots show. In NaCl (Figure 3-10), the corrosion layer is characterized by a low resistance $Mg(OH)_2$ layer and a smaller secondary EDL layer. This shows that the $Mg(OH)_2$ layer is not passive due to the Cl^- attack, and the EDL in this buffer shows high charge mobility, leading to easy migration of Mg^{2+} away from the corrosion sites and H_2O and H_3O^+ to the substrate to be reduced to form H_2 gas. Over 8 hours (Figure 3-10B) the magnitude and relative shape of each time constant remained similar. Thus the similar corrosion kinetics for both timepoints in NaCl. In HBSS the layers are similar in shape, indicating similar kinetics of the passive layer, but the total magnitude of both the passivation layer and the EDL increases in resistance over 8 hours, suggesting the accumulation of a more protective layer in HBSS despite increased Cl^- levels. This indicates that other ions, Ca^{2+} and PO_4^{3-} were incorporating themselves into this layer [8, 40].

3.5.3. Good Buffers – HEPES, MES, PIPES and TRICINE

3.5.3.1. HEPES

The HEPES buffer has the highest buffer capacity at a pH of 7.4 due to its pKa. HEPES has been reported to lead to faster corrosion than bicarbonate buffers in SBF [14]. Higher buffer capacity means that the pH will take longer to rise for an equivalent corrosion rate, delaying the formation of a passive layer. At pH of 7.4 before significant corrosion can take place, the HEPES buffer by itself was not significantly more aggressive in NaCl solutions than bicarbonate and other buffers. The corrosion potential of the HEPES-buffered NaCl was lower than TRIS-buffered NaCl but higher than HCO_3 (Figure 3-4). E_{Corr} in HEPES-buffered HBSS was lower than HEPES-buffered NaCl, and followed the trend of both HCO_3 and TRIS by increasing slightly over the 8 hours of immersion while the corrosion layer stabilized. i_{Corr} dropped significantly after 8 hours in NaCl, but did not change as significantly (within error) for HBSS with the HEPES buffer. HEPES had lower corrosion rates than HCO_3 in NaCl, but faster rates than in HCO_3. This is evidence of HEPES holding a more stable pH layer across solutions, when the corrosion is not affected by the formation of a carbonate layer. HEPES exhibited very little change in cathodic kinetics over 8 hours (Figure 3-9A). The decrease in anodic kinetics and increase in potential is therefore responsible for the decreased corrosion rate over time. In NaCl, HEPES shows the characteristic 2 time constant corrosion resistance of a partially protective $Mg(OH)_2$ layer (Figure 3-10A). After 8 hours, this $Mg(OH)_2$ layer developed, increasing the protection of the film resistance as seen in Figure 3-10B. This layer thus accounts for the decrease in corrosion current density observed in HEPES-buffered NaCl. In HBSS, similar time constants are visible for HEPES (Figure 3-11) but the magnitude of the increase in $Mg(OH)_2$ layer protectiveness is much smaller. This suggests that the $Mg(OH)_2$ layer is being attacked at a faster rate, as one would expect due to the increased Cl^- content of HBSS. The fact that this layer is not more pronounced further suggests that the Ca^{2+} and PO_4^{3-} content have not begun to contribute to the protective layer while the local pH remains near 7.4.

3.5.3.2. MES and PIPES

MES and PIPES, similar in chemical structure to HEPES, followed similar trends to the HEPES buffer but corrosion currents were much lower in either solution than HEPES, TRIS, or Tricine. MES and PIPES had the lowest final anodic reaction rates in NaCl (Figure 3-6) and along with HCO_3, the lowest in HBSS as well (Figure 3-8). MES showed decreasing anodic kinetics in NaCl and a decrease in both cathodic and anodic rates in HBSS (Figure 3-9B). Similar trends were seen in PIPES (Figure 3-9C). This decreasing corrosion rate can be linked to the low buffer capacity, leading to local pH rise and passivation of the substrate. Indeed, large film resistances can be seen for both MES and PIPES in NaCl (Figure 3-10), where increasing $Mg(OH)_2$ film resistance matches HEPES but to a greater extent in PIPES and MES due to the lower buffer capacity. This behaviour is repeated to a greater extent in HBSS, and the behaviour matches that of bicarbonate, suggesting that the formation of the film is further resistant to corrosion. The large EDL suggests a nonconductive ceramic layer that may include carbonates and phosphates, similar to the data collected for bicarbonate buffering. Again, the difference here is the larger pH rise that is accompanied by a similar amount of corrosion, leading to this passive behaviour and the low measured corrosion current densities.

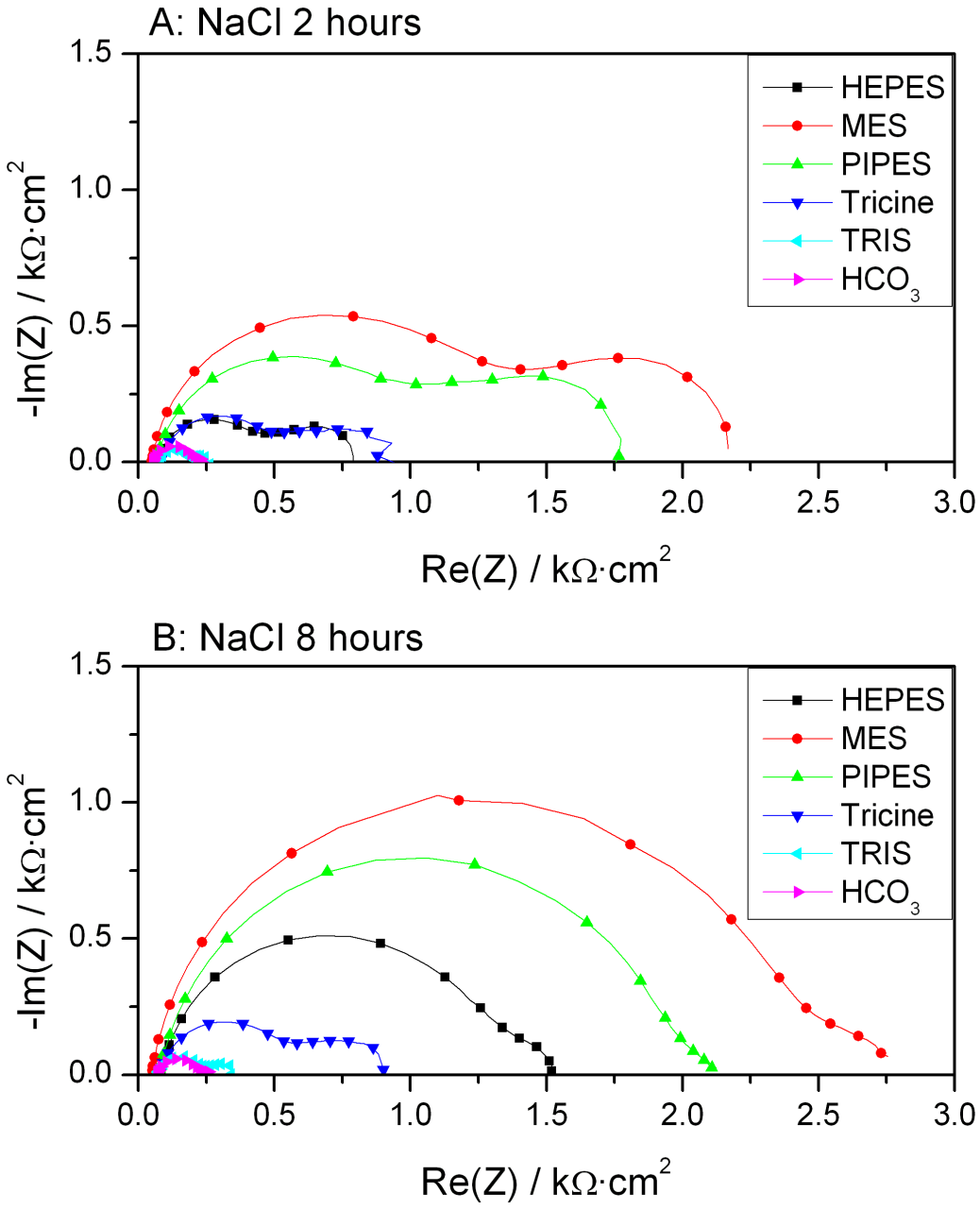

Figure 3-10: Nyquist plot of Mg in NaCl A) after 2 hours and B) after 8 hours.

3.5.3.3. TRICINE

Once settled, i_{Corr} in Tricine was similar to TRIS and HEPES in NaCl and HBSS, as one might expect due to the similar buffer capacities. Tricine in NaCl shifted in E_{Corr} over 8 hours as the corrosion layer settled, resulting in a small decrease in corrosion current density. A similar trend was seen in HBSS. Anodic and cathodic kinetics remained relatively consistent for each solution over the test period (Figure 3-9D). Although Tricine had the

lowest measured conductivity of the buffer set (Figure 3-3) this did not appear to significantly affect the measured corrosion current densities. Tricine did show the lowest potential after 8 hours in HBSS of all buffers (Figure 3-8). The steady corrosion kinetics are apparent from the Nyquist plots, where the same 2 time constant behaviour can be seen over the corrosion period in NaCl (Figure 3-10). The corrosion layer of the $Mg(OH)_2$ and the associated EDL for Tricine starts out very similar to that of HEPES. However, unlike HEPES, the coating layer does not change much in terms of either time constant shape or magnitude. In HBSS, the layer properties were similar. No large change in passivation behaviour was observed. Like TRIS and HEPES, the buffer capacity of Tricine was high enough to inhibit the formation of additional insoluble layers in HBSS that could otherwise slow the reaction rates.

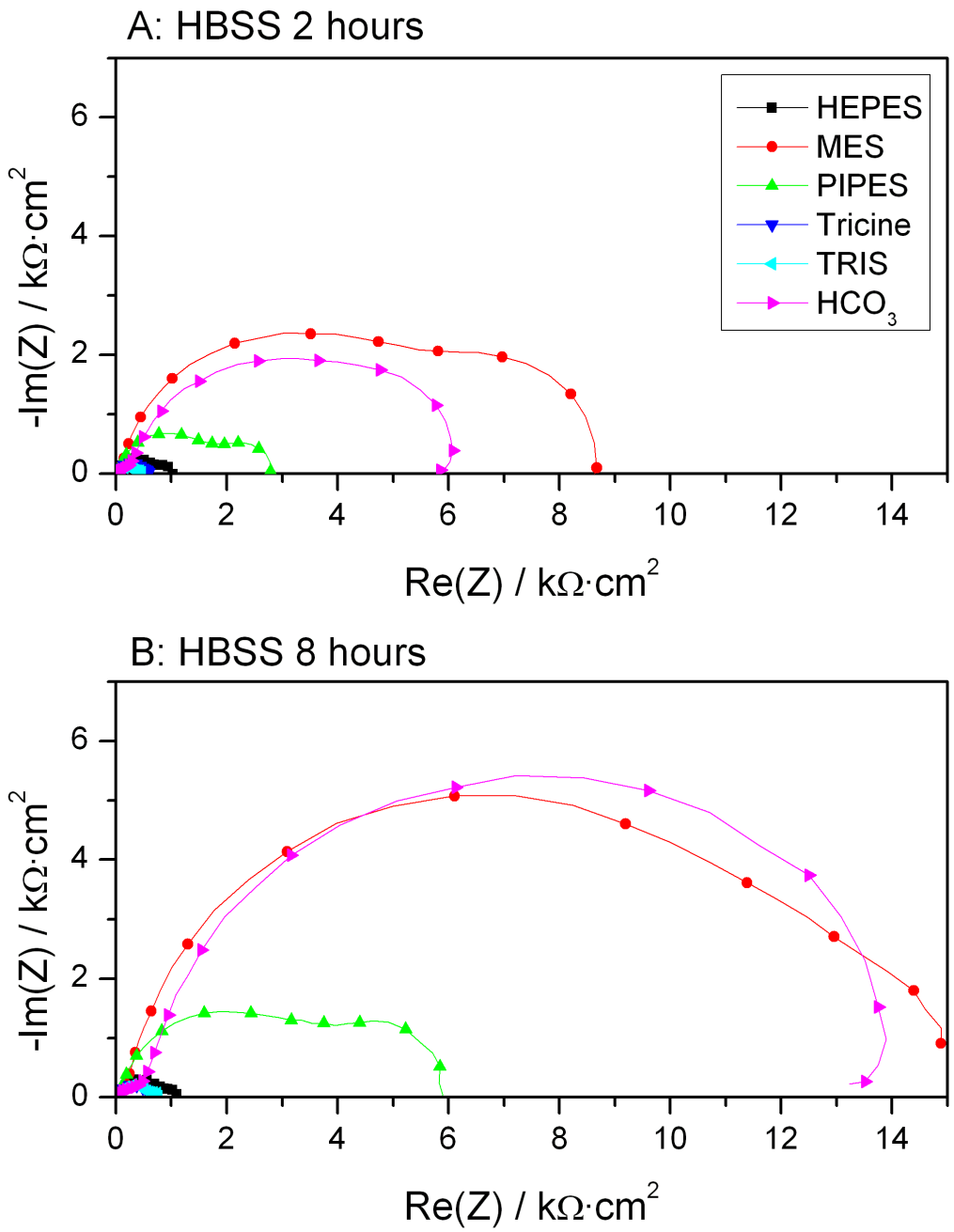

Figure 3-11: Nyquist plots of Mg in HBSS after A) 2 and B) 8 hours.

The relationship between the buffer capacity and measured corrosion rate is especially important to *in vitro* tests. The goal of a suitable *in vitro* test will be to reliably assess the corrosion properties of the material. As shown here, the actual corrosion rates can be quite different for different buffering agents in the same solutions using the same substrate even

though the measured bulk pH of the solution remains the same. The local pH rise near the surface and diffusion rate has a clear effect. The chemistry of the buffer molecule may be important as well, despite the design criterion for these buffering agents to have low interactions with the ions in body fluids [19].

3.6. The Effect of Carbonate Concentration versus Buffer Capacity

The bicarbonate/carbon dioxide buffer system that is chemically if not functionally identical to the *in vivo* buffering systems, and thus is often used for *in vitro* models [40]. In practice, the buffer system itself has a large effect on the total relationship. The corrosion properties in HCO_3 depend on its interactions with other salts in the SBF, as evident by the disparity between corrosion in simple NaCl solutions and HBSS. The carbonate ions detected in the corrosion layer in HCO_3 buffered solutions suggest they play a role in the reduction of the corrosion rate [40]. The solubility of ceramic compounds such as carbonates and phosphates depend on pH, and the local pH rise at the Mg surface can lead to the precipitation of protective layers [8]. Thus, the buffer capacity, which controls this local pH rise, can also affect the deposition of these layers. The local pH rise can also be responsible for the passivation by $Mg(OH)_2$. Thus, the difference in corrosion rate between HCO_3 and another buffer is affected by the buffer capacity as well. As HCO_3 has a poor buffer capacity on its own, the low measured corrosion rates might have more to do with the limitations of the *in vitro* gas exchange than the actual carbonate concentration itself.

To investigate the relationship between buffering capacity and the deposition of protective carbonate layers to carbonate concentration, a further test was performed. HBSS solutions buffered with HEPES and HCO_3 was compared to HBSS co-buffered with 25mM HEPES and 25mM HCO_3 in a 5% CO_2 atmosphere. Thus, the effect of the increased buffer capacity due to the added HEPES on the corrosion rates can be measured.

The corrosion potential of the combined buffer solution was lower than either HEPES or HCO_3 by itself (Figure 3-12). Corrosion current density was high initially, but over time lowered to within the margin of error of that of HEPES alone. It did not drop to the levels of HCO_3 by itself. The higher buffer capacity of the HEPES in the presence of HCO_3 prevented

the formation of the protective layer that forms on the corrosion surface. It can be inferred that a higher pH is required to slow the corrosion rate, and these layers will not form at idealized *in vitro* conditions. This effect can be seen by the lack of anodic reaction shift in the HCO_3 + HEPES buffer compared to the large shift of HCO_3 alone (Figure 3-13).

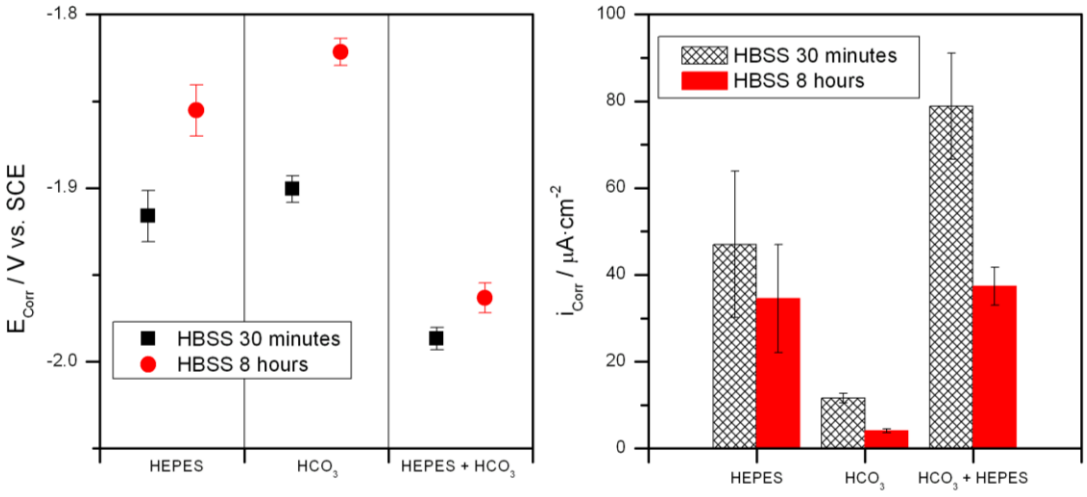

Figure 3-12: E_{Corr} and i_{Corr} as a function of buffer type and corrosion time in HBSS.

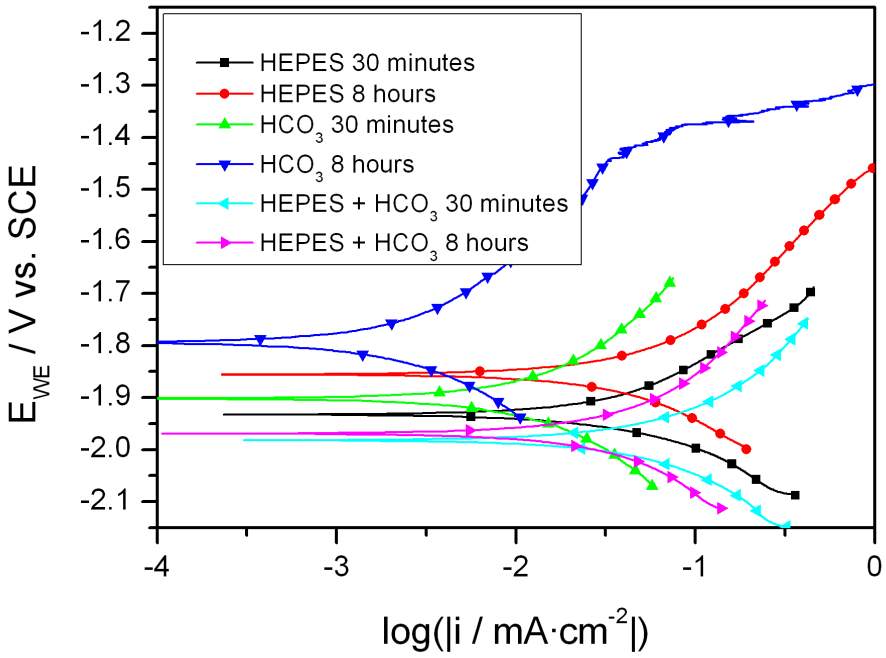

Figure 3-13: Polarization in HBSS with HEPES and HCO_3 compared with both individual buffer solutions.

The impedance data confirms the relationship between buffer capacity and corrosion layer formation. The Nyquist plot of HBSS in HEPES + HCO_3 in Figure 3-14 shows the corrosion behaviour was dominated by a single time constant, with very little additional impedance due to the formation of a passive layer. Thus, at these Cl^- concentrations, and a pH held very close to 7.4, Mg is not passive, and undergoes active corrosion. In HEPES alone, a small second time constant, due to the local pH rise improving the formation of $Mg(OH)_2$ layer appears on the surface [40]. This effect is not as apparent in the co-buffer system, due to the total increased buffer capacity. The large impedance of the carbonate layers in the HCO_3 buffered HBSS only forms without the extra HEPES buffering capacity. It can be concluded that the reduced corrosion observed in these buffers is due to the limitation of the buffering capacity of the component. Thus, the assessment of corrosion properties *in vitro* will be highly dependent on the buffering capacity and local mechanisms for the measured outcome.

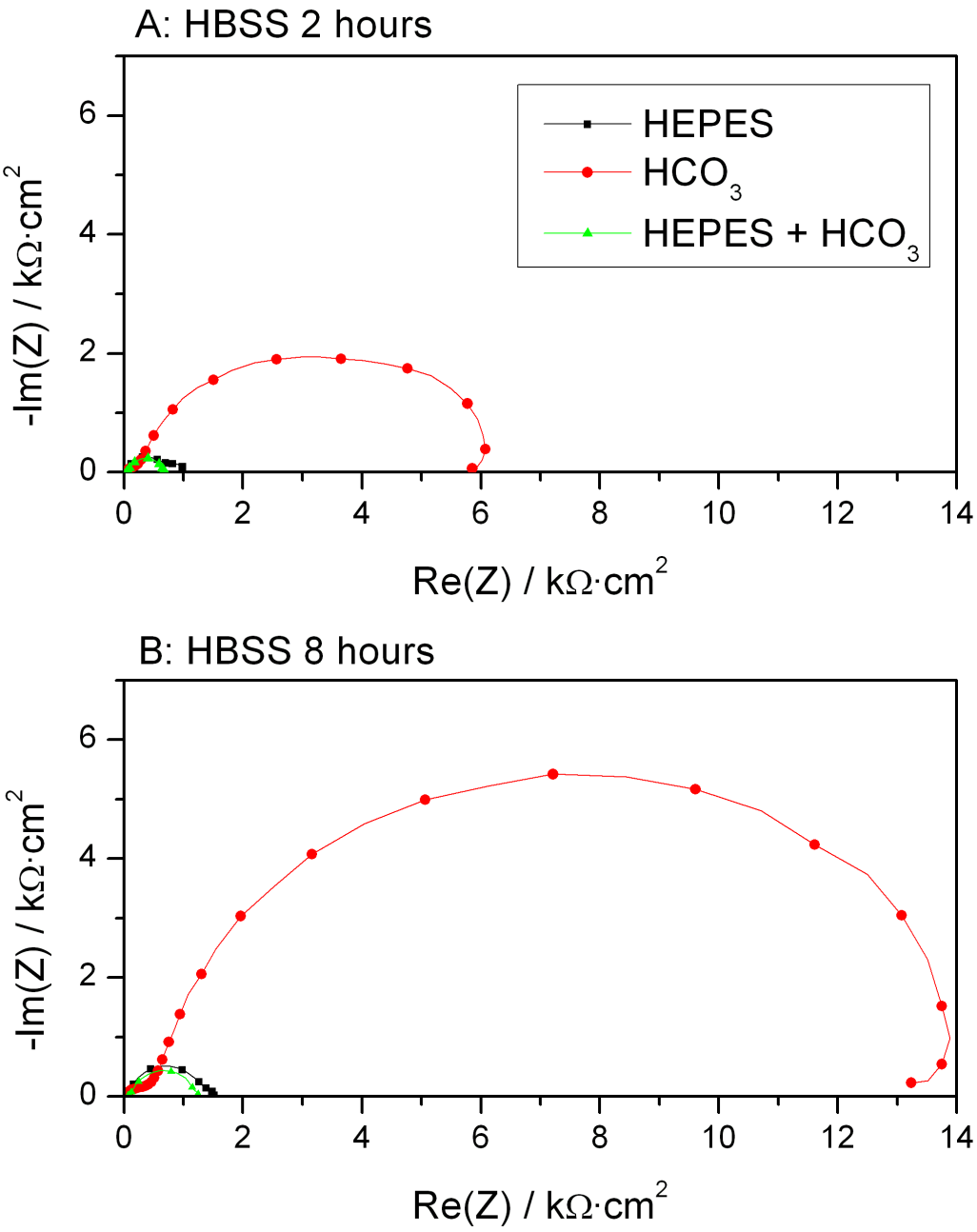

Figure 3-14: Nyquist plot of Mg in HBSS with HCO_3 and HEPES.

3.7. General Discussion on Buffer Choice and Corrosion Measurement:

The *in vitro* corrosion response of pure Mg varies greatly with the selection of the buffering agent. In particular, the measured corrosion rate can be significantly different across different buffering systems even before corrosion of the substrate can significantly change the bulk pH of the test solution.

3.7.1. Buffer Capacity

The buffer capacity is very important in the assessment of the corrosion rate of Mg alloy systems, since the dissolution (namely the anodic reaction) of Mg *in vitro* is very sensitive to pH [5]. The ability of a chemical buffer to resist pH changes at the surface becomes highly important when attempting to accurately model and predict corrosion. Furthermore, buffer systems can react differently in different *in vitro* corrosion media. The amount of difference measured in a simple Cl^- solution versus a more complex solution like HBSS will depend on the buffer agent and buffer capacity. It becomes apparent that the use of a bicarbonate buffer *in vitro* simply because it is the same chemistry as found *in vivo* is not necessarily a solution to the problem as low buffer capacity and solution dependencies can drastically alter the corrosion mechanisms and rates of the measured solution [14, 41]. Therefore, care must be taken to identify and design the parameters of buffer concentration and reaction rate to ensure *in vitro* tests are comparable to each other and to *in vivo* applications. If these are not addressed, it would be possible for a poorly buffered *in vitro* system to report low corrosion rates for a particular alloy or coating, yet behave very differently under the active controlled body system at the implant site. Chemical buffers such as TRIS and the Good buffers can be useful in keeping the pH constant in solutions. The effect of these chemicals on the corrosion rate must be considered. Despite the low interaction with metal ions, these buffers all have different pKas, and thus different capacities and properties in the presence of a corrosion reaction. Therefore, it will be necessary to use care and consistency when using buffered *in vitro* solutions to model the body and investigate corrosion properties in physiological fluids.

3.7.2. E_{Corr} vs. i_{Corr}

An overview of all data points for each buffer is shown on a semi-log plot of E_{Corr} vs. i_{Corr} in Figure 3-15. The global trend is increasing i_{Corr} with decreasing E_{Corr}. The trend of each buffer family with respect to E_{Corr} and i_{Corr} tells us about the relationship between potential and the current density of the corroding sample. HCO_3 follows a fairly linear trend with little variation. In contrast, a buffer such as MES has much larger errors based on each point. MES in particular shows little trend in E_{Corr} over a wide range of i_{Corr}. This suggests a wide variation in corrosion rates independent of the potential driving force. The variation suggests it may not be a good choice of a buffer for consistency across multiple *in vitro* solutions. This can also be said of TRIS, which shows the strange behaviour of apparently increasing i_{Corr} with increasing potential, with the exception of an outlying point. PIPES, Tricine, and HEPES have similar trends following a linear pattern. The trend seems to be steeper than HCO_3. This means the variation in corrosion rate is more independent of variations in E_{Corr} across solutions and time points, a desirable property when consistency in corrosion rate measurements is wanted. Of these buffers, HEPES has the highest buffer capacity at pH 7.4. Therefore, if all else is equal, more pH control can be gained from HEPES per molar addition than any other buffer. That, and HEPES track record and study in the literature for cell culture work recommend HEPES as the buffer of choice for *in vitro* corrosion measurements of Mg in simple SBFs.

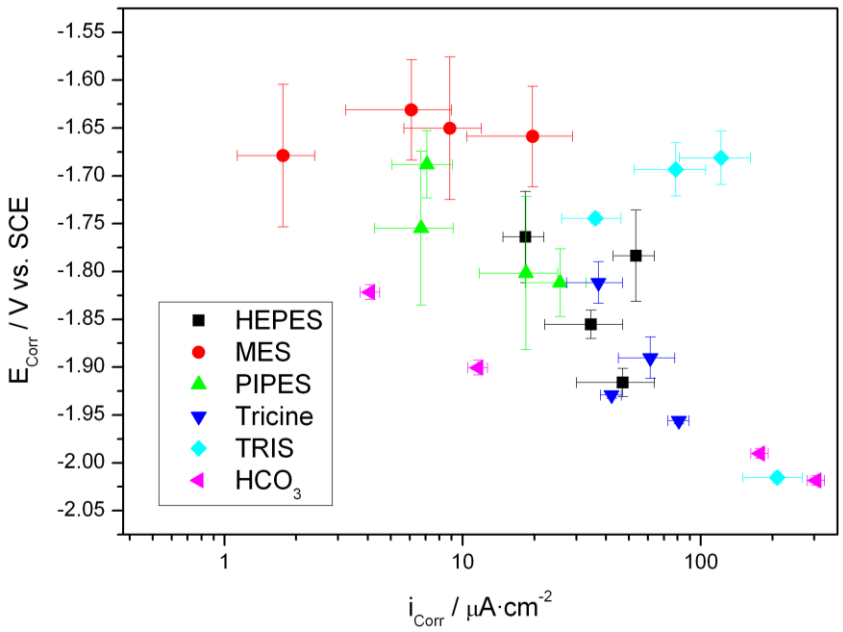

Figure 3-15: i_{Corr} vs. E_{Corr} for all buffered solutions.

3.8. Summary of the Electrochemical Corrosion Properties of Mg in Buffered Solutions

In vitro corrosion behaviour of pure Mg strongly depends on the pH present at the surface of the Mg. Chemical buffers with different buffer capacities can have large effects on the initial corrosion rates even when the bulk pH of the solution is the same. The composition of the SBF has an effect on the passivation layer that forms based on the buffer response. In particular, the relationship between Cl^- concentration and local pH affects the passivation tendencies of the $Mg(OH)_2$ layer, and therefore the ultimate corrosion rate. The local pH depends on the initial corrosion rate and the buffer capacity. The result is the choice of buffer influences the corrosion rate even if it does not directly interact with the corrosion reactions.

Buffer response is also affected by the presence of other inorganic salts in the solution. When pH is increased, protective phases including Ca^{2+}, PO_4^{3-} and CO_3^{2-} can deposit on the surface. When buffer capacity is low enough, these phases slow the reaction in SBFs that contain these ions, leading to different corrosion rates than would be expected from simple Cl^- solutions. Even though it is chemically similar to the body's *in vitro* buffering system, HCO_3 buffers under a partial CO_2 atmosphere have a low buffering capacity and lead to the formation of protective films that greatly inhibit the corrosion reaction. The response is due to the local pH rise that occurs as a function of the performance of the buffer *in vitro*, that may or may not be expected to be mirrored *in vivo*. When the HCO_3 buffer is supplemented with additional buffering capacity from a zwitterionic buffer, the enhanced control of the local pH does not allow the protective layer to form. The ultimate corrosion rate *in vivo* will therefore be heavily influenced by the effectiveness of the body's active pH control systems. This effect should therefore be taken into account when designing *in vitro* corrosion tests and making conclusions about the ultimate *in vivo* corrosion rates based on performance *in vitro*.

3.8.1. The Interaction of HEPES with Mg Ions in Solution

3.8.2. Determining the interaction between Mg and HEPES

For a chemical buffer such as HEPES to be used *in vitro*, it is important to make sure the interaction with the metal and the surrounding solution is kept to a minimum. In fact, the ideal case is that the buffer has no interaction except to perform its function. This is not the case for the HCO_3 buffer, as the carbonate ions become incorporated into the passive layer [40, 41]. The corrosion potential differs slightly across buffered solutions. The differences can be attributed to differences in the layers that form, the diffusion of ions, and if the system has reached steady state, and the local pH. However, the possibility exists that the differences are caused by the direct interaction of the HEPES molecule with the Mg. It could be the case that the HEPES directly accelerates the corrosion of Mg by participating in the corrosion reaction, or that HEPES changes the potential, and therefore the corrosion rate, by removing free Mg ions through binding to form a complex. The original formulator of HEPES for use as a biological buffer tested the interaction with a number of metal ions, including Mg and found it negligible [19]. But the purpose of Good's focus was not Mg corrosion, where local Mg concentrations may be much higher than physiological levels. The best way to confirm that HEPES is not interfering with the corrosion reaction is to measure the interaction between Mg and HEPES directly. This can be examined using nuclear magnetic resonance spectroscopy.

3.8.3. Nuclear Magnetic Resonance Spectroscopy

Solution-state nuclear magnetic resonance spectroscopy (NMR) was used to explore the potential for complexation between Mg and HEPES. Samples were prepared by adding 23.83 g/L of HEPES to distilled H_2O to form a 100 mM HEPES solution, giving an initial pH of 5.31. The pH was then increased to 7.40 ± 0.01 by adding 3.4 mL of ~1 M NaOH solution. Varying amounts of magnesium chloride hexahydrate (99.0%, M2670, Sigma Aldrich) was then dissolved into the HEPES solution to give the desired Mg concentrations of 1, 10, 25 and 100mM $MgCl_2$. These concentrations were chosen to evaluate the behaviour due to increasing Mg^{2+} concentration in solution from a level of normal blood serum (of 1.5mM) up to high levels that could be expected at the surface of a corroding block of Mg.

NMR was then performed with a Varian VNMR 500 (Agilent Technologies, Lexington, MA, USA) at 500 MHz. A glass insert tube filled with deuterium oxide (D_2O) was employed to provide a lock signal for the instrument and acetonitrile was used to provide a reference without interacting directly with the test solution. All solutions were analysed at 23°C, ambient temperature at the location of the instrument. The uncertainty of the NMR measurements was estimated at ~0.002 ppm based on the maximum fluctuation of the acetonitrile standard across all NMR tests.

3.8.4. Interaction Measurements

NMR resolved two distinct peaks assigned to the protons in the HEPES molecule that we would expect to be most affected by the formation of a metal ion complex. These hydrogen atoms are located near the negative charge on the zwitterions and would be most affected by the presence of Mg^{2+} ions with a correlating shift in the field energy level at resonance. The proposed complex behaviour is shown in Figure 3-16 [42]. The change in chemical shift induced by the presence of $MgCl_2$ is not large enough to be significant at lower concentrations of $MgCl_2$, although a substantial chemical shift change was observed at the highest concentration (100 mM) (Figure 3-17). The change in chemical shift was larger when the concentration of HEPES was increased from 25 mM to 100 mM.

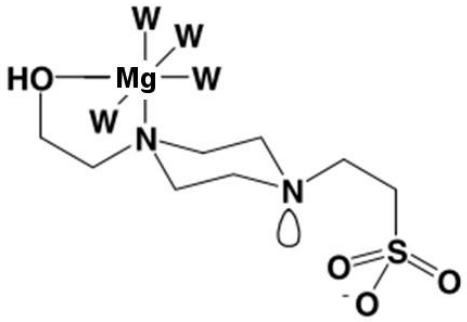

Figure 3-16: Shape of the proposed Mg-HEPES complex.

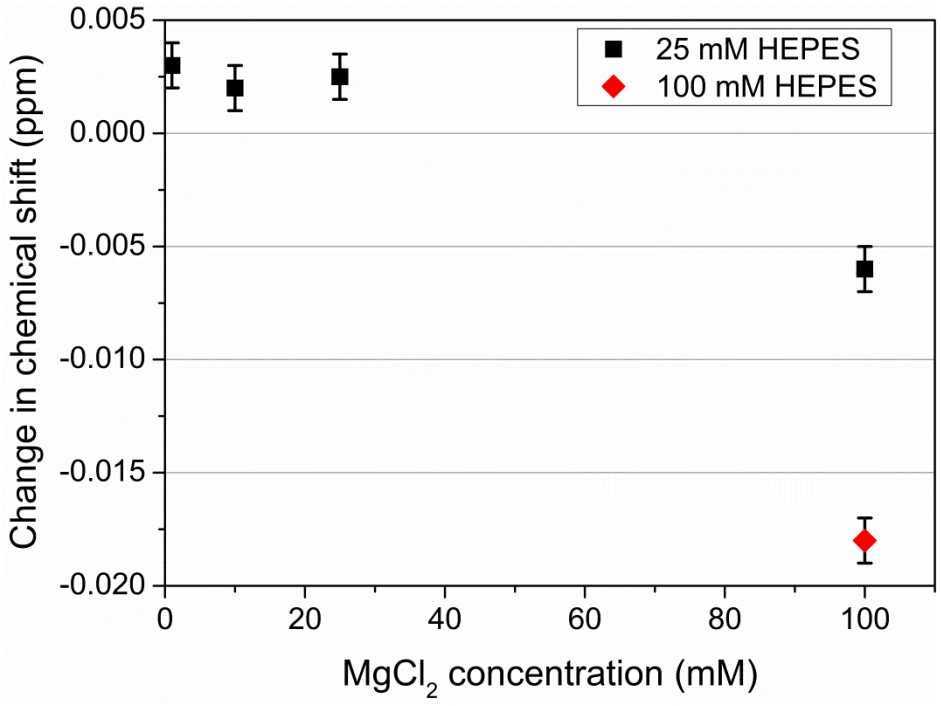

Figure 3-17: Change in chemical shift as a function of $MgCl_2$ concentration from the 25 mM HEPES reference solution. Magnitude of peak shifts in 100 mM $MgCl_2$ versus the reference HEPES solutions for HEPES concentrations of 25 mM and 100 mM are also shown.

The possible chemical interaction between Mg and HEPES was explored further with NMR spectroscopy, based on the 'apparent' relationship between mass loss and hydrogen evolution rates [14, 40]. To support this hypothesis, a recent study by Xin *et al.* investigating the effect of a TRIS buffer on the corrosion of pure Mg found that the TRIS-HCL compound that formed during the buffering process lowered the corrosion potential slightly while increasing the corrosion rate [43]. It was suggested that TRIS-HCL consumes the OH^- generated by the corrosion process, accelerating the oxidation of Mg to Mg^{2+}. They also found increased pitting corrosion in the early stages in the presence of the buffer [43]. Thus, it is also possible that the chemical structure of HEPES itself is leading to enhanced corrosion of Mg. It was hypothesised that part of the HEPES structure is able to react with the OH^- group in the $Mg(OH)_2$ layer itself. This would decrease the effectiveness of the $Mg(OH)_2$ layer in hindering corrosion by presenting the underlying Mg substrate to the corrosion medium. Alternatively, HEPES may be interfering with the spontaneous CaP precipitation process that is normally associated with immersion in an SBF. The EIS results in HEPES buffered solutions show the corrosion layer does not form as large as the HCO_3, PIPES or MES buffered solutions. Since these are also the buffers with lower capacity, this suggests that the

difference is due to the local pH rather than direct interaction with the corrosion layer (Figure 3-11).

As an alternate mechanism for HEPES effect on the corrosion rate, it could be supposed that the negative charges on the deprotonated zwitterions are able to attract, and thus form complexes with, the Mg^{2+} in solution. In theory, this would decrease the concentration of aqueous Mg^{2+} in the vicinity of the corrosion surface, with the change in ionic concentration thus affecting the rate of the corrosion reaction and perhaps also affecting the potential of the Mg^{2+}/Mg redox couple. One of Good's criteria for HEPES was to have low interaction with salts in the solution [19]. The Mg^{2+}-HEPES complexation behaviour was examined by Good by looking for displacement of the titration curves when $MgCl_2$ was added, indicating whether Mg complex formation was competing with H^+. The experiment reported negligible binding in the case of Mg^{2+}, as well as Ca^{2+}, Mn^{2+} and Cu^{2+} [19]. HEPES has been found to form weak complexes with Pb(II) [44]. Others have reported complexation behaviour with HEPES and Cu(II), contrary to Good's original estimations [19].

It is assumed that if HEPES forms a significant complex with Mg^{2+} ions in solution at a pH of 7.4, then the presence of the ion will affect the nearby protons on the HEPES molecule and cause a change in observed chemical shift for those protons. The change in chemical shift observed will be the weighted average of the complex and the free ligand. Thus, a larger change is indicative of greater proportion of the HEPES complex at any given time. Based on the work of Sokolowska *et al.* [42], the complex formation with a divalent metal ion is assumed to be nearest to the proton NMR peaks near 3.8 ppm. Chemical shift due to protons away from the coordination site remained constant with varying Mg^{2+} concentration. This indicates the changes at relevant peaks are due to complex interaction. The changes in the chemical shifts of the relevant peaks are compared in Figure 3-17. At lower $MgCl_2$ concentrations (*i.e.* 1 to 25 mM), the trends indicate some interaction with increased $MgCl_2$ although the chemical shifts are small and lie within the uncertainty of the experiments. This observation suggests Good *et al.* were correct in assuming that HEPES has no significant interaction with Mg^{2+} at the levels typically seen in cell cultures. However, a significantly larger chemical shift in the peak energy level is apparent at a $MgCl_2$ concentration of 100 mM (Figure 3-17). This may be evidence of a small equilibrium constant for the complex, which for low concentrations of $MgCl_2$ comparatively little complex formation exists in solution and is difficult to detect with NMR. However, the concentration of the complex in solution

will increase with increasing concentrations of Mg^{2+} in accordance with Le Chatelier's principle. Moreover, actively corroding Mg is not at equilibrium. As the process occurs, the local concentration of Mg^{2+} near the substrate of corroding Mg is expected to be much higher than that found in the plasma of the human body.

The corrosion rate of magnesium in a specific medium is directly related to the type of passivation layer formed [6]. The passivation layer may consist of $Mg(OH)_2$, $MgCO_3$ or other compounds and will exist in equilibrium with the magnesium ion concentration in the medium. However, if a complex forms between Mg^{2+} and HEPES, this effectively removes Mg^{2+} from solution, changing the equilibrium conditions with the protective coating. Furthermore, the presence of the complex will affect the redox potential. As the passivation layer decreases, more bare metal is exposed to solution, and the corrosion rate can increase. The relationship is shown in Equation 3-6. The magnesium compound MgX (where X is $(OH)_2$, CO_3, or other anion) equilibrium is affected by the interaction between Mg^{2+} and the HEPES molecule to for a complex between Mg and the deprotonated HEPES ligand (L). As such, the interactions with the HEPES molecules may become more important, and may no longer be negligible.

$$MgX \rightleftharpoons X + Mg^{2+} + HEPES \rightleftharpoons MgL \qquad \text{Equation 3-6}$$

For this study, the NMR results show shifts that qualitatively indicate a complex may be formed (Figure 3-17). The equilibrium constant remains unknown, although the magnitude of the chemical shifts and the titration experiments by Good would indicate it is quite small. Quantification of this effect on corrosion is difficult to separate from other factors, but since the interactions are small, the pH and the resulting passivation layers seem to account for the corrosion changes between HEPES and other buffers. As such, if proper care is taken to understand the passivation layer properties, HEPES will be a suitable buffer for the assessment of corrosion protective coatings *in vitro*.

The HEPES buffer may be used to effectively control the pH. Compared to a carbonate buffer, buffer capacity is higher and calcium phosphate deposition is lower. These lead to faster observed corrosion rates in HEPES [40]. Additionally, it is shown that the corrosion rate of Mg is higher in solutions containing these ions. This is due to the lower local pH due to the effect of the buffer. Furthermore, although at concentrations of magnesium near *in*

vivo levels the interaction between HEPES and Mg is small, higher concentrations show shifts in the NMR spectra than may correspond to an interaction or complex between these two species. During corrosion, this may have an effect on the mechanism and rates and should be considered when doing experiments in this buffer solution where either very high concentrations of HEPES are used and/or large amounts of Mg^{2+} ions will be collected in solution. For these cases, further experiments to quantify this effect may be necessary.

3.9. Recommendations on Buffer Usage for *in vitro* Tests

The results from the electrochemical tests show that a number of these buffers are suitable for Mg corrosion studies. All of the buffer systems have their own properties, and therefore some are more desirable than others. HCO_3 stands out as the obvious choice for biocorrosion studies based on its *in vivo* analogue. However, in practice in the lab, the characteristics of the buffer system vary greatly depending on the *in vitro* SBF choice, and the time of immersion. The role of carbonate in the passive layer at elevated pH coupled with the relatively low buffer capacity and diffusion speed with the atmosphere inside an incubator lead to passivation properties that may not be analogous *in vivo*. Indeed, bicarbonate buffered *in vitro* solutions have slower corrosion rates than observed *in vivo* [41]. More importantly for measuring the protective effects of a coating, the lack of consistency in the corrosion mechanism may make it difficult to accurately determine the absolute corrosion protection provided.

The zwitterionic chemical buffers reported by Good provide a buffer system with higher buffer capacity than HCO_3 without interacting with the corrosion layer. Of these buffers, HEPES has the highest capacity per concentration at pH of 7.4. The electrochemical data shows that the corrosion reactions and layers are consistent enough that there is no compelling reason to choose one of the other buffers over HEPES for these corrosion studies. The wider use of HEPES in the literature for Mg corrosion studies over the other zwitterionic buffers also makes cross study comparisons easier. When the interactions of HEPES with Mg were measured, the complex behaviour was very small at biological concentrations of Mg^{2+} and 25mM HEPES. Larger interaction was detected at high concentrations of Mg. At the corrosion surface, the local ion concentration will be higher than normal. Also, the buffer will keep the pH lower at the surface than HCO_3. The HEPES may therefore cause corrosion

reaction rates faster than what would be expected *in vivo* [14]. With the individual advantages of both HEPES and HCO_3, both are appropriate buffers for *in vitro* corrosion tests. By performing tests in both buffered solutions, the properties and differences of these buffers can be quantified and compared. This will effectively give lower and upper bounds for the expected corrosion rate *in vivo*, and allow greater understanding of the individual contributions of pH, carbonate ion reactions, and passive layer performance of Mg and protective coatings and surface treatments. Therefore, the following studies will make use of both buffer systems for comparative purposes.

3.10. References

1. Park, J.B. and J.D. Bronzino, eds. *Biomaterials Principles and Applications*. 2003, CRC Press: Boca Raton. 250.
2. Ng, W.F., K.Y. Chiu, and F.T. Cheng, *Effect of pH on the in vitro corrosion rate of magnesium degradable implant material.* Materials Science and Engineering: C, 2010. **30**(6): p. 898-903.
3. Kirkland, N.T., N. Birbilis, and M.P. Staiger, *Assessing the corrosion of biodegradable magnesium implants: A critical review of current methodologies and their limitations.* Acta Biomaterialia, 2012. **8**(3): p. 925-936.
4. Zhao, M.-C., M. Liu, G.-L. Song, and A. Atrens, *Influence of pH and chloride ion concentration on the corrosion of Mg alloy ZE41.* Corrosion Science, 2008. **50**(11): p. 3168-3178.
5. Ralston, K.D., G. Williams, and N. Birbilis, *Effect of pH on the Grain Size Dependence of Magnesium Corrosion.* Corrosion, 2012. **68**(6): p. 507-517.
6. Song, G.L. and A. Atrens, *Corrosion Mechanisms of Magnesium Alloys.* Advanced Engineering Materials, 1999.
7. Song, G. and A. Atrens, *Understanding Magnesium Corrosion - A Framework for Improved Alloy Performance.* Advanced Engineering Materials, 2003. **5**(12): p. 837-858.
8. Gray-Munro, J.E. and M. Strong, *The mechanism of deposition of calcium phosphate coatings from solution onto magnesium alloy AZ31.* Journal of Biomedical Materials Research Part A, 2009. **90A**(2): p. 339-350.
9. Boron, W.F. and E.L. Boulpaep, eds. *Medical Physiology*. 2nd ed. 2008, Saunders: New York.
10. Hall, J.E., *Guyton and Hall Textbook of Medical Physiology*. 11th ed. 2010, Amsterdam: Elsevier.
11. Tait, W.S., *An Introduction to Electrochemical Corrosion Testing for Practicing Engineers and Scientists*. 1994: PairODocs Publications.

12. Kirkland, N.T., J. Lespagnol, N. Birbilis, and M.P. Staiger, *A survey of bio-corrosion rates of magnesium alloys.* Corrosion Science, 2010. **52**(2): p. 287-291.

13. Helgason, C.D. and C.L. Miller, *Basic Cell Culture Protocols*. 3rd ed. Methods in Molecular Biology, ed. J.M. Walker. Vol. 290. 2005, Totowa, NJ: Humana Press. 384.

14. Yamamoto, A. and S. Hiromoto, *Effect of inorganic salts, amino acids and proteins on the degradation of pure magnesium in vitro.* Materials Science and Engineering: C, 2009. **29**(5): p. 1559-1568.

15. Xu, L., F. Pan, G. Yu, L. Yang, E. Zhang, and K. Yang, *In vitro and in vivo evaluation of the surface bioactivity of a calcium phosphate coated magnesium alloy.* Biomaterials, 2009. **30**(8): p. 1512-1523.

16. Song, Y., S. Zhang, J. Li, C. Zhao, and X. Zhang, *Electrodeposition of Ca-P coatings on biodegradable Mg alloy: In vitro biomineralization behavior.* Acta Biomaterialia, 2010. **6**(5): p. 1736-1742.

17. Shi, P., W.F. Ng, M.H. Wong, and F.T. Cheng, *Improvement of corrosion resistance of pure magnesium in Hanks' solution by microarc oxidation with sol-gel TiO2 sealing.* Journal of Alloys and Compounds, 2009. **469**(1-2): p. 286-292.

18. Chen, Y., Y. Song, S. Zhang, J. Li, C. Zhao, and X. Zhang, *Interaction between a high purity magnesium surface and PCL and PLA coatings during dynamic degradation.* Biomedical Materials, 2011. **6**: p. 025005-025005.

19. Good, N.E., G.D. Winget, W. Winter, T.N. Connolly, S. Izawa, and M.M. Singh, *Hydrogen Ion Buffers for Biological Research.* Biochemistry, 1966. **5**(2): p. 467-477.

20. Chen, S., S. Guan, B. Chen, W. Li, J. Wang, L. Wang, S. Zhu, and J. Hu, *Corrosion behavior of TiO2 films on Mg–Zn alloy in simulated body fluid.* Applied Surface Science, 2011. **257**(9): p. 4464-4467.

21. Meng, E.C., S.K. Guan, H.X. Wang, L.G. Wang, S.J. Zhu, J.H. Hu, C.X. Ren, J.H. Gao, and Y.S. Feng, *Effect of electrodeposition modes on surface characteristics and corrosion properties of fluorine-doped hydroxyapatite coatings on Mg-Zn-Ca alloy.* Applied Surface Science, 2011. **257**(11): p. 4811-4816.

22. Zhao, L., C. Cui, Q. Wang, and S. Bu, *Growth characteristics and corrosion resistance of micro-arc oxidation coating on pure magnesium for biomedical applications.* Corrosion Science, 2010. **52**(7): p. 2228-2234.

23. Liu, G.Y., J. Hu, Z.K. Ding, and C. Wang, *Bioactive calcium phosphate coating formed on micro-arc oxidized magnesium by chemical deposition.* Applied Surface Science, 2011. **257**(6): p. 2051-7.

24. Wei, Z., H. Du, and E. Zhang, *The formation mechanism and biocorrosion property of CaSiO3/CaHPO4 · 2H2O composite conversion coating on the extruded Mg-Zn-Ca alloy for bone implant application·.* Surface and Interface Analysis, 2011. **43**: p. 791-794.

25. Chen, X.B., N. Birbilis, and T.B. Abbott, *A simple route towards a hydroxyapatite-Mg(OH)2 conversion coating for magnesium.* Corrosion Science, 2011. **53**(6): p. 2263-2268.

26. Salunke, P., V. Shanov, and F. Witte, *High purity biodegradable magnesium coating for implant application.* Materials Science and Engineering: B, 2011. **176**(20): p. 1711-1717.

27. Keim, S., J.G. Brunner, B. Fabry, and S. Virtanen, *Control of magnesium corrosion and biocompatibility with biomimetic coatings.* Journal of Biomedical Materials Research - Part B Applied Biomaterials, 2011. **96 B**(1): p. 84-90.

28. Kannan, M.B. and L. Orr, *In Vitro mechanical integrity of hydroxyapatite coated magnesium alloy.* Biomedical Materials, 2011. **6**(4): p. 045003 (11 pp.)-045003 (11 pp.).

29. Waterman, J., A. Pietak, N. Birbilis, T. Woodfield, G. Dias, and M.P. Staiger, *Corrosion resistance of biomimetic calcium phosphate coatings on magnesium due to varying pretreatment time.* Materials Science and Engineering: B, 2011. **176**(20): p. 1756-1760.

30. Desmarais, W.T., D.L. Bienvenue, K.P. Bzymek, R.C. Holz, G.A. Petsko, and D. Ringe, *The 1.20 Å Resolution Crystal Structure of the Aminopeptidase from Aeromonas proteolytica Complexed with Tris: A Tale of Buffer Inhibition.* Structure, 2002. **10**(8): p. 1063-1072.

31. Illingworth, J.A., *A common source of error in pH measurements.* Biochemical Journal, 1981. **195**(1): p. 259-262.

32. Chun-Yan, Z., Z. Rong-Chang, L. Cheng-Long, and G. Jia-Cheng, *Comparison of calcium phosphate coatings on Mg-Al and Mg-Ca alloys and their corrosion behavior in Hank's solution.* Surface and Coatings Technology, 2008. **204**(21-22): p. 3636-3640.

33. Cui, X., Y. Yang, E. Liu, G. Jin, J. Zhong, and Q. Li, *Corrosion behaviors in physiological solution of cerium conversion coatings on AZ31 magnesium alloy.* Applied Surface Science, 2011. **257**(23): p. 9703-9709.

34. Hu, J., C. Zhang, B. Cui, K. Bai, S. Guan, L. Wang, and S. Zhu, *In vitro degradation of AZ31 magnesium alloy coated with nano TiO 2 film by sol-gel method.* Applied Surface Science, 2011. **257**(21): p. 8772-8777.

35. Lei, T., C. Ouyang, W. Tang, L.-F. Li, and L.-S. Zhou, *Enhanced corrosion protection of MgO coatings on magnesium alloy deposited by an anodic electrodeposition process.* Corrosion Science. **52**(10): p. 3504-3508.

36. Ping, L., L. Yin, G. Meiqing, F. Haidong, and X. Xinhua, *Corrosion and drug release properties of EN-plating/PLGA composite coating on MAO film.* Materials Science & Engineering: C (Materials for Biological Applications), 2011. **31**(7): p. 1285-9.

37. Zhang, C.Y., J.C. Gao, and C.L. Liu. *Effect of fluoride treatment on corrosion property of AZ31 magnesium alloy in Hank's solution*. 2011. Changsha, China: Trans Tech Publications.

38. Stellwagen, E., J.D. Prantner, and N.C. Stellwagen, *Do zwitterions contribute to the ionic strength of a solution?* Analytical Biochemistry, 2008. **373**(2): p. 407-409.

39. Warrel, D.A., *Oxford Textbook of Medicine*. 4 ed, ed. T.M. Cox, J.D. Firth, and E.J. Benz Jr. Vol. 3. 2003, New York: Oxford University Press.

40. Kirkland, N., J. Waterman, N. Birbilis, G. Dias, T. Woodfield, R. Hartshorn, and M. Staiger, *Buffer-regulated biocorrosion of pure magnesium.* Journal of Materials Science: Materials in Medicine, 2012. **23**(2): p. 283-291.

41. Willumeit, R., J. Fischer, F. Feyerabend, N. Hort, U. Bismayer, S. Heidrich, and B. Mihailova, *Chemical surface alteration of biodegradable magnesium exposed to corrosion media.* Acta Biomaterialia, 2011. **7**(6): p. 2704-2715.

42. Sokolowska, M. and W. Bal, *Cu(II) complexation by "non-coordinating" N-2-hydroxyethylpiperazine-N'-2-ethanesulfonic acid (HEPES buffer).* Journal of Inorganic Biochemistry, 2005. **99**(8): p. 1653-1660.

43. Xin, Y. and P.K. Chu, *Influence of Tris in simulated body fluid on degradation behavior of pure magnesium.* Materials Chemistry and Physics, 2010. **124**: p. 33-35.

44. Soares, H.M.V.M. and P.C.F.L. Conde, *Electrochemical investigations of the effect of N-substituted aminosulfonic acids with a piperazinic ring pH buffers on heavy metal processes which may have implications on speciation studies.* Analytica Chimica Acta, 2000. **421**(1): p. 103-111.

CHAPTER 4: Biomimetic Calcium Phosphate Coatings

4.1. Introduction

4.1.1. Calcium Phosphates

The necessary requirement for using Mg as a biodegradable implant is to control the rapid corrosion of such an implant in the aggressive *in vivo* environment [1, 2]. Surface modifications (e.g. coatings) that are able to reduce corrosion rates to acceptable levels while remaining biocompatible can provide a solution. Calcium phosphates (CaP) occur naturally as minerals in bone tissue. For this reason, CaPs have been studied extensively for orthopaedic applications as coatings to increase the cellular response to titanium (Ti) implants [3]. Calcium phosphate coatings also help to increase the implant integration into the bone [4, 5].

For magnesium, it follows that a CaP coating will be biocompatible, as they are on Ti [4-6]. And indeed, studies on CaP coated Mg alloys show an increase in biocompatibility and osteoconductivity [7]. Unlike Ti, Mg needs a coating that will also protect the subsurface from corrosion. CaPs are fairly insoluble in physiological conditions [3], and are thus able to be used for corrosion protection. Using different CaP coatings to slow corrosion of magnesium is an area of active research [7-12].

CaP can take many different forms, each with their own properties. Some relevant calcium phosphate phases that can form in solution and their properties are listed in Table 4-1. Monocalcium phosphate (MCPM) is too water soluble to be found in bone [3]. Dicalcium phosphate dihydrate (DCPD) is slightly more stable, and will start to precipitate in aqueous solutions at pH ~4-5.5. While it is still fairly soluble at physiological conditions, it may be beneficial as a bioresorbable implant because DCPD is an intermediate phase in bone mineralization [13]. Similarly, octacalcium phosphate (OCaP) plays a role in biomineral formation [14]. The mineral component of bone itself is carbonated calcium deficient apatite (CDA) [15]. CDA is similar in structure to hydroxyapatite (HA) but with lacunae in the lattice. In bone, substitutions of carbonate and non-apatitic phosphate break up the crystal

structure [16, 17]. These substitutions play a vital role in increasing the activity and solubility of the bone for its formation and dissolution [18]. HA is the most stable and least soluble CaP with the exception of fluorapatite. HA is often the choice for coating Ti implants, where the coating is intended to be permanent [19-21]. For bioresorbable implants stoichiometric HA is not necessarily desirable as the goal is to have a coating that can be degraded by the body to allow bone to replace the implant.

Table 4-1: Calcium phosphate properties

Calcium Phosphate	**Abbrev.**	**Chemical Formula**	**Ca/P Ratio**	**Solubility ($-\log(K_S)$)**
Monocalcium Phosphate monohydrate	MCPM	$Ca(H_2PO_4)_2 \cdot H_2O$	0.5	1.14
Monocalcium Phosphate anhydrous	MCPA	$Ca(H_2PO_4)_2$	0.5	1.14
Dicalcium phosphate dihydrate (brushite)	DCPD	$CaHPO_4 \cdot 2H_2O$	1.0	6.59
Dicalcium phosphate anhydrous (monetite)	DCPA	$CaHPO_4$	1.0	6.90
Octacalcium phosphate	OCaP	$Ca_8(HPO_4)_2(PO_4)_4 \cdot 5H_2O$	1.33	96.6
Calcium deficient apatite	CDA	$Ca_{10-x}[]_x(HPO_4)_x(PO_4)_{6-x}(OH)_{2-x}[]_x$ $(0<x<2)$	1.33-1.66	Variable, ~85
Amorphous Calcium Phosphate	ACP	$Ca_x(HPO_4)_y(PO_4)_z(OH)_2 \cdot nH_2O$ n = 3.0-4.5	1.2-2.2	25.7-32.7
Hydroxyapatite	HA	$Ca_{10}(PO4)_6(OH)_2$	1.67	116.8

Values as given in [3]
Solubility is estimated at 25° C
[] represent vacancies in the lattice of hydroxyapatite

The composition and structure of the CaP coating will affect the corrosion performance. For example, the degree of crystallinity greatly influences the performance of the CaP *in vivo* [4, 18]. The dissolution rate has been shown to decrease as crystallinity increases [22] and amorphous, glassy phases will be more susceptible to biodegradation [23]. A Mg implant will be expected to degrade fully, and any coating or protection provided must therefore degrade as well. A calcium phosphate coating applied must therefore be soluble enough to degrade away. Highly crystalline HA particles that become loose on Ti particles have been known to cause a foreign body response [24]. Therefore it will be desirable to have a coating that can be completely resorbed by the body. However, the coating must be insoluble enough to provide the necessary corrosion protection. And the coating must be able to be applied to

the Mg implant without damaging the substrate (e.g. exposure to high temperatures during plasma spraying) and without the possibility of including toxic precursors or by-products of the coating process. A method for forming a coating such as this is the biomimetic method.

4.1.1. Biomimetic Coating Method

Though many methods for forming coatings are available (See Chapter 2), the biomimetic method offers the advantages of a simple, low temperature, non-toxic and non line-of-sight process. Biomimetic methods have been studied extensively on Ti implants [4, 6, 15, 25-27]. As such, the biocompatibility is well known. The question that must be answered is whether this coating process can be used effectively on Mg, and how well the coatings will protect the substrate from corrosion.

The biomimetic method is attractive because the simple chemistry employed optimizes the properties needed for the coating [15]. The coating should be just insoluble enough to be stable in the physiological system, without becoming so insoluble they prevent the degradation entirely. Ideally, the formed coating is also similar in composition to biological CaP. The biomimetic method coats the samples by simulating a supersaturated physiological fluid [25]. The ionic composition of this fluid contains the ions found in the body. The coating is performed at body temperature of 37° C. The coating formation is driven by controlling the pH of the solution. The pH is controlled with a CO_2/HCO_3 buffer. The choice of buffer make the use of nonphysiological chemicals unnecessary, thus representing the physiological process as closely as possible. The net result is that all coating parameters are formulated to closely match the physiological conditions. The coatings that form in the biomimetic solution will therefore be similar in properties to the CaP found in natural biominerals. Importantly, if the coatings are stable in the SBF, they should also be stable *in vivo*.

The pH rise during the coating process decreases the solubility of the calcium and phosphate ions in solution, leading to heterogeneous nucleation of CaP on the substrate. Figure 4-1 shows a calculated fractional diagram for calcium phosphate formation based on pH. Calcium and phosphate will be dissolved and exist as ions at very low pH. As the pH is increased, the solubility decreases and calcium phosphate solids become more stable, leading to nucleation of various phases [3]. As the pH increases, the stability of the calcium

phosphate phase increases as well. The biomimetic method brings the pH up to just above the physiological pH of 7.4. The final coating will not be pure HA as predicted by Figure 4-1. The additional ions besides Ca^{2+} and PO_4^{3-} in the biomimetic coating solution will become incorporated into the final CaP phases that form [25]. Mg ions incorporated into the coating have the effect of disrupting the crystal structure, making it more amorphous [15, 28]. Carbonate ions from the buffer has a similar effect that also increases the solubility of the CaP [15]. This results in the coating with good biocompatibility [29]. The question to be answered is can these coatings be used to coat Mg as well as Ti and can they be used to provide the necessary corrosion protection?

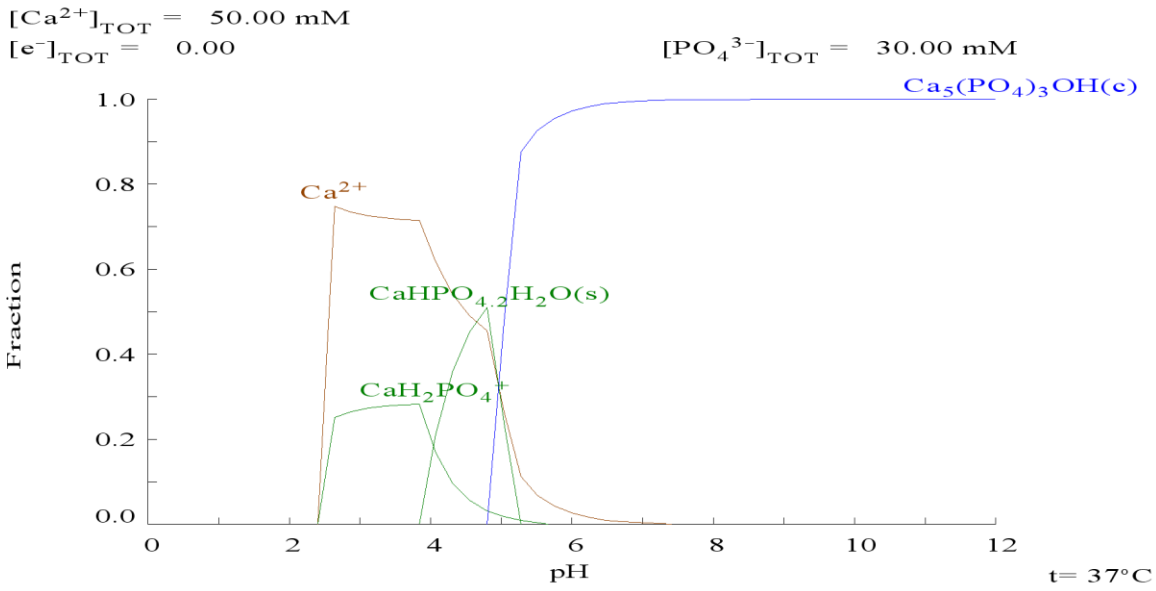

Figure 4-1: Fractional equilibrium diagram for the formation of calcium phosphates as a function of pH.

4.2. Effect of Surface Hydroxide Pretreatment on Biomimetic Formation

4.2.1. The Role of Pretreatment on Biomimetic Calcium Phosphate Nucleation

The nucleation of calcium phosphate compounds on Ti is promoted by titanium hydroxide groups [30]. Other studies have shown alkali pretreatments increase Ti-OH groups on the surface of the TiO_2 layer increase the deposition of calcium phosphates due to the increase in surface energy [31]. Various alkali pretreatments have been developed to form this layer [32-39]. Such treatments increase the deposition of CaP by modifying the natural titanium oxide passivation layer. The increase in surface energy by these treatments help promote heterogeneous nucleation of CaP on the metal surface [31].

Given the role of hydroxide groups on the surface of Ti for biomimetic coating formation, will they also play an important role on Mg? If so, can they be used to optimize the coating process for corrosion resistance? Magnesium in aqueous solutions will readily react with water to form $Mg(OH)_2$ [40]. It is hypothesized that formation of this layer via pretreatment will influence the deposition of the biomimetic CaP film and have a subsequent important effect on corrosion rates *in vitro*. This study was conducted to measure the effect of a magnesium hydroxide pretreatment has on the formation and ultimate corrosion protection of biomimetic calcium phosphate coatings.

4.2.2. Experimental Methods

4.2.2.1. Pretreatments

Pure Mg (99.98% pure, Timminco Inc., Toronto, Canada) and pure Ti was cut into 15 × 15 × 5 mm samples and polished to 1200 grit using successive SiC papers. Samples were ultrasonically cleaned in ethanol for 2 minutes and air dried. Pretreatments were done in distilled H_2O, or NaOH solutions at 100°C. Pretreatment samples were treated in pure H_2O for 0, 15, or 30 minutes or 1M NaOH for 15 or 30 minutes to form a $Mg(OH)_2$ layer. Following pretreatment samples were rinsed with distilled water and allowed to dry in air.

4.2.2.2. Biomimetic Coating

Biomimetic coatings were performed on substrates in concentrated simulated body fluid (SBF). Samples were coated using a modification of the process described by Habibovic et al. [25]. This used two modified SBF solutions with compositions as described in Table 4-2. Both solutions have been modified to reduce chloride ions (Cl^-) to prevent excessive corrosion of Mg during the coating process. Each modified SBF contains ions present in physiological solutions but at higher concentrations to promote CaP formation. The solutions are designed to form a complete, adherent coating. Solution 1 uses a higher concentration of carbonate ions (CO_3^{2-}) to promote amorphous formation of CaP. Solution 2 is low in Mg^{2+} because it is known to inhibit crystalline apatite formation [28, 41]. The pH of the solution was controlled during the process by dissolving carbon dioxide gas (CO_2) in the solution. One litre of Solution 1 was heated to 37 °C and $CO_{2\,(g)}$ was bubbled through for 15 minutes to reach a pH of 6. The CO_2 was then removed, substrates were immersed in the solution, and air was bubbled through the solution for 24 hours. The solution was stirred with a magnetic stirrer to ensure uniform ionic concentrations. After 24 hours the solution pH rose to approximately 9. The samples were removed and rinsed with distilled water. Solution 2 was prepared the same way, at 37 °C and pH of 6 using CO_2. The samples were immersed and air was bubbled through the solution for a further 24 hours. When the treatment was complete samples were removed from the solution, rinsed with ethanol, and allowed to dry in air.

Table 4-2: Chemical composition of coating solutions

Solution 1	**g/L**	**Solution 2**	**g/L**
$CaCl_2$	1.65	$CaCl_2$	1.65
KH_2PO_4	0.3	KH_2PO_4	0.3
$MgSO_4.7H_2O$	1.8	NaCl	7.0
$Na_2HPO_4.4H_2O$	0.4	$Na_2HPO_4.4H_2O$	0.4
$NaHCO_3$	2.27	$NaHCO_3$	0.35

4.2.2.3. Characterization

To study the morphology, coated samples were analyzed with a scanning electron microscope (JEOL 7000F FE-SEM). Samples were sputter coated in gold to prevent charging during analysis. Energy dispersive X-ray spectroscopy (EDS) was performed on separate samples coated with carbon to identify elements present and estimate the calcium to phosphorus ratio. X-ray diffraction (XRD) was performed using a low glancing angle XRD (PANalytical X'Pert-Pro MPD PW3040/60) to identify the crystal structure of the coating. Fourier transform infrared spectroscopy (FTIR) was performed using transmittance FTIR (Perkin Elmer Spectrum One) by mechanically removing the coating and grinding with a mortar to form a mull with NUJOL mineral oil. The mull was placed between two potassium bromide (KBr) plates for analysis.

4.2.3. Surface Treatment for Formation of Biomimetic CaP on Mg

4.2.3.1. The Formation of Biomimetic Coatings on Mg

The biomimetic coating process is designed to promote heterogeneous nucleation of CaP on the surface of the metal as the solution undergoes a pH rise. The first stage of the coating is done to form a carbonate rich layer that covers the surface. This then provides a platform for the deposition of the second layer of the coating [36]. Homogeneous nucleation of CaPs in solution was also observed to occur in the coating solution. Due to the mechanism of deposition on Ti being accelerated by Ti-OH groups at the surface, it was hypothesized that the formation of a similar layer on Mg would promote biomimetic coating on Mg. For biomimetic deposition on Ti, the Ti-OH has a slight negative surface charge when immersed in a solution with a pH of 7.4, i.e. the body [31]. These negatively charged points provide places for positively charged calcium ions to attach to the surface, and thus lead to formation of the apatite layer. This step was observed to be unnecessary for Mg. The biomimetic coating process deposited a CaP coating on the surface of all the Mg substrates, regardless of pretreatment. Figure 4-2 A, B, C shows the formation of calcium phosphates by biomimetic treatment on titanium based on surface treatments. As reported in the literature, the alkali heat treatment is beneficial to nucleation on the surface of the Ti [31]. Figure 4-2 A that the untreated Ti substrate nucleates CaP at a relatively few number of points on the surface.

Once nucleated, the growth of the CaP is preferred on the existing points, leading to large areas of uncovered Ti and a few round CaP clusters. When treated in H_2O for 15 minutes at 100° C, Ti generates more of the surface OH groups that promote apatite deposition [42]. Alkali heat treatment is much more effective, 30 minutes in NaOH forms a calcium hydroxide layer that covers the entire surface (Figure 4-2C) [33, 35, 36].

The biomimetic coating process designed for Ti was successfully employed to coat Mg substrates. The morphology of the final coatings is shown in Figure 4-2 D, E, and F. The Mg samples were coated completely regardless of pretreatment. CaP was detected over the entire surface of the untreated sample (Figure 4-2 D), as well as samples treated with H_2O (E) and NaOH (F). The Mg surface needs very little help to create a surface hydroxide layer that the CaP favors for nucleation in the biomimetic solutions. Mg is very reactive, and thus will oxidize to form $Mg(OH)_2$ on the surface in an aqueous environment even at low temperature [43]. Furthermore, in the Cl^- containing biomimetic solutions, the Mg substrates will corrode. The corrosion of the substrate will form a local pH rise near the surface due to the reduction of H_2O. The elevated pH causes further super saturation of the already concentrated calcium solution. The result is the formation of CaP on the Mg surface [8].

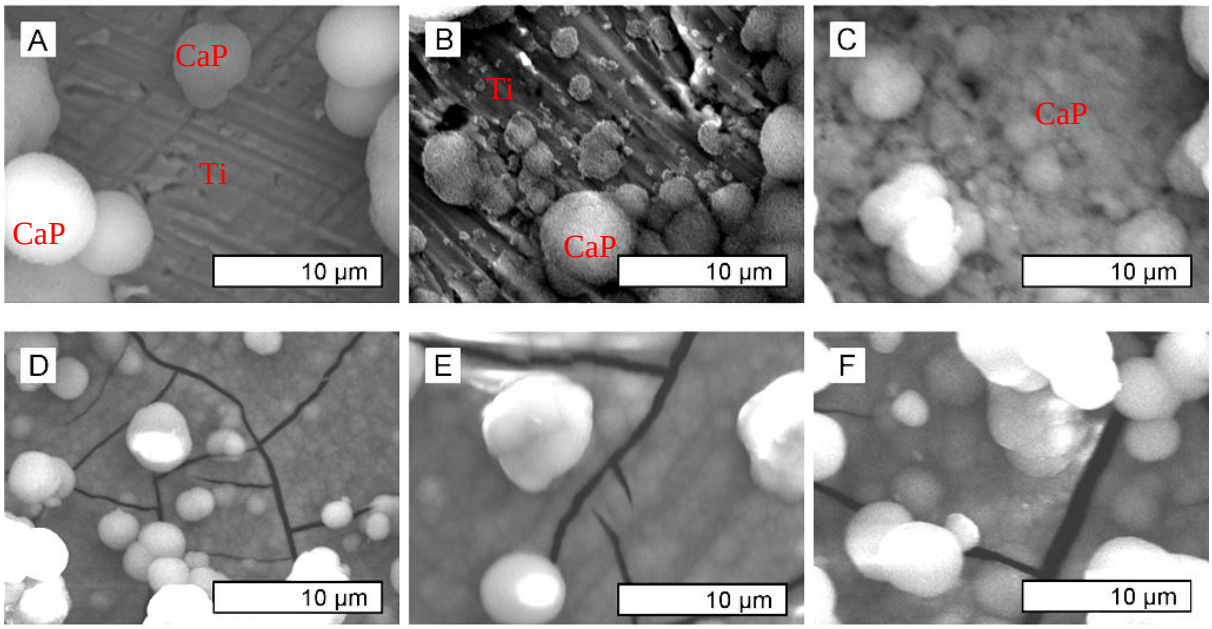

Figure 4-2: Comparison of calcium phosphate nucleation via biomimetic coating on titanium substrates vs Mg substrates for various surface pretreatments. Ti pretreated with A) no treatment, B) 15 minute H_2O, C) 30 minute NaOH then biomimetic coated. Mg pretreated with D) no treatment, E) 15 minute H_2O, F) 30 minute NaOH then biomimetic coated.

4.2.3.2. Effect of Surface Treatment on Coating Morphology

Having established that biomimetic coatings can be easily formed on Mg regardless of pretreatment, the question becomes does pretreatment time and composition significantly change the properties of the created coatings? To investigate this, the morphology of the surface treatments and final coatings was investigated under a SEM. The surface of samples after the pretreatment step, then coating in the first biomimetic solution, and finally after the complete coating after both solutions was examined. Figure 4-3 tables the results. Untreated Mg after polishing is shown in Figure 4-3 A. After 15 minutes of immersion in H_2O at 100° C, needle-like structures of $Mg(OH)_2$ form on the surface, as is typical in aqueous solutions (Figure 4-3 B) [44]. By 30 minutes immersion time, the $Mg(OH)_2$ surface coating has completely covered the Mg surface. In NaOH solutions, the coating was formed even faster. Complete coverage was achieved at both 15 (D) and 30 (E) minutes. The morphology of the layer in NaOH was quite different compared to H_2O. Once the hydroxide layer is complete, this layer is passive under these conditions, meaning that the hydroxide layer protects the substrate from further oxidation [40]. This limits the effect that longer pretreatments will be able to have. Therefore, the study was limited to 30 minutes as the full layer had formed.

After the pretreatments, the Mg samples were immersed into the first biomimetic coating solution. The composition of the solution (Table 4-2) is high in Mg^{2+} and HCO_3^-. The purpose of this is to promote a more amorphous coating structure that will cover the entire surface [26]. This first step of the coating is used on Ti to promote faster deposition of the second, thicker CaP layer [45]. The Mg^{2+} and HCO_3^- inhibit crystalline growth to form a more soluble CaP layer. This layer then acts as a site for nucleation of additional CaP. Furthermore, because it is slightly soluble, the dissolution of this layer in the second biomimetic solution will increase the local ion concentration near the surface and also help to promote the formation of the final layer. Also, the coating solution is modified to be lower in Cl^- than reported in the literature due to the corrosive effect of chloride on Mg [46, 47]. On Mg, all pretreatment samples formed a CaP coating in solution 1 that covered the entire sample (Figure 4-3 F-J). The layer exhibited similar morphology regardless of pretreatment, another indicator that the pretreatment step on Mg is nowhere near as important as it is on Ti.

Large plate-like crystal flakes were present on the top of this coating for all samples. At certain nucleation sites, larger crystals formed at irregular intervals.

Following the coating process in solution 1, the samples were coated in the second biomimetic solution for a further 24 hours to create the final biomimetic coating. The second solution is low in Mg and lower in carbonate in order to lead to a more crystalline and therefore more stable coating. The amount of Cl^- is much higher than solution 1, but the Mg has already been covered by a protective CaP coating that will prevent corrosion while the ultimate coating is formed. The increased NaCl has been shown to increase the coating deposition on the surface of the implant by favouring heterogeneous nucleation at the surface over homogeneous nucleation in the solution [48]. When the samples are coated, the slightly soluble first CaP layer provides nucleation sites for additional CaP deposition [45].

Given the similarities in morphology of the first coating, it is not surprising that the final morphology of the CaP coatings are similar as well (Figure 4-3 K-O). The entire surface of the substrates were covered with the final coating for all pretreatment levels. The coating was not even in thickness, as large round and flake like CaP deposits grew from the surface of this layer as well. A striking feature of the final coating morphology with pretreatment is the number and amount of cracks and defects present after the coating is dried. These types of defects appear on other biomimetic coatings in the literature on titanium substrates [6, 15, 38, 45]. For Ti, the corrosion resistance is not terribly important. However, for Mg the corrosion resistance is the main purpose of the coating. So although the ultimate morphology did not change much with pretreatment, the amount and severity of the defects varied, and this may become important for the corrosion resistance of this style of coating.

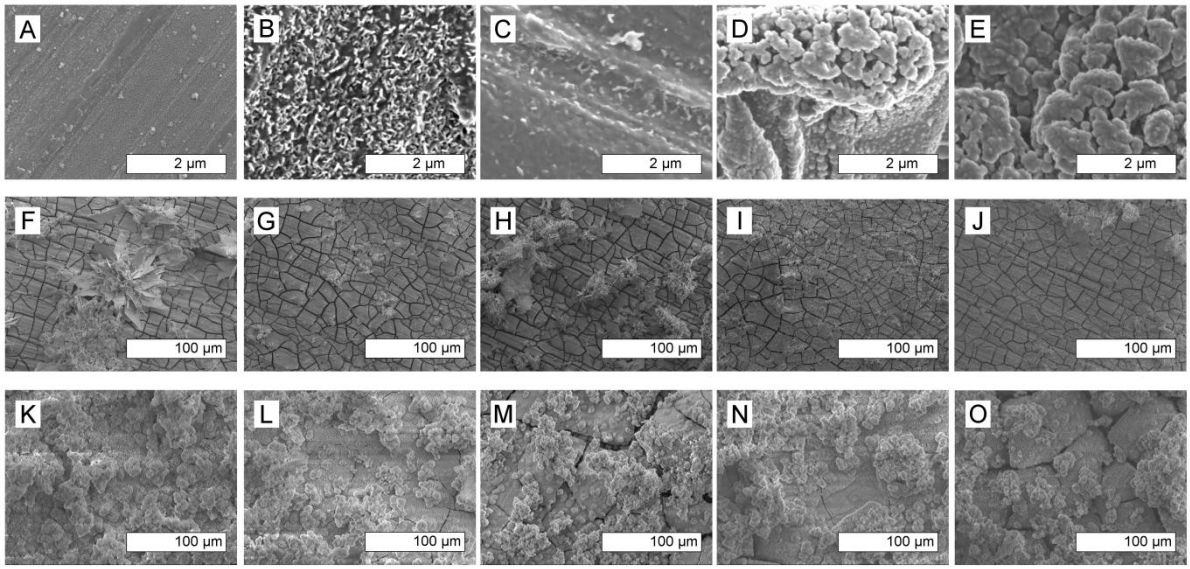

Figure 4-3: Surface morphology for Mg after A) no pretreatment, B) 15 minutes H_2O, C) 30 minutes H_2O, D) 15 minutes NaOH, E) 30 minutes NaOH pretreatment. Surface after biomimetic coating solution 1 applied for F) no pretreatment, G) 15 minutes H_2O, H) 30 minutes H_2O, I) 15 minutes NaOH, J) 30 minutes NaOH pretreatment, and after the full 2 step coating is applied for K) no pretreatment, L) 15 minutes H_2O, M) 30 minutes H_2O, N) 15 minutes NaOH, O) 30 minutes NaOH pretreatment.

4.2.3.3. Pretreatment Effect on Ca/P ratio by EDS

EDS was used to estimate the Ca/P ratio of the coated samples. This was done as a quick method for measuring the differences in composition. EDS is not extremely precise for elemental composition on 3D structures such as the surface of these coatings due to possible edge effects [49]. Therefore, the samples were tested at multiple locations and the averages of the ratios of Ca to P energy peak intensities were collected (Figure 4-4). A more detailed study of the composition of the coatings and their formation is explained below in section 4.3. This comparison was to determine if there was a significant change in the composition based on pretreatment. After the first coating step, the Ca/P ratio of the created coating was quite low. The high amount of Mg^{2+} and CO_3^{2-} in solution promoted deposition of a substituted, calcium deficient CaP structure [15, 28].

Once the second coating was applied, the Ca/P ratio was higher. This was as expected due to the nature of the solution. Solution 2 contained no Mg and a much smaller amount of carbonate. This should promote the deposition of a more insoluble calcium phosphate compound. Figure 4-4 shows that after the second coating is applied, the Ca/P ratio observed

were within the instrument error for EDS. It can thus be concluded that the pretreatment has little effect on the ultimate Ca/P ratio of the final coating.

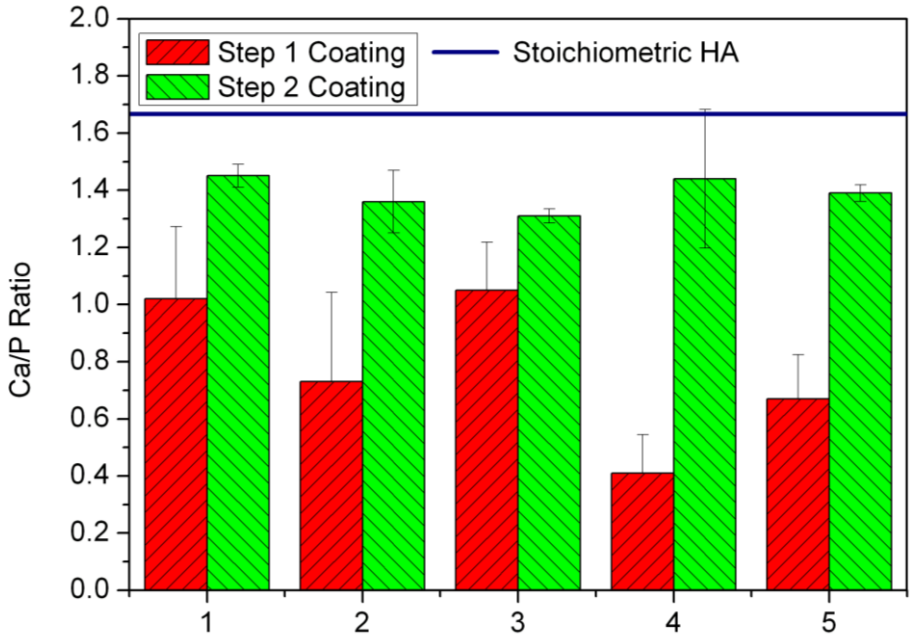

Figure 4-4: Calcium to phosphorous ratio by EDS of coated Mg samples after coating in biomimetic solution 1 and then solution 2. 1) No pretreatment, 2) 15 minutes H2O, 3) 30 minutes H2O, 4) 15 minutes NaOH, 5) 30 minutes NaOH.

4.3. Pretreatment Effect on Coating Characteristics on Mg

To further investigate the compositional and formation effects of the coatings, the H_2O pretreatments were subjected to further tests. Because the composition by EDS and the morphology was very similar, the study was limited to Mg with no pretreatment (designated Mg 0), pretreated in H_2O at 100° C for 15 minutes (Mg 15) and 30 minutes (Mg 30). These were chosen to represent the range of no initial hydroxide layer to a fully formed layer that coats the entire surface (Figure 4-3 A-C). The differences in biomimetic coatings that form will help determine what, if any change the pretreatment has on the composition.

For magnesium substrates, the greatest increase in mass after the coating process was observed for the untreated Mg 0, and decreased with increasing pretreatment time (Figure 4-5). The formation of these groups is not nearly as critical on Mg as it is on Ti, as Mg is much more reactive, and will readily react to form $Mg(OH)_2$ in aqueous solutions [47].

Pretreatment to form this layer is therefore not necessary, and may not even be beneficial for coating formation. In this case, greater final coating mass corresponded with less surface treatment. By observing the SEM morphology of the coating, it is clear that the coatings contain numerous defects, and part of the coating may be flaking off in the coating solution instead of remaining on the substrate. Low adhesion is a commonly reported property of biomimetic coatings, but can be increased by modifying the surface roughness [15, 32]. From SEM observation crack density and size was found to increase with longer surface treatment. Thus it appears that although a longer pretreatment period may promote CaP nucleation, it might subsequently result in a lower adhesion of the coating as a whole, resulting in parts of the coating flaking off in solution and a decrease in total coating mass at the end of the process.

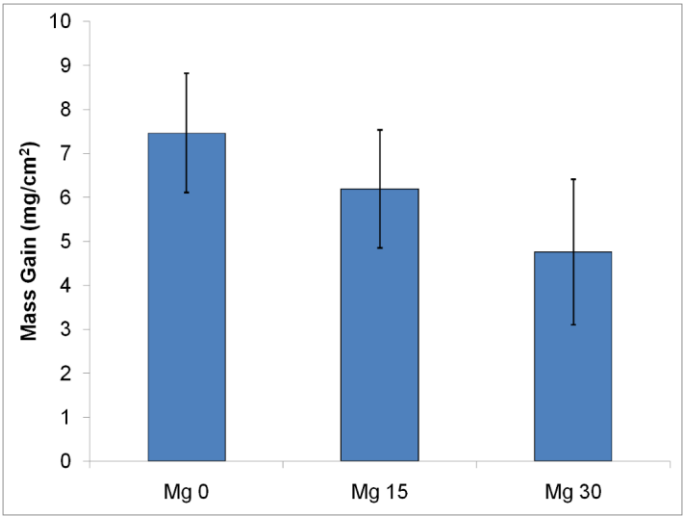

Figure 4-5: Mass change after biomimetic coating.

XRD shows peaks matching calcium phosphate compounds. The structure was not a single phase, as detected by fitting to available powder diffraction files. Peaks close to values for calcium deficient apatite were observed on samples at 2θ near 26 and 32 degrees (Figure 4-6) [50]. Additional peaks suggest DCPD [51], calcium magnesium carbonates [52], or other calcium phosphates may be present. For uncoated Mg, the XRD scan did not detect all of the peaks expected from the powder diffraction file [53]. The reason for this may be that the sample does not necessarily meet the requirements for good powder diffraction. Specifically, they may not meet the requirement for small, randomly oriented crystals [49]. The Mg substrate was taken from a cast ingot with fairly large grain size. As such, the XRD of the pure Mg misses some of the peaks. The limitations of this method also can apply to the

coated samples, as there may be some directionality to the CaP phases formed on the surface. Also, the wide peaks denote low crystallinity, and shifted peaks are indicative of lattice substitutions by other ions [15].

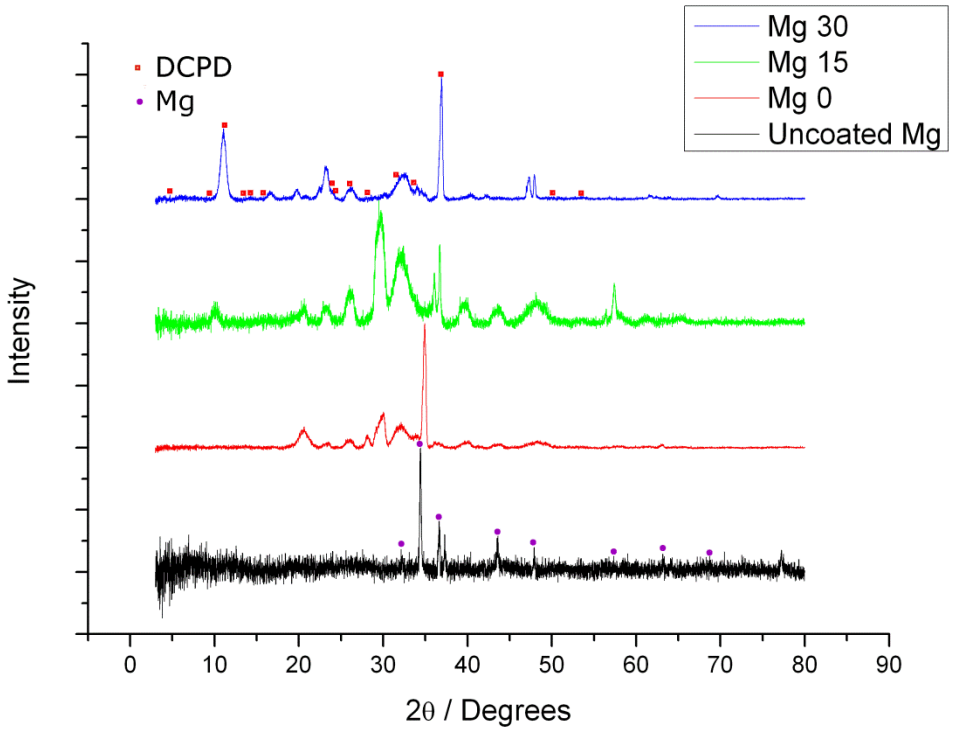

Figure 4-6: XRD of biomimetic coated samples Mg 0, Mg 15, and Mg 30.

The calcium to phosphate ratio, as measured by EDS, was found to be below that of the stoichiometric HA. As previously mentioned, this is due to substitutions in the lattice. In the apatite lattice, calcium can be replaced by small amounts of magnesium and sodium, and phosphates can be replaced by carbonate ions [25]. During the biomimetic coating process, these ions were incorporated into the coating. Mg is found to be present in significant quantities due to the corrosion of the substrate during the coating process. This is mostly due to the Cl^- ions which are present in solution. The corrosion mechanism of magnesium in physiological fluid is strongly related to the presence of chloride ions, which destroy the passivation layer of $Mg(OH)_2$ [40, 54, 55]. Removing all of the chloride ions from the coating solutions may help to slow the corrosion, and limit the amount of Mg that makes its way into the coating. Substitutions and interstitial Mg in the lattice affects the growth of the CaP crystal structure [15, 28]. The Mg present in the lattice inhibits the growth of crystalline

apatite. FTIR results confirm carbonate in the lattice, identified by the presence of C-O bonds, identified at 1420 and 875 cm^{-1} (Figure 4-7) [3]. Carbonate has a similar effect of breaking up and distorting the crystal structure, as well as allowing possible phase additions of calcium carbonate ($CaCO_3$). From a biomimetic coating standpoint, these additions are desirable to simulate natural bone, which is not pure crystalline HA [15]. However, from the perspective of corrosion, these phases are more soluble in solution, and therefore may provide less protection. The next step is therefore to measure the corrosion rate of these coatings *in vitro*.

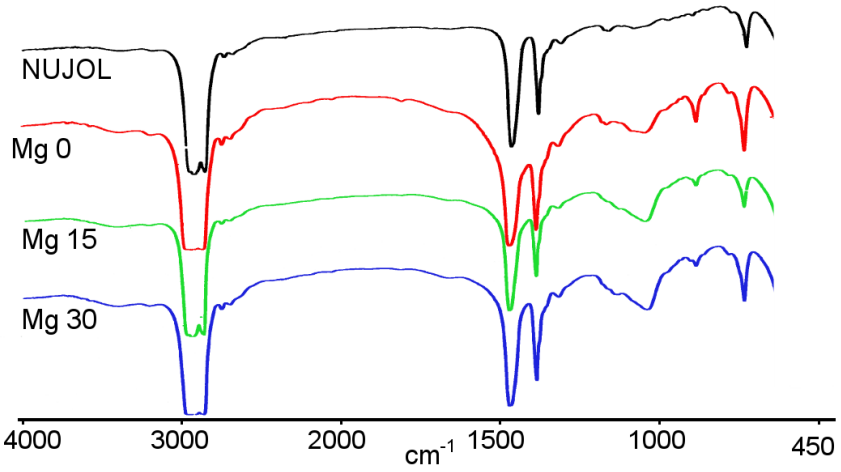

Figure 4-7: FTIR of biomimetic coated samples Mg 0, Mg 15, and Mg 30.

4.4. Corrosion Protection vs. Pretreatment

4.4.1. Corrosion Testing

4.4.1.1. Electrochemical Methods

Electrochemical tests were carried out to measure the corrosion rate. Experiments were carried out in 0.8% NaCl and Hanks' Balanced Salt Solution (HBSS) at 37°C ± 0.5 °C and pH of 7.4 ± 0.05, buffered with 4-(2-hydroxyethyl)-1-piperazineethanesulfonic acid (HEPES) (25mM). 300 mL of solution was used per test. The area of the working electrode was 1 cm^2. Potentiodynamic polarization (PDP) and electrochemical impedance spectroscopy (EIS) tests were performed. A three electrode setup was used with a Pt counter electrode and a saturated calomel reference electrode (SCE). PDP tests were carried out after 20 minutes in solution to

allow the open circuit potential to stabilize. PDP tests utilized a scan rate of 1 mV/s, and scanned over the range OCP – 0.100 V to Ref + 0.500 V. EIS scans were performed every 30 min over a period of 24 hours to evaluate the change in corrosion resistance with time. A 10mV peak to peak signal from OCP across a frequency range from 50 kHz to 20 mHz.

4.4.1.2. Corrosion Properties of the Pretreatment Alone

When exposed to H_2O, the surface of the Mg metal oxidizes to form a passive layer of $Mg(OH)_2$ [43]. Pretreatment in H_2O at 100°C provided a $Mg(OH)_2$ layer for the coatings to form on. The pretreatment morphology of the $Mg(OH)_2$ on surface is shown in Figure 4-3 A B and C. Untreated Mg is referred to as Mg 0, treatment in H_2O for 15 minutes is labelled Mg 15, and Mg 30 is 30 minutes of treatment. After 15 minutes in the pretreatment bath, the morphology of the hydroxide layer grows into a flake like structure. By 30 minutes of immersion, the magnesium hydroxide has grown into a dense layer covering the sample completely. While this hydroxide layer is passive at high pH or low Cl^- levels [47], the effect on corrosion at physiological pH needs to be measured to determine if the pretreatment layer contributes to the corrosion resistance of the final biomimetic coating.

To determine the effect of the pretreatment layer on corrosion resistance, samples were tested in 0.8% NaCl solution using EIS over 24 hours. Figure 4-8 shows the total film resistance of each group of samples. The error bars represent ± 1 standard deviation. Significant differences in the corrosion resistance were not observed. Mg 0 and Mg 15 were very similar, while Mg 30 had slightly less resistance, though not significantly so, than the other samples. This was expected as $Mg(OH)_2$ is very soluble in Cl^- containing solutions [40]. This demonstrated that the pretreatment layer did not itself significantly contribute to the corrosion resistance of the final coating. Any differences, therefore, can be attributed to the calcium phosphate coating.

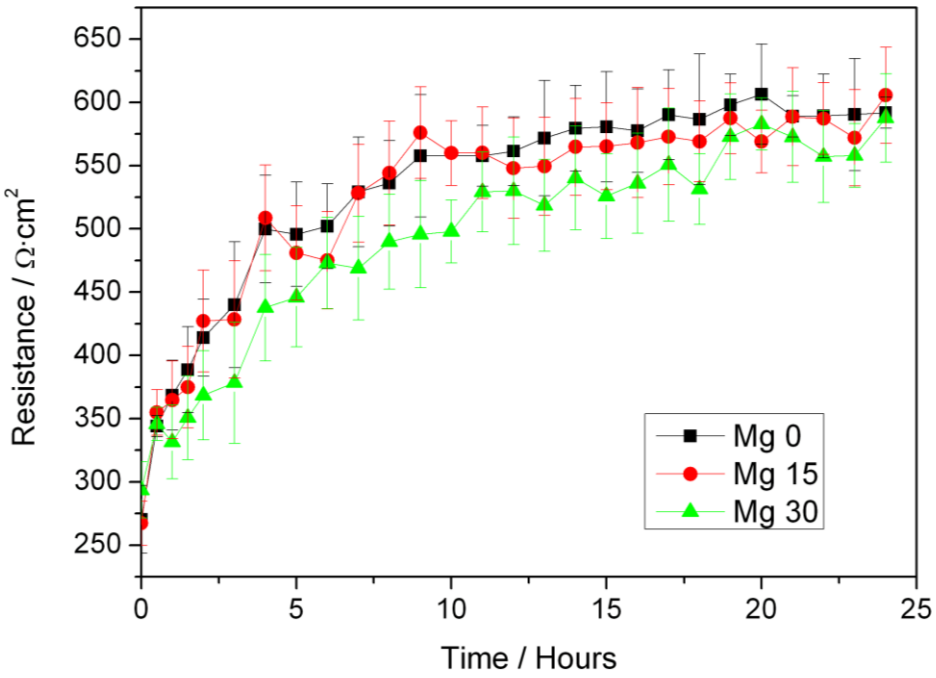

Figure 4-8: Polarization resistance of uncoated Mg samples with applied H_2O treatments in NaCl.

4.4.2. Biomimetic Coatings Corrosion Protection in NaCl and HBSS

4.4.2.1. Polarization Behaviour

PDP displayed a decrease in corrosion current density (i_{Corr}) for all coated samples (Figure 4-9). Tafel-type analysis was performed on the linear regions of the plot, using the Tafel slopes from between 50 and 250 mV away from the corrosion potential, to provide an approximation of the corrosion current density (Table 4-3). The overall corrosion rate drops due to the calcium phosphate coating. The coating decreases the available surface area susceptible to corrosion. The lowest corrosion current density from the Tafel-type fit was observed on samples with no pretreatment. These also displayed the greatest gain in mass after the coating process. It therefore makes sense that initially they will provide the greatest corrosion protection. The CaP phases present here should be fairly insoluble under these conditions [3, 15], however phases containing carbonates will be more soluble than HA for example, and may contribute to the decreasing corrosion protection of the coating. More importantly, the corrosion reactions continue through the defects and cracks in the layer. The greater amount of physical defects in pretreated samples, as seen in Figure 4-3 L and M, show higher corrosion current densities than the sample with no pretreatment.

All of the biomimetic coatings reduced both the cathodic and anodic reactions of the Mg. The greatest reduction in the reactions was observed on Mg 0, the sample with no pre-treatment. Mg 15 reduced the cathodic reaction nearly as much as Mg 0, but the anodic reaction was considerably higher. This is an indicator that there are defects in the coating that allow corrosion to occur, leading to the dissolution of the Mg. Mg 30 had the largest cathodic kinetics, suggesting the coating was porous enough to allow the diffusion of water to the sites, but the coating provided enough coverage to slow the anodic kinetics considerably. The PDP can give an initial estimate of the corrosion behaviour, but does not show changes in behaviour over time. Anodic polarisation of the samples during PDP can cause significant corrosion to take place on the Mg, meaning each sample can only be accurately tested once. Therefore, in order to evaluate the changes in corrosion properties over time, EIS was used.

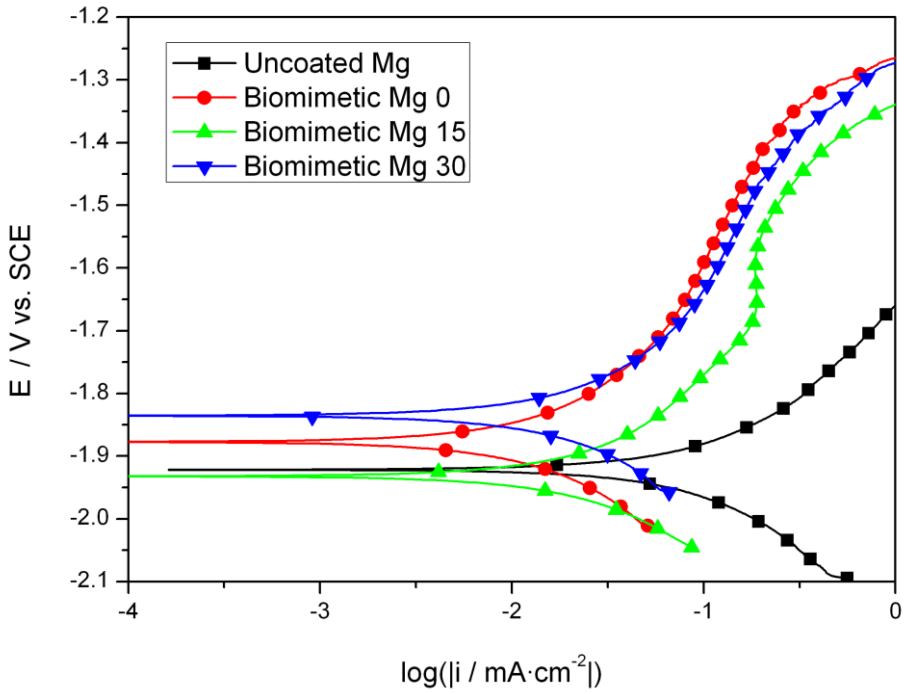

Figure 4-9: Polarization of biomimetic coatings in HBSS.

Table 4-3: corrosion values obtained by electrochemical analysis

Sample	E_{Corr} (V)	i_{Corr} HBSS PDP ($\mu A/cm^2$)	R_P NaCl Initial ($\Omega \cdot cm^2$)	R_P HBSS Initial ($\Omega \cdot cm^2$)	R_P NaCl 24 h ($\Omega \cdot cm^2$)	R_P HBSS 24 h ($\Omega \cdot cm^2$)
Uncoated Mg	-1.921	62.6	270	249	591	885
Mg 0	-1.877	10.9	2961	2935	1370	2446
Mg 15	-1.931	16.8	1952	2109	780	2502
Mg 30	-1.835	12.7	2524	2023	845	3657

4.4.2.2. Polarization Resistance

EIS was performed in both NaCl and HBSS solution to identify the coating corrosion properties over a period of 24 hours. Corrosion resistance was estimated by fitting an equivalent circuit to the Nyquist plots of the frequency response. The change in the corrosion resistance over time was then plotted in NaCl (Figure 4-10) and in HBSS (Figure 4-11). Representative Nyquist plots in NaCl and HBSS for 1 and 24 hours are shown in Figure 4-12. The morphology of the coating of each sample is compared to the damage sustained due to corrosion in HBSS after the 24 hour EIS tests is shown in Figure 4-13.

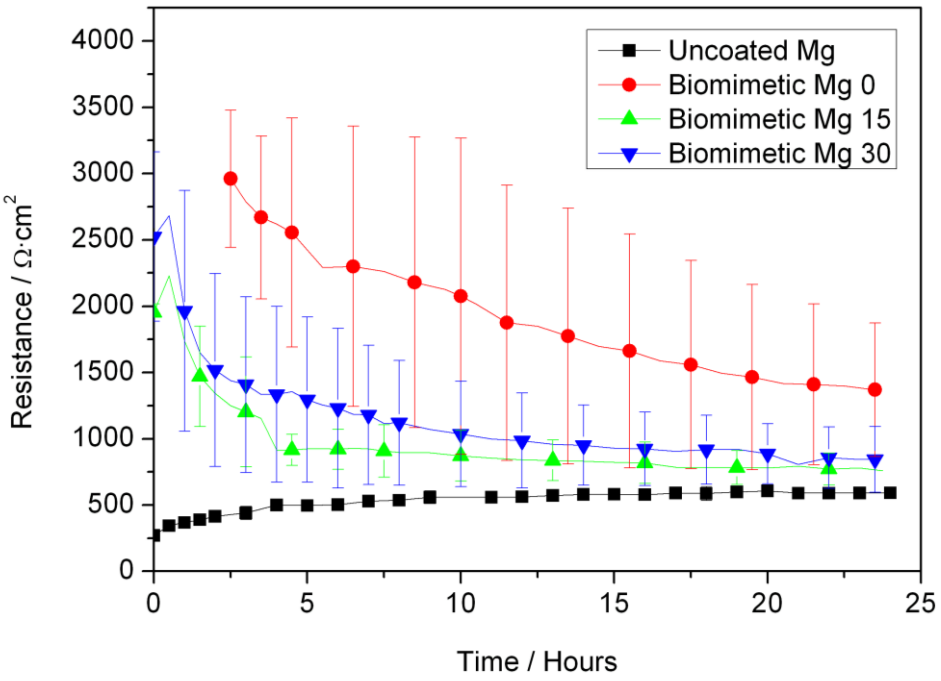

Figure 4-10: Corrosion resistance of biomimetic coated samples in NaCl.

In NaCl, the initial corrosion resistance of the coating was high but fell as the experiment proceeded. By 24 hours the corrosion resistances of all samples had fallen significantly. This decrease can be attributed to the formation of defects in the coating (Figure 4-13). Pitting occurs beneath the coating through cracks, undercutting the coating, and decreasing the adhesion. This lead to the eventual failure of the coating in small sections, leaving areas of bare Mg completely exposed to the solution (Figure 4-13F). Figure 4-16 A shows the corrosion layers at 1 hour consisted of a two time constant system that is typical of a porous coating layer and the EDL with the solution [56]. Over the 24 hour period, the magnitude of the resistance for the film time constant decreased due to the decrease in the coverage of the coatings as the cracks and defects formed. The subsequent increase in area exposed to solution leads to the additional decrease in the EDL resistance. EIS data in NaCl shows that for all time points over 24 hours, the coating with no pretreatment had the highest corrosion resistance. The larger EDL time constant corresponded with the visual observation of the fewer, less severe defects present on the Mg 0 samples. This also corresponded to the greatest mass increase in coating deposition of the tested samples. Therefore, the pretreatment to form a hydroxide layer on the Mg surfaces was not beneficial for depositing a defect free biomimetic coating.

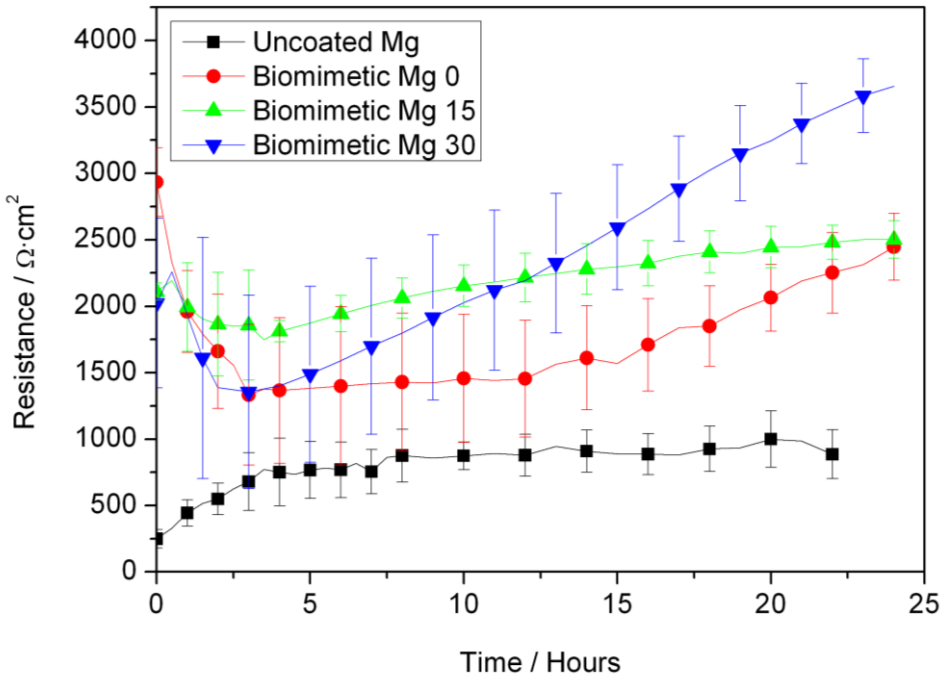

Figure 4-11: Corrosion resistance of biomimetic coated samples by EIS in HBSS over 24 hours.

Corrosion in HBSS was very different compared with NaCl (Figure 4-11). After an initial decrease, the corrosion resistance began to increase with time. In HBSS, the coating becomes more protective as corrosion occurs. This can be attributed to the presence the additional ions in HBSS. Corrosion between cracks creates a local pH rise, leading to additional precipitation of calcium phosphates on the surface of magnesium. This phenomenon has been documented for magnesium in SBFs [2, 57]. This pH rise occurs precisely where the coating is weakest, leading to increasing corrosion resistance with time. It was observed that longest pretreatment time led to the highest ultimate corrosion resistance after 24 hours. This suggests the $Mg(OH)_2$ layer was beneficial overall for the nucleation of calcium phosphates in HBSS. These results show that the pretreatment layer has an effect on the formation of the coating and the subsequent corrosion performance. However, this effect did not occur until after the coating became damaged, as the corrosion resistance started off high, dropped quickly, then began to climb (Figure 4-11). For Mg 0 and Mg 15, the final polarization resistance at 24 hours was slightly higher than the initial resistance after 1 hour. Nyquist plots show the rise was due to the increase in the film resistance due to the deposition of additional CaP from the HBSS (Figure 4-12 B). But the EDL film resistance remained very low. This means there were still plenty of defects for which solution could attack the

substrate through the coating. This also explains the lack of significant cathodic protection observed by PDP (Figure 4-9).

The defect problem with the coatings was clearly observed under SEM. Figure 4-13 F shows that the Mg 30 sample had a particular large effect as a whole section of the coating has delaminated and left the underlying Mg substrate exposed. The Mg 30 samples ultimately had the highest corrosion resistance in HBSS despite the obvious defects, and the poor performance in NaCl. The additional protection can be explained by the deposition of CaP from the HBSS. As Ca^{2+} ions are not present in the NaCl solution, this effect was not seen in those tests. In HBSS, the subsequent corrosion of the Mg due to the porous coating allowed local pH rises to deposit the CaP necessary to improve the coating as the increased EDL resistance shows (Figure 4-12 B). The drop, then subsequent rise in resistance is characteristic of this behaviour, which can be thought of as akin to a passivation effect. The effect is not seen on the bare Mg substrate because diffusion and the buffer keep the pH low enough near the surface to slow the CaP nucleation. When the pH rise happens inside of a crack, diffusion is retarded enough that the local pH can cause supersaturation of Ca ions, and thus subsequent deposition. So while the longer pretreatment seemed to lead to the largest polarization resistance in HBSS after 24 hours, this was due to the coating having the most defects. In NaCl, the highest corrosion resistance coating is the one most effective in preventing Cl^- attack, which was samples without pretreatment. In HBSS the protection also depends on additional CaP from the *in vitro* solution, and pretreatment was beneficial for this effect.

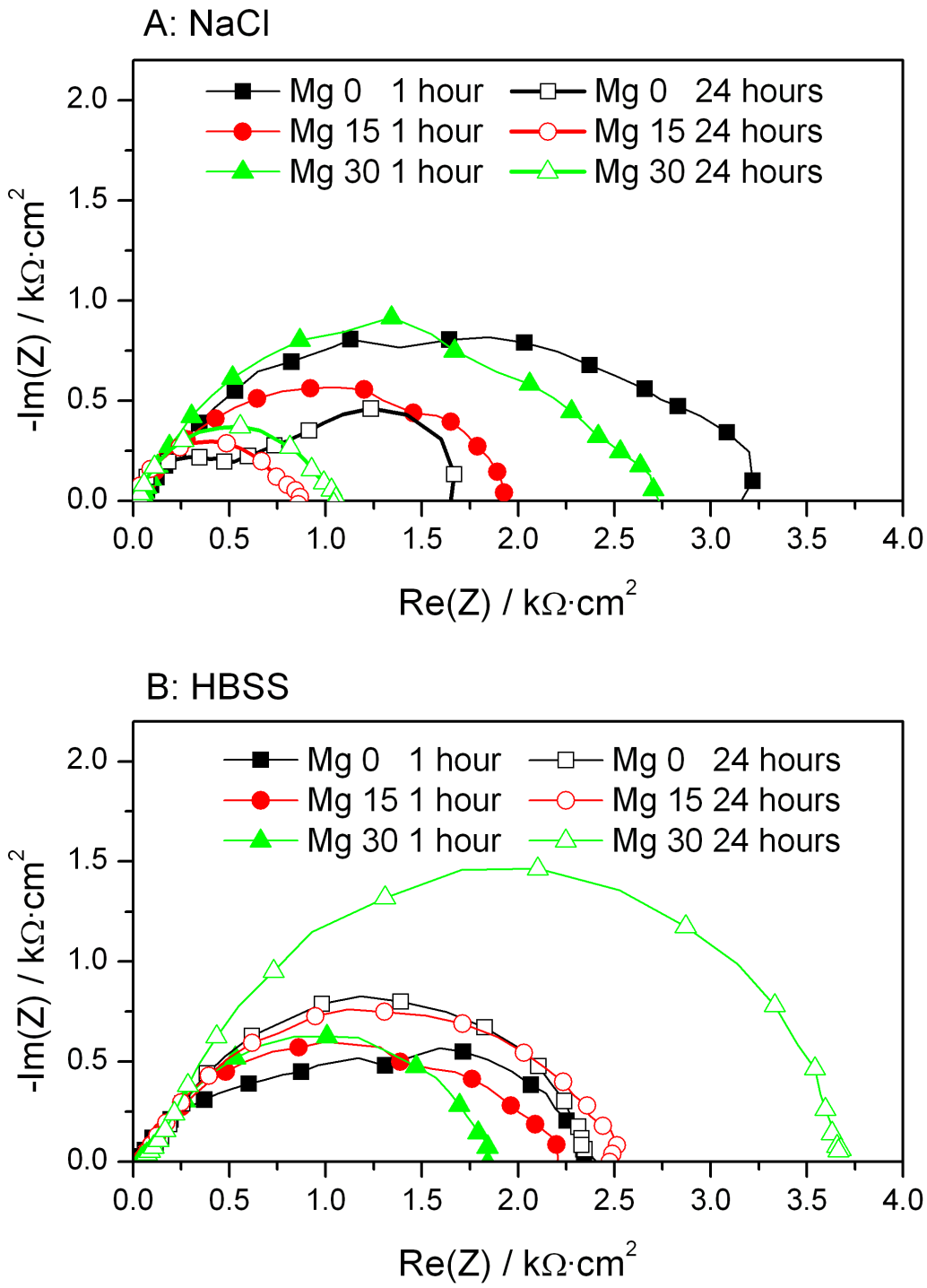

Figure 4-12: Nyquist plots of impedance data for pretreated biomimetic samples in NaCl (A) and HBSS (B) over 24 hours.

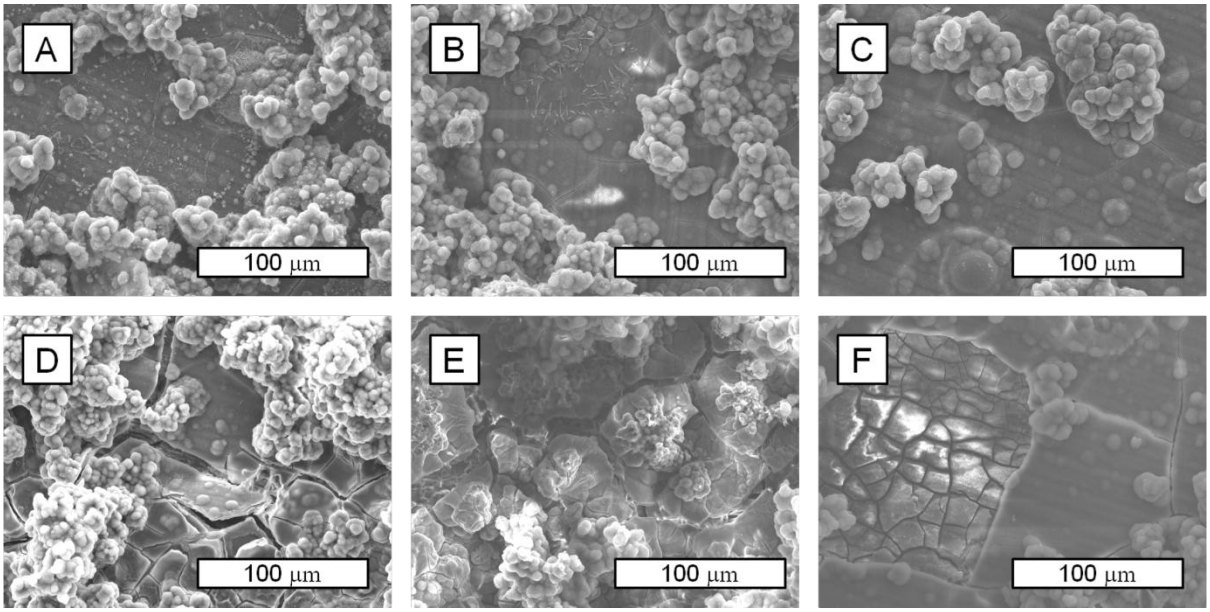

Figure 4-13: Scanning electron micrographs of biomimetic samples before corrosion Mg 0 (A), Mg 15 (B), Mg 30 (C) and after corrosion 24 hours in HBSS Mg 0 (D), Mg 15 (E) and Mg 30 (F).

4.4.3. Conclusion on the Pretreatment Effect on Corrosion Protection

The effect of $Mg(OH)_2$ pretreatments on the formation and corrosion protection of biomimetic calcium phosphate coatings was examined. It was not critical to pretreat magnesium to nucleate a CaP coating on Mg. Instead, longer pretreatment times led to a greater amount of cracks and defects in the coating layer. More defects lead to faster corrosion underneath the coating, which would eventually lead to pieces of coating breaking off in solution. In a simple NaCl solution, this results in decreasing corrosion protection with time. When calcium and phosphate ions were added to the solution, the $Mg(OH)_2$ pretreatment layer promoted additional nucleation of CaPs. This led to increased corrosion resistance during the 24 hour test. The results of the study show that pretreatment is not necessary for biomimetic coating of Mg and the corrosion properties are not necessarily improved by pretreatment. The increase in coating polarization resistance due to CaP nucleation was a surprising result. The pretreatment in this case seemed to improve the deposition. If this mechanism can be leveraged to improve the corrosion properties of the biomimetic coatings, it may help with the ultimate goal of providing the protection needed for an implant. The amount and severity of the defects in the coating do pose significant

concern for the ultimate utility of biomimetic coatings. If they cannot be improved to prevent localized corrosion, they will not be an acceptable protection method, despite their other desirable properties. The coatings will be required to withstand corrosive environments long enough that the bone can heal. The length of time the coating provides protection and whether or not this protection persists requires more observations past 24 hours. Therefore, longer term corrosion tests will be necessary to evaluate the performance.

4.5. Electrochemical Investigation of the Formation of Biomimetic Coatings

Biomimetic coatings form easily on Mg. They do not require the hydroxide pretreatment necessary for Ti. If we want to identify and optimize the coating process, it will be necessary to assess the deposition mechanics. The formation of the biomimetic coatings takes place in an aqueous solution. Therefore, electrochemical monitoring can be used to measure the formation of the coating. EIS can be used to measure the film resistance as a function of immersion time. This charge transfer resistance will be related to the coverage and porosity of the biomimetic coating as it forms. In this way the deposition and rise in protectiveness can be measured with coating time. The results will shed light on the mechanisms and critical stages of coating formation.

4.5.1.1. Methods

a Mg sample was mounted in epoxy with a copper wire connected to the back. This left one metal face exposed to provide a uniform electrode for measurement in the coating solution. No pretreatment was applied to the sample. A polycarbonate fixture was created to hold the exposed Mg face parallel to a flat Pt counter electrode. The distance between electrodes was 2 cm. A saturated calomel electrode (SCE) was used as a reference and placed between the two electrodes. The setup was immersed into the biomimetic coating solution and coated with the same process described in section 4.2.2.2. While immersed in the coating solution, the potential with respect to the reference electrode was monitored continuously, and an EIS scan was taken once every 2 hours to assess the progress of the coating.

4.5.1.2. Coating Formation

The electrochemical data for the formation of the coatings is shown in Figure 4-15. The potential of the electrode with respect to the reference was fairly variable, and quite noisy. The noise is probably an artefact of the coating solution environment. The bubbling of the gas through the solution, the oscillations of the stirrers, and the switching of the thermoregulator may contribute to the noise on both the working and reference electrodes. This is in addition to the deposition of the coating itself.

The initial response of each solution was quite varied for the first 3 to 4 hours. The OCP varied the most over theses ranges as the solution and electrodes settled. This was also a period of activity in the solution, as the pH rise was quite significant early on, especially in solution 1 (Figure 4-14). Once settled, the polarization resistance of the solution climbed linearly as the coating deposition progressed. The rise in pH promotes the deposition of more and more CaP on the surface [25], thus leading to more corrosion protection. However, the rise in pH will also promote slower corrosion kinetics due to the formation of the $Mg(OH)_2$ layer. It is therefore necessary to attempt to decouple these effects, though they are closely related. It should also not be forgotten that the polarization resistance in these solutions is not directly comparable to *in vitro* corrosion response due to the very different ionic compositions as well as pH.

The Nyquist plots in solution show the time constants of the coating growing (Figure 4-16). In solution 1, the initial response is dominated by the single large time constant of the uncoated Mg. Over the 24 hours, the coating forms and the 2 time constant behaviour appears. The resulting layer deposition increases the corrosion resistance as this layer is deposited. The porosity and solubility of the CaP phases formed in solution 1 limit the protectiveness of the overall coating. By coating the substrate in the second biomimetic coating solution, the higher Ca content CaP phases deposit and form the more protective second layer. The polarization resistance increases slowly with pH as the coating is deposited over the 24 hours.

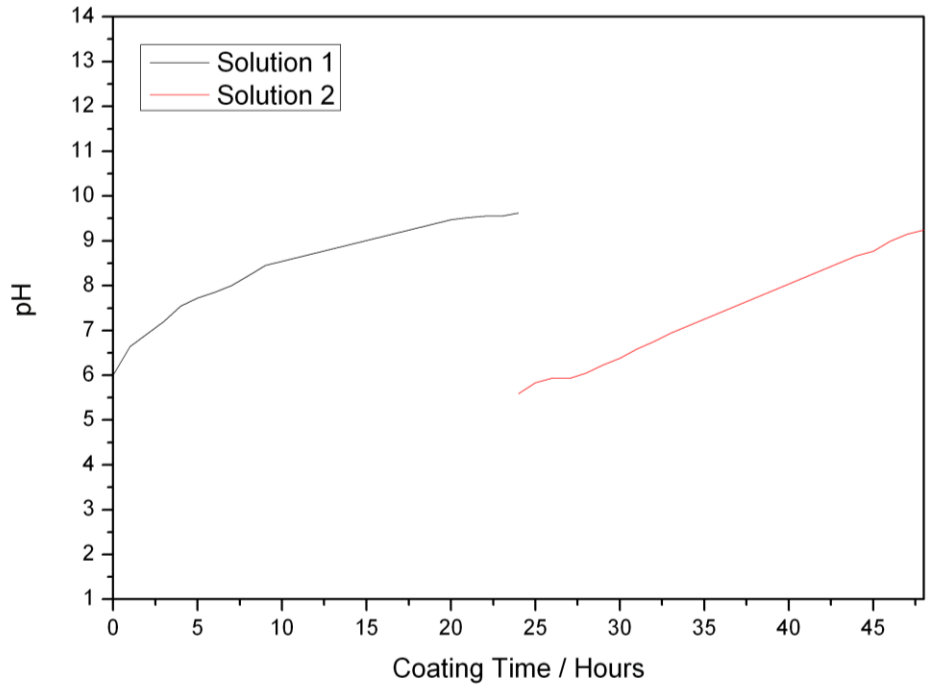

Figure 4-14: pH monitored over time in biomimetic coating Solutions 1 and 2 over the 48 hour coating process.

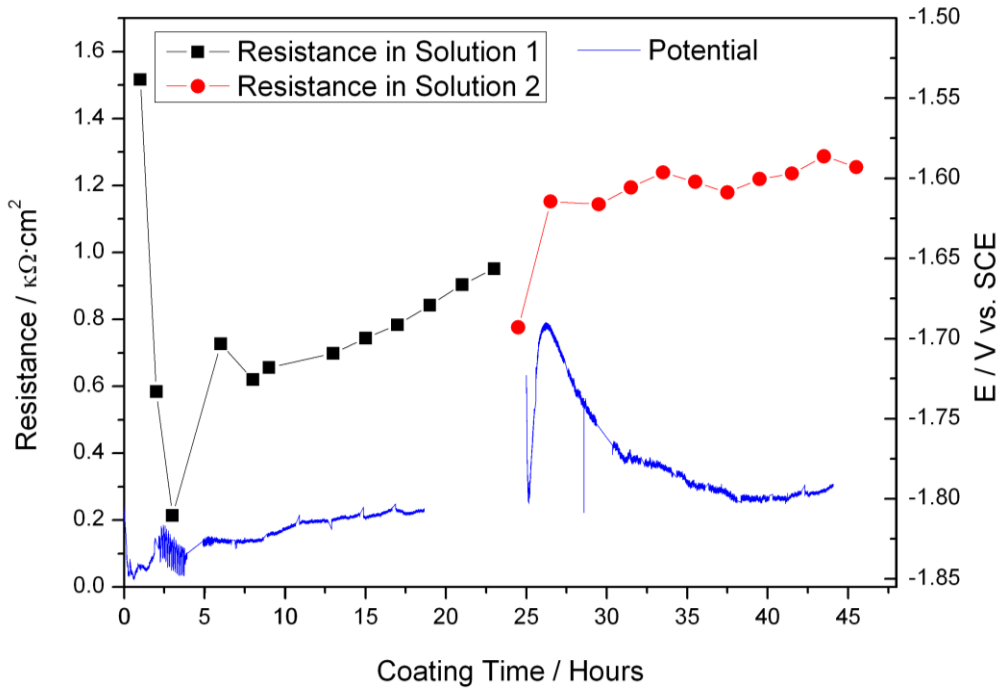

Figure 4-15: Polarization resistance and potential of Mg during the biomimetic coating procedure over 48 hours in Solutions 1 and 2.

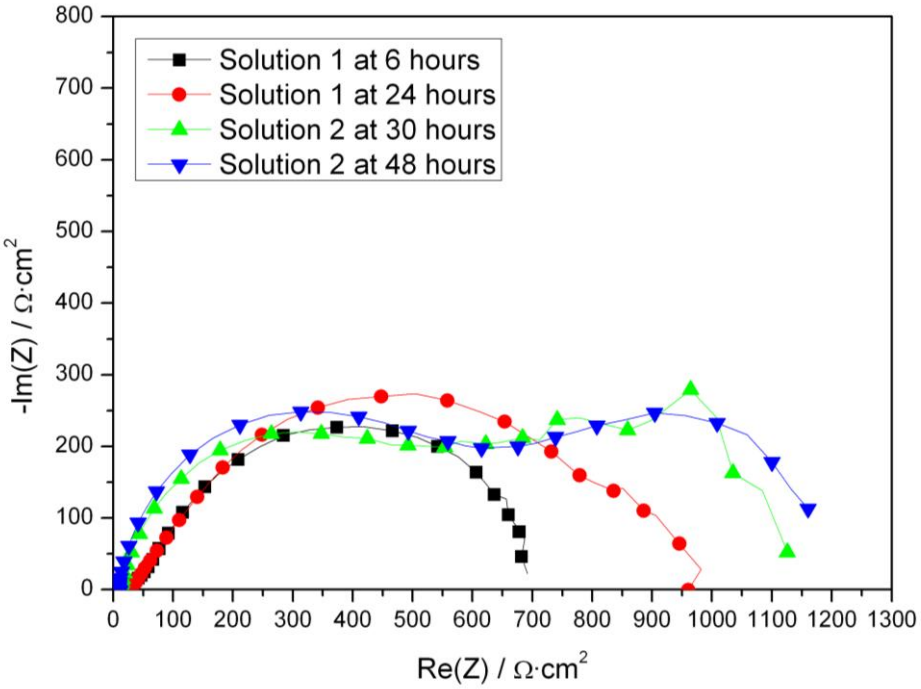

Figure 4-16: Nyquist plots during the formation of the coating in biomimetic Solutions 1 and 2.

4.6. Effect of Buffer on Measured Corrosion Rates

As evident in Chapter 3, the electrochemical behaviour of the Mg is dependent on the buffer system as well as the *in vitro* solution. The use of the HEPES buffer keeps the pH near the initial value of 7.40, has limited interaction with the corrosion reactions and the corrosion of the Mg at different rates will have less of an effect on the measurement error due to the changing pH. However, the HEPES buffer is chemically quite different than the buffer mechanisms *in vivo*. Indeed, the lower carbonate HEPES buffered tests typically express corrosion rates faster than seen in animal models [58]. The use of the bicarbonate, or HCO_3 buffer is more chemically similar to in vivo, but of course the mechanism is not quite the same *in vitro*. The buffering of carbonate ions is increased in the body by metabolism of hydrocarbons [59, 60]. In simple CO_2 atmospheres however, the buffer capacity is significantly decreased. Therefore, the corrosion rate is usually underestimated *in vitro* when this buffer is used [61]. To determine the effect of the change in buffer system on the coated Mg, the corrosion behaviour in HCO_3 and HEPES was compared by EIS and PDP in HBSS.

The total polarization resistance in each solution from 1 to 7 hours immersion of the biomimetic coated samples is shown in Figure 4-17. The biomimetic coatings for this study were given no pretreatment. The early corrosion behaviour was focused on, to detect the changes in the solution before the corrosion caused much pH rise, and before the coatings began to fail severely, thus altering the results. In this way the direct effect of the different buffers could be observed on the samples. As with uncoated Mg, the bicarbonate buffer caused more rapid increases in the resistance of the corrosion layer, due to the deposition of the carbonates with the high pH. This is similar to what happens over time with the Mg in HBSS [8], but the lower buffer capacity and the greater amount of HCO_3^- increase the rate. The resistance in HBSS + HCO_3 doubles over 7 hours, while the HEPES buffered solutions the coating resistance was fairly constant.

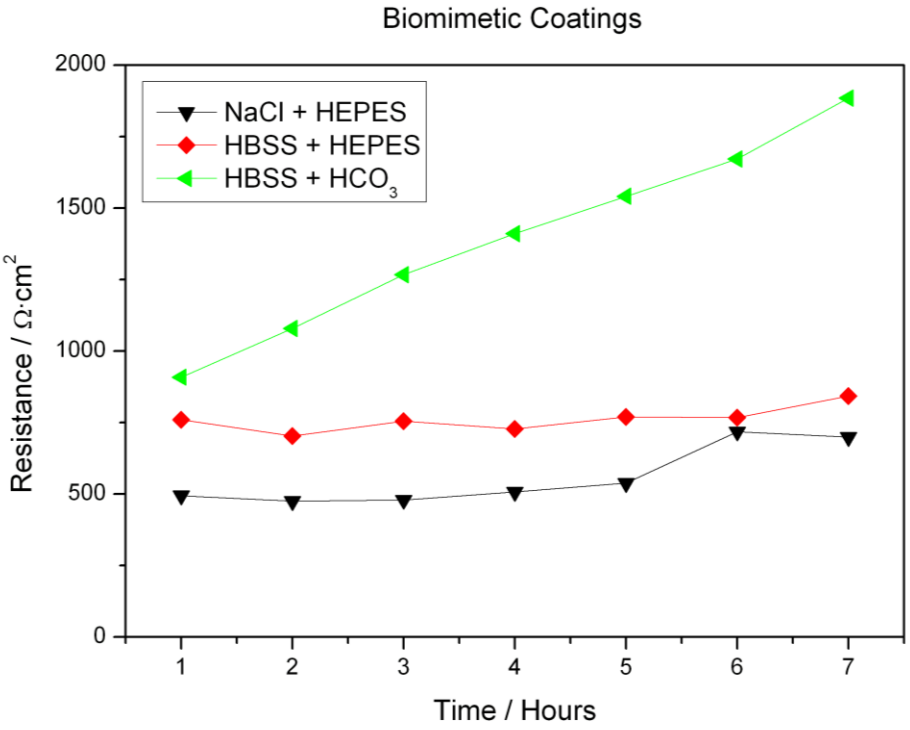

Figure 4-17: Early stage polarization resistance of biomimetic coatings in solutions buffered with HEPES and HCO_3.

PDP scans for all samples are displayed in Figure 4-18. The data supports the same conclusions. HEPES buffered NaCl and HBSS solutions show little change in corrosion kinetics for either the anodic or cathodic reactions over 8 hours. The HCO_3 buffered solution shows the biomimetic coating decreases the cathodic kinetics slightly and the anodic kinetics

significantly. This is consistent with the effect noted in Chapter 3. The carbonate in calcium containing solutions quickly forms a layer that in this case, augments the corrosion protection of the biomimetic layer, hence the drop in the anodic reaction. This layer is still porous though, as evident by the only slight decrease in cathodic kinetics. Overall, the measured corrosion rate of the coated samples is also dependant on the buffer solution, further affirming the need for the *in vitro* testing environment to be consistent and relevant to obtain good data.

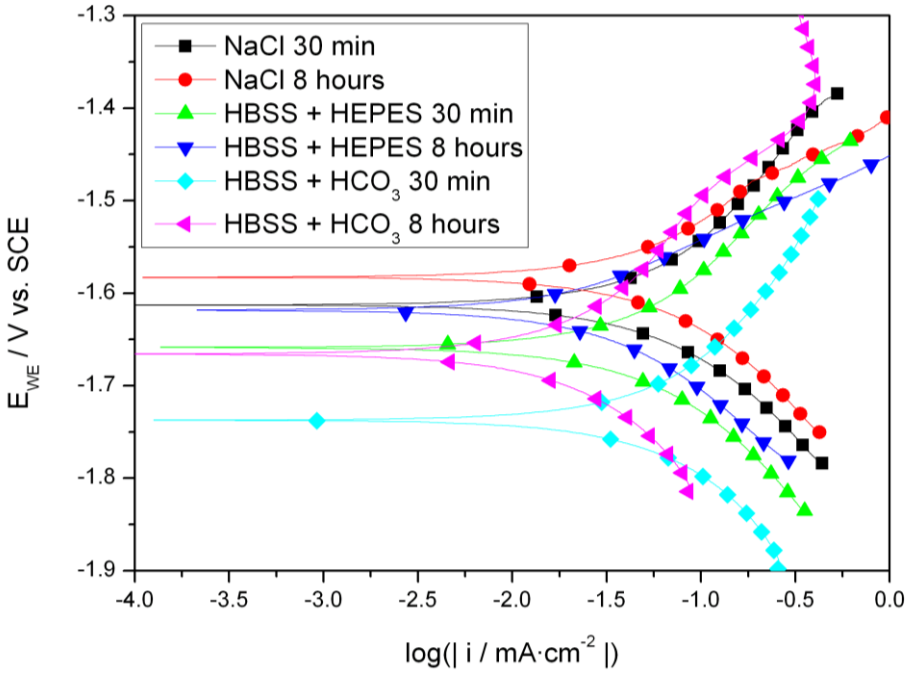

Figure 4-18: Polarization of biomimetic coatings in HEPES and HCO_3 buffered solutions at 30 minutes and 8 hours.

4.7. Conclusions

The biomimetic coatings formed easily on Mg without the need for any surface treatment. The coatings were able to protect from corrosion, but not completely. The surface treatment compromises the integrity (in terms of corrosion resistance) of the coatings by causing the formation of defects and such. The corrosion protection thus falls with time in NaCl as corrosion occurs beneath the coating through defects.

The surface treatment did seem to improve the deposition of additional CaP phases from the solution, thus leading to the decreasing, then increasing corrosion resistance in HBSS. The mechanism for this is documented for Mg in SBF [8] and in vivo [62]. The biomimetic coatings help promote this mechanism, leading to increased corrosion resistance in HBSS.

The corrosion resistance of the coatings is linked to the integrity of the coating by the amount of defects present. The severity of these defects is what will limit the total effectiveness of the corrosion resistance. Optimizing the initial coating creation, as well as the deposition of additional CaP from physiological solutions will help to bring up the total protectiveness to where they can be used *in vivo*. The continued corrosion through the defects remains a problem. If they cannot be improved to prevent localized corrosion, they will not be an acceptable solution, despite their other desirable properties. The coatings will be required to withstand corrosive environments long enough that the bone can heal. The 24 hour tests show that the corrosion occurs beneath the defects, but the rise or fall of the corrosion resistance depends on the environment. These short 24 hour tests do not indicate whether or not this protection persists. Therefore, longer term corrosion tests were eventually necessary to evaluate the performance.

4.8. References

1. Staiger, M.P., A.M. Pietak, J. Huadmai, and G. Dias, *Magnesium and its alloys as orthopedic biomaterials: A review.* Biomaterials, 2006. **27**(9): p. 1728-1734.
2. Witte, F., N. Hort, C. Vogt, S. Cohen, K.U. Kainer, R. Willumeit, and F. Feyerabend, *Degradable biomaterials based on magnesium corrosion.* Current Opinion in Solid State and Materials Science, 2008. **12**(5-6): p. 63-72.
3. León, B. and J.A. Jansen, *Thin Calcium Phosphate Coatings for Medical Implants*. 2008: Springer.
4. Barrere, F. and C.M.v.d. Valk, *Osteogenecity of octacalcium phosphate coatings applied on porous metal implants.* Journal of Biomedical Materials Research Part A, 2003. **66A**(4): p. 779-788.
5. Barrere, F., C.M. van der Valk, G. Meiger, R.A.J. Dalmeijer, K. De Groot, and P. Layrolle, *Osteointegration of biomimetic apatite coating applied onto dense and porous metal implants in femurs of goats.* Journal of Biomedical Materials Research Part B: Applied Biomaterials, 2003. **67B**(1): p. 655-665.
6. Zhu, L., X. Ye, G. Tang, N. Zhao, Y. Gong, Y. Zhao, J. Zhao, and X. Zhang, *Biomimetic coating of compound titania and hydroxyapatite on titanium.* Journal of Biomedical Materials Research Part A, 2007. **83A**(4): p. 1165-1175.
7. Xu, L., F. Pan, G. Yu, L. Yang, E. Zhang, and K. Yang, *In vitro and in vivo evaluation of the surface bioactivity of a calcium phosphate coated magnesium alloy.* Biomaterials, 2009. **30**(8): p. 1512-1523.

8. Gray-Munro, J.E. and M. Strong, *The mechanism of deposition of calcium phosphate coatings from solution onto magnesium alloy AZ31.* Journal of Biomedical Materials Research Part A, 2009. **90A**(2): p. 339-350.
9. Hiromoto, S. and A. Yamamoto, *High corrosion resistance of magnesium coated with hydroxyapatite directly synthesized in an aqueous solution.* Electrochimica Acta, 2009. **54**(27): p. 7085-7093.
10. Hu, J., C. Wang, W.C. Ren, S. Zhang, and F. Liu, *Microstructure evolution and corrosion mechanism of dicalcium phosphate dihydrate coating on magnesium alloy in simulated body fluid.* Materials Chemistry and Physics, 2010. **119**(1-2): p. 294-298.
11. Wu, C., Z. Wen, C. Dai, Y. Lu, and F. Yang, *Fabrication of calcium phosphate/chitosan coatings on AZ91D magnesium alloy with a novel method.* Surface and Coatings Technology, 2010. **204**(20): p. 3336-3347.
12. Yang, J.X., Y.P. Jiao, F.Z. Cui, I.-S. Lee, Q.S. Yin, and Y. Zhang, *Modification of degradation behavior of magnesium alloy by IBAD coating of calcium phosphate.* Surface and Coatings Technology, 2008. **202**(22-23): p. 5733-5736.
13. Basu, B., D.S. Katti, and A. Kumar, *Advanced Biomaterials: Fundamentals, Processing, and Applications*. 2009: John Wiley & Sons.
14. Chow, L.C. and E.D. Eanes, *Octacalcium Phosphate*. 2001: Karger Publishers.
15. Barrere, F., *Biomimetic Calcium Phosphate Coatings: Physicochemistry and Biological Activity*. 2002, University of Twente: Enschede.
16. Rey, C., B. Collins, T. Goehl, I. Dickson, and M. Glimcher, *The carbonate environment in bone mineral: A resolution-enhanced fourier transform infrared spectroscopy study.* Calcified Tissue International, 1989. **45**(3): p. 157-164.
17. Rey, C., J. Lian, M. Grynpas, F. Shapiro, L. Zylberberg, and M.J. Glimcher, *Non-apatitic environments in bone mineral: FT-IR detection, biological properties and changes in several disease states.* Connective tissue research, 1989. **21**(1-4): p. 267-273.
18. Rey, C., *Calcium phosphate biomaterials and bone mineral. Differences in composition, structures and properties.* Biomaterials, 1990. **11**: p. 13-15.
19. Epinette, J.-A. and M.T. Manley, *Fifteen Years of Clinical Experience with Hydroxyapatite Coatings in Joint Arthroplasty*. 2003: Springer.
20. Chen, D., E.H. Jordan, M. Gell, and M. Wei, *Apatite formation on alkaline-treated dense TiO2 coatings deposited using the solution precursor plasma spray process.* Acta Biomaterialia, 2008. **4**(3): p. 553-559.
21. Gross, K.A. and C.C. Berndt, *Thermal processing of hydroxyapatite for coating production.* Journal of Biomedical Materials Research, 1998. **39**(4): p. 580-587.
22. Klein, C.P.A.T., P. Patka, J.G.C. Wolke, J.M.A. de Blieck-Hogervorst, and K. de Groot, *Long-term in vivo study of plasma-sprayed coatings on titanium alloys of tetracalcium phosphate, hydroxyapatite and α-tricalcium phosphate.* Biomaterials, 1994. **15**(2): p. 146-150.
23. Buser, D., R.K. Schenk, S. Steinemann, J.P. Fiorellini, C.H. Fox, and H. Stich, *Influence of surface characteristics on bone integration of titanium implants. A histomorphometric study in miniature pigs.* Journal of Biomedical Materials Research, 1991. **25**(7): p. 889-902.
24. Whitehead, R.Y., W.R. Lacefield, and L.C. Lucas, *Structure and integrity of a plasma sprayed hydroxylapatite coating on titanium.* Journal of Biomedical Materials Research, 1993. **27**(12): p. 1501-1507.
25. Habibovic, P., F. Barrere, C.A. van Blitterswijk, K. de Groot, and P. Layrolle, *Biomimetic hydroxyapatite coating on metal implants.* Journal of the American Ceramic Society, 2002. **85**(3): p. 517-22.

26. Kokubo, T., *Formation of biologically active bone-like apatite on metals and polymers by a biomimetic process.* Thermochimica Acta, 1996. **280-281**: p. 479-490.
27. Lin, C.-M. and S.-K. Yen, *Biomimetic growth of apatite on electrolytic TiO2 coatings in simulated body fluid.* Materials Science and Engineering: C, 2006. **26**(1): p. 54-64.
28. Bigi, A., G. Falini, E. Foresti, A. Ripamonti, M. Gazzano, and N. Roveri, *Magnesium influence on hydroxyapatite crystallization.* Journal of Inorganic Biochemistry, 1993. **49**(1): p. 69-78.
29. Landi, E., A. Tampieri, M. Mattioli-Belmonte, G. Celotti, M. Sandri, A. Gigante, P. Fava, and G. Biagini, *Biomimetic Mg- and Mg,CO3-substituted hydroxyapatites: synthesis characterization and in vitro behaviour.* Journal of the European Ceramic Society, 2006. **26**(13): p. 2593-2601.
30. Kasuga, T., H. Kondo, and M. Nogami, *Apatite formation on TiO2 in simulated body fluid.* Journal of Crystal Growth, 2002. **235**(1-4): p. 235-240.
31. Wang, X.J., Y.C. Li, J.G. Lin, P.D. Hodgson, and C.E. Wen, *Apatite-inducing ability of titanium oxide layer on titanium surface: The effect of surface energy.* Journal of Materials Research, 2008. **23**(6): p. 1682-1688.
32. Baker, K.C., M.A. Anderson, S.A. Oehlke, A.I. Astashkina, D.C. Haikio, J. Drelich, and S.W. Donahue, *Growth, characterization and biocompatibility of bone-like calcium phosphate layers biomimetically deposited on metallic substrata.* Materials Science and Engineering: C, 2006. **26**(8): p. 1351-1360.
33. Kim, H.M., F. Miyaji, T. Kokubo, and T. Nakamura, *Effect of heat treatment on apatite-forming ability of Ti metal induced by alkali treatment.* Journal of Materials Science: Materials in Medicine, 1997. **8**(6): p. 341-347.
34. Kim, H.M., F. Miyaji, T. Kokubo, S. Nishiguchi, and T. Nakamura, *Graded surface structure of bioactive titanium prepared by chemical treatment.* Journal of Biomedical Materials Research, 1999. **45**(2): p. 100-107.
35. Kim, H.-M., F. Miyaji, T. Kokubo, and T. Nakamura, *Preparation of bioactive Ti and its alloys via simple chemical surface treatment.* Journal of Biomedical Materials Research, 1996. **32**(3): p. 409-417.
36. Kokubo, T., F. Miyaji, H.M. Kim, and T. Nakamura, *Spontaneous Formation of Bonelike Apatite Layer on Chemically Treated Titanium Metals.* Journal of the American Ceramic Society, 1996. **79**(4): p. 1127-1129.
37. Nishiguchi, S., T. Nakamura, M. Kobayashi, H.-M. Kim, F. Miyaji, and T. Kokubo, *The effect of heat treatment on bone-bonding ability of alkali-treated titanium.* Biomaterials, 1999. **20**(5): p. 491-500.
38. Wen, H.B., J.G.C. Wolke, J.R. de Wijn, Q. Liu, F.Z. Cui, and K. de Groot, *Fast precipitation of calcium phosphate layers on titanium induced by simple chemical treatments.* Biomaterials, 1997. **18**(22): p. 1471-1478.
39. Zhang, Q. and Y. Leng, *Electrochemical activation of titanium for biomimetic coating of calcium phosphate.* Biomaterials, 2005. **26**(18): p. 3853-3859.
40. Song, G. and A. Atrens, *Understanding Magnesium Corrosion - A Framework for Improved Alloy Performance.* Advanced Engineering Materials, 2003. **5**(12): p. 837-858.
41. Barrere, F., C.A. van Blitterswijk, K. de Groot, and P. Layrolle, *Nucleation of biomimetic Ca-P coatings on Ti6Al4V from a SBF×5 solution: influence of magnesium.* Biomaterials, 2002. **23**(10): p. 2211-2220.
42. Li, P., C. Ohtsuki, T. Kokubo, K. Nakanishi, N. Soga, and K. de Groot, *The role of hydrated silica, titania, and alumina in inducing apatite on implants.* Journal of Biomedical Materials Research, 1994. **28**(1): p. 7-15.

43. Friedrich, H.E., *Magnesium Technology : Metallurgy, Design Data, Applications*, ed. H.E. Friedrich and B.L. Mordike. 2006, Heidelberg: Springer.
44. Wang, P., C. Li, H. Gong, H. Wang, and J. Liu, *Morphology control and growth mechanism of magnesium hydroxide nanoparticles via a simple wet precipitation method.* Ceramics International, 2011. **37**(8): p. 3365-3370.
45. Barrère, F., P. Layrolle, C.A. van Blitterswijk, and K. de Groot, *Biomimetic calcium phosphate coatings on Ti6Al4V: a crystal growth study of octacalcium phosphate and inhibition by Mg2+ and HCO3−.* Bone, 1999. **25**(2, Supplement 1): p. 107S-111S-107S-111S.
46. Zhao, M.-C., M. Liu, G.-L. Song, and A. Atrens, *Influence of pH and chloride ion concentration on the corrosion of Mg alloy ZE41*. Corrosion Science, 2008. **50**(11): p. 3168-3178.
47. Song, G.L. and A. Atrens, *Corrosion Mechanisms of Magnesium Alloys.* Advanced Engineering Materials, 1999.
48. Barrere, F., C.A. van Blitterswijk, K. de Groot, and P. Layrolle, *Influence of ionic strength and carbonate on the Ca-P coating formation from SBFx5 solution.* Biomaterials, 2002. **23**(9): p. 1921-1930.
49. Leng, Y., *Materials characterization : introduction to microscopic and spectroscopic methods*. 2008, Singapore ; Hoboken, NJ: J. Wiley. xii, 337 p.
50. *PDF 04-013-6614*. 2006, International Center for Diffraction Data: Newton, PA.
51. *PDF 01-074-6549*. 1962, International Center for Diffraction Data: Newton, PA.
52. *PDF 04-012-6929*. 1998, International Center for Diffraction Data: Newton, PA.
53. *PDF 04-007-2050*. 1978, International Center for Diffraction Data: Newton, PA.
54. Wang, Y., M. Wei, J. Gao, J. Hu, and Y. Zhang, *Corrosion process of pure magnesium in simulated body fluid.* Materials Letters, 2008. **62**(14): p. 2181-2184.
55. Xin, Y., K. Huo, H. Tao, G. Tang, and P.K. Chu, *Influence of aggressive ions on the degradation behavior of biomedical magnesium alloy in physiological environment.* Acta Biomaterialia, 2008. **4**(6): p. 2008-2015.
56. Tait, W.S., *An Introduction to Electrochemical Corrosion Testing for Practicing Engineers and Scientists*. 1994: PairODocs Publications.
57. Rettig, R. and S. Virtanen, *Time-dependent electrochemical characterization of the corrosion of a magnesium rare-earth alloy in simulated body fluids.* Journal of Biomedical Materials Research Part A, 2008. **85A**(1): p. 167-175.
58. Yamamoto, A. and S. Hiromoto, *Effect of inorganic salts, amino acids and proteins on the degradation of pure magnesium in vitro.* Materials Science and Engineering: C, 2009. **29**(5): p. 1559-1568.
59. Boron, W.F. and E.L. Boulpaep, eds. *Medical Physiology*. 2nd ed. 2008, Saunders: New York.
60. Hall, J.E., *Guyton and Hall Textbook of Medical Physiology*. 11th ed. 2010, Amsterdam: Elsevier.
61. Willumeit, R., J. Fischer, F. Feyerabend, N. Hort, U. Bismayer, S. Heidrich, and B. Mihailova, *Chemical surface alteration of biodegradable magnesium exposed to corrosion media.* Acta Biomaterialia, 2011. **7**(6): p. 2704-2715.
62. Witte, F., V. Kaese, H. Haferkamp, E. Switzer, A. Meyer-Lindenberg, C.J. Wirth, and H. Windhagen, *In vivo corrosion of four magnesium alloys and the associated bone response.* Biomaterials, 2005. **26**(17): p. 3557-3563.

CHAPTER 5: Modified Biomimetic Coatings for Improved Protection

5.1. Introduction

The biomimetic coating was successfully applied to the Mg substrates, and as shown, it reduced the early corrosion rate *in vitro*. The defects in the ceramic coating were the dominant cause of the failure of the biomimetic coatings. The deposition on the surface of a compact, defect free coating was not improved by the hydroxide pretreatments. The final coatings had more defects which led to more corrosion in NaCl solutions when pretreatment was used than when it was not. The use of the pretreatment, which is so necessary on Ti implants, is not beneficial for Mg. This calls into question the need for the 2 stage biomimetic coating phase. This process, designed to promote deposition on Ti [1, 2] is not optimized for Mg. The structure and composition of the biomimetic coatings are desirable for biocompatibility [3-5] and osteoconductivity [6, 7]. These are properties that should be retained in the coatings if possible. The need is for the biomimetic coatings to provide more corrosion protection. This was not initially a design consideration for the biomimetic coating since Ti is very corrosion resistant. Given the defects and corrosion properties of the coatings in simple NaCl solutions, it is uncertain if these coatings can be made to protect the implant for the required duration. Furthermore, since the deposition of biomimetic coatings on Mg is not nearly as difficult, the formation mechanisms and whether the first step helps or hinders the corrosion properties has not been investigated.

The study presented here will investigate the formation of the biomimetic coatings using the first solution to create the amorphous carbonated coating followed by the higher chloride final coating step compared with simply using the second step of the biomimetic coating process to create the coating directly. The composition and structure of the coatings will be examined to find out how the first stage impacts the final coating layer on Mg. The corrosion properties of these coatings will be assessed over a longer term test of 14 days to investigate if the corrosion resistance will last in solution.

5.2. Materials and Methods

5.2.1. Coating Process

Pure Mg substrates were cut to dimensions of 15 × 15 mm, polished to 1200 grit and rinsed with ethanol. Biomimetic coatings were prepared as described in Chapter 4 will be referred to as Biomimetic 1. The biomimetic coatings were formed by coating the samples in solution 1 for 24 hours, followed by coating in solution 2 for 24 hours (Table 4-2). The modified coatings (Biomimetic 2) were coated only in solution 2 for 24 hours. The coatings created were examined after every process with normal and glancing angle (GA) XRD. The glancing angle XRD was done with a fixed X-ray incidence angle of 5 degrees and while the detector was moved from 5 to 80 degrees to capture the full diffraction pattern.

5.2.2. Hydrogen Evolution

Hydrogen evolution was conducted for coated samples over 14 days. Four samples of each experimental group were tested. Samples were coated with silicone sealant for H_2 evolution tests on all faces except one to ensure only one face was exposed. Each sample was immersed into 500 mL of HBSS buffered with 25mM HEPES and adjusted to pH of 7.4 at a temperature of 37° C. A 50 mL glass burette was attached to a glass funnel, inverted over the sample and filled with solution. Hydrogen gas collected was measured at least once per day for 14 days. The solution was replaced every 72 hours to keep the pH and ionic composition of the fluid at the appropriate conditions.

5.2.3. Electrochemical tests

Electrochemical tests were carried out to measure the corrosion rate. Experiments were carried out in 103mM NaCl and Hanks' Balanced Salt Solution (HBSS) at 37°C ± 0.5 °C and pH of 7.4 ± 0.05, buffered with 4-(2-hydroxyethyl)-1-piperazineethanesulfonic acid (HEPES) (25mM). 300 mL of solution was used per test. The area of the working electrode was 1 cm^2. Potentiodynamic polarization (PDP) and electrochemical impedance spectroscopy (EIS) tests were performed. A three electrode setup was used with a Pt counter electrode and a saturated calomel reference electrode (SCE). PDP tests were carried out after 20 minutes in solution to allow the open circuit potential to stabilize. PDP tests utilized a scan rate of 1 mV/s, and scanned over the range OCP – 0.100 V to Ref + 0.500 V. EIS scans were performed every 30

min over a period of 24 hours to evaluate the change in corrosion resistance with time. It used a 10mV peak to peak signal from OCP across a frequency range from 50 kHz to 20 mHz.

5.2.4. Buffered tests

Buffered tests were carried out in HBSS with either 25mM HEPES or 26mM HCO_3 as described in Chapter 3. Electrochemical tests were carried out in an incubator at 37° C. HCO_3 buffered tests were performed with a controlled 5% CO_2 atmosphere to bring the pH to 7.4. HEPES buffered tests were performed at ambient atmospheric CO_2 levels.

5.3. Results and Discussion

5.3.1. Formation of the Coating

The biomimetic coatings formed easily in Solution 2 without the first coating in Solution 1. The final composition was very similar for both coatings after the final treatment as shown in Figure 5-1. The glancing angle XRD proved to be very useful in determining the composition of the thin coatings on Mg. The low angle maximized the intensity of the diffracted X-rays from the coating relative to the substrate. The normal scans are dominated by the Mg peaks, and the coating is barely detectable in some cases. This is due to the X-rays penetrating the coatings and the signal is therefore being dominated by the underlying substrate. For the low angle scans, the composition of the coating is much more detectable. As with the previous samples, the mixture of phases and structure of the coatings made absolute crystal structure identification difficult. After coating in the first biomimetic solution, no direct match to a single crystal structure was found, although EDS reveals the composition to be composed of a semi-crystalline carbonated CaP [8].

After coating in the second solution, the samples matched peaks close to Mg and carbonate substituted dicalcium phosphate dihydrate (DCPD) [9]. The wide peaks again suggest very low crystallinity, and small crystallite sizes as would be expected from DCPD where the lattice is disrupted by substitutions [10, 11]. The coatings on both samples coated with solution 1 then solution 2 were very similar in crystal structure to the samples coated with solution 2 only. The substituted DCPD solution is formed from the composition of the biomimetic coating solution [12], and should therefore not be greatly influenced by the first

step of the coating. This first step was designed to provide a base for the CaP to nucleate onto for Ti, as Ti by itself does not otherwise distribute the biomimetic coating evenly [2]. On Mg, the corrosion of the Mg in the Cl^- containing solution promotes the direct deposition of CaP on the surface [13]. Biomimetic solution 1 is lower in Cl^- content than the process reported by Habibovic et al. [12]. This prevents significant corrosion to the substrate in coating solution 1. However, some corrosion in the biomimetic solution may be desirable since the corrosion was found to actually accelerate the coating deposition. As the XRD shows, skipping the first biomimetic coating solution had little effect on the crystal structure of the final coating. Further, the observed morphology (Figure 5-3 B and C) shows that the coating deposited completely over the surface regardless of the first biomimetic coating.

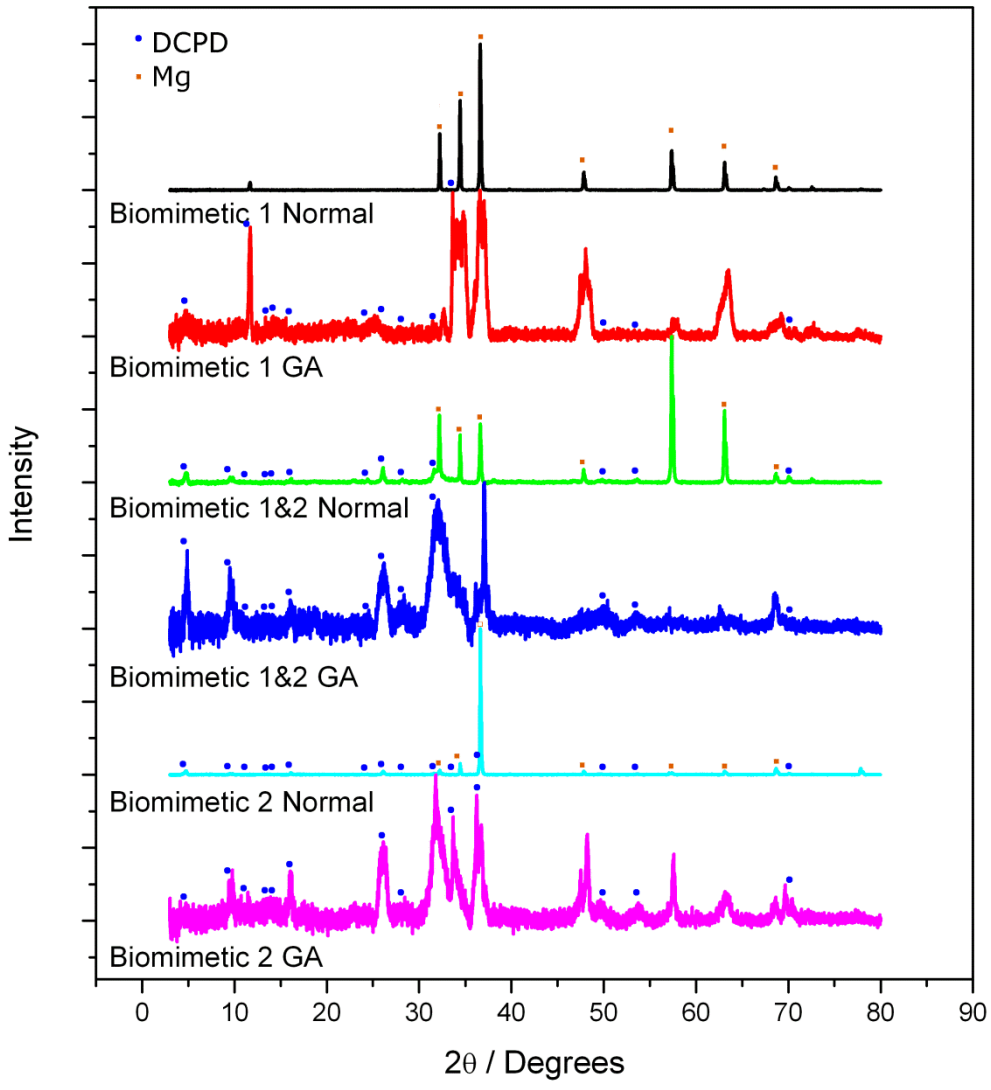

Figure 5-1: XRD Normal and Glancing Angle (GA) for samples after coating in biomimetic solution 1, then biomimetic solution 2, and samples coated with biomimetic solution 2 only.

5.3.2. Corrosion Results

5.3.2.1. The Effect of Coating Process on the Hydrogen Evolution

The hydrogen evolution results show the difference in corrosion properties over 14 days (Figure 5-2). For uncoated surfaces, the corrosion rate is quite rapid, and increases with greater surface roughness [14]. The hydrogen evolution rate for the polished sample in the early portion displays positive curvature, indicative of accelerating corrosion rate. The cause of this is the nonuniform pitting of the sample that occurs, leading to greater surface area and thus greater corrosion [14, 15]. However, there is an inflection point in the curve, after 150 hours the corrosion rate begins to decelerate. This is an artefact of the calcium phosphates that form on the surface from dissolved salts found the in the bloodstream, and therefore also in these *in vitro* environments [13, 16]. This layer provides the protection that allows the corrosion to decrease in the latter stages of the test. Unfortunately, due to the limited amount of calcium available, the total corrosion that must take place before this occurs is unacceptable for implants, as by 150 hours, already significant corrosion has taken place, generating 10 mL/cm^2 H_2 gas, well above the estimates of tolerable H_2 evolution of ~0.01 mL/cm^2/day [17].

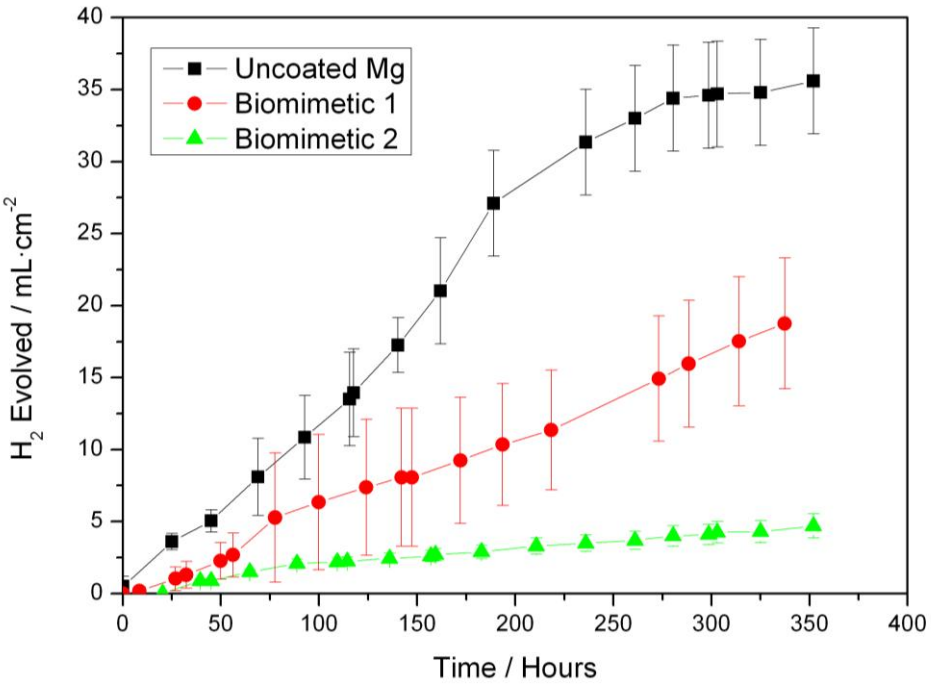

Figure 5-2: Hydrogen evolution over 14 days for samples.

The formation of the calcium phosphate on the surface of the biomimetic coatings led to an eventual protective CaP coating on the surface. EDS confirmed that the composition was calcium phosphate with Mg and other ions from the SBF detected in trace amounts. The morphology of the coating after 14 days in SBF on the corroded Mg is shown in Figure 5-3 D. The coating had cracks and defects that would allow corrosion, although the corrosion rate dropped considerably compared to the early stages of the bare Mg. The crystal structure of the corroded surface was investigated with XRD (Figure 5-4). The CaP phases were very amorphous, and no real peak match could be found. The amount of corrosion that took place to form the coating was considerable. Therefore, the Mg^{2+} concentration at the surface would have been very high. . All of this magnesium is likely to have limited the crystallinity of the coating and led to a highly amorphous calcium-magnesium phosphate deposit [10, 11].

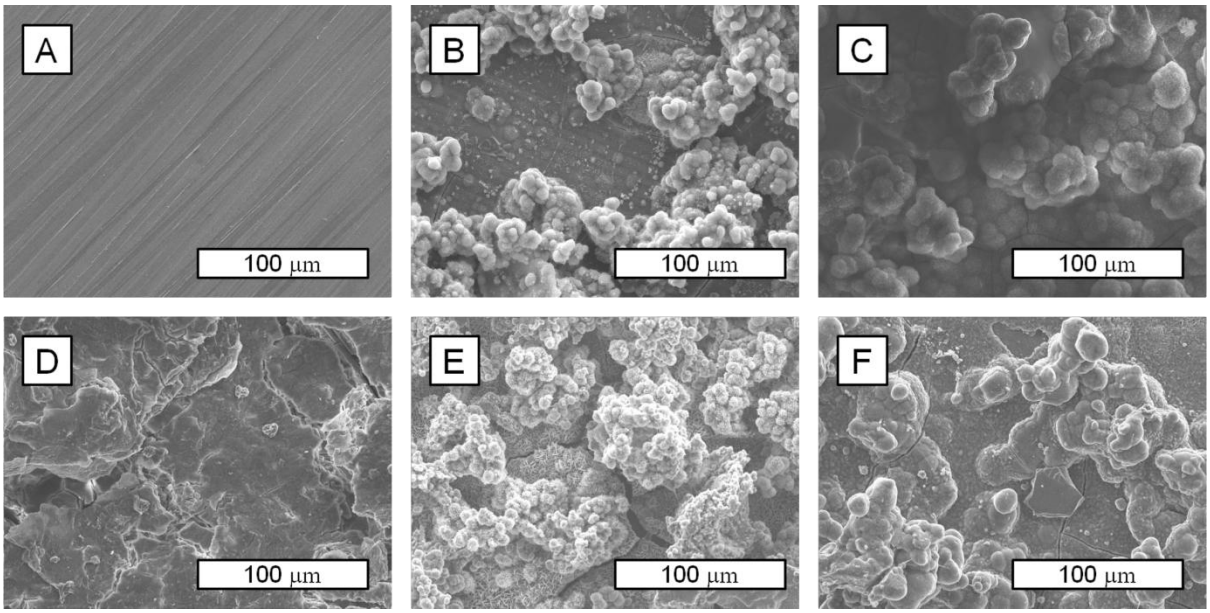

Figure 5-3: Scanning electron micrographs of uncorroded A) bare Mg, B) biomimetic coating, C) biomimetic 2 coating; morphology of D) bare Mg, E) biomimetic coating, F) biomimetic 2 coating corroded in HBSS for 14 days.

The biomimetic coatings are a method of simulating the formation of this layer, using the inorganic salts at higher concentration of Ca and PO_4^{3-} to promote the protective layer, while using low concentrations of Cl^- to prevent significant corrosion during the coating process. Instead of waiting for the layer to form *in situ*, the layer is applied first to provide corrosion protection. As shown before, these biomimetic layers can provide corrosion protection [18-20]. In this study both biomimetic coatings 1 and 2 protected the surface, leading to less corrosion and therefore less H_2 generation during the early stages of the corrosion. Despite

similar compositions, the biomimetic 2 coatings were more protective than the biomimetic 1 coatings. Biomimetic 1 coatings had low corrosion rates with little variation between samples until ~60 hours into the corrosion tests. Following that, the defects in the coating allowed corrosion to occur, accelerating the corrosion rate [19]. The accelerating rate of corrosion was quite variable across samples, leading to the large variation seen in Figure 5-2. The corrosion continued across the remainder of the 14 day test at a relatively steady rate.

In contrast to biomimetic 1 coatings, biomimetic 2 coatings remained much more corrosion resistant across the 14 days. The low variation across samples shows that although defects and cracks occurred in the coating, they did not grow or become worse as time passed in the solutions (Figure 5-3 C, F). The biomimetic 2 coatings formed the same semi-crystalline, substituted DCPD phases as the final coatings for biomimetic 1 (Figure 5-1). The difference is the layer it was formed on. Like the pretreatments in Chapter 4, the deposition of the first layer of amorphous CaP was unnecessary for the formation of the coating. However, this layer is more soluble than the final layer due to the high concentration of carbonates and lower relative amounts of Ca [8]. The solubility of this layer led to the formation of defects and delamination of the coating from the substrate at various points, leaving the Mg exposed to corrosive solution (Figure 5-3 E). This was not observed on the biomimetic 2 coatings, which although some corrosion took place, the overall integrity to the coating was not diminished over the test (Figure 5-3 F). When corroded, the coating underwent the deposition of additional CaP from the solution, and this helped to keep the effect of the defects from dominating the corrosion properties. Figure 5-4 shows that after the 14 day test, the phase of the CaP converted itself from mainly substituted, low crystalline DCPD to substituted, semi-crystalline Ca deficient apatite structure [21], a thermodynamically more stable phase [22]. This conversion of DCPD was also seen by Hu et al. after immersion in SBF [20].

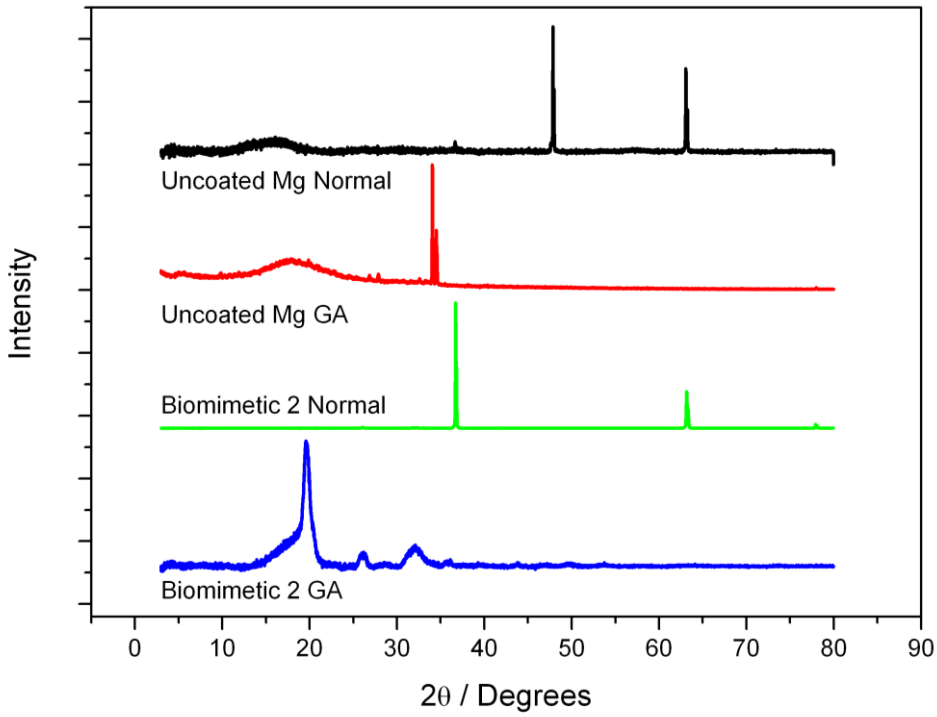

Figure 5-4: XRD after corrosion for 14 days in HBSS of uncoated Mg and biomimetic 2 coated samples (normal and glancing angle).

5.3.2.2. Effect of Coatings on Polarization Resistance

The impedance properties of the coatings show the effects of the defects and overall created integrity of the coatings. Figure 5-5A shows the Nyquist plots of the initial polarization of each coating in NaCl + HEPES and HBSS + HEPES after 1 hour in solution. The aggressive NaCl solutions, which contain no Ca^{2+} or PO_4^{3-} to deposit an insoluble layer, display the coating resistance to Cl^- attack, and the subsequent EDL resistance through the pores in the coatings. The larger resistance of the Biomimetic 2 coatings show that the deposited coating has fewer defects than the biomimetic 1 coating. This effect is also seen in HBSS. In this solution, the deposition of the additional CaPs becomes important [13]. While in NaCl after 7 hours (Figure 5-5B) the resistance of the coatings is not improved, the biomimetic 2 coating in HBSS shows increased resistance indicated by the increased impedance. This growth is not matched by the biomimetic 1 coatings. The deposition requires a pH rise to promote the nucleation [13, 23]. For Biomimetc 1 coatings with large cracks and defects, the diffusion is too great, and this formation is much slower. The Biomimetic 2 coatings have smaller defects, and are thus diffusion limited, and this effect is seen earlier. This helps the Biomimetic 2 coatings reduce the corrosion and hydrogen evolution *in vitro*.

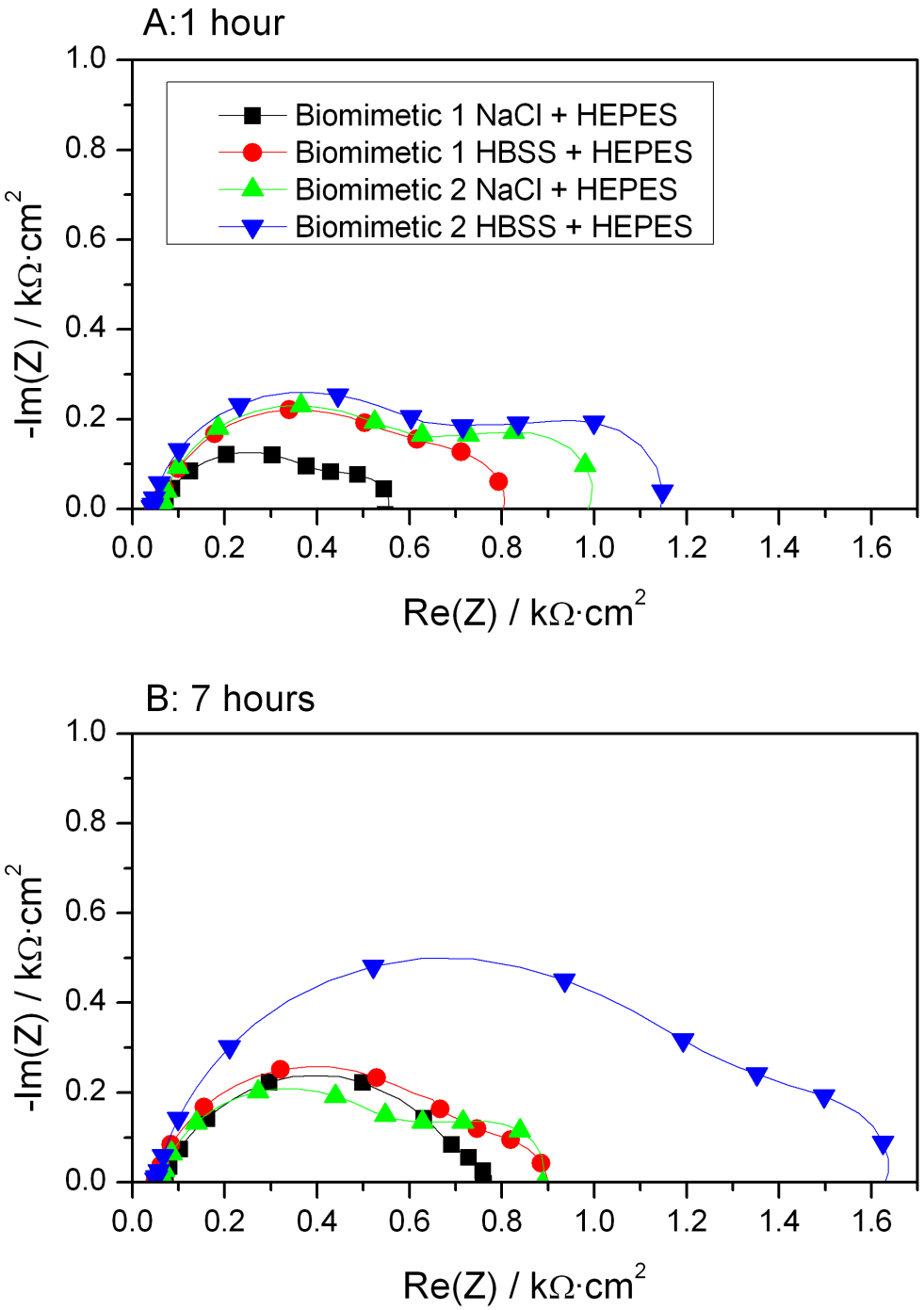

Figure 5-5: Nyquist plots of biomimetic coating 1 and 2 in NaCl and HBSS buffered with HEPES at 1 and 7 hours immersion.

5.3.3. Effect of Buffer Type on the Corrosion Measurements

The type of buffer used for the *in vitro* tests can also affect the measured corrosion rate as demonstrated in Chapter 3. E_{Corr} and i_{Corr} for both coatings is compared to uncorroded Mg in NaCl and HBSS buffered with HEPES, as well as HBSS buffered with HCO_3 (Figure 5-6).

The initial corrosion potential of all of the biomimetic 2 coatings was lower than the Biomimetic 1 coatings. The better protection of these layers prevented Mg^{2+} ion formation at the surface, keeping the E_{Corr} low. The slower corrosion rate by the more complete coatings is also preventing the corrosion layer from stabilizing as quickly for these coatings as well. However, the i_{Corr} for all Biomimetic 2 samples was lower than Biomimetic 1 samples, as indicated by the better coating properties. The bicarbonate buffered solutions led to much lower corrosion rates than HEPES buffered samples. This effect was seen on both biomimetic coatings, but the effect was particularly significant for biomimetic 2 coatings.

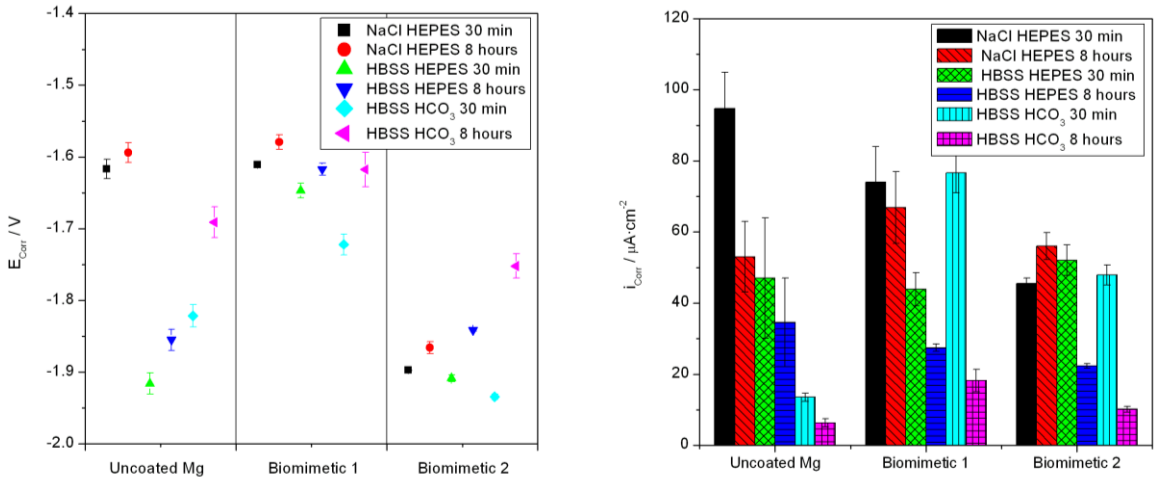

Figure 5-6: E_{Corr} and i_{Corr} for biomimetic 1 and biomimetic 2 coated samples.

PDP of the Biomimetic 2 coating reveals the origins of this effect. Like the Mg, when the HCO_3 buffer contains Ca ions, the passive carbonate layer that forms prevents corrosion [24]. Figure 5-7 shows that over the first 8 hours, the anodic reaction rate is slowed due to the formation of these layers. This is not seen in NaCl solutions, where the only mechanism of corrosion is the chloride ion attack. In HBSS, the anodic reaction rate drops while the cathodic reaction remains relatively unchanged. The HCO_3 buffer enhances this effect due to the lower buffer capacity and the high concentration of carbonate ions available to form calcium carbonate phases.

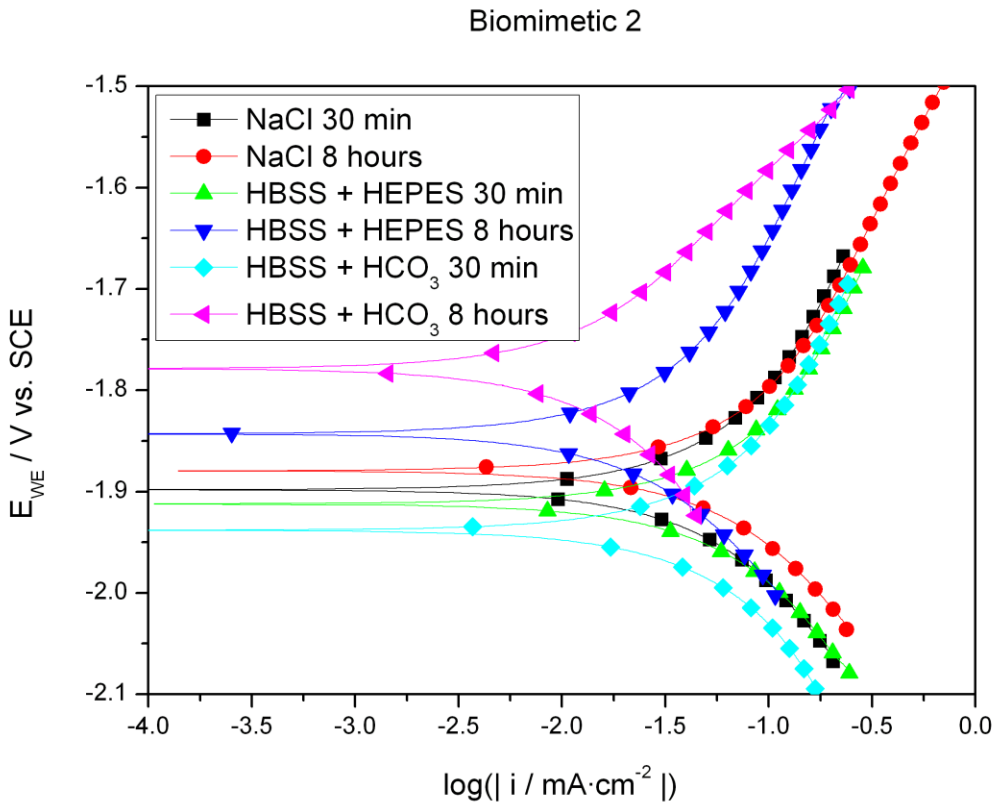

Figure 5-7: Polarization of Biomimetic 2 coatings in HEPES and HCO_3 buffered solutions.

Thus, the resistance to corrosion of the coating goes up in the bicarbonate buffered HBSS as immersion time increases (Figure 5-8). This effect is not seen in NaCl for either coating, or in HBSS for biomimetic 1. Biomimetic 2 coatings improve slightly in HBSS due to the CaP deposition effect [13]. However, both coatings show constant improvement in HCO_3 solutions. The difference between these two effects is shown by the Nyquist plots over 1 and 7 hours (Figure 5-9). The growth of the EDL time constant surpasses the coating resistance for both coatings over 7 hours in HCO_3 solutions. The decreased area available to corrosion due to the pH rise and the deposition of the carbonates accounts for the lower corrosion current due to the anodic shift. Therefore, the measured corrosion and hydrogen evolution over 14 days in HEPES buffered solutions will likely be higher than the corrosion rate experienced in a HCO_3 buffered solution, such as *in vivo*.

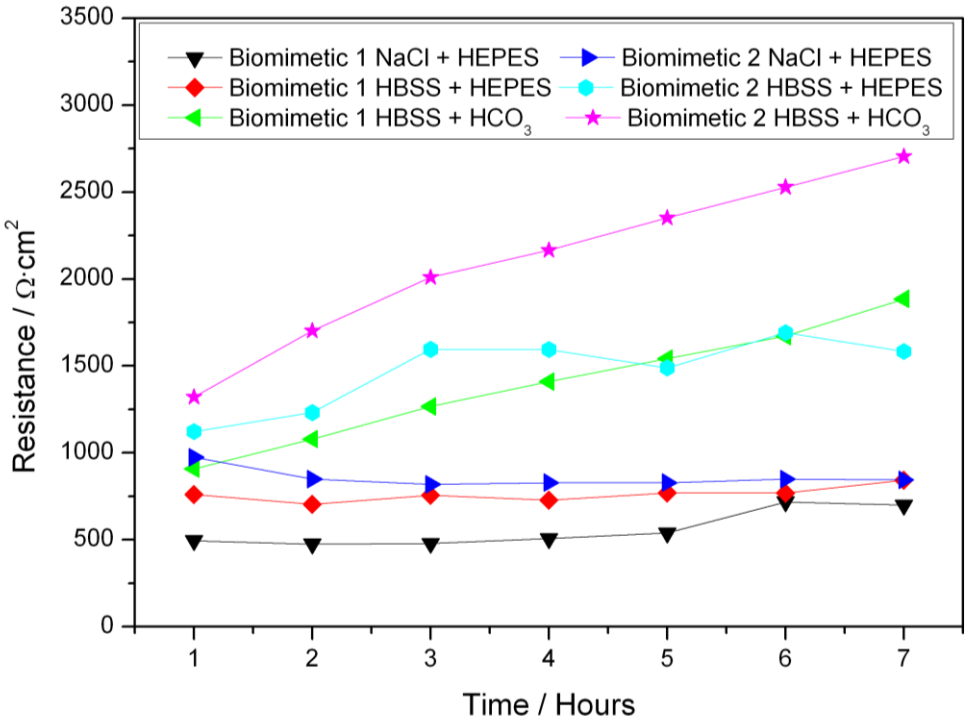

Figure 5-8: Polarization resistance over 7 hours of both biomimetic coatings in HEPES and HCO_3 buffered solutions.

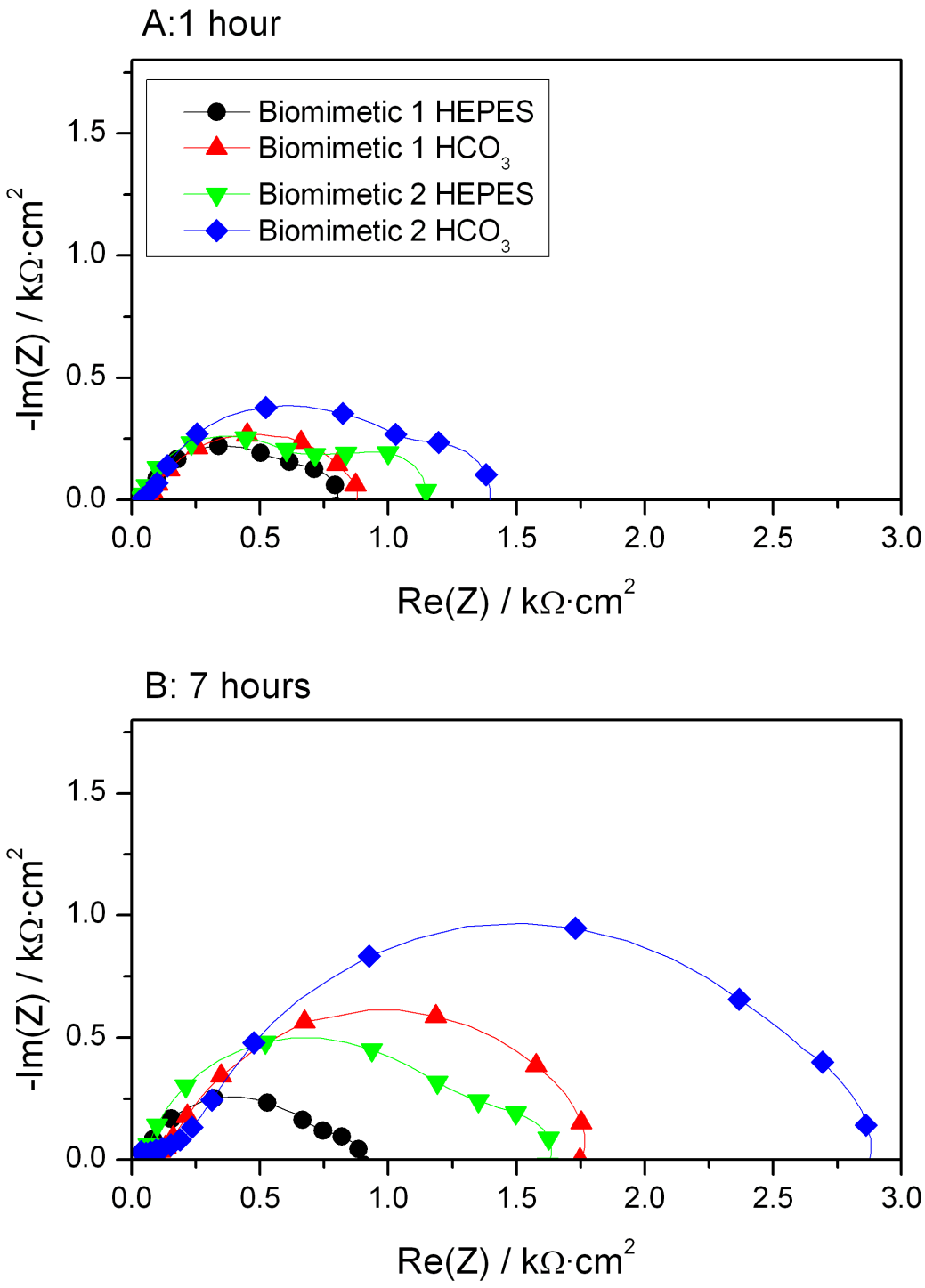

Figure 5-9: Nyquist plots of coated samples in HBSS buffered with HEPES or HCO3 at A) 1 and B) 7 hours.

5.4. Conclusions

The experimental data here unambiguously shows that the high Mg amorphous carbonated CaP first step in the coating is not required for deposition of the biomimetic coating on Mg, like it is on Ti [1, 2]. The availability of Mg^{2+} ions and pH rise from the corrosion of the Mg provides enough nucleation potential on Mg to provide a full coverage coating. This is a major difference between that and Ti, where there is no corrosion and the high carbonate solution is needed to provide the inhibition of large crystals that the Mg^{2+} ions perform here. The deposition of the final biomimetic 2 coatings was similar in composition and crystal structure to the substituted DCPD biomimetic coatings created with the first step [8]. The corrosion protection was found to be much greater without this step, as the biomimetic 2 coatings produced minimal H_2 gas over the course of the 2 week immersion test in HBSS. This low level of H_2 generation puts the coatings in range of predicted acceptable levels of H_2 generation *in vivo* [17]. Over the 14 day test, the phase of the calcium phosphate coatings changed from mostly DCPD to a calcium deficient apatite structure. This more stable phase is less soluble and provides more protection than the amorphous phase that formed on uncoated Mg [22]. The corrosion protection provided by these coatings was still limited by the defects and corrosion through the coating, rather than the dissolution of the coating itself. The defects and the corrosion problem they present remain a challenge for the use of these coatings *in vivo*. The biomimetic 2 coatings did show some signs that the deposition of additional CaP from solution helped to repair the defects and extend the protection. If this mechanism can be optimized and utilized it may help provide a coating with better protection properties.

The choice of buffer was shown to have an effect on both the measured rates of corrosion and the mechanism of corrosion that takes place. The HEPES buffer proved to be more aggressive than the bicarbonate buffer due to the better control of the pH rise and the lack of carbonate phases contributing to the corrosion layer. The measured corrosion rates in HEPES are thus expected to be faster than the HCO_3 in vitro tests. In vivo tests are more difficult to determine, but it seems likely that the HEPES buffer will provide the upper bound of the corrosion rate, as it's expected that the HCO_3 buffer *in vivo* will present slower rather than faster corrosion [24].

5.5. References

1. Bigi, A., E. Boanini, B. Bracci, A. Facchini, S. Panzavolta, F. Segatti, and L. Sturba, *Nanocrystalline hydroxyapatite coatings on titanium: a new fast biomimetic method.* Biomaterials, 2005. **26**(19): p. 4085-4089.
2. Wen, H.B., J.G.C. Wolke, J.R. de Wijn, Q. Liu, F.Z. Cui, and K. de Groot, *Fast precipitation of calcium phosphate layers on titanium induced by simple chemical treatments.* Biomaterials, 1997. **18**(22): p. 1471-1478.
3. Zhu, L., X. Ye, G. Tang, N. Zhao, Y. Gong, Y. Zhao, J. Zhao, and X. Zhang, *Biomimetic coating of compound titania and hydroxyapatite on titanium.* Journal of Biomedical Materials Research Part A, 2007. **83A**(4): p. 1165-1175.
4. Baker, K.C., M.A. Anderson, S.A. Oehlke, A.I. Astashkina, D.C. Haikio, J. Drelich, and S.W. Donahue, *Growth, characterization and biocompatibility of bone-like calcium phosphate layers biomimetically deposited on metallic substrata.* Materials Science and Engineering: C, 2006. **26**(8): p. 1351-1360.
5. Kim, H.-M., F. Miyaji, T. Kokubo, and T. Nakamura, *Preparation of bioactive Ti and its alloys via simple chemical surface treatment.* Journal of Biomedical Materials Research, 1996. **32**(3): p. 409-417.
6. Barrere, F. and C.M.v.d. Valk, *Osteogenecity of octacalcium phosphate coatings applied on porous metal implants.* Journal of Biomedical Materials Research Part A, 2003. **66A**(4): p. 779-788.
7. Barrere, F., C.M. van der Valk, G. Meiger, R.A.J. Dalmeijer, K. De Groot, and P. Layrolle, *Osteointegration of biomimetic apatite coating applied onto dense and porous metal implants in femurs of goats.* Journal of Biomedical Materials Research Part B: Applied Biomaterials, 2003. **67B**(1): p. 655-665.
8. Barrere, F., *Biomimetic Calcium Phosphate Coatings: Physicochemistry and Biological Activity*. 2002, University of Twente: Enschede.
9. *PDF 01-074-6549*. 1962, International Center for Diffraction Data: Newton, PA.
10. Bigi, A., G. Falini, E. Foresti, A. Ripamonti, M. Gazzano, and N. Roveri, *Magnesium influence on hydroxyapatite crystallization.* Journal of Inorganic Biochemistry, 1993. **49**(1): p. 69-78.
11. Barrere, F., C.A. van Blitterswijk, K. de Groot, and P. Layrolle, *Nucleation of biomimetic Ca-P coatings on Ti6Al4V from a SBF×5 solution: influence of magnesium.* Biomaterials, 2002. **23**(10): p. 2211-2220.
12. Habibovic, P., F. Barrere, C.A. van Blitterswijk, K. de Groot, and P. Layrolle, *Biomimetic hydroxyapatite coating on metal implants.* Journal of the American Ceramic Society, 2002. **85**(3): p. 517-22.
13. Gray-Munro, J.E. and M. Strong, *The mechanism of deposition of calcium phosphate coatings from solution onto magnesium alloy AZ31.* Journal of Biomedical Materials Research Part A, 2009. **90A**(2): p. 339-350.
14. Nguyen, T.L., Blanquet, A., Staiger, M.P., Dias, G.J., Woodfield, T.B.F., *On the role of surface roughness in the corrosion of pure magnesium in vitro.* Journal of Biomedical Materials Research Part B, 2012. **In Press**.

15. Alvarez, R.B., H.J. Martin, M.F. Horstemeyer, M.Q. Chandler, N. Williams, P.T. Wang, and A. Ruiz, *Corrosion relationships as a function of time and surface roughness on a structural AE44 magnesium alloy.* Corrosion Science, 2010. **52**(5): p. 1635-1648.
16. Rettig, R. and S. Virtanen, *Time-dependent electrochemical characterization of the corrosion of a magnesium rare-earth alloy in simulated body fluids.* Journal of Biomedical Materials Research Part A, 2008. **85A**(1): p. 167-175.
17. Song, G., *Control of biodegradation of biocompatable magnesium alloys.* Corrosion Science, 2007. **49**(4): p. 1696-1701.
18. Keim, S., J.G. Brunner, B. Fabry, and S. Virtanen, *Control of magnesium corrosion and biocompatibility with biomimetic coatings.* Journal of Biomedical Materials Research - Part B Applied Biomaterials, 2011. **96 B**(1): p. 84-90.
19. Waterman, J., A. Pietak, N. Birbilis, T. Woodfield, G. Dias, and M.P. Staiger, *Corrosion resistance of biomimetic calcium phosphate coatings on magnesium due to varying pretreatment time.* Materials Science and Engineering: B, 2011. **176**(20): p. 1756-1760.
20. Hu, J., C. Wang, W.C. Ren, S. Zhang, and F. Liu, *Microstructure evolution and corrosion mechanism of dicalcium phosphate dihydrate coating on magnesium alloy in simulated body fluid.* Materials Chemistry and Physics, 2010. **119**(1-2): p. 294-298.
21. *PDF 04-013-6614*. 2006, International Center for Diffraction Data: Newton, PA.
22. León, B. and J.A. Jansen, *Thin Calcium Phosphate Coatings for Medical Implants*. 2008: Springer.
23. Lorenz, C., J.G. Brunner, P. Kollmannsberger, L. Jaafar, B. Fabry, and S. Virtanen, *Effect of surface pre-treatments on biocompatibility of magnesium.* Acta Biomaterialia, 2009. **5**(7): p. 2783-2789.
24. Yamamoto, A. and S. Hiromoto, *Effect of inorganic salts, amino acids and proteins on the degradation of pure magnesium in vitro.* Materials Science and Engineering: C, 2009. **29**(5): p. 1559-1568.

CHAPTER 6: Improving the *in vitro* Corrosion Resistance of Biomimetic Calcium Phosphate Coatings for Mg using a Calcium Hydroxide Layer

Biomimetic calcium phosphate coatings have been studied to improve the corrosion resistance of biodegradable magnesium alloys. The corrosion resistance of these coatings was found to be limited by the defects in the coating [1, 2]. A method for improving the corrosion response of these coatings is therefore needed if biomimetic coatings are to be used for corrosion protection. In this study, a calcium hydroxide under layer was applied to improve the properties of these biomimetic coatings. The *in vitro* corrosion response was studied using hydrogen evolution and electrochemical techniques. It was found that the calcium hydroxide layer increased the corrosion resistance of the coatings. The coatings created had fewer defects than the unmodified biomimetic coatings. Over time, the calcium hydroxide layer also prevented the defects in the coating from growing, leading to longer lasting protection. The results of this study suggest calcium hydroxide coatings can significantly improve the corrosion protection of a biomimetic coating system.

6.1. Introduction

Biomimetic coatings have been shown to be able to reduce the corrosion rate of Mg. This, coupled with the biocompatibility [3-5] and osteogenic properties [6-8] of these coatings make them ideal candidates for corrosion protection of a degradable implant. However, as the previous work has shown, these coatings are often undermined by the presence of defects and pores that allow local corrosion to continue beneath the coating. This results in a loss of mechanical strength before new bone has healed so it may carry the physiological loads. Moreover, the release of H_2 gas at rates above which the surrounding tissue can safely dispose of it needs to be avoided in a clinical setting. The degradation rate needs to remain very low during the initial phase of tissue recovery, then degrade completely at a rate low enough that hydrogen gas does not accumulate [9]. The exact rates will depend on the type and site of the implant, however, the corrosion protection provided by the biomimetic coatings must not be compromised by too many defects. While steps can be taken to reduce

the amounts of defects created as presented in Chapter 4 and 5, the implant needs to also be protected from defects that may form during or after implantation due to mechanical or thermal stresses.

Recalling that magnesium is a very active metal [10], with a standard reduction potential of -2.37 V, any Mg left exposed to an aqueous solution will oxidize at physiological conditions. When magnesium corrodes in water, the net reaction is $Mg_{(s)} + 2H_2O \rightarrow Mg(OH)_2 + H_{2(g)}$ [11, 12]. $Mg(OH)_2$ is fairly insoluble in water. If part of this layer dissolves, or is removed by mechanical means, the metallic magnesium beneath corrodes and re-passivates the surface, by forming additional $Mg(OH)_2$. This protects from further corrosion. This mechanism does not serve to protect in the body because Cl^- acts a catalyst to speed up the reaction [11]. The Cl^- replaces OH^- in the layer, but is much more water soluble than $Mg(OH)_2$ [13]. The high concentration of Cl^- *in vivo* means the passive layer is not protective in the body, leading to fast degradation rates. A protection mechanism is required at the Mg substrate that will react to the solution in the same manner as a passive layer, forming an insoluble barrier beneath any defects that appear during processing or use. Once again taking a biomimetic approach, the development of a self-healing property or mechanism that provides the required level of protection from the corrosion medium could be envisaged in order to "heal" defects as they appear.

Unfortunately, as previous chapters describe, the biomimetic coatings are fraught with problems. During the coating process, adhesion of the coating to the surface and complete coverage are necessary to prevent internal corrosion of the implant. Any defects can lead to corrosion underneath the coating, leading to lower adhesion of the coating and increasing corrosion rates [2]. Calcium phosphates are much more brittle than the underlying substrate. As such, the likelihood of defects is high for a load bearing implant. Therefore a coating that is not as sensitive to defects is desirable. Furthermore, the coating process in chemical solutions often allows, and in some cases, partially relies on the corrosion of Mg to deposit the CaP [1, 18]. Magnesium corrosion releases Mg^{2+} ions in solution, and these ions can have a negative effect on the solution coating by inhibiting the formation of crystalline apatite [25], favouring more soluble phases [14]. The deposition of CaP and calcium carbonates from *in vitro* [18] and *in vivo* [26] are interesting phenomena, as they presents us with a possible mechanism for imitating passivation, using the chemistry of the surrounding fluids. As seen in Chapters 4 and 5, the additional nucleation of calcium compounds on the Mg can

increase the protection of the layer and slow corrosion. Unfortunately, the deposition of such compounds is limited in the deposition rate and insolubility, due to the relatively low amount of Ca available in the body, with typical blood plasma containing only 2.5 mM Ca^{2+} [27]. To increase the protection this provides, an additional source of calcium at the defect sites is required.

Calcium hydroxide ($Ca(OH)_2$) is often used as a biomaterial in dental applications [28]. The application of a calcium hydroxide coating can be used to provide a pretreatment or act as a sublayer to a top layer of calcium phosphate. Such a layer could possibly be used to increase the protective properties of the biomimetic coatings. It is hypothesised that the deposition of a $Ca(OH)_2$ underlayer will encourage the formation and reformation of the biomimetic CaP layer. It is thought that disassociation of $Ca(OH)_2$ should provide a ready supply of Ca^{2+} to form CaP, while the OH^- raises the pH and promotes further CaP deposition.

Once the final CaP coating is applied and immersed in a corrosive *in vitro* or *in vivo* environment, a slightly soluble calcium base layer exists just below the surface. Any cracks that form, or defects from the original coating, will lead to corrosion of this layer. In an *in vivo* solution, the phosphate ions present can react with the calcium ions to precipitate a new layer CaP at the defects. This happens naturally on Mg in physiological solutions [18], but the rate of coverage and deposition was found to be too slow and hence not sufficiently protective of the Mg substrate (Chapter 5). This study shows the improvement of a biomimetic calcium phosphate coating using an electrochemical assisted deposition (ECAD) coating of calcium hydroxide for corrosion protection of biomedical magnesium.

6.2. Materials and Methods

6.2.1. Preparation of Calcium Hydroxide Coatings

Pure Mg (99.98% Timminco) samples were cut to 15 × 15 mm sections and mounted in epoxy with a copper wire attached at the back for electrical connection, and one face exposed for deposition. This provided a consistent surface area for both coating deposition and corrosion measurement. Samples were polished to 1200 grit with SiC. Samples were then ultrasonically cleaned in ethanol for 5 minutes and allowed to dry in air.

6.2.2. Calcium Hydroxide Coating

ECAD samples were coated using a standard 3 electrode setup with a saturated calomel electrode (SCE) as the reference and a flat Pt plate as the counter electrode. The sample face was mounted parallel to the counter electrode, at a distance of 1 cm in a 2M $Ca(NO_3)_2$ solution. Potentiostatic coating performed with -3.2V volts vs. the SCE reference for 10 min. Following deposition, samples were rinsed with ethanol and allowed to dry in air.

6.2.3. Biomimetic Calcium Phosphate Coating

After ECAD coating, samples were biomimetically coated using the modified 5x concentrated simulated body fluid (SBF) in the process described in Chapter 5 [2]. The pH of the solution was controlled during the process by dissolving carbon dioxide gas (CO_2) in the solution. One litre of biomimetic coating solution 2 was heated to 37 °C and $CO_{2\ (g)}$ was bubbled through for 15 minutes to attain a pH of 6. The CO_2 was then removed, samples were immersed in the solution, and air was bubbled through the solution for 24 hours. The solution was stirred with a magnetic stirrer to ensure uniform ionic concentrations. After 24 hours the solution pH rose to approximately 8. The samples were removed, and rinsed with distilled water, and allowed to dry in air at room temperature.

6.2.4. Characterization

Coatings created were characterized by scanning electron microscopy (SEM) (JEOL 7000F FE-SEM), energy dispersive X-ray Spectroscopy (EDS) and X-Ray Diffraction Spectroscopy (XRD) (PANalytical X'Pert-Pro MPD PW3040/60) were used to determine composition. Sample preparation was carried out as described in Chapter 4.

6.2.5. Corrosion Testing

Corrosion tests were carried out to measure the corrosion rate. Experiments were carried out in Hanks' Balanced Salt Solution (HBSS) at 37 ± 0.5 °C and pH of 7.4 ± 0.05, buffered with 4-(2-hydroxyethyl)-1-piperazineethanesulfonic acid (HEPES) (25mM). 500 mL of solution was used per sample for each hydrogen evolution test. Glass burettes were used to collect the hydrogen gas and measure the total hydrogen evolved with a precision of ± 0.1 mL. Corrosion solution was refreshed every 72 hours to keep pH and ionic composition relatively

constant. 5 samples of each biomimetic, ECAD + biomimetic, and uncoated Mg were measured. The H_2 Evolution was monitored for a total of 14 days.

Electrochemical tests were performed by potentiodynamic polarization (PDP) and electrochemical impedance spectroscopy (EIS). A three electrode setup was used with a Pt counter electrode and a saturated calomel reference electrode (SCE). 300 mL of HBSS was used for each test. The area of the working electrode was 1 cm^2. PDP tests were carried out after 20 minutes in solution to allow the open circuit potential to stabilize. PDP tests utilized a scan rate of 1 mV/s, and scanned over the range OCP – 0.100 V to Ref + 0.500 V. EIS scans were performed once every hour over a period of 72 hours to evaluate the change in corrosion resistance with time. An AC 10mV peak to peak signal from OCP across a frequency range from 50 kHz to 20 mHz was used.

6.3. Results and Discussion:

6.3.1. Calcium Hydroxide Layer Formation by ECAD:

Electrodeposition proved to be useful for depositing a calcium hydroxide coating on the samples. The coating produced by ECAD in concentrated 2M $Ca(NO_3)_2$ solution was dense and covered the entire surface more or less uniformly (Figure 6-2A). The coating exhibited no areas that were not covered. The coating consisted of $Ca(OH)_2$ as confirmed by XRD (Figure 6-3) and EDS. The ECAD process required an overvoltage to create a calcium hydroxide coating through the reduction of water (Figure 6-1). The surface of the magnesium was held at -3.2 V (vs. SCE). The current through the cathode reduced water in the solution (Equation 6-1).

$$2\ H_2O + 2\ e^- \rightarrow H_{2(g)} + 2\ OH^- \qquad \text{Equation 6-1}$$

$$Ca^{2+} + 2\ OH^- \rightarrow Ca(OH)_{2(s)} \qquad \text{Equation 6-2}$$

The increase in pH had the effect of decreasing the solubility of Ca^{2+} ions in solution, resulting in the precipitation of solid calcium hydroxide on the surface of the substrates (Equation 6-2). The coating can be formed very quickly, a 10 µm thick layer formed in just 10 minutes of deposition (Figure 6-2). Once formed, the $Ca(OH)_2$ acts as an electrical

insulator, limiting the amount of current output during the electrostatic coating process. This limits the total thickness that may be achieved and longer deposition times were not found to significantly increase the coating thickness. 10 minutes was used to attain complete coverage of the surface. The coating did cover the entire surface relatively uniformly after 10 minutes of treatment, and had enough adhesion that it did not readily scratch or flake away.

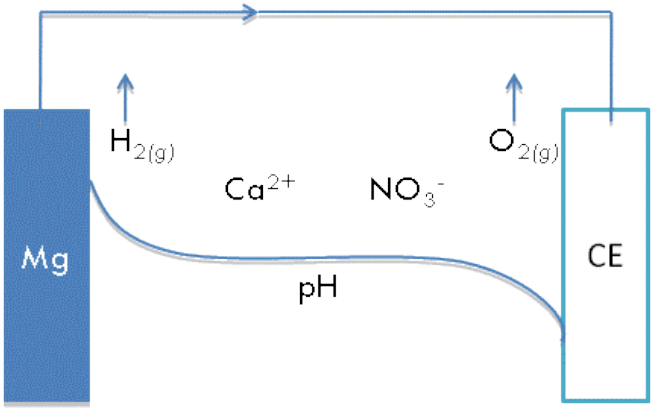

Figure 6-1: Schematic of the ECAD process.

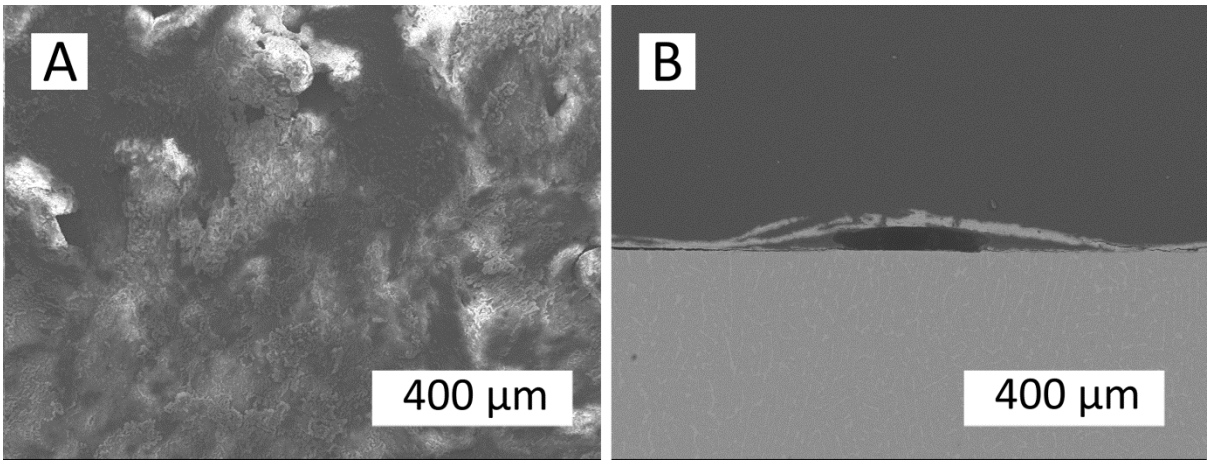

Figure 6-2: Scanning electron microghraphs of ECAD $Ca(OH)_2$ coating (A) and cross section of a bubble defect (B).

The coating method does present a few problems. The hydrogen gas evolved forms in bubbles that block $Ca(OH)_2$ formation at the interface, resulting in volcano-like defect, as reported by Kumar et al. [29]. Figure 6-2B shows the cross section of such a gas bubble defect in the coating. The gas bubbles can be minimized by stirring and or shaking to remove them more quickly from the surface. This will also have the effect of dispersing the pH rise near the surface, and since the ECAD process relies on the reduction of water, there is no way

to eliminate the hydrogen gas bubbles completely. As such, another method for depositing the calcium hydroxide layer might ultimately be found to be more suitable.

6.3.2. The Formation of the Biomimetic Coating on the Calcium Hydroxide Layer

After the $Ca(OH)_2$ layer was deposited on the magnesium, a calcium phosphate layer was applied to the surface. The biomimetic coatings can be applied on top of other types of coatings [23], and the $Ca(OH)_2$ served as a suitable surface for deposition. The biomimetic coating created flake like structure of a calcium phosphate compound on the surface (Figure 6-4). According to the glancing angle XRD (Figure 6-3), the coating formed mainly dicalcium phosphate dihydrate, or brushite [30]. The biomimetic layer produced on the surface of the ECAD coated material is slightly different to the biomimetic layers produced on bare magnesium substrates in morphology (Figure 6-4A and B). The difference can be attributed to differences in crystal growth and nucleation as well as small changes in composition due to the Ca rich ECAD layer.

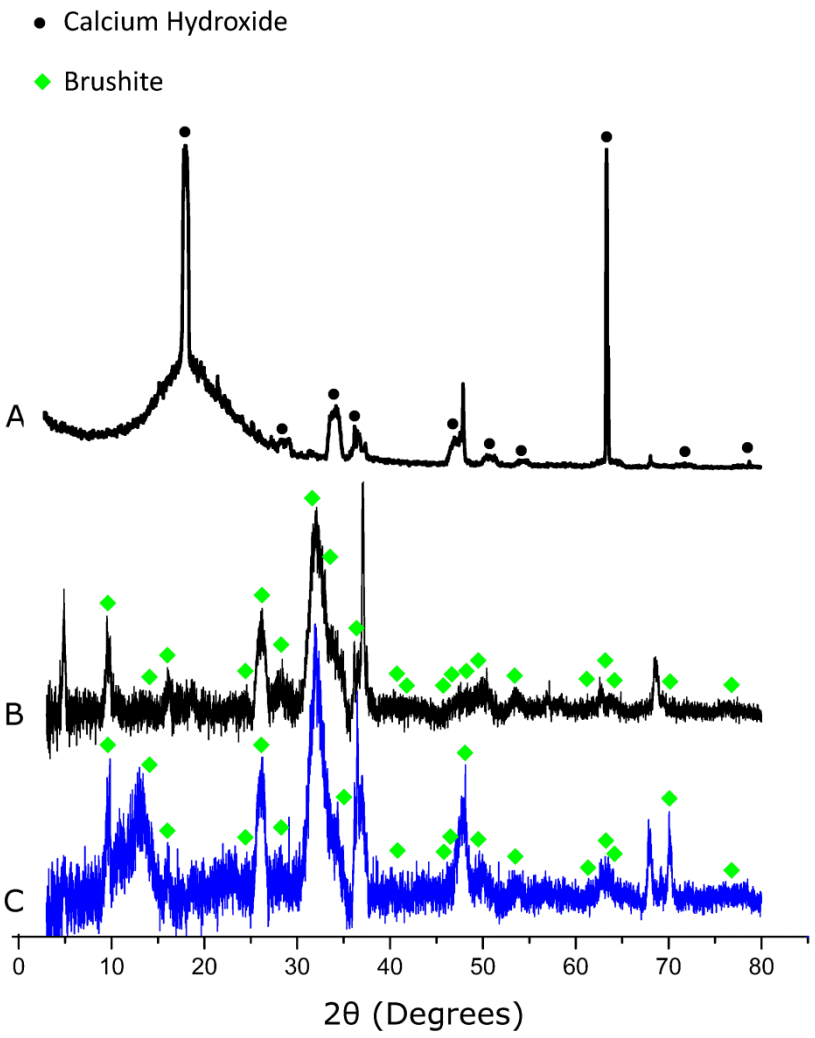

Figure 6-3: GA-XRD of $Ca(OH)_2$ coating by ECAD (A), biomimetic coating (B), and ECAD + biomimetic coating (C).

Biomimetic coatings can protect against magnesium corrosion by themselves, however the coatings tend to have a few problems. The coatings are deposited in solutions similar to the body fluids, and therefore often include additional phases and ionic substitutions in the crystal lattice. While these increase the biocompatibility compared to crystalline synthetic CaP [4, 7] the resulting phases also tend to increase the solubility [15], and thus decrease the corrosion resistance. Substitutions in the lattice with Mg is typically high, especially on a Mg substrate, which tends to corrode during the process, creating a high Mg^{2+} concentration near the surface of the substrate. Mg^{2+} has the effect of decreasing the crystallinity of the calcium phosphate [25]. For ECAD samples, the corrosion of the magnesium during the biomimetic coating was mitigated by the calcium hydroxide coating. Rather than the Mg substrate corroding in the coating solution, the $Ca(OH)_2$ protected it. The pH rise that helps form

coatings in solution due to magnesium corrosion [18] can instead be created by the dissolution of calcium hydroxide. This could help to prevent so many Mg ions from getting into the coating. Mg ions break up the lattice [31] and this ultimately creating a more soluble and less protective coating.

Additionally, The $Ca(OH)_2$ layer provided a surface of calcium that is slightly soluble for the CaP layers to convert to and nucleate on. The phosphate groups in the biomimetic solution can replace hydroxide groups on the surface of the ECAD layer to form the more insoluble calcium phosphates. CaP then provides sites for further nucleation of the biomimetic coating. This could account for the differences observed in the morphology (Figure 6-4) and composition between the two coatings (Figure 6-3).

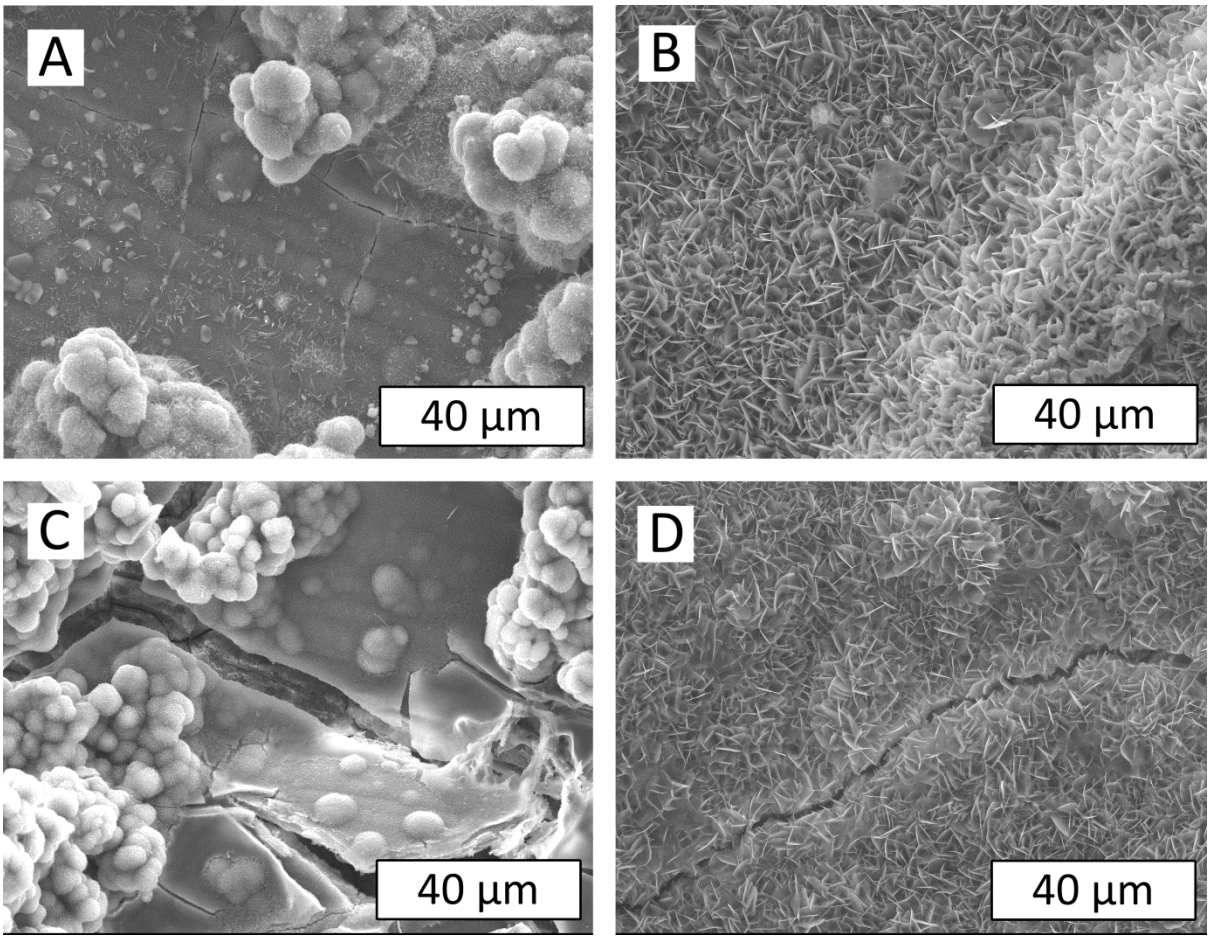

Figure 6-4: Biomimetic 1 coating before (A) and after corrosion in HBSS for 24 hours (C). ECAD + biomimetic coat before (B) and after corrosion in HBSS for 24 hours (D).

6.3.3. The Effect on Corrosion Protection of the ECAD + Biomimetic Coating

Corrosion protection of coatings was assessed in HBSS at 37 °C to simulate the chemical conditions found in human body fluid. The corrosion mechanism to be studied was the protection against chloride ion attack as well as the deposition of calcium phosphate compounds on the surface from the SBF [18]. Hence, HBSS was chosen for the tests because it contains these salts without the complication of other compounds such as proteins. The use of the HEPES buffer prevents the corrosion reaction from changing the pH of the solution without the need for an active pH control system such as that found in the body. The corrosion solutions were used for up to 72 hours, after which the pH of the solution was kept within ± 0.1 for all samples by the HEPES buffer.

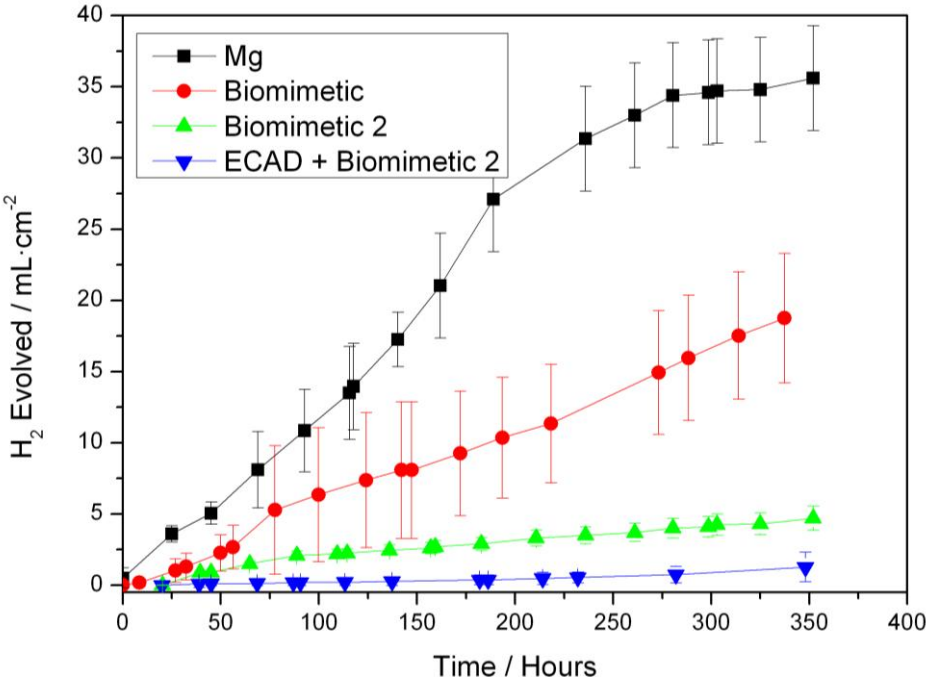

Figure 6-5: Total hydrogen evolved over 14 days.

The corrosion rate was monitored by hydrogen gas evolution in order to examine the longer term corrosion behaviour of these coatings(Figure 6-5). The hydrogen evolution of the ECAD modified coatings was compared to uncoated Mg and both coatings described in earlier chapters. The uncoated samples exhibited rapid corrosion. For uncoated samples, the curvature of the early part of the graph showed accelerating corrosion rate. This is due to

local pitting of the Mg surface [32]. This effectively increased the surface area available to the solution, leading to an accelerating corrosion rate. Later, this rate slowed as the calcium phosphate was deposited on the surface of the Mg [33]. This layer begins to protect the surface. As such, beyond ~250 hours of corrosion in SBF the corrosion rate decelerates. But already significant amounts of H_2 gas had been generated, by 350 hours the average amount of gas per sample is 35.6 mL (Table 6-1). So to form this protective layer in SBF required a large amount of corrosion to occur. This is unacceptable for degradable implants as the mechanical strength of the implant needs to survive during the initial stages of healing [34].

Table 6-1: Comparison of corrosion values

Coating	**I_{corr} ($\mu A \cdot cm^{-2}$)**	**R_P at 72 (hours ($\Omega \cdot cm^2$)**	**H_2 at 14 days ($mL \cdot cm^{-2}$)**
ECAD + Biomimetic	3.4	8547	1.3
Biomimetic 2	16.8	3280	4.7
Uncoated Mg	34.8	1640	35.6

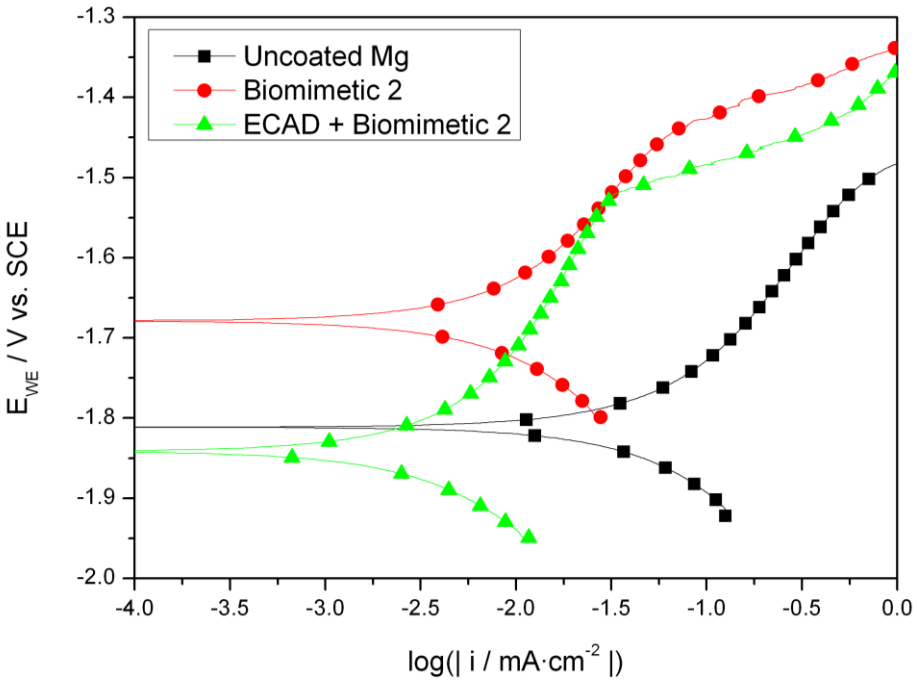

Figure 6-6: Potentiodynamic polarization curves for selected samples after 72 hours immersion.

The biomimetic coatings are applied to simulate this process and create the protective coating before it is exposed to the solution. The biomimetic 2 coatings protect the substrate from corrosion by blocking the corrosive environment from the underlying Mg. Indeed, early in the life of the coating both of the biomimetic calcium phosphates provided much greater protection from the corrosive environment than the uncoated counterparts (Figure 6-5). The PDP tests showed the biomimetic coating had a lower corrosion current density (Figure 6-6) than the uncoated Mg, and a corresponding higher polarization resistance (Figure 6-7). The lower current density was due to the smaller portion of exposed area to the solution. Thus, there was a decrease in the anodic reaction rate. The corrosive solution cannot attack the magnesium where it is protected by the calcium phosphate coating. However, there were cracks and defects in the coating where the corrosion could continue, as seen in Figure 6-3A. These cracks create an imperfect coating that allows the corrosion reaction to progress. This effect can be seen by the two time constant frequency response to polarization that corresponds to a porous coating (Figure 6-9). The biomimetic 2 coating exhibits a resistance and capacitance of the coating itself and one for the electrolytic double layer (EDL) that forms the interface with the metal to solution. Contrast this to the uncoated Mg which exhibits a single semicircle corresponding to the EDL without significant contribution of a coating layer. Thus, the corrosion rate and corresponding H_2 generation is lower for biomimetic coated samples, but the defects in the biomimetic coating still allowed corrosion to occur.

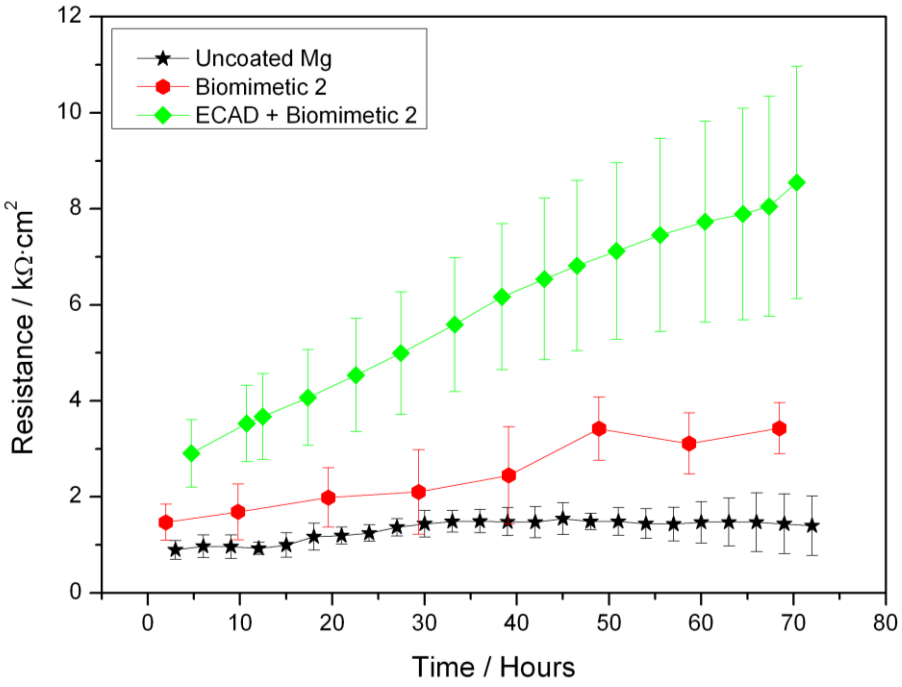

Figure 6-7: Total coating polarization resistance over 72 hours immersion in HBSS.

Over time, the biomimetic coating properties changed. While the polarization resistance was relatively steady over the first 72 hours, the corrosion rate remained relatively low. Later on, the coatings begin to fail. The size of the defects increased, as seen in Figure 6-4C. The brushite coating created were not as stable as apatite coatings, as they can partially dissolve in SBF [14]. Furthermore, as the substrate was attacked underneath, the coatings would delaminate from the surface, exposing more area for corrosion [2]. As this happened, the average amount of corrosion increased. The variability of the coating increased as well, as coatings delaminated nonuniformly across the sample population. Figure 6-5 shows this trend of increasing corrosion, although the rate is still less than the uncoated samples. Clearly the biomimetic coatings protect from corrosion, but the defects allow some corrosion to occur. If coatings such as these are to be used for slowing the corrosion rate, this problem of corrosion through defects in a metastable biomimetic coating is a significant challenge.

The ECAD coatings attempt to solve this problem by using the $Ca(OH)_2$ under layer to enhance the corrosion resistance of the biomimetic coatings. The $Ca(OH)_2$ is slightly soluble in the biomimetic coating solutions, leading to better coverage and conversion of the coating.

The initial polarization resistance of the ECAD coatings are higher than the biomimetic coatings (Figure 6-7). There is a corresponding decrease in the corrosion current density measured by PDP in Figure 6-6 as well. Compared with the uncoated Mg, the ECAD coating decreases both the anodic and cathodic reaction rates. While both coatings slow the anodic reaction the ECAD coating also affects the cathodic reaction, leading to the much lower H_2 formation rate. This indicates that the layer formed after the biomimetic coating process, while similar in composition leaves a smaller area of defects though which to continue the corrosion reaction. The polarization resistance over the first 72 hours displayed an interesting trend. The ECAD coated samples actually increased in polarization resistance as time passed in the corrosion solution. This indicates that as the samples were immersed, the protective qualities of the coating actually increased.

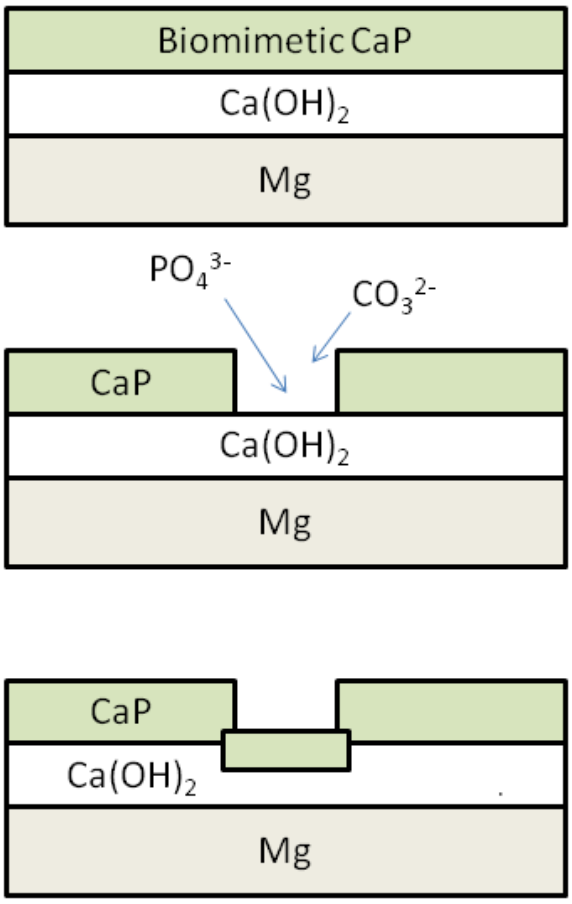

Figure 6-8: Schematic of the proposed self-healing process that occurs with the introduction of a $Ca(OH)_2$ coating *via* ECAD.

The mechanism of this can be explained by the high concentration of calcium in the layer under the biomimetic coating (Figure 6-8). As the calcium hydroxide dissolves, the ions combine with phosphate ions in solution to form insoluble calcium phosphate phases at the corrosion sites. This effectively blocks corrosion and preserves the integrity of the coating, which exhibits much less damage after exposure to the solution (Figure 6-4D). Contrast this with the corrosion of the Mg substrate on the biomimetic only coated samples. The subsequent release of free Mg^{2+} ions inhibited the formation of calcium phosphates [25] and does not repassivate the defects (Figure 6-4C). This benefit was very pronounced over the 14 days of corrosion. While H_2 generation is large for the other samples, the ECAD coatings preserve their integrity and only allow a small amount of corrosion, only evolving an average of 1.3 mL of H_2 over the test period (Table 6-1). The improvement in the coating properties over time allowed this coating to remain intact and protective for a much longer period of time than the biomimetic coating by itself.

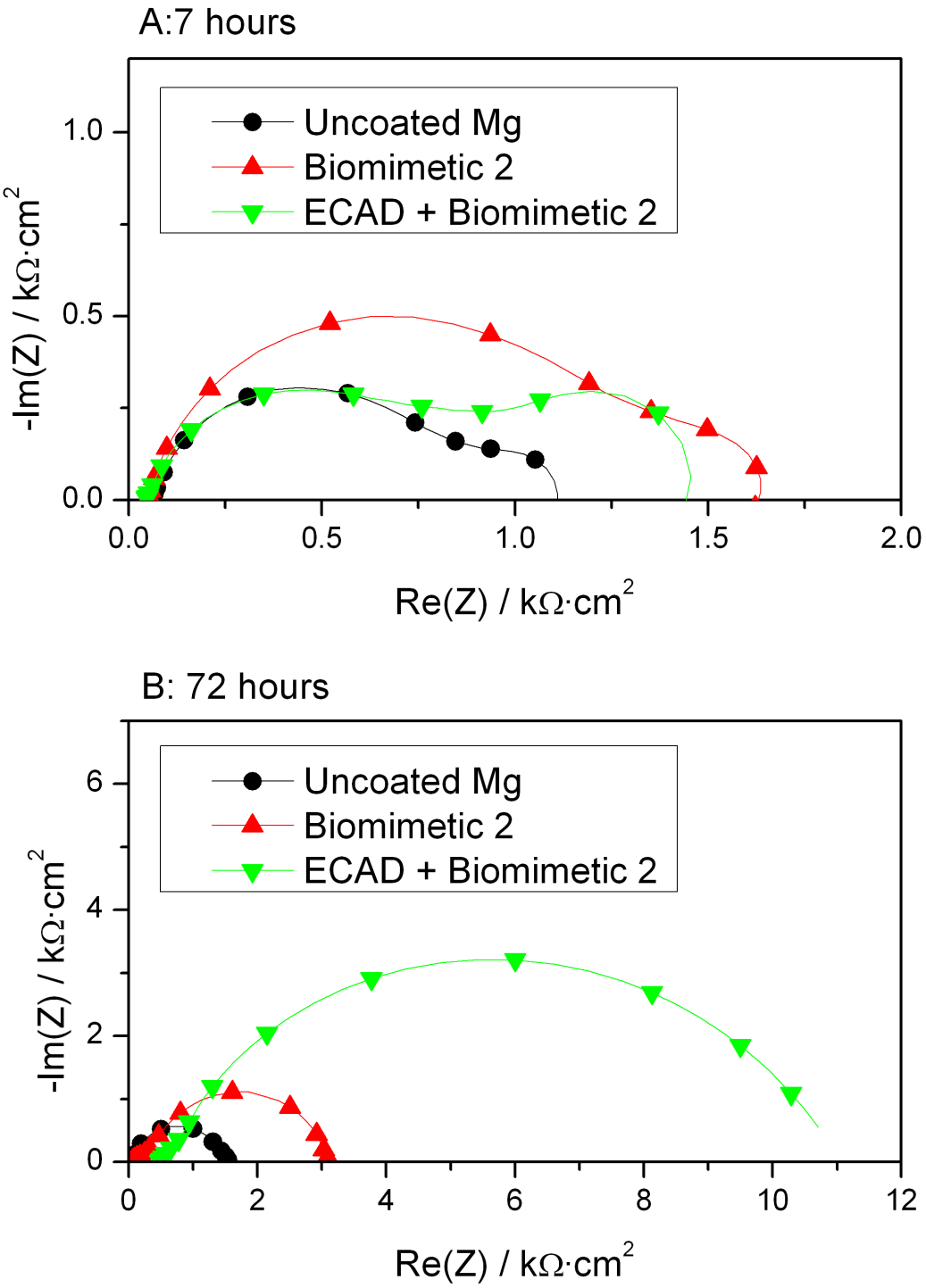

Figure 6-9: Nyquist plots of impedance data for representative samples at 7 and 72 hours immersion in HBSS.

The ECAD coating polarization resistance showed the typical 2 time constant porous coating behaviour in the early stages (Figure 6-9A). Over time, a single time constant grew to

dominate the corrosion behaviour (Figure 6-9B). The decreased amount of defects made the coating resistance dominant and the corresponding effect of the EDL less prevalent. At low frequencies, the uncertainty on the ECAD coatings was relatively large, which may have obscured the secondary time constant that the coating was expected to exhibit. From the polarization behaviour over time (Figure 6-7), it can be seen that the ECAD coatings are quite variable in performance compared to the biomimetic coatings. This suggests that the coatings are very sensitive to the coating parameters. The volcano shaped defects due to the ECAD process may have left areas of lower calcium hydroxide coverage that adversely affected the performance of the coatings. Further investigations into controlling the properties of this layer are therefore needed. However, the effect on the stability and corrosion protection of the biomimetic coatings suggest this coating method is promising as a step toward overcoming the barriers to using biomimetic coatings for corrosion protection of magnesium implants.

6.3.4. Crystal Structure Changes after Corrosion of ECAD Coated Samples

The proposed mechanism of the ECAD $Ca(OH)_2$ coatings is the $Ca(OH)_2$ dissolves and combines with phosphate and carbonate ions to seal the gap and defects in the outer biomimetic layer. The changes in coating composition support this mechanism. Figure 6-10 shows the X-ray diffraction patterns for the samples after the 2 week hydrogen evolution tests. As previously discussed, the uncoated Mg undergoes corrosion, raising the pH near the surface, and eventually depositing a magnesium calcium carbonate phosphate layer. This layer is very amorphous, as seen by the very wide hump in the diffraction pattern. Whereas highly crystalline structures have sharp, well defined peaks, this layer has little long range order in the structure [35]. The biomimetic coatings, composed mostly of DCPD [30] began showing peaks of apatites [36], converting the existing structure to a more stable phase. However, this coating did not repair the defects, leaving large gaps for corrosion to occur (Figure 6-4).

The ECAD layer below the biomimetic coating did not significantly alter the phases present, as these samples also displayed peaks of semi-crystalline DCPD. In addition to these peaks, peaks matching calcium magnesium carbonate appeared (Figure 6-10) [37]. The coating also

showed the formation of amorphous structures at low angles similar to that of uncoated Mg. This is evidence of very small crystal sizes of the newly deposited calcium compounds [35].

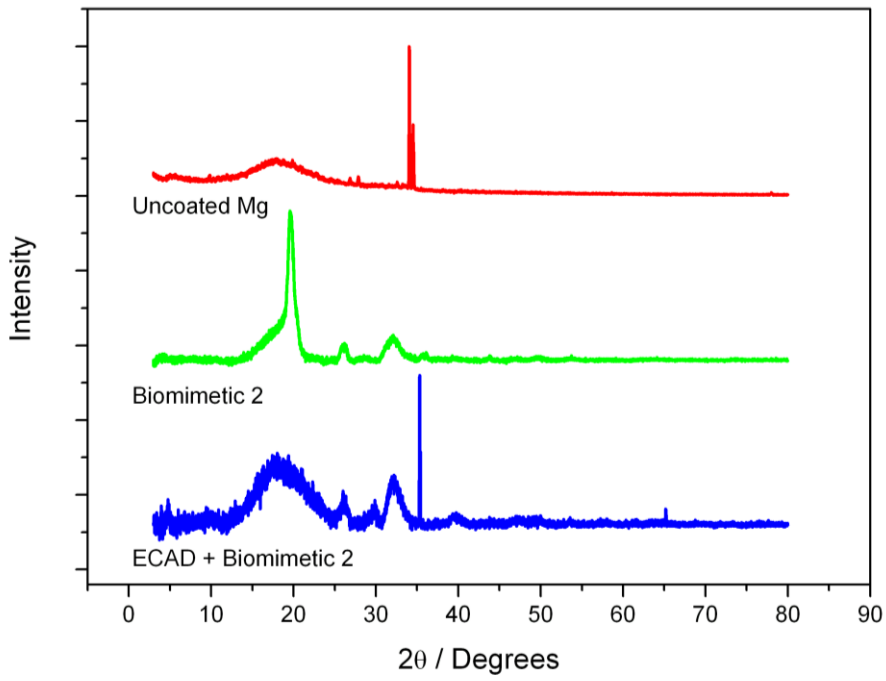

Figure 6-10: GA-XRD of uncoated Mg, Biomimetic 2 coatings, and ECAD + Biomimetic 2 coatings in HBSS + HEPES at 14 days immersion time.

6.4. Effect of Buffer Choice on Corrosion of ECAD + Biomimetic Coated Samples

Corrosion of ECAD coated samples in HCO_3 was not vastly different compared with other types of biomimetic coatings in the HCO_3 buffer system. The early corrosion properties of the ECAD coated samples in all solutions were very similar in E_{Corr} and i_{Corr} to the Biomimetic 2 samples (Figure 6-11). The polarization in NaCl and HBSS over the first 8 hours was nearly identical in HEPES buffered solutions for all of the ECAD samples (Figure 6-12). This is evidence that the early corrosion behaviour is more related to the initial condition of the coating. The difference in the corrosion reactions do not take place until after the samples have been corroding long enough for the self healing properties of the ECAD layer to alter the corrosion behaviour as shown in Figure 6-6. However, the lower buffer capacity and high carbonate content of the HCO_3 buffered HBSS shows the large

anodic protection for the ECAD coated samples after 8 hours, and the polarization resistance of the layer has the steepest increase as well (Figure 6-13).

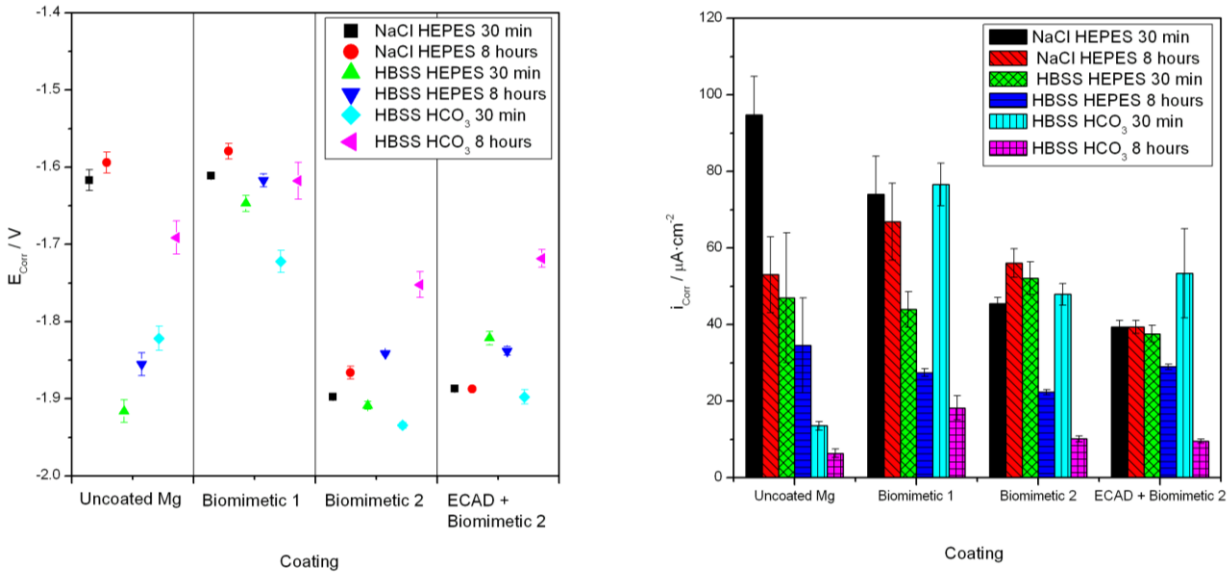

Figure 6-11: E_{Corr} and i_{Corr} of uncoated Mg, biomimetic coatings 1 and 2, and ECAD + biomimetic 2 coatings in solutions buffered with HEPES and HCO_3.

Overall, the fact that the HCO_3 buffers react similarly to all of these coatings gives us confidence that the corrosion reaction *in vitro* will be similar with the carbonate buffer, and therefore similar to the actual carbonate buffer presented *in vivo*. It is expected that the self healing properties of the coating will continue to repair the defects that are present for any of these solutions, provided phosphate and carbonate are present, both of which are plentiful *in vivo*. Of course, this will need to be tested with more complicated *in vitro* solutions to make sure the properties are the same, such as with the addition of amino acids and proteins. Finally, the coatings will need to actually be tested *in vivo* to make sure they will perform as expected. However, the corrosion properties *in vitro* remain very promising to solve the mechanical problems that arise from defective biomimetic coatings.

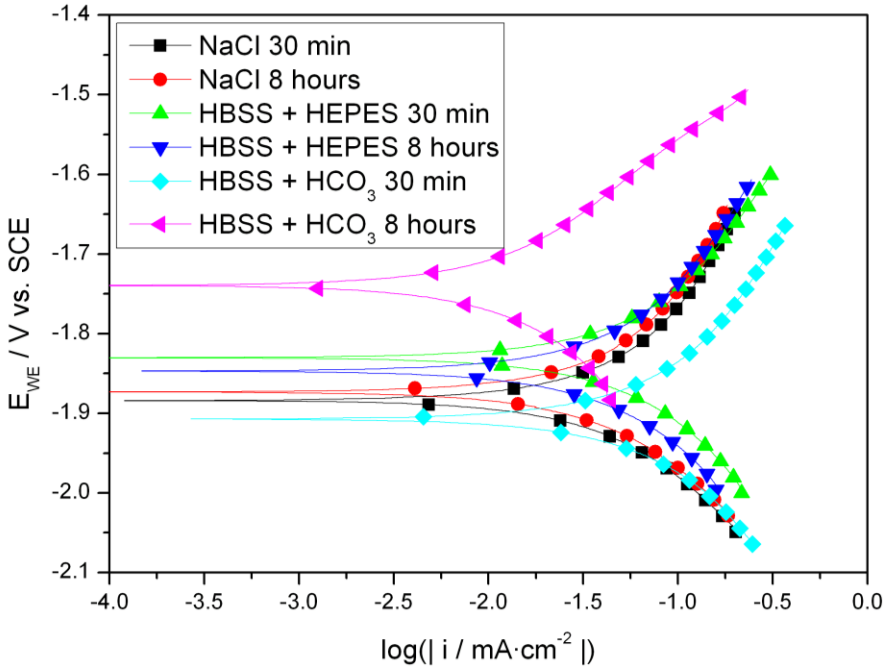

Figure 6-12: PDP of ECAD + Biomimetic 2 coated samples in solutions buffered with HEPES and HCO_3.

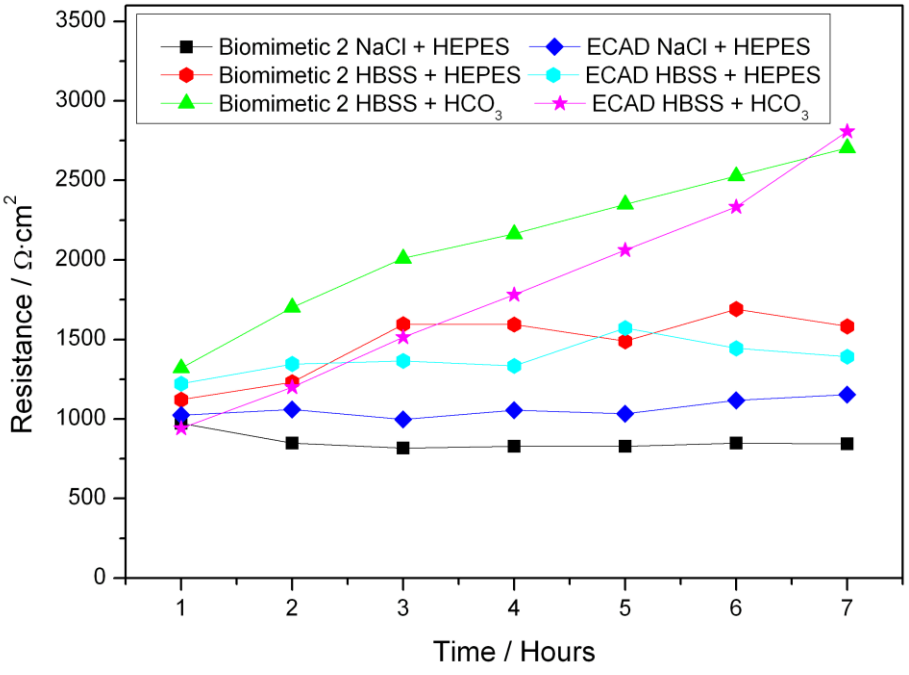

Figure 6-13: Early stage polarization resistance of Biomimetic 2 and ECAD + Biomimetic 2 coatings in solutions buffered with HEPES and HBSS.

6.5. Conclusions

ECAD of calcium hydroxide can increase the corrosion protection of the biomimetic coating. The ECAD coating provides a more resistant biomimetic coating with fewer defects. The corrosion protection did not degrade over time for the ECAD coatings as it did for the biomimetic coatings. The ECAD method for deposition of the $Ca(OH)_2$ was found to be effective with very short deposition times. However, volcano shaped defects and bubbles in the coating were observed, which may decrease the overall protectiveness of the coatings. The biomimetic coating was deposited onto the ECAD layer, and this layer did not significantly change the final composition or structure of the layer. The amount of defects in the final layer was lower, leading to higher initial corrosion resistance. It was concluded that the $Ca(OH)_2$ layer promotes the deposition of a complete and low defect biomimetic coating.

The real benefit of the ECAD $Ca(OH)_2$ was the improvement to the corrosion properties of the coating over time. As corrosion progressed, the protectiveness of the ECAD coatings increased due to the calcium rich layer depositing additional protective calcium phosphates at corrosion sites. The availability of a semisoluble calcium rich layer to deposit in the defects greatly improved the corrosion resistance as corrosion occurred. This led to the coating remaining intact with few defects after the corrosion period, and very little H_2 gas generated over the 14 day experiment. This can be translated into very low corrosion of the substrate, and therefore the mechanical properties will be retained, and the H_2 that is generated can be safely removed. For a biodegradable implant application where corrosion behaviour is critical, a self healing coating such as the one describe here may provide much better corrosion properties than typical biomimetic coatings by themselves. Therefore, the calcium hydroxide layers are promising as a route to improving the corrosion resistance of biomimetic coatings.

As with other coatings, the differences between the in vitro test with HEPES and HCO_3 buffer systems were tested. As HEPES has higher buffer capacity than HCO_3 *in vitro,* and does not accurately represent the carbonate ions in the body, it could be the case that the mechanisms of corrosion will not be quite the same when the coating system is moved from *in vitro* to *in vivo*. The performance of the ECAD + biomimetic coating in HCO_3 buffered HBSS was actually more corrosion resistant than in HEPES. The additional carbonate ions and larger pH rise led to earlier deposition of calcium compounds, further protecting the

substrate. The good initial performance of the coating in HCO_3 buffered solutions indicates that the mechanism of protection this coating provides will persist in other solutions and remain more protective in carbonated buffered solutions such as the body.

6.6. References

1. Lorenz, C., J.G. Brunner, P. Kollmannsberger, L. Jaafar, B. Fabry, and S. Virtanen, *Effect of surface pre-treatments on biocompatibility of magnesium.* Acta Biomaterialia, 2009. **5**(7): p. 2783-2789.
2. Waterman, J., A. Pietak, N. Birbilis, T. Woodfield, G. Dias, and M.P. Staiger, *Corrosion resistance of biomimetic calcium phosphate coatings on magnesium due to varying pretreatment time.* Materials Science and Engineering: B, 2011. **176**(20): p. 1756-1760.
3. Baker, K.C., M.A. Anderson, S.A. Oehlke, A.I. Astashkina, D.C. Haikio, J. Drelich, and S.W. Donahue, *Growth, characterization and biocompatibility of bone-like calcium phosphate layers biomimetically deposited on metallic substrata.* Materials Science and Engineering: C, 2006. **26**(8): p. 1351-1360.
4. Kokubo, T., *Formation of biologically active bone-like apatite on metals and polymers by a biomimetic process.* Thermochimica Acta, 1996. **280-281**: p. 479-490.
5. Dekker, R.J., J.D. de Bruijn, M. Stigter, F. Barrere, P. Layrolle, and C.A. van Blitterswijk, *Bone tissue engineering on amorphous carbonated apatite and crystalline octacalcium phosphate-coated titanium discs.* Biomaterials, 2005. **26**(25): p. 5231-5239.
6. Barrere, F. and C.M.v.d. Valk, *Osteogenecity of octacalcium phosphate coatings applied on porous metal implants.* Journal of Biomedical Materials Research Part A, 2003. **66A**(4): p. 779-788.
7. Barrere, F., C.M. van der Valk, G. Meiger, R.A.J. Dalmeijer, K. De Groot, and P. Layrolle, *Osteointegration of biomimetic apatite coating applied onto dense and porous metal implants in femurs of goats.* Journal of Biomedical Materials Research Part B: Applied Biomaterials, 2003. **67B**(1): p. 655-665.
8. Zhu, L., X. Ye, G. Tang, N. Zhao, Y. Gong, Y. Zhao, J. Zhao, and X. Zhang, *Biomimetic coating of compound titania and hydroxyapatite on titanium.* Journal of Biomedical Materials Research Part A, 2007. **83A**(4): p. 1165-1175.
9. Song, G., *Control of biodegradation of biocompatable magnesium alloys.* Corrosion Science, 2007. **49**(4): p. 1696-1701.
10. Song, G. and A. Atrens, *Understanding Magnesium Corrosion - A Framework for Improved Alloy Performance.* Advanced Engineering Materials, 2003. **5**(12): p. 837-858.
11. Song, G.L. and A. Atrens, *Corrosion Mechanisms of Magnesium Alloys.* Advanced Engineering Materials, 1999.
12. Mueller, W.-D., M. Lucia Nascimento, and M.F. Lorenzo de Mele, *Critical discussion of the results from different corrosion studies of Mg and Mg alloys for biomaterial applications.* Acta Biomaterialia, 2010. **6**(5): p. 1749-1755.
13. Friedrich, H.E., *Magnesium Technology : Metallurgy, Design Data, Applications*, ed. H.E. Friedrich and B.L. Mordike. 2006, Heidelberg: Springer.
14. Barrere, F., *Biomimetic Calcium Phosphate Coatings: Physicochemistry and Biological Activity*. 2002, University of Twente: Enschede.

15. León, B. and J.A. Jansen, *Thin Calcium Phosphate Coatings for Medical Implants*. 2008: Springer.
16. Xu, L., F. Pan, G. Yu, L. Yang, E. Zhang, and K. Yang, *In vitro and in vivo evaluation of the surface bioactivity of a calcium phosphate coated magnesium alloy.* Biomaterials, 2009. **30**(8): p. 1512-1523.
17. Li-li, T., W. Qiang, G. Fang, X. Xiao-song, Q. Jian-hong, and Y. Ke, *Preparation and characterization of Ca-P coating on AZ31 magnesium alloy.* TRANSACTIONS OF NONFERROUS METALS SOCIETY OF CHINA, 2010. **20**(Suppl. 2): p. S648-S654-S648-S654.
18. Gray-Munro, J.E. and M. Strong, *The mechanism of deposition of calcium phosphate coatings from solution onto magnesium alloy AZ31.* Journal of Biomedical Materials Research Part A, 2009. **90A**(2): p. 339-350.
19. Hiromoto, S. and A. Yamamoto, *High corrosion resistance of magnesium coated with hydroxyapatite directly synthesized in an aqueous solution.* Electrochimica Acta, 2009. **54**(27): p. 7085-7093.
20. Hu, J., C. Wang, W.C. Ren, S. Zhang, and F. Liu, *Microstructure evolution and corrosion mechanism of dicalcium phosphate dihydrate coating on magnesium alloy in simulated body fluid.* Materials Chemistry and Physics, 2010. **119**(1-2): p. 294-298.
21. Wu, C., Z. Wen, C. Dai, Y. Lu, and F. Yang, *Fabrication of calcium phosphate/chitosan coatings on AZ91D magnesium alloy with a novel method.* Surface and Coatings Technology, 2010. **204**(20): p. 3336-3347.
22. Yang, J.X., Y.P. Jiao, F.Z. Cui, I.-S. Lee, Q.S. Yin, and Y. Zhang, *Modification of degradation behavior of magnesium alloy by IBAD coating of calcium phosphate.* Surface and Coatings Technology, 2008. **202**(22-23): p. 5733-5736.
23. Habibovic, P., F. Barrere, C.A. van Blitterswijk, K. de Groot, and P. Layrolle, *Biomimetic hydroxyapatite coating on metal implants.* Journal of the American Ceramic Society, 2002. **85**(3): p. 517-22.
24. Lin, C.-M. and S.-K. Yen, *Biomimetic growth of apatite on electrolytic TiO2 coatings in simulated body fluid.* Materials Science and Engineering: C, 2006. **26**(1): p. 54-64.
25. Bigi, A., G. Falini, E. Foresti, A. Ripamonti, M. Gazzano, and N. Roveri, *Magnesium influence on hydroxyapatite crystallization.* Journal of Inorganic Biochemistry, 1993. **49**(1): p. 69-78.
26. Witte, F., V. Kaese, H. Haferkamp, E. Switzer, A. Meyer-Lindenberg, C.J. Wirth, and H. Windhagen, *In vivo corrosion of four magnesium alloys and the associated bone response.* Biomaterials, 2005. **26**(17): p. 3557-3563.
27. Warrel, D.A., *Oxford Textbook of Medicine*. 4 ed, ed. T.M. Cox, J.D. Firth, and E.J. Benz Jr. Vol. 3. 2003, New York: Oxford University Press.
28. Desai, S. and N. Chandler, *Calcium Hydroxide-Based Root Canal Sealers: A Review.* Journal of Endodontics, 2009. **35**(4): p. 475-480.
29. Kumar, M., H. Dasarathy, and C. Riley, *Electrodeposition of brushite coatings and their transformation to hydroxyapatite in aqueous solutions.* Journal of Biomedical Materials Research, 1999. **45**(4): p. 302-310.
30. *PDF 01-074-6549*. 1962, International Center for Diffraction Data: Newton, PA.
31. Song, Y., S. Zhang, J. Li, C. Zhao, and X. Zhang, *Electrodeposition of Ca-P coatings on biodegradable Mg alloy: In vitro biomineralization behavior.* Acta Biomaterialia, 2010. **6**(5): p. 1736-1742.
32. Wang, Y., M. Wei, J. Gao, J. Hu, and Y. Zhang, *Corrosion process of pure magnesium in simulated body fluid.* Materials Letters, 2008. **62**(14): p. 2181-2184.

33. Rettig, R. and S. Virtanen, *Time-dependent electrochemical characterization of the corrosion of a magnesium rare-earth alloy in simulated body fluids.* Journal of Biomedical Materials Research Part A, 2008. **85A**(1): p. 167-175.
34. Kannan, M.B. and L. Orr, *In Vitro mechanical integrity of hydroxyapatite coated magnesium alloy.* Biomedical Materials, 2011. **6**(4): p. 045003 (11 pp.)-045003 (11 pp.).
35. Leng, Y., *Materials characterization : introduction to microscopic and spectroscopic methods*. 2008, Singapore ; Hoboken, NJ: J. Wiley. xii, 337 p.
36. *PDF 04-013-6614*. 2006, International Center for Diffraction Data: Newton, PA.
37. *PDF 04-012-6929*. 1998, International Center for Diffraction Data: Newton, PA.

CHAPTER 7: Effect of Amino Acids and Proteins on the *in vitro* Corrosion Rates of Coatings on Mg

In vitro tests necessarily reduce the complexity of the actual *in vivo* environment. The corrosion mechanism of Mg is influenced by the amount of Cl^- present, as well as the inorganic salts that are present in physiological fluids. These simple test environments are suited to corrosion protection measurements for coatings and other surface treatments that seek to reduce the attack of Cl^- to the underlying Mg, thus limiting the corrosion rate. This will be a key function if the mechanical properties of an otherwise fast degrading Mg or Mg alloy are to be retained in load bearing applications. However, the actual environment faced does not contain only these ions, and therefore and understanding of how these coatings react with more complicated corrosion environments will be necessary to understand the actual degradation mechanisms and rates.

Organic elements such as amino acids and proteins are present in the body. While these do not necessarily react directly with the electrochemical corrosion reactions, they have been reported to affect the corrosion rates of degradable Mg implants *in vitro* [1]. The adsorption or adherence to the surface of biomaterials by these organic molecules can affect the corrosion rate of the Mg. Therefore, understanding the influence they have on the mechanisms of coated samples will be necessary for optimizing and designing *in vivo* corrosion response of a coated Mg implant.

7.1. MEM: the Addition of Amino Acids

The cell culture medium Eagle's Minimum Essential Medium (MEM) is a formula containing ionic compounds similar to the body and other *in vitro* solutions as well as a number of amino acids to provide a suitable environment for cell cultures. It is quite widely used for cell culture and has utilized in studies of Mg corrosion as well [2].

Amino acids affect the buffer capacity of the *in vitro* solutions [3]. The additional buffering may therefore affect the corrosion rates by keeping the pH lower than it would be without

them. They may also chelate with Mg and inhibit the formation of the insoluble Mg compounds that form the passive layer, decreasing the corrosion resistance [2]. It has also been reported that the amino acids can be adsorbed onto the surface Mg alloys and increase the corrosion resistance [4].

The addition of the amino acids to measure corrosion rate bridges the gap between simple ionic solutions and more complicated protein solutions for corrosion testing. As such, MEM has been used for *in vitro* corrosion tests. Chen et al. used MEM as a more realistic corrosion environment to test a hydroxyapatite coating [5]. Others have used Dulbecco's Modified Eagle Medium (DMEM), a version of MEM with additional amino acids present to test the corrosion response [6]. Proteins can be added to MEM to create a more realistic medium for corrosion testing [7, 8].

Proteins can also influence the corrosion properties of metals [9]. Protein interaction is important to the biocompatibility of implants as well [10]. Proteins are built of chains of amino acids. The structures of proteins typically have functional groups on the outside of the protein that can be polar, nonpolar, hydrophilic or hydrophobic, thus creating a complex surface. The overall charge of which depends on the pH of the environment for a given protein with a given isoelectric point[10]. The charge and surface composition will affect the adsorption rates of the proteins on the surface. The adsorption of these proteins can affect the corrosion surface and thus the interactions will be important for corrosion behaviour. Foetal bovine serum (FBS) has been used to provide proteins for *in vitro* SBFs for corrosion tests [7, 8, 11, 12]. FBS is taken from the blood plasma of a calf fetus. It's often used for cell culture work for the amount of growth factors it contains as well as the low number of antibodies [13]. FBS contains proteins amounting to 30-45 g/L [14] with the majority of the protein composition made of bovine serum albumin (BSA) [15]. This is the bovine equivalent of human serum albumin, which accounts for about half of the blood serum protein in humans. BSA can be purified from bovine blood more cheaply than complete FBS can be procured. For the corrosion tests here for cost and simplicity, BSA was added to determine the effect of proteins on the corrosion properties of the coated samples. The amount of protein added to the MEM for corrosion tests was 40 g/L as used by Rettig and Virtanen [16, 17], and later Kirkland [11], as an accurate representation of the physiological amounts of HSA in the body.

The corrosion properties of Mg and Mg alloys have been shown to be affected by the addition and concentration of proteins. Studies show adding proteins have been shown to slow corrosion of various Mg alloys [2, 12, 18-20]. However, the effect is not always clear due to the complex nature of the interactions. Mueller et al. reported corrosion rates of pure Mg in PBS increase when BSA is added to 0.1% but then decrease as further BSA is added (up to 10%). This trend depended on alloy as well, AZ31 showed very little change in corrosion rate across BSA concentrations, while LAE442 had steadily increasing i_{Corr}. Kirkland et al. showed that the addition of 10% FBS slowed the corrosion rate of a number of alloys as well as pure Mg in MEM [11]. However, increasing additions of BSA to MEM solutions from 20 to 60 g/L led to increasing corrosion rates for pure Mg, although all were ultimately lower than MEM alone. These varying trends suggest the corrosion influence of proteins is more complicated than the simplistic adsorption model, as proteins in solution has a complicated effect on the passivation layers that form [21]. In an effort to investigate the effect proteins have on the corrosion properties of biomimetic coated samples, the coatings were investigated in MEM with and without BSA.

7.1.1. Materials and Methods

7.1.1.1. Corrosion Media

Solutions of Eagle's Minimum Essential Medium (MEM) were prepared with and without bovine serum albumin (BSA) at 40g/L. The solution composition is given in Table 7-1. The solutions were buffered to an initial pH of 7.40 with 25mM HEPES and NaOH at a temperature of 37 degrees C. Bicarbonate buffered solutions were tested in an incubator with a 5% CO_2 atmosphere.

Table 7-1: Composition of corrosion media

Component	Human plasma (HP)	Hank's balanced salt solution (HBSS)[a]	Minimum essential medium (MEM)[c]	MEM + bovine serum albumin (MEM+BSA)[d]
Na^+	142	145	117.4	117.4
Cl^-	103	144.6	123.5	123.5
K^+	5.0	5.8	5.4	5.4
Ca^{2+}	2.5	1.3	1.8	1.8
Mg^{2+}	1.5	0.4	0.4	0.4
HPO_4^{2-}	1.0	0.8	1	1
SO_4^{2-}	0.5	0.4	0.4	0.4
D-Glucose	5	5.5	5.5	5.5
Bicarbonate (HCO_3^-)	22-30	± 26.2	± 26.2	± 26.2
HEPES	-	± 25	± 25	± 25
Phenol red	-	0.03	0.03	0.03
Albumin (g/L)	34-54	-	-	40

All concentrations in mmol/L unless otherwise stated.
Concentrations of inorganic blood contents given as in [22].
[a] (H1641, Sigma-Aldrich), [b] (E7510, Sigma-Aldrich), [c] (56414C, Sigma-Aldrich), [d] (MP Biomedical NZ Ltd)

7.1.1.2. Coatings

Pure Mg samples were prepared (Helmholtz-Zentrum Geesthacht). Samples were polished up to 600 grit SiC paper and rinsed with ethanol. Biomimetic coatings were carried out as described in Chapter 5. ECAD + Biomimetic coatings were carried out as described in Chapter 6.

7.1.1.3. Electrochemical Testing

PDP was used at 30 min of settling time and at 8 hours to determine the polarization resistance and the change in polarization resistance for the early stages of corrosion. 5 tests were performed per timepoint to determine the uncertainty of both the experiments and the Tafel-fit extrapolations. PDP scans went from 150 mV below OCP to 250 mV above OCP or to 1mA applied current. Scans were performed at a rate of 1 mV/s.

EIS was used to measure the polarization resistance of the coating and corrosion layers. One sample from each group was monitored once per hour from 1 to 7 hours immersion. Frequency range from 50kHz to 30 mHz was used. The amplitude of the signal was 10mV, and 5 measurements per frequency were averaged.

7.2. Effect of Amino Acids on the Corrosion Properties of Mg

7.2.1. Uncoated Mg

The polarization behaviour in MEM was compared to that of HBSS. Table 7-1 shows the compositions of both fluids are similar, and have the same Mg^{2+} ion content. However, MEM has slightly lower Cl^- as well as higher Ca^{2+} and PO_4^{3-} concentrations. The difference here might suggest slightly decreased corrosion rates and slightly increased CaP formation in solution. The polarization of uncoated Mg in both solutions showed that E_{Corr} is higher in MEM than in HBSS once the layer has settled (Figure 7-1). The corrosion current density is initially higher in MEM than in HBSS. This is counterintuitive given the higher E_{Corr}, and lower amount of Cl^- in MEM. Higher corrosion could be observed due to the increased buffer capacity provided by amino acids [3], as well as the proposed mechanism that amino acids chelate with Mg^{2+} and inhibit passive layer formation [2].

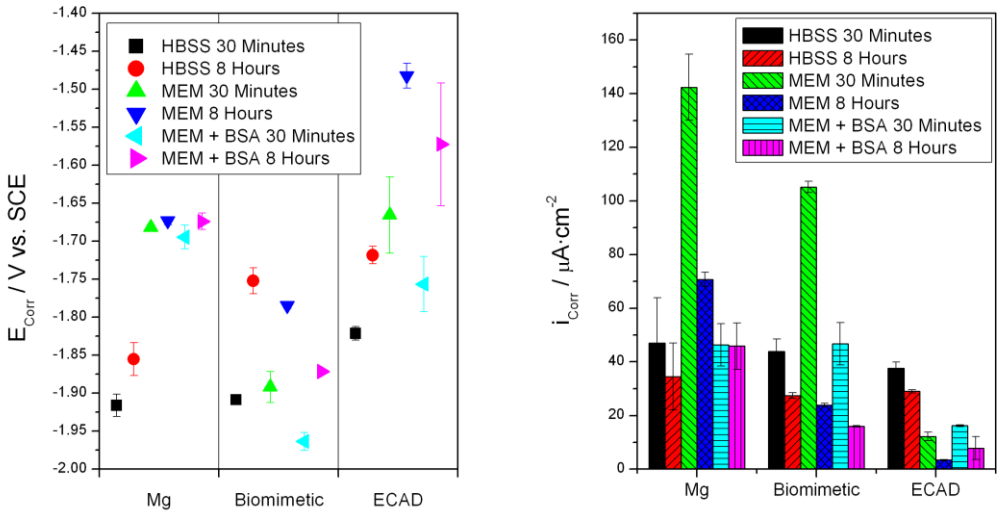

Figure 7-1: Corrosion potential and current density for coated samples with and without amino acids and proteins.

With a similar composition of inorganic ions, and the addition of a number of amino acids which may act as charge carriers, the possibility exists that the higher current measurements were an artefact of solution conductivity. The conductivity of the solutions was measured with a conductivity meter and it was determined MEM had slightly lower conductivity than HBSS with HEPES, showing that this was not the case (Figure 7-2).

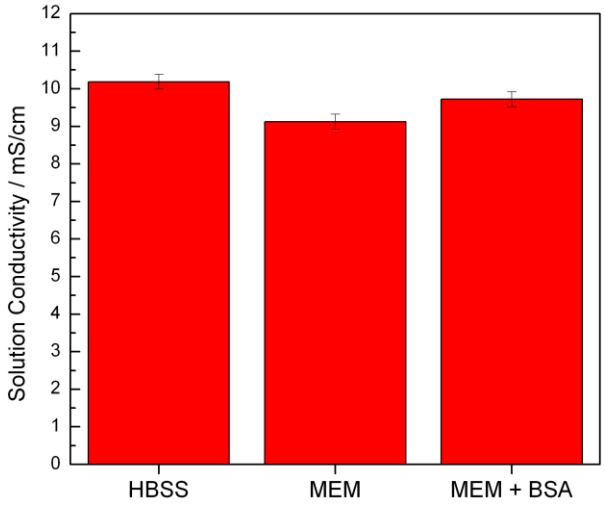

Figure 7-2: Solution Conductivity at 37° C with the HEPES buffer.

7.2.2. The effect of MEM on the Corrosion of Coated Samples

Figure 7-3 reveals the polarization behaviour of coated samples in HBSS vs MEM. The reaction kinetics displays a trend across samples. The increase in both E_{Corr} and i_{Corr} in MEM over HBSS was primarily due to the large increase in the cathodic kinetics. The anodic kinetics were similar in both solutions, possibly decreased slightly for pure Mg, although this was not the dominant effect. While it has been reported that the polarization resistance of steel and aluminium was increased by amino acids [23, 24], polarization resistance was lower in MEM for uncoated Mg over the first 7 hours (Figure 7-4). For each time point, both the film and EDL resistance was lowered by the presence of the amino acids. Therefore adsorption of amino acids resisting corrosion is not slowing corrosion in the short term. Instead the opposite effect is taking place. The lower passive film resistance supports the findings of Yamamoto et al. [2]. Resistance increased with time, doubling after 7 hours.

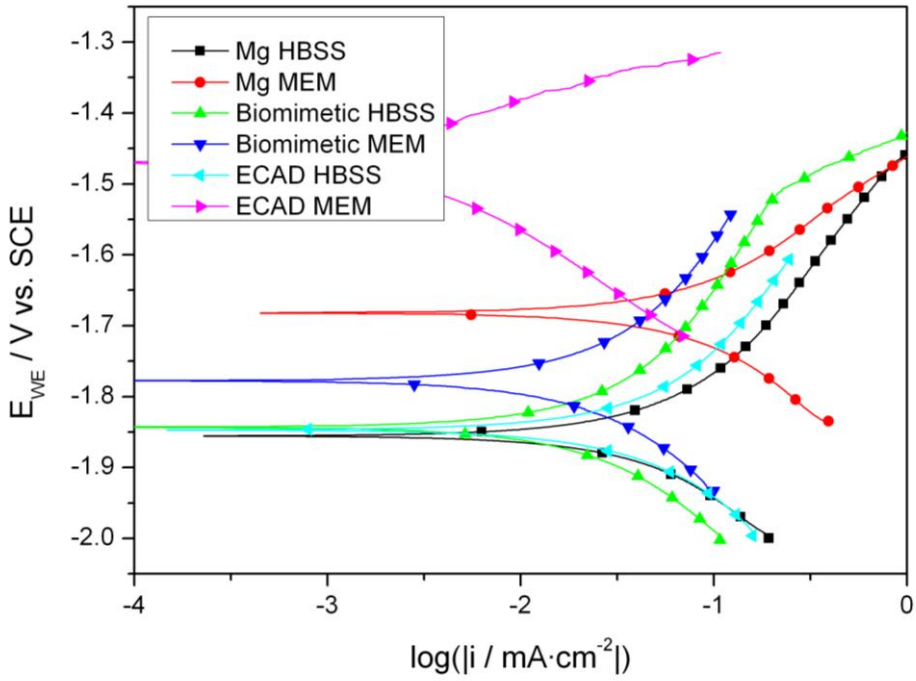

Figure 7-3: PDP in HBSS vs. MEM buffered with HEPES at 8 hours immersion.

Coated samples exhibit similar behaviour in the presence of amino acids. The polarization of biomimetic coatings show that the cathodic reaction was again increased in MEM. Unlike uncoated Mg, this shift was accompanied by a decrease in the anodic kinetics. The anodic kinetics do not offset the corrosion density initially, but after 6 hours the effect is to bring the biomimetic coated sample in MEM below the corrosion rate in HBSS. This behaviour is mirrored by the polarization resistance. The biomimetic coated samples have lower resistance in MEM initially, but by 7 hours the film resistance is almost equal. This, coupled with the more noble potential leads to a reduction in the corrosion rate. The ECAD coating increases these differences even more dramatically. In MEM the cathodic reaction rate is much higher, although not quite so high as uncoated Mg. The large decrease in the anodic reaction in MEM indicates that the ECAD layer accounts for the decrease seen in the corrosion rate. With the improved properties of the coating, the amino acids do not have the effect on the uncoated Mg. The interference in the growth of the passivation layer does not affect the ECAD coating as it does the uncoated and biomimetic coated samples.

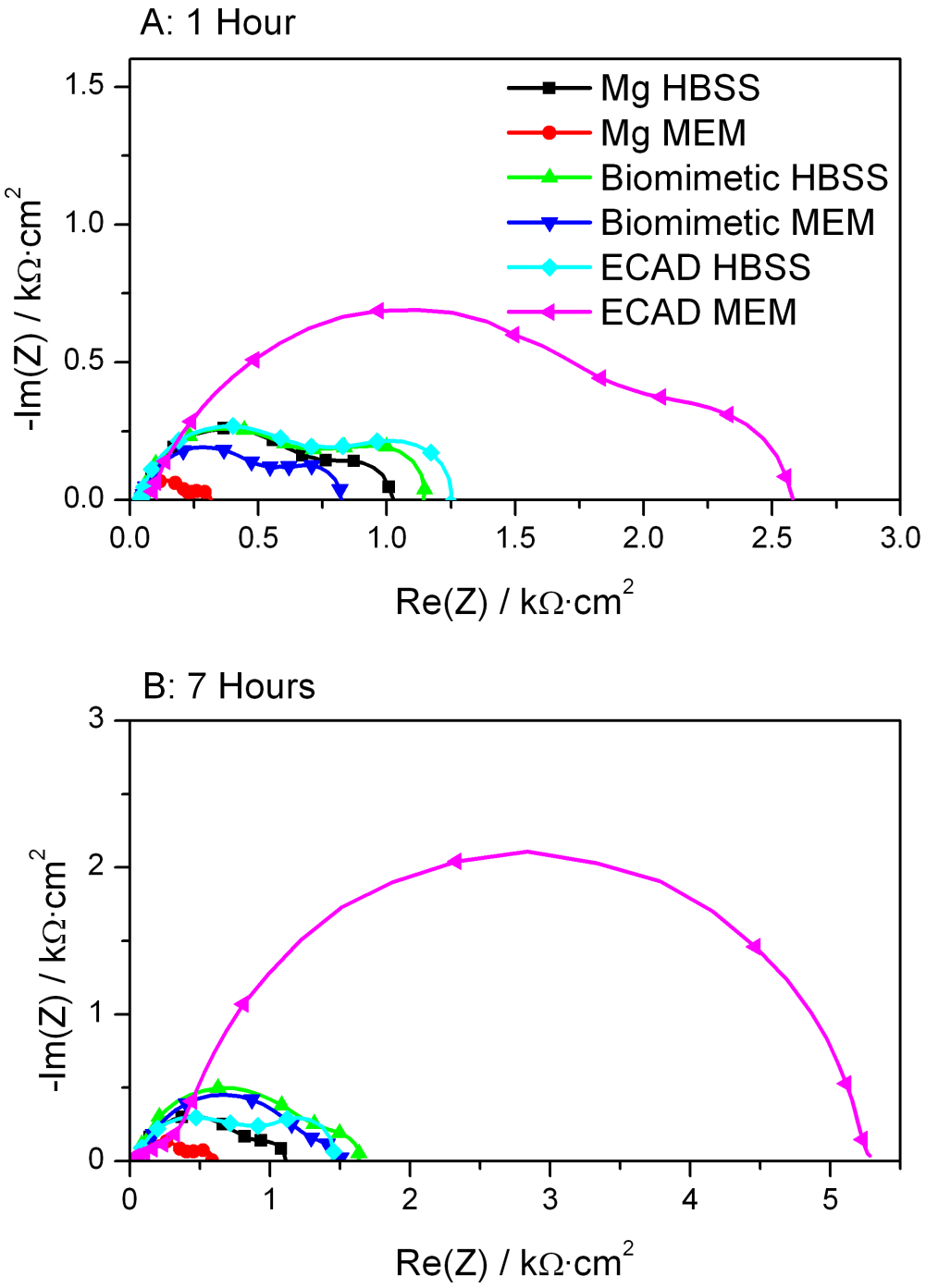

Figure 7-4: EIS of all samples in HBSS and MEM buffered with HEPES at 1 (A) and 7 (B) hours immersion.

7.3. The Effect of Proteins on Corrosion Properties of Coated Samples

7.3.1. Uncoated Mg

Uncoated Mg displayed highly invariant corrosion potential in both MEM and MEM + BSA over the duration of the tests (Figure 7-1 A). The proteins do not directly interact with the corrosion of pure Mg in solution. For uncoated Mg, the proteins decreased the cathodic and anodic kinetics at 30 minutes (Figure 7-5) and 8 hours (Figure 7-6) without changing the corrosion potential significantly. The effect of proteins is reported to be in the adsorption to form a protective layer [18, 19]. The total corrosion current density for Mg in MEM was initially high, over 140 $\mu A/cm^2$ but decreased rapidly over the 8 hours of testing (Figure 7-1B). The decrease can be attributed to the formation of the hydroxide layer, the charge separation, and the local pH rise with the immersion time decreasing the corrosion rate. In Figure 7-7A the PDP of the uncoated samples shows that over the test, there was a slight drop in both the anodic and cathodic branches, consistent with the formation of a the corrosion layer. This is confirmed by EIS in Figure 7-8 A and B as Mg in MEM shows the 2 time constant system characterizing a semi-protective hydroxide layer. After 8 hours, the total impedance of both the oxide layer and the EDL increased, indicating the corrosion film became slightly more protective as corrosion occurred and the layer formed. Figure 7-9 shows the slow and steady rise of this resistance.

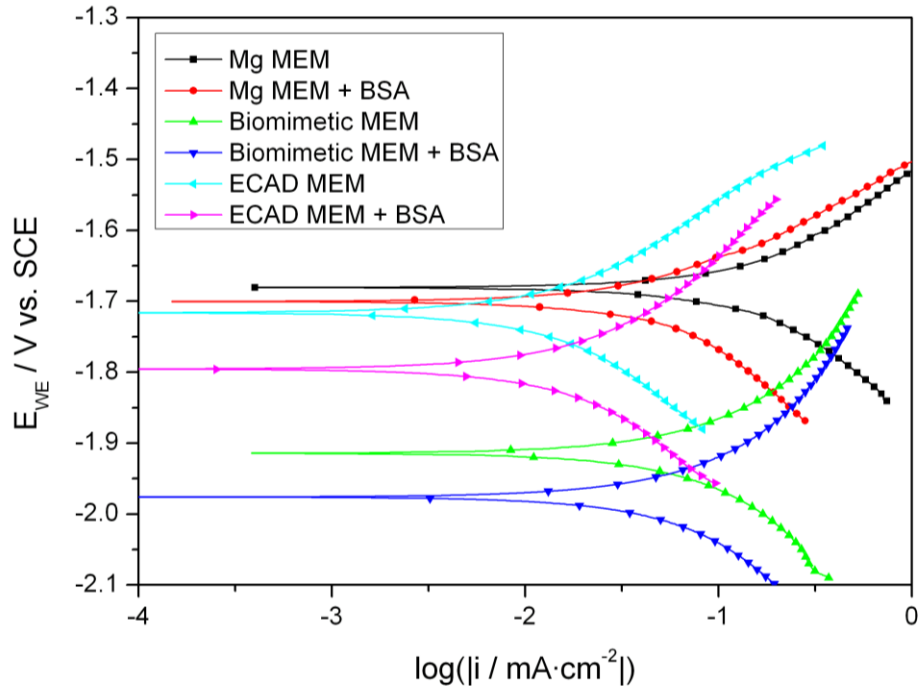

Figure 7-5: PDP of all samples in MEM and MEM + BSA at 30 minutes.

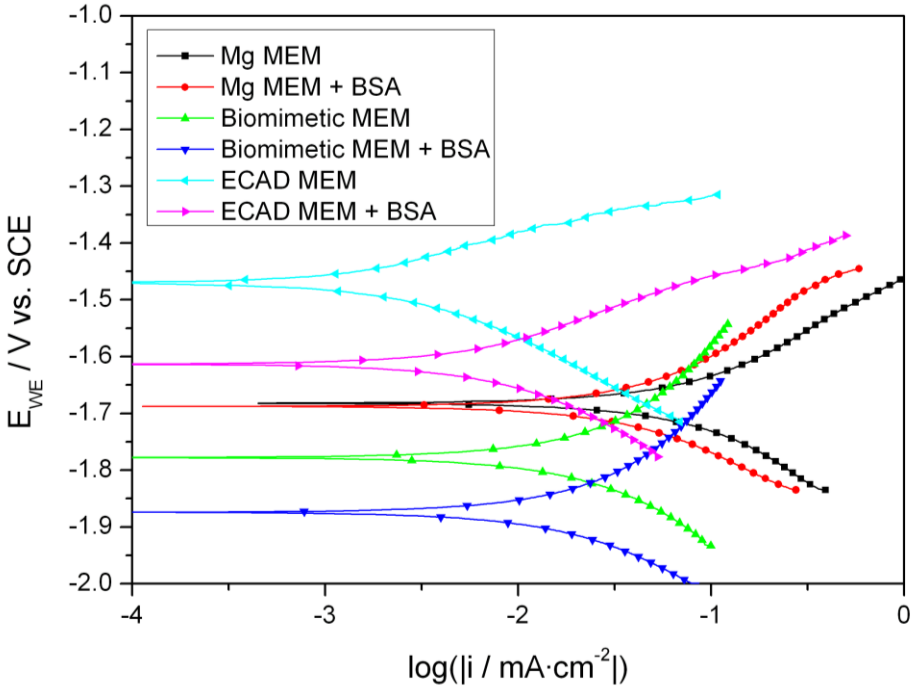

Figure 7-6: PDP of all samples in MEM and MEM + BSA at 8 hours.

When albumin is added to the solution, the E_{Corr} does not change much, but the corrosion current density drops considerably. The variation in i_{Corr} is greater as well. Figure 7-7 shows that after 30 minutes, BSA addition decreases the cathodic reaction greatly and the anodic reaction somewhat. After 8 hours, it is observed that the anodic and cathodic reactions are suppressed by the albumin, as the anodic reaction decreases with time in the BSA solutions (Figure 7-7 A). The total corrosion current density is thus fairly constant in BSA over the 8 hours for pure Mg. The Nyquist plots in Figure 7-8 show that the relative shape is similar to MEM though the resistances are increased in magnitude, and furthermore stays relatively constant over the test period. The explanation for this is found in the proteins impeding corrosion by attaching to the surface and forming a protective layer as reported elsewhere [16-19]. Albumin has been shown to increase E_{Corr} of Mg by decreasing the anodic reaction rate on AZ91 [18], as well as increase the anodic reaction rate on WE43 and LAE442 [25]. Over the time period here, both anodic and cathodic reactions decreased with addition of BSA as reported by Kirkland [26], and along with the EIS data the mechanism seems to be adsorption of proteins to the Mg surface creates a layer that partially protects by reducing the effective surface area available to corrosion. The reported effect that chelating metal ions with the proteins would increase the corrosion rate [9] was not apparent in this study, as has previously been reported for pure Mg [21].

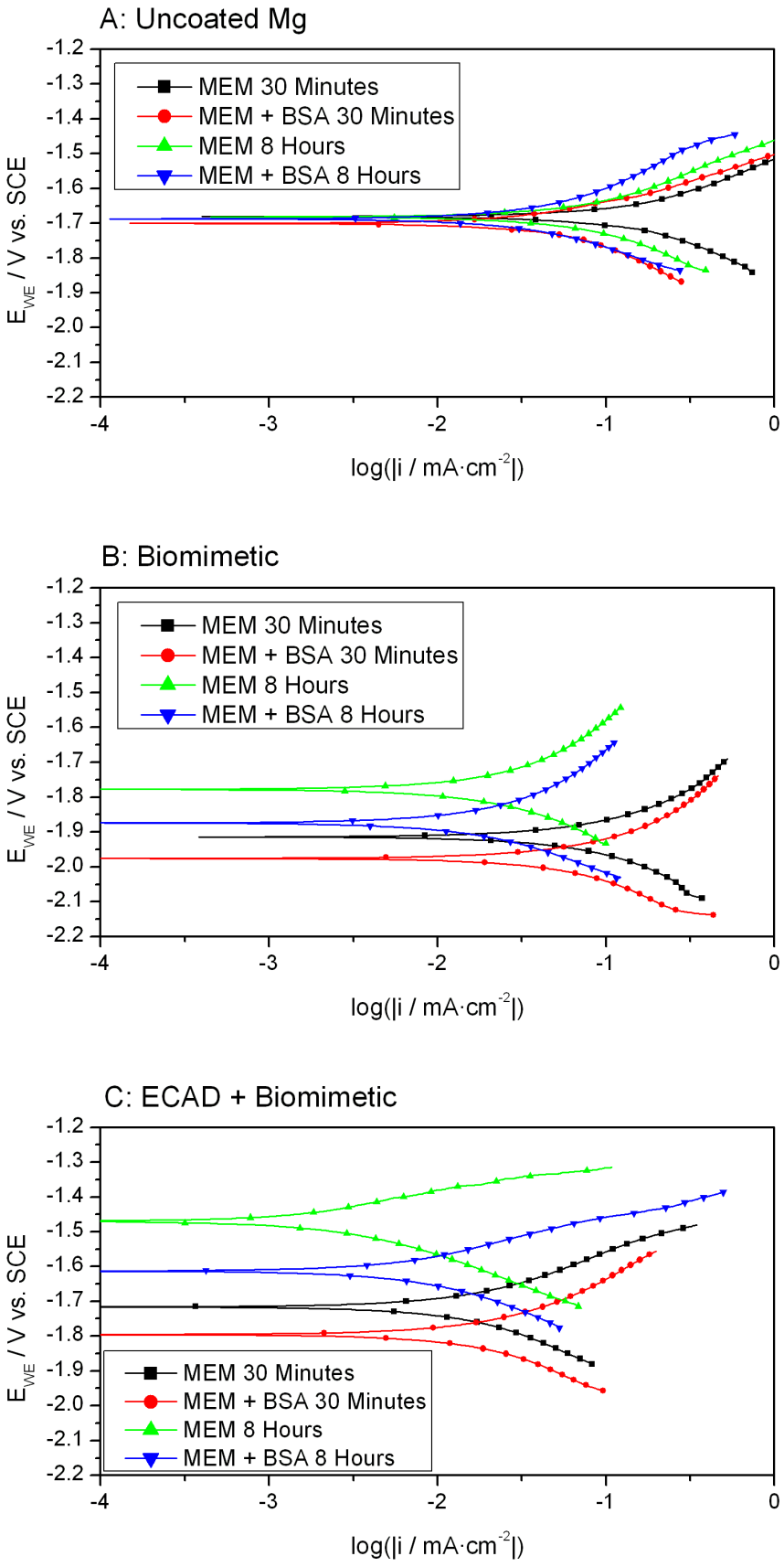

Figure 7-7: PDP over time in MEM and MEM + BSA for A) uncoated Mg, B) Biomimetic coated and C) ECAD coated samples.

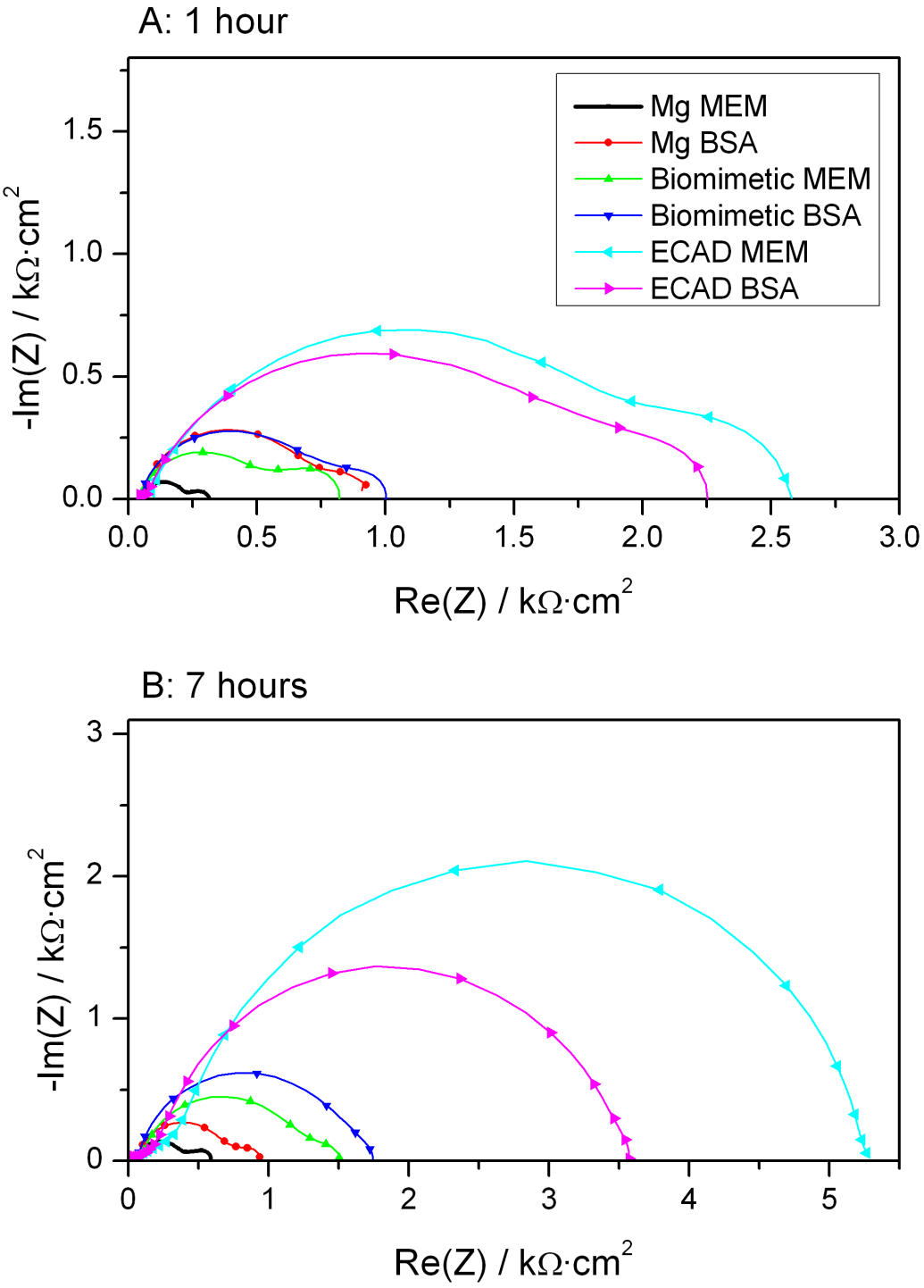

Figure 7-8: EIS of solutions with and without proteins at 1 (A) and 7 (B) hours.

7.3.2. Biomimetic Coated Mg in Protein Solutions

The biomimetic coatings had the effect of reducing the corrosion potential in the short run, but this increased towards the direction of the uncoated samples in both solutions over the 8 hours of testing (Figure 7-1). The corrosion current density behaved in a similar manner to what would be expected for these coated samples. The early corrosion rates in both solutions are quite high, but decrease as time goes on. The rate drops with increasingly noble potentials, as the corrosion layer forms and the coating reduces the corrosion rate. Here, the addition of proteins provided a decrease in the corrosion rate early on, and this protection was improved over the 8 hour test. Comparing the polarization behaviour in Figure 7-5, the protection early on due to the proteins comes from a decrease in the cathodic kinetics. This is again the case with the biomimetic coatings after 8 hours (Figure 7-6) where the lower cathodic kinetics provides a lower corrosion current density despite an increase in anodic kinetics due to the more negative potential.

In Figure 7-7B, the trend of increasing time shows that the cathodic kinetics of each solution remained fairly constant over the test period. The decrease in anodic kinetics therefore drives the reduction in corrosion current density. The decrease in the corrosion reaction is due to the improvement in properties of the layers that form. For the coated samples, BSA resulted in less anodic shift than MEM alone. The corrosion layer here also exhibits the typical 2 time constant system of a semi-porous coating (Figure 7-8). After an hour in solution, the additional proteins in the BSA solution increase the magnitude of the layer resistance, suggesting the proteins are adsorbing on the surface and reducing the area vulnerable to corrosion. Interestingly, the size of the impedance of the biomimetic coated sample in BSA is comparable to the uncoated Mg at this time in BSA, which is larger than the impedance of the biomimetic coated sample in MEM alone. Thus the presence of proteins in this solution radically changes the corrosion layer properties. Indeed, the initial corrosion current density in MEM and MEM + BSA is higher and nearly equal to (within error) the corrosion rates of uncoated Mg in MEM + BSA. Thus, the reduction of corrosion rate at least initially due to proteins is significant. Unfortunately, the barrier to corrosion that the proteins provide does not appear to provide lasting protection, as the corrosion rate by impedance of the uncoated Mg in protein-containing solutions stays constant or rises over the test period.

The biomimetic coatings, which have some corrosion initially, show slightly improving rates over the 8 hours of testing whereby the total impedance improves as the layer on the biomimetic coatings approaches steady state, while the proteins alone do not provide the lasting protection of these calcium phosphates. The biomimetic coating is porous [27], and the local pH rise inside these pores lead to decreasing corrosion rates as corrosion occurs. This accounts for the decrease in anodic reaction rate over time and the improvement in the film resistance. When proteins are added to the solutions, the film resistance improves even further. The corrosion potential is lower, leading to an increase in anodic kinetics, but despite this the overall corrosion current density is lowered by proteins for biomimetic coated samples.

7.3.3. ECAD + Biomimetic Coatings:

The ECAD improvement to the biomimetic coatings is also apparent in the protein solutions. The corrosion resistance of the coatings is greatly improved over the standard biomimetic coatings in simple SBFs as described in Chapter 6. The corrosion potential of ECAD coated samples was quite variable for these tests. Early E_{Corr} values are near that of uncoated Mg, and the potential becomes more positive as time progresses in either solution. i_{Corr} is initially much lower than other uncoated and coated samples, as a testament to the improved formation and composition of the coating structure. Again, in MEM and MEM + BSA, the coating properties improve over time and the corrosion current density drops over the 8 hour test.

In MEM + BSA, the ECAD coating i_{Corr} is down but more variable and not lower than ECAD in MEM alone. At 30 minutes, the addition of proteins to the MEM solution causes a decrease in the cathodic reactions, as with the other samples (Figure 7-5). However, this is coupled with an increase in the anodic kinetics when proteins are added. This trend is also apparent after 8 hours. So while the proteins appear to adsorb and impede the diffusion of solution to the metal, slowing the production of hydrogen gas, they also prevent/slow the reformation of calcium phosphates on the surface of the biomimetic coating due to the ECAD calcium hydroxide layer [28]. As such, the total protection of these coatings takes longer to show up in protein solutions. However, the phenomenon is still passive enough to provide

the most corrosion protection in protein solutions. At 1 hour (Figure 7-8A) the total impedance of ECAD samples in both protein solutions is showing a large coating impedance and a large additional EDL impedance as the solution moves into the pores of the coating. At 7 hours (Figure 7-8B) the impedance has grown, and the coating resistance shows small capacitance, as the insulating properties of the coating resist build up of charge, and the EDL impedance is relatively large, as there is now very little defects and pores in the coating for corrosion to occur. Again, here the proteins impede the process, and the impedance in BSA is lower in this solution than MEM alone. The proteins slow the self healing mechanism of the ECAD coatings, leading to a larger measured corrosion rate. However, both ECAD coatings in both solutions show the characteristic improvement over time that is the mechanism of the coating system (Figure 7-9). Therefore, in more complicated SBFs that include amino acids and proteins, the ECAD layer of calcium hydroxide still provides increased corrosion protection for biomimetic coatings.

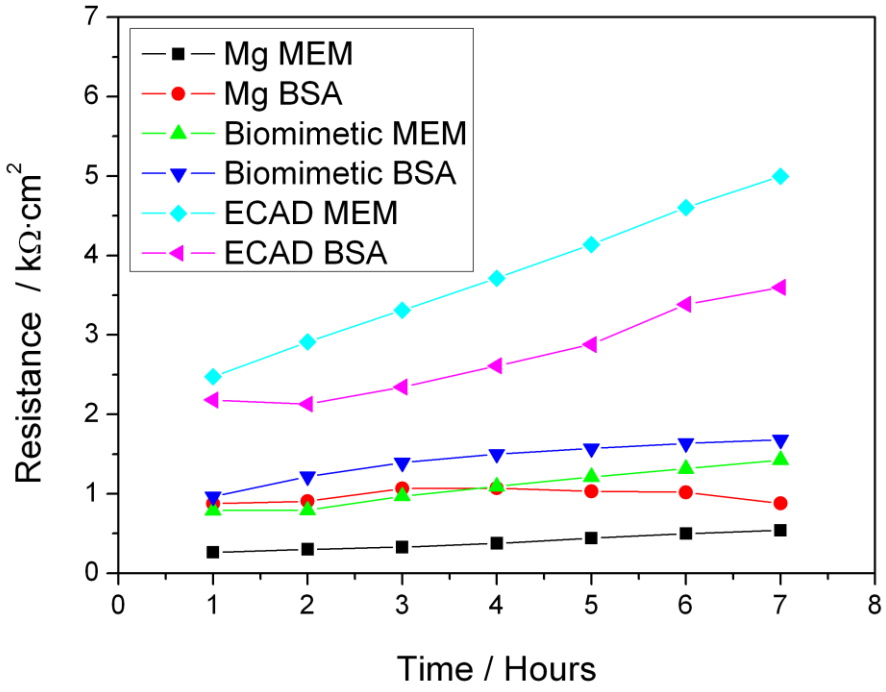

Figure 7-9: EIS over time total polarization resistance.

The response of the coatings across all MEM solutions and time points shows the mechanisms of the coatings in these protein solutions (Figure 7-10). The corrosion potential of uncoated Mg has a low correlation with i_{Corr}. The large changes in corrosion rate are not accompanied by changes in E_{Corr} which suggests that the proteins do not strongly interact with the corrosion reactions and products. Instead, the rate changes arise due to the limited diffusion as a result of the forming layer [19, 21]. Biomimetic coatings follow a trend as the corrosion occurs on the coated samples E_{Corr} and i_{Corr} increase and decrease, respectively, with time. Proteins in solution shift this curve down to lower corrosion rates and lower potentials due to the adsorption layer that both retards the corrosion current density and slows the formation of the layer. ECAD coated samples corrosion rates correlate closely to $i_{Corr.}$ Where the corrosion potential becomes more noble, the corrosion decreases. Here, the protein additions actually increase the measured corrosion rate for each time point, as they retard the repair of the coating layer. However, this will not prevent the self healing mechanism of these coatings from continuing to improve as corrosion occurs, protecting the substrate from corrosion damage for extended periods of time.

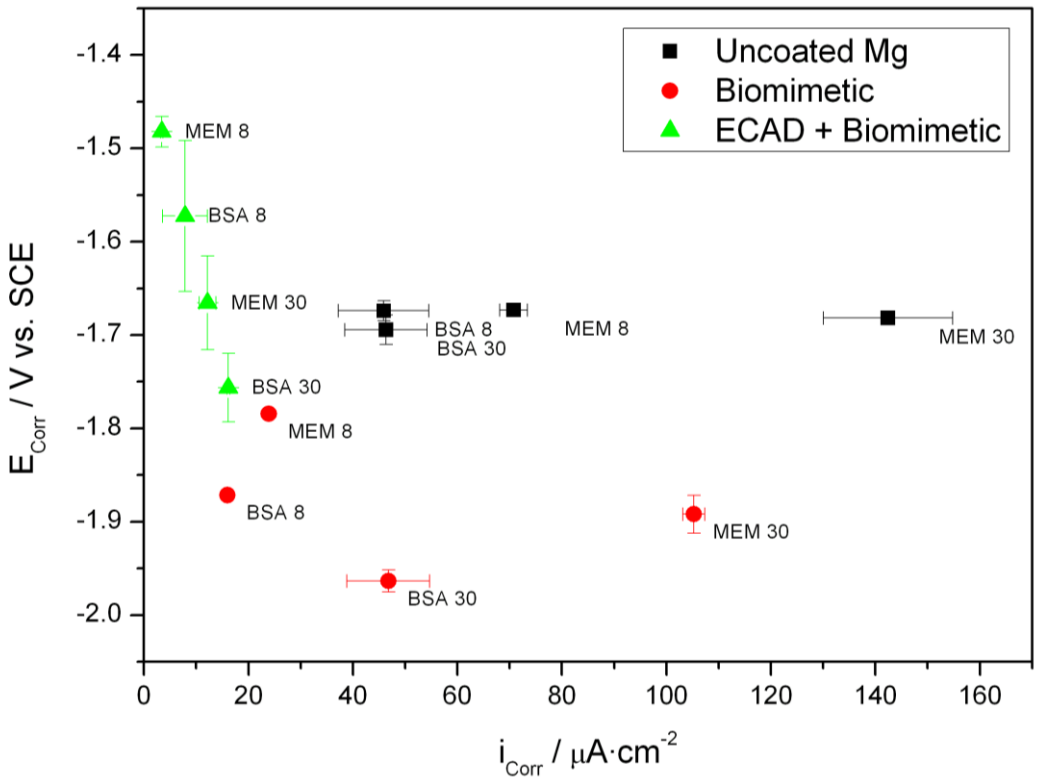

Figure 7-10: E_{Corr} vs. i_{Corr} for uncoated and coated samples in MEM and BSA.

7.4. Buffer Choice and the Presence of a CO_2 Atmosphere on Amino Acids and Proteins in Solution

The choice of buffering agent has been shown to have a great effect on the corrosion measurements of Mg, as discussed in Chapter 3. The difference in buffer capacity and chemical composition is responsible for changing the corrosion layer that forms and the local pH the corroding surface is exposed to. Proteins, and protein-surface interactions are highly sensitive to the pH [10]. The pH will affect the binding of albumin to divalent ions such as Ca^{2+} [29]. The binding reaction of Mg^{2+} is similar and competes at the same sites [30]. Albumin-Mg^{2+} binding has been shown to exhibit changes in binding behaviour between pH 7 and 7.5 [31]. Therefore the buffer choice and passivation properties will directly influence the effect these proteins have on the measured corrosion rate, due to the effects of the local pH. Because the binding increases at with pH [29] the greater variation in pH with a CO_2/HCO_3 buffer due to its lower capacity could affect the corrosion potential and the formation of the passive layer. Additionally, the changes in surface charges with pH may affect the adsorption rate and therefore the protective properties [10].

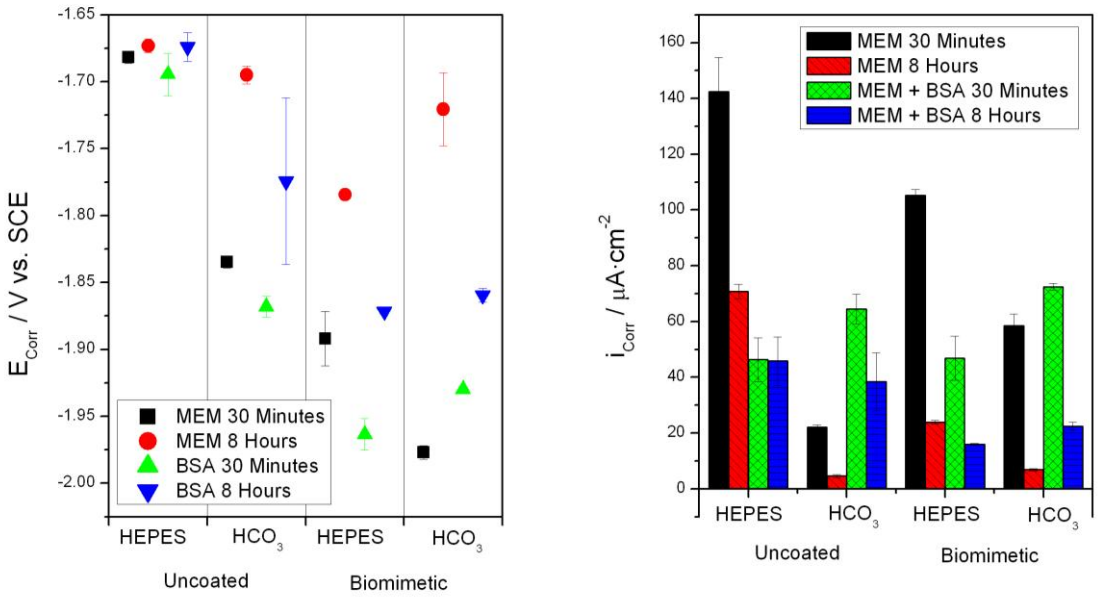

Figure 7-11: E_{Corr} and i_{Corr} of coated samples with HEPES and HCO_3 buffers.

Figure 7-11 shows E_{Corr} and i_{Corr} at 30 minutes and 8 hours for both HEPES and HCO_3 buffered protein solutions. As seen previously, in HEPES buffered solutions E_{Corr} does not change much when BSA is added. In HCO_3 buffered systems, the addition of proteins lowers E_{Corr}. Uncoated Mg in HEPES buffered MEM solutions have high initial i_{Corr} that falls as the corrosion progresses. For MEM + HCO_3, i_{Corr} by 30 minutes is quite low, and by 8 hours it is even lower, forming a large passive layer. This is similar to the corrosion behaviour in HBSS and HCO_3 where the passive hydroxide and carbonate layer forms to impede corrosion [32].

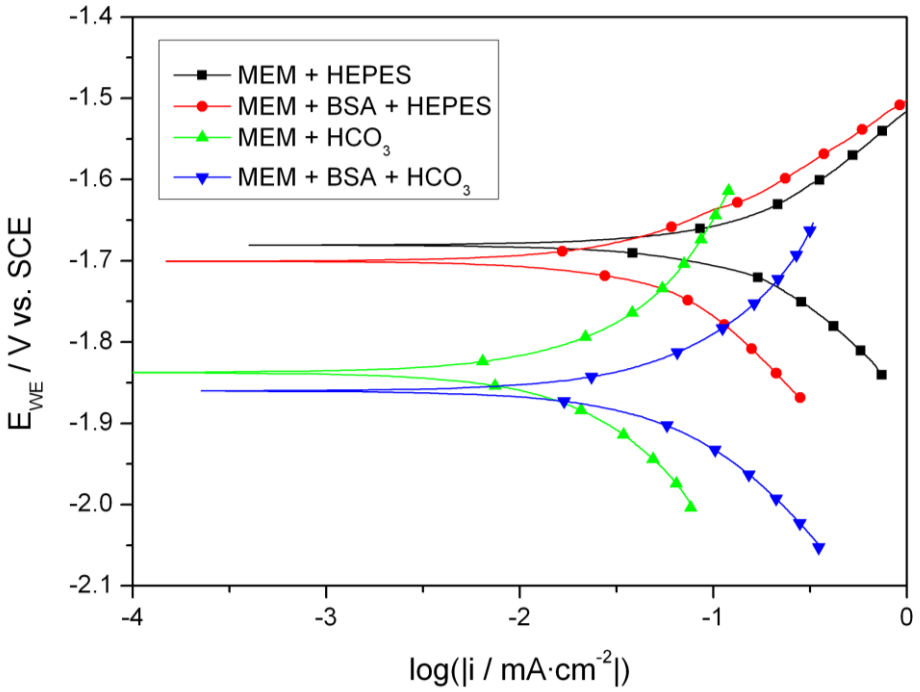

Figure 7-12: PDP of uncoated Mg after 30 minutes in HEPES and HCO3 buffered protein solutions.

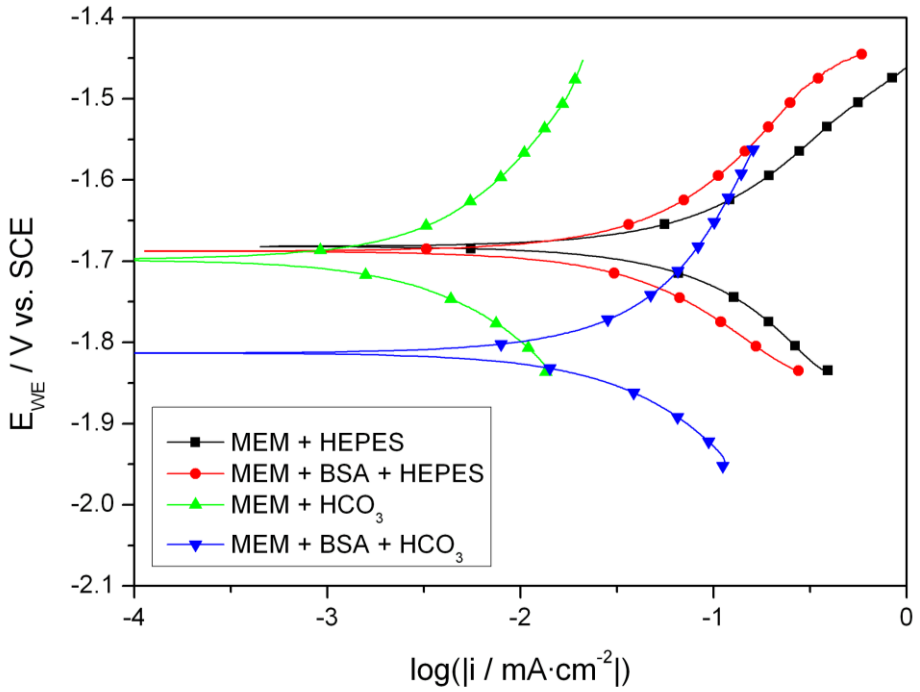

Figure 7-13: PDP of protein solutions and uncoated Mg after 8 hours.

Once proteins are added, the HCO_3 buffered solutions have much higher corrosion current densities, between 40 and 60 $\mu A \cdot cm^{-2}$. This suggests the passivation layer formed in the HCO_3 buffer is impeded by proteins. The polarization of uncoated Mg at 30 minutes (Figure 7-12) shows that the carbonate buffer exhibits large decreases in cathodic kinetics and a smaller decrease in anodic kinetics. With the addition of BSA, the decrease in anodic kinetics is lessened, possibly due to the proteins interfering with the protective passivation layer that forms in the HCO_3 buffer. After 8 hours, the HCO_3 buffer in MEM creates a massive drop in both anodic and cathodic kinetics of roughly equal magnitude, leading to the very small change in E_{Corr}. When proteins are present, the cathodic kinetics are decreased, but the anodic kinetics remain similar to the HEPES buffered BSA solution. The explanation is found in the limitation of the formation of the passive layer, perhaps by proteins taking up Ca^{2+} ions and preventing the calcium carbonates from forming on the surface. The lower E_{Corr} might also be explained by binding of Mg^{2+} ions, which would occur in the presence of the higher pH [29]. The fact that the HEPES buffered reaction kinetics drop only slightly with BSA addition agrees with other findings that the influence of the buffer, specifically CO_2/HCO_3 buffer, is instrumental in the reduced corrosion rate [21].

Figure 7-18 shows the Nyquist plots of uncoated Mg in both MEM and MEM + BSA over the first 7 hours. The large EDL resistance in MEM buffered with HCO_3 initially shows the insulation the passive layer provides in the bicarbonate buffered solution. This effect increases as time passes, corrosion occurs, the pH rises and the layer becomes more passive (Figure 7-16). Both solutions containing albumin show similar impedance layers, in either buffer initially. Instead of the low capacitance primary coating layer with a high resistance EDL of the MEM/HCO_3 layer, the larger initial time constant appears as the result of the semi permeable protein layer resisting charge transfer, which causes the drop in the anodic and cathodic reactions. Closer examination of the Nyquist plot (Figure 7-19) shows that the uncoated Mg in MEM + BSA buffered with HCO_3 actually shows 3 distinct time constants. The first is the small passivation layer presented by the carbonate and hydroxide layer, followed by a layer of proteins, and finally the smaller charge transfer resistance from the electrolytic double layer itself. The smaller size of the first and third time constant in this systems is evidence of the proteins inhibiting the passivation that provides such protection in MEM and HCO_3 alone.

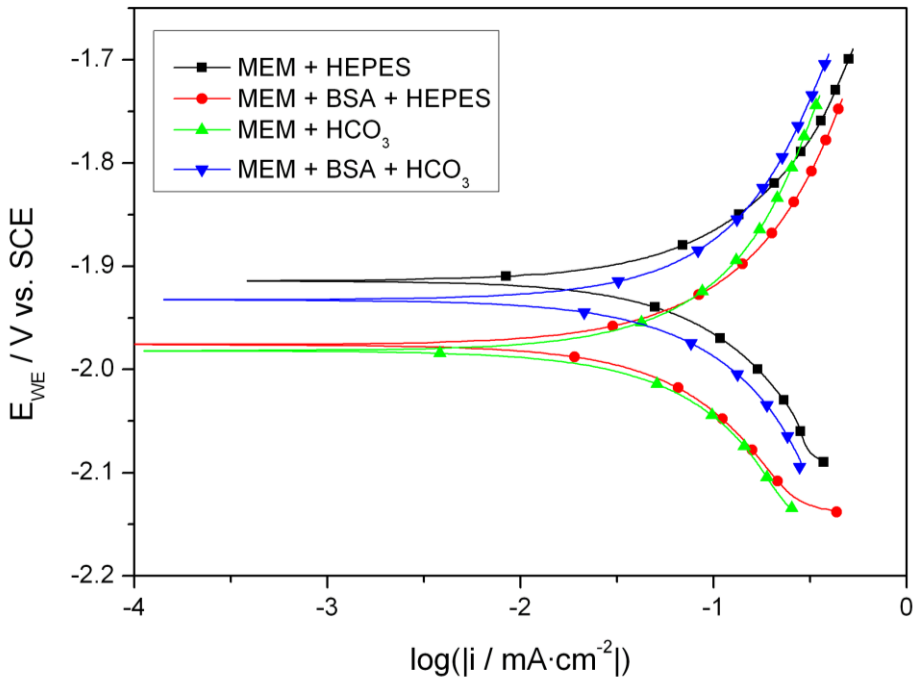

Figure 7-14: PDP of biomimetic coated samples in protein solutions at 30 minutes.

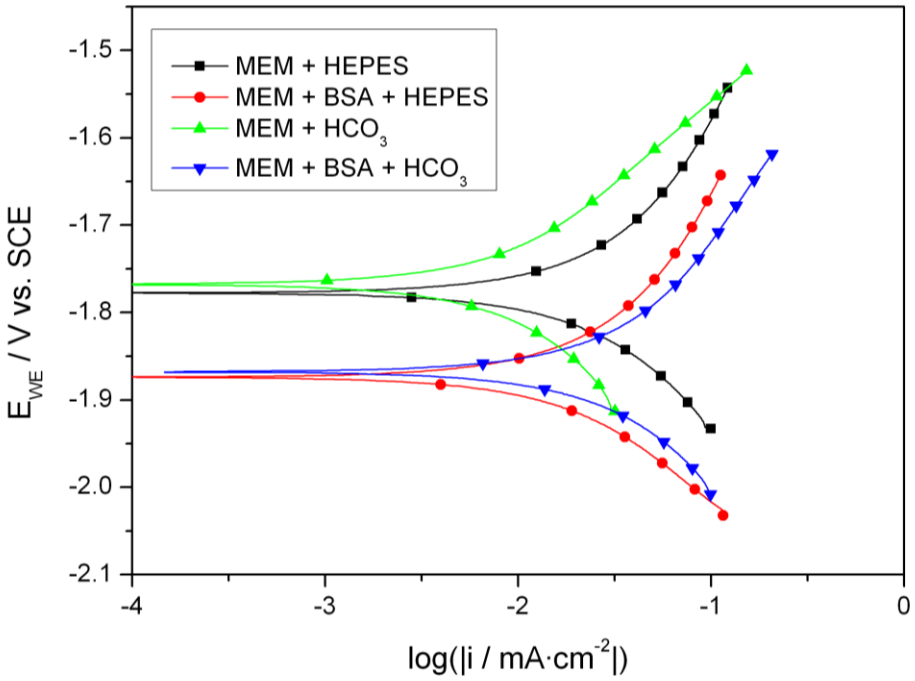

Figure 7-15: PDP of protein solutions on biomimetic coated samples after 8 hours.

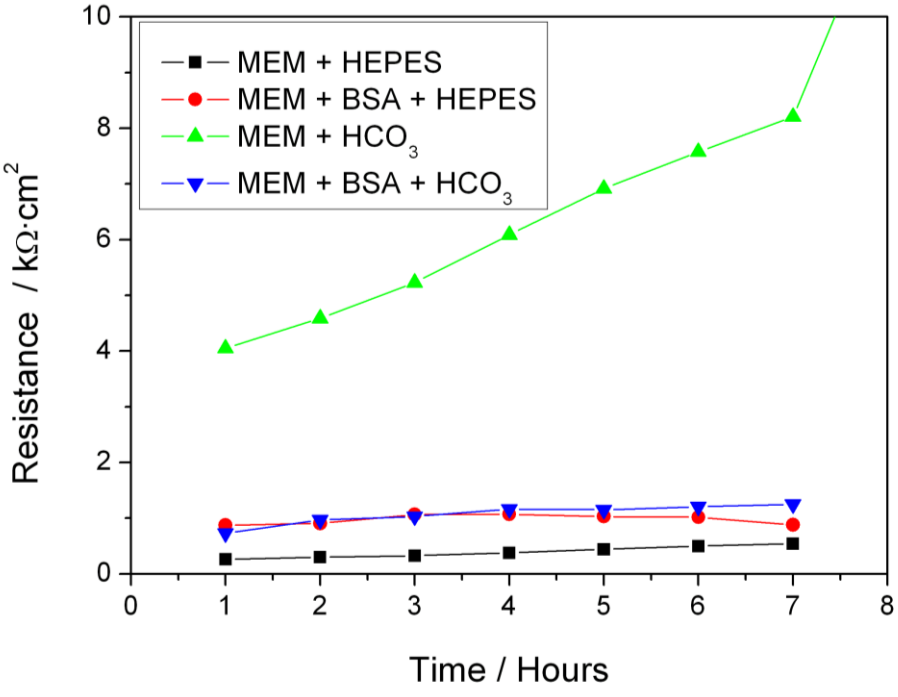

Figure 7-16: Polarization resistance in MEM and MEM + BSA of uncoated Mg samples with buffers.

For biomimetic coated samples, the CO_2 buffer results in decreased anodic and cathodic kinetics for MEM solutions at 30 minutes (Figure 7-14). With the addition of proteins, the anodic kinetics decrease, but the cathodic kinetics are increased by the CO_2 buffer. This follows the trend seen before with uncoated Mg. After 8 hours, the difference between these two buffer systems becomes more pronounced (Figure 7-15). By this time, both layers have had a chance to settle, and HCO_3 buffer reduces both reactions in MEM, but when albumin is present, the cathodic kinetics remain increased, and the anodic kinetics are slightly higher as well. The inhibitory effects of the proteins on the passivation layers causes the same effect on these coated samples, by blocking the passivation of the pores in the coatings. Past 8 hours, the protective layer that formed in MEM on bare Mg did not seem to persist, as the corrosion resistance dropped significantly (Figure 7-17). Thus, the layer in the presence of amino acids does not seem to last. The biomimetic coatings in MEM + HCO_3 also displayed a great increase in the passive properties of the coating. This layer persisted over the 24 hour test. However, with the addition of BSA, the protective effect of the low capacity HCO_3 buffer was much less pronounced, and the corrosion rates were more typical of what one would expect at pH 7.4.

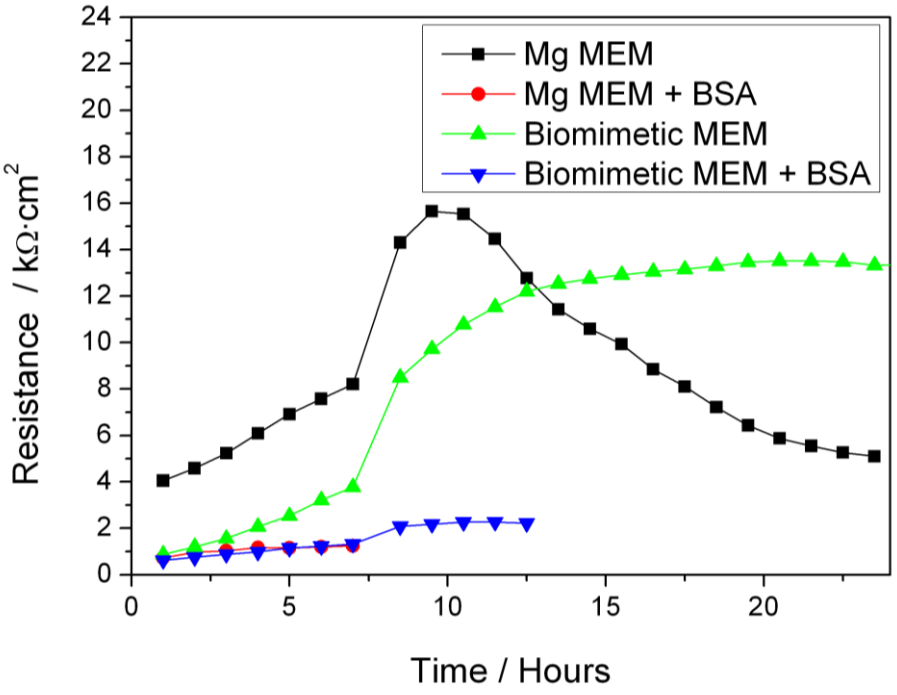

Figure 7-17: Polarization resistance of biomimetic coated samples in HCO_3 buffered protein solutions.

The Nyquist plots show the coating resistances grow with time (Figure 7-20), and the bicarbonate buffered sample in MEM leads the pack due to the resistance layer that forms. The lower resistance of the biomimetic coated sample will be an artefact of the lower corrosion rate than uncoated Mg alone, where the pH rise quickly outpaces the buffer capacity, forming the insoluble calcium and magnesium carbonates that supplement the magnesium hydroxide layer. When the coating is added, the pH change rises more slowly, giving the bicarbonate ion and CO_2 atmosphere time to equilibrate, leading to the less protective layer. With proteins binding to free Ca^{2+} and Mg^{2+} ions in solution [9, 29], these ions are effectively less available to form the insoluble salts that prevent the corrosion. Thus, the kinetics of the reactions differs depending on the buffer choice for each system. With a complicated environment such as the body, it will be important to understand the effects each component will have on the ultimate corrosion reactions and passivation properties expected at the implant site.

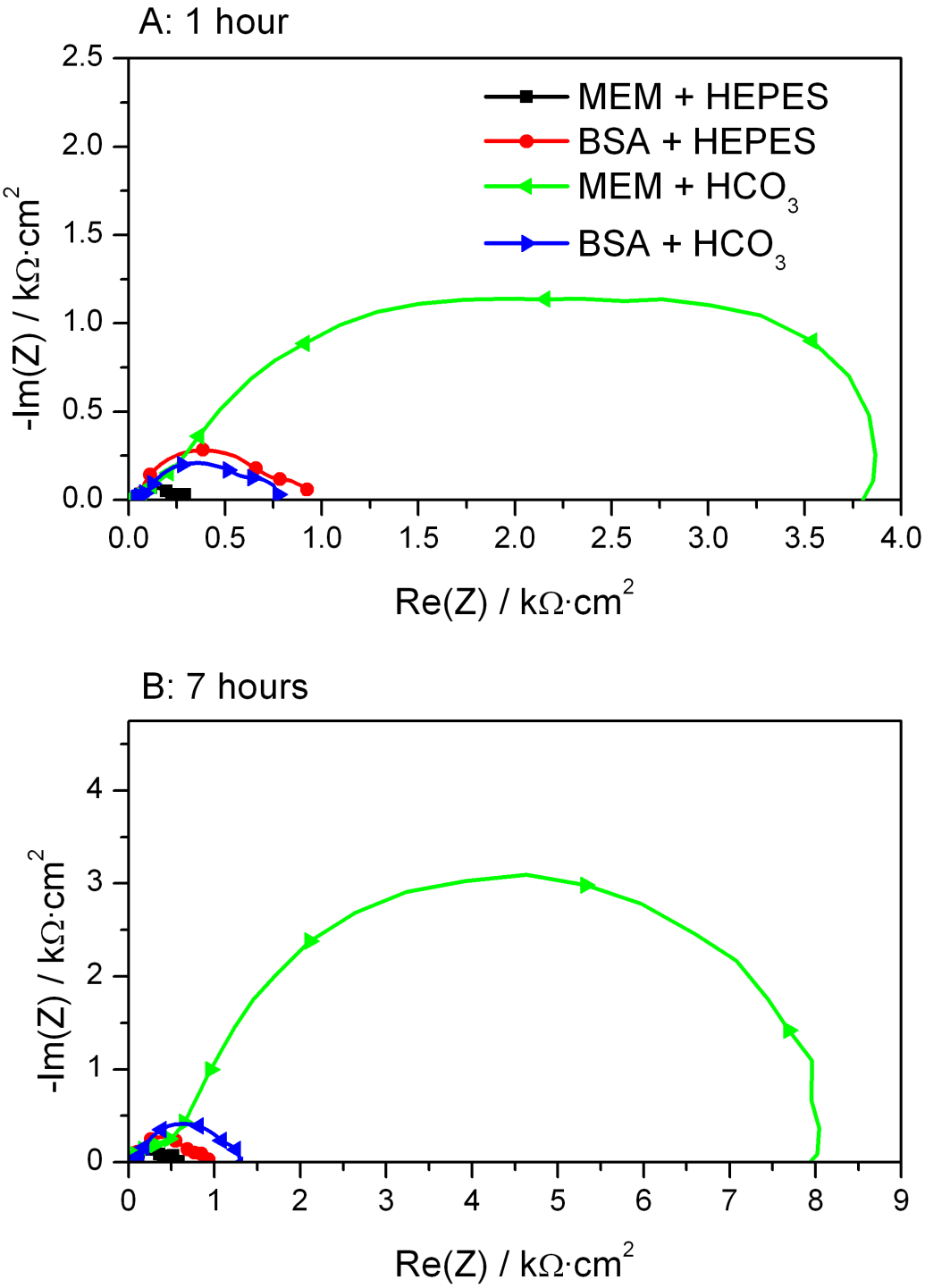

Figure 7-18: Nyquist plots of uncoated Mg in protein solutions buffered with HCO_3.

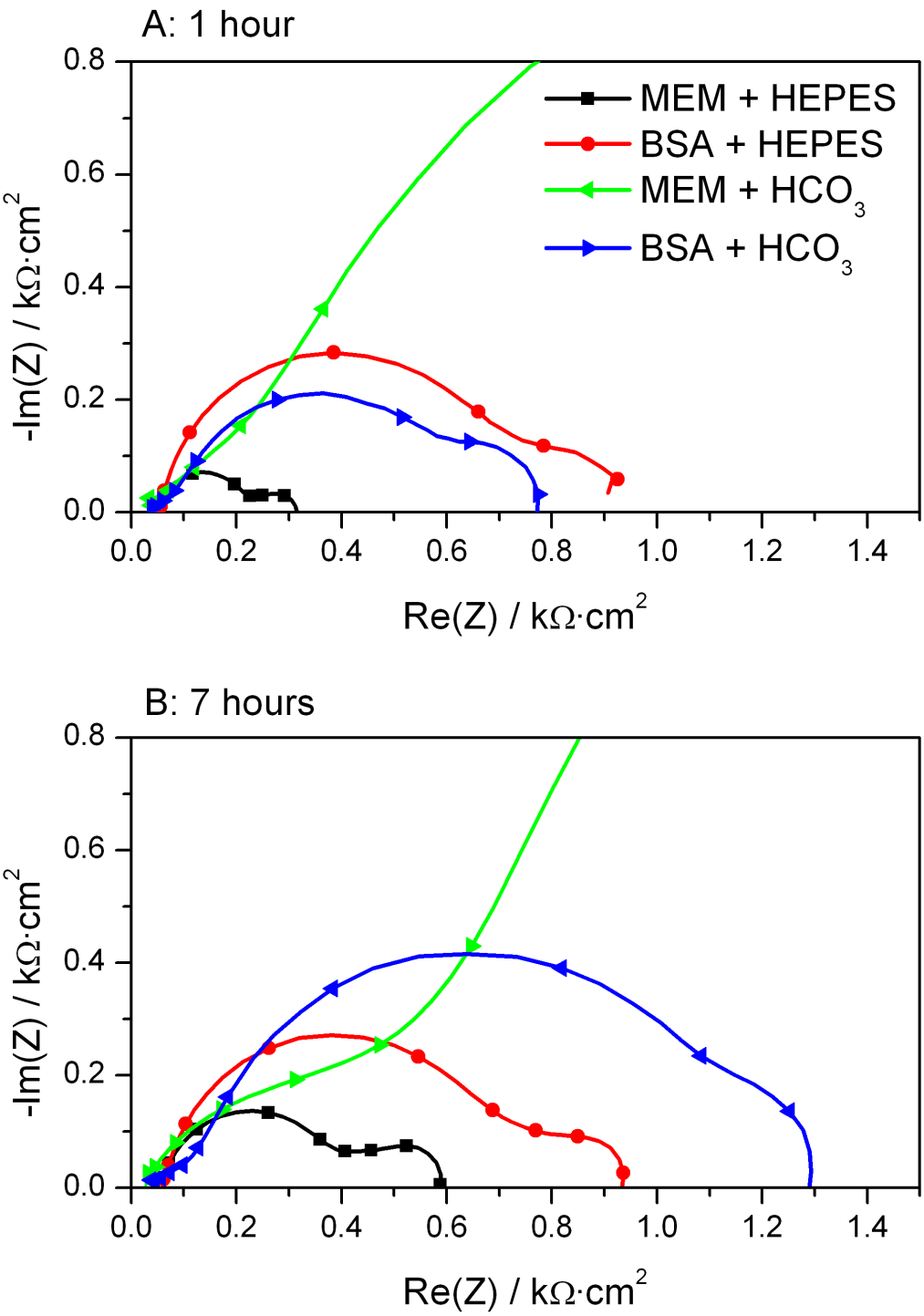

Figure 7-19: Nyquist plots of uncoated Mg in protein solutions buffered with HCO_3 detail.

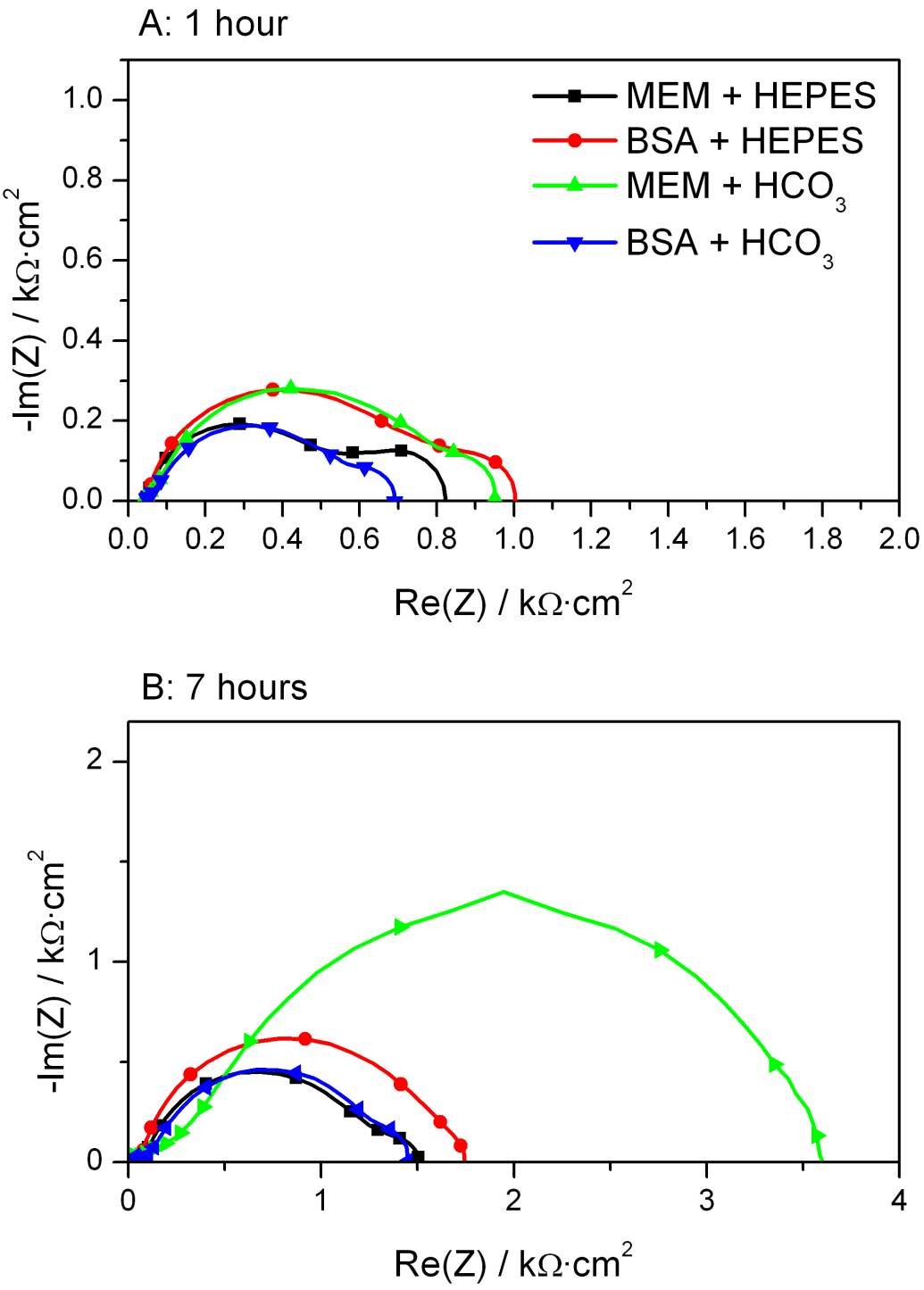

Figure 7-20: Nyquist plots of biomimetic coated samples in protein solutions buffered with HCO_3.

The relationship between E_{Corr} and i_{Corr} for uncoated and coated samples in the protein solutions vs. buffer type is compared in Figure 7-21. The uncoated Mg in HEPES, displaying no real great passive behaviour showed no strong correlation with regard to E_{Corr} and i_{Corr}.

All other samples tested displayed the expected trend of decreasing i_{Corr} with increasing E_{Corr}. As the layers settled in the solution, the corrosion rates dropped as over time for all of these samples, the difference is only the impeding corrosion layer that forms, whether due to proteins, the buffer, or both.

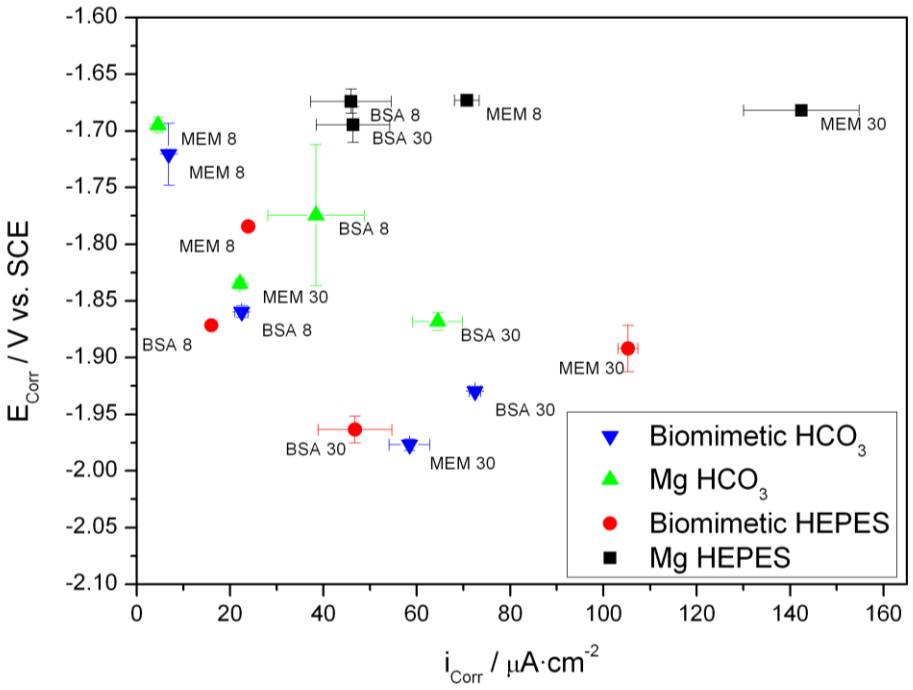

Figure 7-21: E_{Corr} vs. i_{Corr} plots for uncoated Mg and biomimetic coated samples for different buffer types on MEM and MEM + BSA.

7.5. Conclusions

It is clear from these results that both amino acids and proteins had an effect on the corrosion reactions *in vitro*. It will be important to understand the individual effects *in vitro* if effective models and predictions are to be developed by *in vivo* testing. The early corrosion rates of uncoated Mg were accelerated by the change from HBSS to MEM as the SBF, despite the lower amount of Cl^-, and slightly lower solution conductivity. The increased buffer capacity that the amino acids provide [3] explains this effect. The higher rather than lower E_{Corr} measured for Mg suggests the chelation of Mg^{2+} ions is not the dominant factor in the early corrosion mechanisms as has been proposed for the rate acceleration [2]. The increased buffer capacity and inhibition of passive layer formation are therefore likely to be

responsible. Adsorption of amino acids did not slow the early rates of corrosion for uncoated Mg like they do on other metals [23, 24]. It can be concluded that the overall effect of the amino acids is to increase the corrosion rate *in vitro*, and it would be expected to contribute to the corrosion rate *in vivo* as well.

The amino acids accelerate the corrosion rate and decrease the resistance of the coating and passive layer on the biomimetic coated samples as well. The mechanism of corrosion on the biomimetic coated samples was similar to uncoated Mg, reduced to a smaller area by the insoluble CaP coating. Amino acids accelerated the corrosion of the coated Mg through the defects similar to uncoated samples. Corrosion of the ECAD modified coatings was different. The $Ca(OH)_2$ layer below is designed to dissolve and promote the deposition of additional CaP at the defect sites where corrosion is taking place. Thus, in the more aggressive environment of the MEM, the corrosion rate of the ECAD coated sample decreased, and the coatings became more protective. Overall, this data suggests that the use of MEM *in vitro* can accelerate the corrosion rates of Mg, and the presence of amino acids *in vivo* may lead to higher *in vivo* corrosion rates that one might expect by doing *in vitro* tests without amino acids. These tests also show that the ECAD modification for corrosion protection by biomimetic coatings is enhanced by the amino acids. This ECAD coating remained corrosion resistant even in these more aggressive solutions.

The corrosion environment and thus the overall corrosion rate were affected by the proteins, It was found that the proteins reduced the corrosion of uncoated Mg in solution by the adsorption of proteins to the surface [18, 19]. The effect of increasing corrosion on uncoated Mg by chelating of metal ions with proteins was not a significant contribution to the early corrosion kinetics in this study [21]. The corrosion rates were dominated by the pH and Cl^- ions and the relative area available for corrosion.

The proteins affected the corrosion through biomimetic coatings as well. With the addition of proteins, the extra impedance provided by the adsorption to the surface led to better passive properties of the exposed metal. The reduction in corrosion rate shows that the proteins facilitate the barrier the biomimetic coating provides. The corrosion through the defects was lessened when the proteins were present. Therefore, in a high protein solution such as the body, it could be expected that this effect will reduce the corrosion rate of the biomimetic coated samples further than the measurements made in vitro.

The addition of proteins also reduced the diffusion of salts to the $Ca(OH)_2$ layer of ECAD coated samples. The total corrosion resistance of the ECAD coatings is improved by the corrosion and deposition of the salts to this layer. Therefore, the protein additions slowed the formation of this layer, leading to a corrosion resistance increase at a slower rate than the ECAD coated samples in MEM alone. However, the ultimate corrosion rates of these samples were lower than the biomimetic coated samples alone. It can be concluded that the proteins slowed the self healing mechanism but did not stop it, and this method still provided improved protection over the other coatings.

The behaviour of the protein solutions with different buffer systems was also found to be relevant to the corrosion reactions. In NaCl and HBSS solutions the presence of the carbonate buffer exhibited a low capacity and rapid carbonate film formation that reduced corrosion rates. This also occurred when amino acids were present. However, once BSA was added, the layer formation was impeded and the total corrosion resistance dropped much closer to that of the HEPES buffered solutions. The proteins appear to interfere with the layer formation by binding to salts [9, 29]. This is further evidence that the HCO_3 buffered systems may not be the most physiologically relevant just because of the chemical equivalency. Of course, this is only a single type of protein addition. The actual physiological system has many different types of proteins, and the behaviour is complex. Therefore, further *in vitro* and *in vivo* tests will be needed to understand the effects of each different type of protein. The different solutions and buffers all agreed on the relative corrosion protection provided by each coating, but for the exact rates and mechanisms, the effect of the proteins is not trivial, and may result in greater or lesser protection than expected from simple SBFs, depending on the solution and the buffering agent.

7.6. References

1. Virtanen, S., *Biodegradable Mg and Mg alloys: Corrosion and biocompatibility.* Materials Science and Engineering: B, 2011. **176**(20): p. 1600-1608.

2. Yamamoto, A. and S. Hiromoto, *Effect of inorganic salts, amino acids and proteins on the degradation of pure magnesium in vitro.* Materials Science and Engineering: C, 2009. **29**(5): p. 1559-1568.
3. Malda, J., T.B.F. Woodfield, M. Radisic, S. Levenberg, C. Oomens, F.P. Baaijens, P. Svalander, and G. Vunjak-Novakovic, *Cell Nutrition : In Vitro and In Vivo.* Tissue Engineering : A Textbook, 2008(1): p. 327-362.
4. Gu, X.N., Y.F. Zheng, and L.J. Chen, *Influence of artificial biological fluid composition on the biocorrosion of potential orthopedic Mg-Ca, AZ31, AZ91 alloys.* Biomedical Materials, 2009. **4**(6): p. 8.
5. Chen, X.B., N. Birbilis, and T.B. Abbott, *A simple route towards a hydroxyapatite-Mg(OH)2 conversion coating for magnesium.* Corrosion Science, 2011. **53**(6): p. 2263-2268.
6. Carboneras, M., M.C. GarcÃ-a-Alonso, and M.L. Escudero, *Biodegradation kinetics of modified magnesium-based materials in cell culture medium.* Corrosion Science, 2011. **53**(4): p. 1433-1439.
7. Keim, S., J.G. Brunner, B. Fabry, and S. Virtanen, *Control of magnesium corrosion and biocompatibility with biomimetic coatings.* Journal of Biomedical Materials Research - Part B Applied Biomaterials, 2011. **96 B**(1): p. 84-90.
8. Salunke, P., V. Shanov, and F. Witte, *High purity biodegradable magnesium coating for implant application.* Materials Science and Engineering: B, 2011. **176**(20): p. 1711-1717.
9. Clark, G.C.F. and D.F. Williams, *The effects of proteins on metallic corrosion.* Journal of Biomedical Materials Research, 1982. **16**(2): p. 125-134.
10. Latour, R., *Biomaterials: Protein-Surface Interactions*.
11. Kirkland, N.T., *In Vitro Assessment of the Physiological Biocorrosion Behaviour of Magnesium-Based Biomaterials.* 2011.
12. Eliezer, A. and F. Witte, *Corrosion Behaviour of Magnesium Alloys in Biomedical Environments.* Advanced Materials Research, 2010. **95**: p. 17-20.
13. Willmer, E.N., *Cells and Tissues in Culture: Methods, Biology, and Physiology*. 1965, London: Academic Press.
14. Equitech-Bio Inc. *Sterile Filtered Fetal Bovine Serum, US Origin*. 2010 [cited 2010 13/05]; Available from: https://www.equitech-bio.com/Sterile-filtered-fetal-bovine-serum-US-origin.html.
15. Lenter, C., *Geigy Scientific Tables*. 1981, Basle, Switzerland: Ciba-Geigy.
16. Rettig, R. and S. Virtanen, *Time-dependent electrochemical characterization of the corrosion of a magnesium rare-earth alloy in simulated body fluids.* Journal of Biomedical Materials Research Part A, 2008. **85A**(1): p. 167-175.
17. Rettig, R. and S. Virtanen, *Composition of corrosion layers on a magnesium rare-earth alloy in simulated body fluids.* Journal of Biomedical Materials Research - Part A, 2009. **88**(2): p. 359-369.
18. Liu, C., Y. Xin, X. Tian, and P.K. Chu, *Degradation Susceptibility of Surgical Magnesium Alloy in Artificial Biological Fluid Containing Albumin.* Journal of Materials Research, 2007. **22**(7): p. 1806-1814.
19. Liu, C.L., Y.J. Wang, R.C. Zeng, X.M. Zhang, W.J. Huang, and P.K. Chu, *In vitro corrosion degradation behaviour of Mg–Ca alloy in the presence of albumin.* Corrosion Science, 2010. **52**(10): p. 3341-3347.
20. Yang, L., N. Hort, R. Willumeit, and F. Feyerabend, *Effects of corrosion environment and proteins on magnesium corrosion.* Corrosion Engineering, Science and Technology, 2012.

21. Willumeit, R., J. Fischer, F. Feyerabend, N. Hort, U. Bismayer, S. Heidrich, and B. Mihailova, *Chemical surface alteration of biodegradable magnesium exposed to corrosion media.* Acta Biomaterialia, 2011. **7**(6): p. 2704-2715.
22. Warrel, D.A., *Oxford Textbook of Medicine*. 4 ed, ed. T.M. Cox, J.D. Firth, and E.J. Benz Jr. Vol. 3. 2003, New York: Oxford University Press.
23. Ashassi-Sorkhabi, H., Z. Ghasemi, and D. Seifzadeh, *The inhibition effect of some amino acids towards the corrosion of aluminum in 1 M HCl + 1 M H2SO4 solution.* Applied Surface Science, 2005. **249**(1-4): p. 408-418.
24. Ashassi-Sorkhabi, H., M.R. Majidi, and K. Seyyedi, *Investigation of inhibition effect of some amino acids against steel corrosion in HCl solution.* Applied Surface Science, 2004. **225**(1-4): p. 176-185.
25. Mueller, W.-D., M. Lucia Nascimento, and M.F. Lorenzo de Mele, *Critical discussion of the results from different corrosion studies of Mg and Mg alloys for biomaterial applications.* Acta Biomaterialia, 2010. **6**(5): p. 1749-1755.
26. Kirkland, N.T., N. Birbilis, J. Walker, T. Woodfield, G.J. Dias, and M.P. Staiger, *In-vitro dissolution of magnesium–calcium binary alloys: Clarifying the unique role of calcium additions in bioresorbable magnesium implant alloys.* Journal of Biomedical Materials Research Part B: Applied Biomaterials, 2010: p. n/a-n/a.
27. Waterman, J., A. Pietak, N. Birbilis, T. Woodfield, G. Dias, and M.P. Staiger, *Corrosion resistance of biomimetic calcium phosphate coatings on magnesium due to varying pretreatment time.* Materials Science and Engineering: B, 2011. **176**(20): p. 1756-1760.
28. Waterman, J., *Improving in vitro corrosion resistance of biomimetic calcium phosphate coatings for Mg substrates using calcium hydroxide layer.* Corrosion Engineering, Science and Technology, 2012. **47**(5): p. 340-345.
29. Kragh-Hansen, U. and H. Vorum, *Quantitative analyses of the interaction between calcium ions and human serum albumin.* Clinical Chemistry, 1993. **39**(2): p. 202-208.
30. Pedersen, K.O., *Binding of Calcium to Serum Albumin III. Influence of Ionic Strength and Ionic Medium.* Scandinavian Journal of Clinical & Laboratory Investigation, 1972. **29**(4): p. 427-432.
31. Guillaume, Y.C., C. Guinchard, and A. Berthelot, *Affinity chromatography study of magnesium and calcium binding to human serum albumin: pH and temperature variations.* Talanta, 2000. **53**(3): p. 561-569.
32. Xin, Y., K. Huo, H. Tao, G. Tang, and P.K. Chu, *Influence of aggressive ions on the degradation behavior of biomedical magnesium alloy in physiological environment.* Acta Biomaterialia, 2008. **4**(6): p. 2008-2015.

CHAPTER 8: Conclusions

8.1. Coatings and *in vitro* Corrosion Tests

In order for magnesium to be used, the corrosion rate needs to be limited during the early implantation [1]. The coating system is also important, as the properties of Mg and the implant shape will limit the choices of deposition. The ideal coating must be processable at low temperatures and suitable environments due to the melting temperature and reactivity of Mg. The final implant shape may need to be a porous structure, which cannot be coated completely by techniques requiring line of sight. The use of toxic or non-biocompatible precursors and intermediate chemicals during the coating process is not inconceivable, but these must be completely removed before the device is implanted. If the coating process can avoid this concern it will be beneficial.

One of the coating systems in the literature that meets the desired criteria is the biomimetic coating. This coating type has been well documented recently for its biocompatible properties on titanium implants, but has received little attention for Mg. It is biocompatible, imitates natural bone structure, and contains no elements or structures not found in the body anyway. The process is done at body temperature, and is coated in simple solutions that contain no elements that are not found in physiological fluids. The solubility of the phases is similar to natural bone, and thus more insoluble than Mg, and thus can be protective under corrosion conditions, yet less insoluble than the HA used on permanent Ti implants. The biocompatibility and osteogenic properties of biomimetic coatings have already been proven by numerous tests on Ti, which gives us confidence that it will be just as useful in promoting bone growth on degradable implants. The gap in the knowledge is the corrosion properties, as the protection of Ti has not been a design requirement of the coatings. Thus, if the biomimetic coatings can be used to slow the corrosion rate sufficiently, they will be ideal for the in vivo control of the degradation rate of biodegradable Mg implants.

8.2. Buffer Selection for *in vitro* Corrosion Testing

The corrosion rate in vitro is very sensitive to pH. As Mg corrosion causes a pH rise, this will change the corrosion behaviour if it is not mitigated by a buffer system. Electrochemical tests here show that while many buffers are suitable, the properties of the buffers influence the measured corrosion rate. Therefore some are more suitable for *in vitro* tests than others. The *in vivo* buffer chemistry based on CO_2/ HCO_3 is commonly used in the literature. The characteristics of the buffer system vary greatly depending on the *in vitro* SBF choice, and the time of immersion. The role of carbonate in the passive layer at elevated pH coupled with the relatively low buffer capacity and diffusion speed with the atmosphere inside an incubator lead to passivation properties that may not be analogous *in vivo*. Bicarbonate buffered *in vitro* solutions have slower Mg corrosion rates than *in vivo* [2]. With the pH changes that accompany fast corroding Mg, the lack of consistency in the corrosion mechanism makes it difficult to accurately determine the absolute corrosion protection provided.

The zwitterionic chemical buffers provide a buffer system with higher buffer capacity than HCO_3 without depositing to form a corrosion layer. HEPES had the highest buffer capacity of the buffers tested at pH of 7.4. The electrochemical data shows that the corrosion reactions and layers are consistent enough that there is no compelling reason to choose one of the other buffers over HEPES for these corrosion studies. The wider use of HEPES in the literature for Mg corrosion studies over the other zwitterionic buffers makes comparison of results to the available literature easier. When the interactions of HEPES with Mg were measured, the complex behaviour was very small at biological concentrations of Mg^{2+} and 25mM HEPES. Larger interaction was detected at high concentrations of Mg. At the corrosion surface, the local ion concentration will be higher than normal. Also, the pH at the surface will remain lower with HEPES than HCO_3 due to the capacity. The HEPES may therefore cause corrosion reaction rates faster than what would be expected *in vivo* [3]. With the individual advantages of both HEPES and HCO_3, both are appropriate buffers for *in vitro* corrosion tests. By performing tests in both buffered solutions, the properties and differences of these buffers can be quantified and compared. This will bound the corrosion rate expectation in vivo, and allow greater understanding of the individual contributions of pH, carbonate ion reactions, and passive layer performance of Mg and protective coatings and surface treatments. Both of these buffers were used to compare the effect of the carbonate on the corrosion mechanisms *in vitro*. The mechanisms and effect of the buffers on the

measured in vitro corrosion rate allowed us to understand and quantify the corrosion response of protective coatings in vitro. Therefore the properties of these coatings could be investigated and optimized for corrosion resistance without the need for many expensive *in vivo* studies.

8.3. Biomimetic Calcium Phosphate Coatings on Magnesium

8.3.1. Formation on Mg

The use of biomimetic calcium phosphates was well known on Ti. The deposition mechanisms and corrosion properties on Mg were not well known. The favourable qualities of these coating make them ideal for *in vivo* applications if the corrosion rate can be successfully controlled. Thus the properties of the surface on the formation of the coating, the resulting corrosion protection, and the failure mechanisms of these coatings were examined here.

Pretreatment to form a hydroxide layer is known to be important to biomimetic coating deposition on Ti, so its effect on Mg substrates was measured. It was found not to be necessary to pretreat magnesium to nucleate a CaP coating on Mg. Instead, longer pretreatment times led to a greater amount of cracks and defects in the coating layer. More defects lead to faster corrosion underneath the coating, which would eventually lead to pieces of coating breaking off in solution. In a simple NaCl solution, this results in decreasing corrosion protection with time. When calcium and phosphate ions were added to the solution, the $Mg(OH)_2$ pretreatment layer promoted additional nucleation of CaPs. This led to increased corrosion resistance during the 24 hour test. The results of the study show that pretreatment is not necessary for biomimetic coating of Mg and the corrosion properties are not necessarily improved by pretreatment. The increase in coating polarization resistance due to CaP nucleation was a surprising result. The pretreatment in this case seemed to improve the deposition. If this mechanism can be leveraged to improve the corrosion properties of the biomimetic coatings, it may help with the ultimate goal of providing the protection needed for an implant.

The corrosion resistance of the coatings is linked to the integrity of the coating by the amount of defects that are there. The severity of these defects is what will limit the total effectiveness of the corrosion resistance. Optimizing the initial coating creation, as well as the deposition of additional CaP from physiological solutions will help to bring up the total protectiveness to where they can be used in vivo.

The amount and severity of the defects in the coating do pose significant concern for the ultimate utility of biomimetic coatings. If they cannot be improved to prevent localized corrosion, they will not be an acceptable solution, despite their other desirable properties. The coatings will be required to withstand corrosive environments long enough that the bone can heal. The 24 hour tests show that the corrosion occurs beneath the defects, but the rise or fall of the corrosion resistance depends on the environment. The short 24 hour corrosion tests showed some protection, but the failure mechanisms suggested this would not last. Therefore, longer term corrosion tests were eventually necessary to evaluate the performance.

8.4. Modification and Long Term Corrosion of Biomimetic Coatings

The findings from the previous studies on biomimetic coatings showed that the pretreatments and processes to increase the deposition of these coatings on Ti was not necessary or beneficial for the corrosion properties on Mg. This was taken further to examine the individual contribution of both coating steps for the biomimetic coating. The results showed that the high Mg amorphous carbonated CaP first step in the coating is not required for deposition of the biomimetic coating on Mg, in contrast to Ti [4, 5]. The composition and crystal structure of the substituted DCPD biomimetic coatings were found to not be affected by the first coating solution process. The new biomimetic 2 coatings improved the corrosion protection significantly. These coatings produced minimal H_2 gas over the course of the 2 week immersion test in HBSS. This low level of H_2 generation puts the coatings in range of predicted acceptable levels of H_2 generation *in vivo* [6]. Over the 14 day test, the phase of the calcium phosphate coatings changed from mostly DCPD to a calcium deficient apatite structure. This more stable phase is less soluble and provides more protection than the

amorphous phase that formed on uncoated Mg [7]. The corrosion protection provided by these coatings was still limited by the defects and corrosion through the coating, rather than the dissolution of the coating itself. The defects and the corrosion problem they present remain a challenge for the use of these coatings *in vivo*. The biomimetic 2 coatings did show some signs that the deposition of additional CaP from solution helped to repair the defects and extend the protection. This mechanism can be optimized and utilized to provide a coating with better protection properties.

The choice of buffer was shown to have an effect on both the measured rates of corrosion and the mechanism of corrosion that takes place. The HEPES buffer proved to be more aggressive than the bicarbonate buffer due to the better control of the pH rise and the lack of carbonate phases contributing to the corrosion layer. The measured corrosion rates in HEPES are thus expected to be faster than the HCO_3 *in vitro* tests. *In vivo* tests are more difficult to determine, but it seems likely that the HEPES buffer will provide the upper bound of the corrosion rate, as it's expected that the HCO_3 buffer in vivo will present slower rather than faster corrosion [3].

8.5. Self healing Coatings based on Calcium Hydroxide

The defects in the biomimetic coatings present a problem for the use of biomimetic coatings. A defect that appears in the coating either during the deposition, implantation or while implanted will allow localized corrosion to take place below the coating. Additional calcium and phosphate from the physiological solution can coat a Mg implant and slow the corrosion over time. This phenomenon is limited by the low amounts of Ca in typical physiological fluids. The ECAD calcium hydroxide 2 layer biomimetic coating system was invented through this work to provide a self healing mechanism for defect-prone biomimetic CaP coatings.

This ECAD coating increased the corrosion protection of the biomimetic coating. The calcium rich layer also provided a suitable nucleation substrate for the biomimetic coating, and this produced a better coating with less defects than the normal biomimetic coatings. The

self healing mechanism increased the coating corrosion resistance over time, rather than it degrading. The ECAD method met the criteria for the coating methods: low temperature, not line of sight, fast, and non-toxic. However, gas production during the deposition did allow the formation of volcano shaped defects in the ECAD layer. This could be an issue for optimization of the coating, but even with these defects the coating layer was effective. The biomimetic coating was deposited, and the ECAD layer did not significantly change the final composition or structure of the CaP. The amount of defects in the final layer was lower, leading to higher initial corrosion resistance. The $Ca(OH)_2$ layer promotes the deposition of a complete and low defect biomimetic coating.

The major benefit of the ECAD $Ca(OH)_2$ was the self healing effect the coating produced. As corrosion progressed, the protectiveness of the ECAD coatings increased due to the calcium rich layer depositing additional protective calcium phosphates at corrosion sites. The availability of a semi-soluble calcium rich layer to deposit in the defects greatly improved the corrosion resistance as corrosion occurred. This led to the coating remaining intact with few defects to allow the corrosion reaction to progress. The H_2 generation was low, and the pitting below the coating was minimal. For a biodegradable implant application where corrosion behaviour is critical, a self healing coating such as the one describe here may provide much better corrosion properties than typical biomimetic coatings by themselves. Therefore, the calcium hydroxide layer provides a simple, effective means of improving the biomimetic coating corrosion properties without using any toxic elements or processing.

The ECAD coatings performed well with both HEPES and HCO_3 buffer systems. As HEPES has higher buffer capacity than HCO_3 *in vitro*, and does not accurately represent the carbonate ions in the body, it could be the case that the mechanisms of corrosion will not be quite the same when the coating system is moved from *in vitro* to *in vivo*. The ECAD + biomimetic coating in HCO_3 buffered HBSS was more corrosion resistant than the same coating in HEPES. The additional carbonate ions and larger pH rise led to earlier deposition of calcium compounds, further protecting the substrate. The good initial performance of the coating in HCO_3 buffered solutions indicates that the mechanism of protection this coating provides will persist in other solutions and remain more protective in carbonated buffered solutions such as the body.

8.6. The Effect of Amino Acids and Proteins on *in vitro* Testing of Corrosion Resistant Coatings

8.6.1. Amino Acids

Both amino acids and proteins had an effect on the corrosion reactions *in vitro*. The early corrosion rates of uncoated Mg were accelerated by the change from HBSS to MEM as the SBF, despite the lower amount of Cl^-, and slightly lower solution conductivity. The increased buffer capacity that the amino acids provide [8] explains this. Chelation of Mg^{2+} ions has been proposed as a mechanism for the accelerating rate of corrosion in amino acids [3], but the higher rather than lower E_{Corr} measured here does not support that theory, at least during the early stages of corrosion. Adsorption of amino acids did not slow the early rates of corrosion for uncoated Mg like they do on other metals [9, 10]. It can be concluded that the overall effect of the amino acids is to increase the corrosion rate *in vitro*, and it would be expected to contribute to the corrosion rate *in vivo* as well.

The amino acids had the same effect on the biomimetic coated samples, accelerating the corrosion rate and decreasing the resistance of the coating and passive layer. The mechanism of corrosion on the biomimetic coated samples was similar to uncoated Mg, but impeded by the CaP layer. Therefore, the amino acids accelerated the corrosion of the bare Mg through the defects in the same manner. The ECAD modified coatings did not corrode like this, however. The $Ca(OH)_2$ layer below is designed to dissolve and promote the deposition of additional CaP at the defect sites where corrosion is taking place. Thus, in the more aggressive environment of the MEM, the corrosion rate of the ECAD coated sample decreased, and the coatings became more protective. Overall, this data suggests that the us of MEM *in vitro* can accelerate the corrosion rates of Mg, and the presence of amino acids *in vivo* may lead to higher *in vivo* corrosion rates that one might expect by doing *in vitro* tests without amino acids. These tests also show that the ECAD modification for corrosion protection by biomimetic coatings is enhanced by the amino acids. This demonstrates that the coating remains corrosion resistant even in the more aggressive solution.

8.6.2. Proteins

Although they do not directly interact with the corrosion reactions of Mg, proteins affect the environment and thus the overall corrosion rates measured. It was found that the proteins reduced the corrosion of uncoated Mg in solution by the adsorption of proteins to the surface [11, 12]. The effect of increasing corrosion on uncoated Mg by chelating of metal ions with proteins was not a significant contribution to the early corrosion kinetics in this study [2]. The corrosion rates were dominated by the pH and Cl^- ions and the relative area available for corrosion.

Biomimetic coated samples corrosion properties were dependant on the cracks and pores in the coating. With the addition of proteins, the extra impedance provided by the adsorption of proteins to the surface led to better passive properties of the exposed metal. The reduction in corrosion rate shows that the proteins facilitate the barrier the biomimetic coating provides. The corrosion through the defects was lessened when the proteins were present. Therefore, in a high protein solution such as the body, it could be expected that this effect will reduce the corrosion rate of the biomimetic coated samples further than the measurements made in vitro.

When modified with the ECAD layer of $Ca(OH)_2$, the addition of proteins also reduced the diffusion of salts to the layer. The total corrosion resistance of the ECAD coatings is improved by the corrosion and deposition of the salts to this layer. Therefore, the protein additions slowed the formation of this layer, leading to a corrosion resistance increase at a slower rate than the ECAD coated samples in MEM alone. However, the ultimate corrosion rates of these samples were lower than the biomimetic coated samples alone. Therefore, it can be concluded that the BSA slowed the CaP deposition and protection mechanism of these ECAD coatings, but did not stop it, and this method still provided improved protection over the other coatings.

The choice of buffer system was also found to be important in the formation of the corrosion layers and ultimate corrosion protection. In simple ionic NaCl and HBSS solutions the presence of the carbonate buffer exhibited a low capacity and therefore rapid pH rise and film formation that reduced the corrosion rate. In MEM, this was also observed to occur. However, once BSA was added, the layer formation was impeded and the total corrosion resistance dropped to much closer to that of the HEPES buffered solutions. The proteins

interfere with the layer formation by binding to salts [13, 14]. This is further evidence that the HCO_3 buffered systems may not be the most physiologically relevant just because of the chemical equivalency. Of course, this is only a single type of protein addition. The actual physiological system has many different types of proteins, and the behaviour is complex. Therefore, further *in vitro* and *in vivo* tests will be needed to understand the effects of each different type of protein. However, this work shows that the relative protection provided by the coatings remained the same across these solution, and that for the exact rates and mechanisms, the effect of the proteins is not trivial, and may result in greater or lesser protection than expected from simple SBFs, depending on the solution and the buffering agent.

8.7. Concluding Remarks and Future Work

Biomimetic coatings have already proven their value on Ti implants for biocompatibility. These properties, and the processing abilities make them attractive for degradable Mg implants. The need for the coating of Mg implants is to slow the corrosion rate. The results presented here show that the biomimetic coatings can be applied to Mg. The coatings have been shown to provide improved corrosion protection. However, the protection is not complete due to the amount of defects in the coating. By changing the deposition process, and improving the healing mechanism of the coating, the defects can be minimized and sealed. This leads to better corrosion protection, brining the corrosion rates closer to levels that would be acceptable for degradable implants. Overall, these changes bring biomimetic coated degradable Mg implants into the realm of practical applications.

The research does not end here though. The research here has been conducted to accurately model and identify the dominant corrosion behaviour and environments that may be faced *in vivio*. However, the complexity of the physiological environment means the measurements of exact corrosion rates are not yet possible *in vitro.* While the coatings can be optimized for protection against specific elements, they must be tested *in vivo*, using animal models, before clinical trials can begin. The research should continue moving up in complexity, to plasma, cell culture, then animal models. This will also allow the effects of long term

biocompatibility and dissolution behaviour. The data collected here shows the corrosion rate is slowed, which is one goal, but it will also be necessary to measure and optimize the final dissolution properties of these coatings. After all, the implant should not last forever, and must degrade after an appropriate interval. Further optimization of the biomimetic composition, the thickness and morphology of the calcium hydroxide layer, and the adhesion to the substrate will need to be performed. The system could further be improved by linking it with a better alloy as a substrate, or the addition of another element of a composite coating, such as a biodegradable polymer.

Furthermore, the implant and coating remnants must not cause problems as or after they degrade. The use of only biologically present elements gives us confidence that these coatings may be used, but this must be proven *in vivo*. These biodegradable implants must be formulated to provide maximum benefit with minimal harm, so this must be studied and measured. Overall, if this research is done and these obstacles can be overcome, the use of biodegradable Mg metal for temporary orthopaedics can move from the realm of research to the clinic.

8.8. References:

1. Staiger, M.P., A.M. Pietak, J. Huadmai, and G. Dias, *Magnesium and Its Alloys as Orthopedic Biomaterials: A Review.* Biomaterials, 2006. **27**(9): p. 1728-1734.
2. Willumeit, R., J. Fischer, F. Feyerabend, N. Hort, U. Bismayer, S. Heidrich, and B. Mihailova, *Chemical surface alteration of biodegradable magnesium exposed to corrosion media.* Acta Biomaterialia, 2011. **7**(6): p. 2704-2715.
3. Yamamoto, A. and S. Hiromoto, *Effect of inorganic salts, amino acids and proteins on the degradation of pure magnesium in vitro.* Materials Science and Engineering: C, 2009. **29**(5): p. 1559-1568.
4. Bigi, A., E. Boanini, B. Bracci, A. Facchini, S. Panzavolta, F. Segatti, and L. Sturba, *Nanocrystalline hydroxyapatite coatings on titanium: a new fast biomimetic method.* Biomaterials, 2005. **26**(19): p. 4085-4089.
5. Wen, H.B., J.G.C. Wolke, J.R. de Wijn, Q. Liu, F.Z. Cui, and K. de Groot, *Fast precipitation of calcium phosphate layers on titanium induced by simple chemical treatments.* Biomaterials, 1997. **18**(22): p. 1471-1478.
6. Song, G., *Control of biodegradation of biocompatable magnesium alloys.* Corrosion Science, 2007. **49**(4): p. 1696-1701.
7. León, B. and J.A. Jansen, *Thin Calcium Phosphate Coatings for Medical Implants*. 2008: Springer.

8. Malda, J., T.B.F. Woodfield, M. Radisic, S. Levenberg, C. Oomens, F.P. Baaijens, P. Svalander, and G. Vunjak-Novakovic, *Cell Nutrition : In Vitro and In Vivo.* Tissue Engineering : A Textbook, 2008(1): p. 327-362.
9. Ashassi-Sorkhabi, H., Z. Ghasemi, and D. Seifzadeh, *The inhibition effect of some amino acids towards the corrosion of aluminum in 1 M HCl + 1 M H2SO4 solution.* Applied Surface Science, 2005. **249**(1-4): p. 408-418.
10. Ashassi-Sorkhabi, H., M.R. Majidi, and K. Seyyedi, *Investigation of inhibition effect of some amino acids against steel corrosion in HCl solution.* Applied Surface Science, 2004. **225**(1-4): p. 176-185.
11. Liu, C., Y. Xin, X. Tian, and P.K. Chu, *Degradation Susceptibility of Surgical Magnesium Alloy in Artificial Biological Fluid Containing Albumin.* Journal of Materials Research, 2007. **22**(7): p. 1806-1814.
12. Liu, C.L., Y.J. Wang, R.C. Zeng, X.M. Zhang, W.J. Huang, and P.K. Chu, *In vitro corrosion degradation behaviour of Mg–Ca alloy in the presence of albumin.* Corrosion Science, 2010. **52**(10): p. 3341-3347.
13. Kragh-Hansen, U. and H. Vorum, *Quantitative analyses of the interaction between calcium ions and human serum albumin.* Clinical Chemistry, 1993. **39**(2): p. 202-208.
14. Clark, G.C.F. and D.F. Williams, *The effects of proteins on metallic corrosion.* Journal of Biomedical Materials Research, 1982. **16**(2): p. 125-134.

APPENDIX A : Selected coating *in vitro* corrosion studies

Coating Process

Alloys	Polish	Coat Process	Coat Process Sub type	Pretreatment	Coat solution	Ca:P coat soln	Coat soln pH	Coat Temp	coat time	post treat	coating created	Ca:P coat	coat thickness	Ref
Pure Mg, AZ91D	1000	Anodization	50V 5mA/cm2		0.25 M NaOH and 0.1 M Na 2 SiO 3	na			up to 3hrs				10 um	[1]
Pure Mg, AZ91D	1000	Anodization	50V 5mA/cm2		0.25 M NaOH and 0.1 M Na 2 SiO 3	na			up to 3hrs				10 um	[1]
Pure Mg, AZ91D	1000	Anodization	50V 5mA/cm2		0.25 M NaOH and 0.1 M Na 2 SiO 3	na			up to 3hrs				10 um	[1]
Pure Mg, AZ91D	1000	Anodization	50V 5mA/cm2		0.25 M NaOH and 0.1 M Na 2 SiO 3	na			up to 3hrs				10 um	[1]
CP Mg, AZ91D, AM60, MEZ, ZE41	1200	Anodization	20-5mA/cm2		K2SiO3 (1.6%wt) + KOH (1%wt)	na		ambient	30min		anodized			[2]
AZ91D	???	Anodization	Plasma Electrolytic Oxidation		NaOH, Na PO4, Ca acetate, Na Silicate	needs calc	??? (basic)		10 min		MgO, Mg2SiO4			[3]
Pure Mg (99.95%)	2000	Anodization	MAO		NaOH (30 g/L), $Na_2SiO_3 \cdot 9H_2O$ (160 g/L) and $Na_2B_4O_7 \cdot 10H_2O$ (160 g/L)			25C	1-22min		oxide MAO			[4]
Pure Mg	1200	Anodization	TiO2 and F and MgO anodization	NaOH (2 g/l), Na_4SiO_4 (8 g/l) and NaF (2 g/l)	$(Ti(OC_4H_9)_4)$ and isobutanol (C_4H_9OH) in a volume ratio of 1:3.						MAO			[5]
AZ31		Anodization	Microarc Oxidation		30–50 g/L Na2SiO3 and 5 g/L NaOH	na	basic	?	?	Ion beam HIPIB	Mao film		25um	[6]
Mg 6Zn 1-1.5Ca		Anodization	Electrodeposition		KOH 10M				2H	Aneal 450C 6hrs in air	MgOH2		??	[7]
5.5–6.5% Zn, 1.0–1.5% Ca	.05mm alumi	Anodization	Electrodeposition								MgO			[8]

Alloys	Polish	Coat Process	Coat Process Sub type	Pretreatment	Coat solution	Ca:P coat soln	Coat soln pH	Coat Temp	coat time	post treat	coating created	Ca:P coat	coat thickness	Ref
	na													
Pure Mg	600 grit	Anodization		Anodization 2-100V	Hanks modified 1.3mM Ca, .8mM PO4, blood plasma Cl-	1.625	7 (neutral) not mentioned buffer	310 K	up to 40 h		amorphous?	.75-.95	not reported	[9]
AZ91	???	Anodization	30-90V		NaOH 4M						anodized			[10]
Pure Mg (99.9%)	1200	biomimetic			SBF for 5 days 60 mL per 9.5mm dia sample, TRIS buffer	2.5	7.4??? Initial?	RT	5 days	NaOH, air, h2o, NaOH only effective to seal cracks	some kind of CaP, Mg in it	.5 to 2		[11]
Pure Mg	1200	Biomimetic		H2O at 100C for up to 30 min	5x SBF		5 to 8	37	48hrs		Calcium phsophate DCPD + HA		10-20 um	[12]
AZ91D	1500	Biomimetic		Ca(NO3)2 .17M and K2HPO4 0 to .1m titrated in	mSBF	0 to 1.7 pretreat, then	7.4	37 C	3h		DCPD	?	20 um after 5 days	[13]
AZ80	?	Composite MAO + ED		MAO in 50 g/L NaOH, 40 g/L Na 2 SiO 3 , 20 g/L Na 2 B 4 O 7 and 40 g/L Na 3 C 6 H 5 O 7 90V for 40 min	10 g/L Ca (NO 3) 2 and 10 g/L NH 4 H 2 PO 4 . Also 10 mL/L H2O2 done at 7V for 10 min		4.4		10 min		DCPD plus MAO		8-10um MAO 2-4 ED	[14]
AZ81 Die cast	2000	Composite MAO + EN + Polymer	Electroless nickel and plga	MAO in NaOH and NaSiO3	$2NiCO_3{\cdot}3Ni(OH)_2{\cdot}4H_2O$, then PLGA						PLGA EN			[15]
WE42	2000	Composite MAO + PLLA coat				na					MAO/PLLA			[16]
AZ31	1000	Conversion	HF		HF 10 to 40%	na	acidic	RT	72 hrs	none	No xtalline MgF2 detected, too thin? Amorphous? Paper not clear	na	8 to 23 um	[17]
AZ31	2000	Conversion	Hydrothermal		5.66% mass fraction NaOH	na	basic	160 C	1 to		Mg(OH)2	na		[18]

Alloys	Polish	Coat Process	Coat Process Sub type	Pretreatment	Coat solution	Ca:P coat soln	Coat soln pH	Coat Temp	coat time	post treat	coating created	Ca:P coat	coat thickness	Ref
							14		4 hours					
MgZnCa extruded	2000	Conversion	Conversion/solution coat	H3PO4 then NH4F	NaSiO3 (30g/L) and Ca(NO3)2 (30g/L)						CaSiO3 and brushite		6um	[19]
AZ31	3.5 um diamond	conversion	cerium conversion coat		$Ce(NO_3)_3$, with concentrations of 10 g/L, at 60 °C for immersing 5 min and 20 mL/L of hydrogen dioxide solution, H_2O_2 (Fisher Scientific, 30%)			60 C	5 min		Ce conversion			[20]
Powder Met Pure Mg, Cast Pure Mg, AZ31	1200	Conversion	HF		48 wt% HF			RT	24h					[21]
pure Mg	4000	Conversion	MgF in HF	none	HF 48% wt	na	acidic	RT	6 to 24 h (24 reported)		MgF2	na	1.5 um	[22]
AZ31		Conversion	Fluride		HF						HF			[23]
AZ91D		Conversion	phytic acid								phytic acid			[24]
Pure Mg powder met	1500	Conversion	F conversion coating		.01-.3 M KF Cl added in some up to 8gL	na	not said, weak basic my guess		1hr		Mg F posibly, only EDX and theory			[25]
AZ91D	1000	Conversion	HF		70% HF	no	acid				MgF			[26]
AZ81E		conversion	Rare Earth	has Ce SO4, Al as well	look into this more?						Rare Earth conversion			[27]
AM60,	1200	conversion	Molybdate phosphate	ultrasonic acetone	Na_2MoO_4 30 g L^{-1} + $Ca(NO_3)_2$ 4 g L^{-1} + $Mn(Ac)_2$ 6 g L^{-1} +additive 1 g L^{-1} $NaNO_3$ 1 g L^{-1} + HNO_3, also Mo + H3PO4 + NaH2PO440 g L−1	to calc	?	50 C	120s		Molybdate phosphate			[28]
Pure Mg (99.99%)	2000	Conversion and Aerosol Deposition	HF and then HA coat	48% HF at RT for 24 hrs	HA powder heated to 1200 1 hrs then sprayed						MgF2 HA			[29]
Mg–1.0Ca	1000 grit	Electrodeposition	Potentiostatic	none	0.042 M Ca(NO3)2·4H2O and 0.025 M NH4H2PO4		5	40 C	4h		DCPD	NR	thicker	[30]

Alloys	Polish	Coat Process	Coat Process Sub type	Pretreatment	Coat solution	Ca:P coat soln	Coat soln pH	Coat Temp	coat time	post treat	coating created	Ca:P coat	coat thickness	Ref
													than EDS	
AZ31	1000 grit	Electrodeposition	Potentiostatic	none	0.042 M Ca(NO3)2·4H2O and 0.025 M NH4H2PO4		5	40 C	4h		DCPD	NR	thicker than EDS	[30]
Mg 6 wt.% Zn	1000 grit	Electrodeposition	Galvanostat		CaNO3 .042 M, NH4H2PO4 .025 M		4.4			Sat Ca(OH)2 then .1M NaOH 80C for 4h	Formed DCPD, HA, FHA tested			[31]
AZ91	Machined	Electrodeposition	Potentiostatic	1 M NaOH 80 C for 1 hrs	.1 M CaNO3 and NH4H2PO4	1.666667				1 M NaOH 80 C for 1 hrs	HA			[32]
Mg 1.0 Ca	1200	Electrodeposition	Potentiostatic		42mM CaNO32 and NH4H2PO4	1.68	5		20, 60,120, 240 min		Brushite		20-25um	[33]
Mg–Zn–Ca	1000	Electrodeposition	F substituted apatite/ pulsed reverse current PRC in addition to traditional ed TED	40% HF	0.15 mol/L $NaNO_3$, 0.025 mol/L $NH_4H_2PO_4$, 0.042 mol/L $Ca(NO_3)_2$ and 20 mL/L H_2O_2	1.68	5	65 C			FHA	1.44 PRC/1.3 TED		[34]
AZ91D		Electrodeposition	Electrophoretic deposition	MAO	HA particle and chitosan	stoich ha and chitosan	acidic?	25C	30 min		HA-chitosan Ha particles			[35]
Pure, AZ91		Electroplating ionic liquids												[36]
Pure Mg (99.99%)	1200 then electropolished	Polymer	Dip		PLC and PLA in trichloromethane			RT			PLC PLA			[37]
99.98% Mg, SS, and Ti	na	PVD									Mg		100um	[38]
Mg 2% Zn	Diamond W1.5	PVD	Magnetron Sputtering TiO2	ultrasonic acetone ethanol	n/a magnetron sputter	na	na	325 Watt powe	2h		TiO2	na	200 nm	[39]

Alloys	Polish	Coat Process	Coat Process Sub type	Pretreatment	Coat solution	Ca:P coat soln	Coat soln pH	Coat Temp	coat time	post treat	coating created	Ca:P coat	coat thickness	Ref
								r						
AZ31	2000	PVD	Aerosol Deposition								HA/ Chitosan			[40]
AZ31	1000	PVD	Ion Beam Assisted Deposition	Ar beam bombardment to pretreat	Ion beam 20min	HA + 37% CaO powder	na	less than 100C	20min	some anealed 250C 2h, some in H2O 100C 30min for Amorphous -> Xtal HA	CaP			[41]
AZ31	.05 alumina	Sol Gel	Titania		$Ti(OC_4H_9)_4$:EtOH: H_2O:$NH(C_2H_4OH)_2$ = 14:112:2:3				3–5 cm min^{-1}	anneal 200–400 °C for 1–2 h in the vacuum furnace	TiO_2	na		[42]
Mg 1% Ca	???	Sol Gel	Titania		organic sol gel	na	??		12 cm/min	500 C for 2 hrs, repeated several times for thicker coating	TiO2	na	up to thick enough xrd did not penetrate	[43]
ZE41	800	Sol Gel	Silica dip, conventional, dense light		SiO2 TEOS/ethanol/acidulated water 1:1:1 or 4:4:1 or 1:11:1	na			dip 35cm/min	sinter 400 or 500 C 1 or 2 hrs	silica, some others zn, mg only EDS and sem	na	4um	[44]
AZ31	600	Solution Chemistry		Acid Etch	Ca-EDTA: $C_{10}H_{12}N_2O_8Na_2Ca$), potassium dihydrogenphosphate (KH_2PO_4) and sodium hydroxide (NaOH)			363K	10min-6hr		HA, HA OCP	.61-.67	5um	[45]
AZ31	1200	Solution Chemistry	immersion long term	Na2HPO4 60C	NaH2PO4 and CaNO3)2	needs calc	8.9	70C	48h		beta TCP and CaPO3OH	NR	15-20um	[46]
Pure Mg	2000	Solution Chemistry		none	.01 M CaNO3 + Na3PO4 + H3PO4	?	4.5	65	2min	NaOH 10g/L 80C 60 min	HA	1.45	200-300 nm	[47]
mg-1.2 Mn - 1.0 Zn	1000	Solution Chemistry		alkaline 63 C for 15 min, 2% H3PO4 and H2SO4 for -10 sec	phosphating bath MCP and Zn and NO3 - see paper	needs calc	???	???	6min		CaHPO4 dot 2H2O	not accurately measured		[48]

Alloys	Polish	Coat Process	Coat Process Sub type	Pretreatment	Coat solution	Ca:P coat soln	Coat soln pH	Coat Temp	coat time	post treat	coating created	Ca:P coat	coat thickness	Ref
												Ulness XPS?		
Pure Mg	600	Solution Chemistry	Hydrothermal	HNO3 and H2SO4 etch	$C_{10}H_{12}CaN_2Na_2O_8$ (Ca-EDTA) and KH_2PO_4	1	5.9, 8.9, 11.9	RT to 363K	temp ramp then 7.2 ks		HA and/or OCP		3um	[49]
Pure Mg (99.98)	600	Solution Chemistry	Ca-EDTA	Acid Etch	$C_{10}H_{12}CaN_2Na_2O_8$ (Ca-EDTA) and KH_2PO_4		5.9, 8.9, 11.9				HA/OCP			[49]
Pure Mg	.1 um Alumina	Solution Chemistry	Hydrothermal		Ca EDTA, K2HPO4, NaOH	check it	6.3-11.3	368 K	8 or 24 hrs		HA			[50]
Pure Mg	1500	Solution Chemistry	PO4 slowly added	MAO (for corrosion)	.17 M Ca(NO3)2 dribbled in .1M K2HPO4	1.7	?	27 C	5h		DCPD and HA	1.43	10um	[51]
AZ31		Solution Chemistry		Na2CO3 50C 30min, then NaOH 24h room temp, heat treat 140C for 24h	3mM CaCl2 1.8mM Na2HPO4	1.67	5		few min to 1 week		Ca deficient HA	1.1	much greater 10 nm	[52]
Pure Mg	600	Solution Chemistry		HNO3 and H2SO4 etch	$C_{10}H_{12}CaN_2Na_2O_8$ (Ca-EDTA) and KH_2PO_4	1	8.9	313K to 363K	8h or 2h		HA		3um	[53]
Pure, AZ31, AZ61, AZ91	.1um Alumina	Solution Chemistry	Chelate solution chem	none	Ca EDTA, K2HPO4, NaOH	1 to 1.67	5.4-11.3 7.3 for corrosion	368 K	8-16-24 hrs		HA	not reported		[54]
AZ31	1200	Solution Chemistry	Immersion	Acid Etch	$Ca(NO_3)_2$ and $NH_4H_2PO_4$		4	60 C	24hrs		CaP	mixed, TCP??? Mg Phosphates,		[55]
Pure Mg	600	Solution Chemistry	Hydrothermal	nitric sulfuric acid etch	0.25 mol/l Ca-EDTA and 0.25 mol/l KH_2PO_4		8.9	363K	600-28800 s		HA (Mg(OH)2 seen as well)		1.3-9.2 um	[56]

Corrosion Results

Corrosion Solution	Cor Soln Temp	Corrosion Soln Buffer	Corr Soln pH	Solution Refreshed	mass loss max time	Mass loss coat	mass loss control	Ref
0.15M NaCl and SBF	???	??? (none prob)	7 initial	daily				[1]
0.15M NaCl and SBF	???	??? (none prob)	7 initial	daily				[1]
0.15M NaCl and SBF	???	??? (none prob)	7 initial	daily				[1]
0.15M NaCl and SBF	???	??? (none prob)	7 initial	daily				[1]
5wt%	25+/-1	none	7.0 initial					[2]
.9% NaCl	???	none	not stated	not				[3]
SBF 8.035 g/L NaCl, 0.355 g/L NaHCO3, 0.225 g/L KCl, 0.231 g/L K2HPO4·3H2O, 0.311 g/L MgCl2·6H2O, 0.292 g/L CaCl2 and 0.072 g/L Na2SO4	37C	tris + HCl	7.4					[4]
Hanks		TRIS and HCl	7.4					[5]
3.5 NaCl								[6]
Hanks					3 days			[7]
								[8]
none								[9]
								[10]
Dulbeccos Mod Eagle and FBS	37	CO2 5%	7.4 start?	no				[11]
Hanks + NaCl	37	HEPES 6g/l	7.4	no	24 hours			[12]
SBF (similar to hanks)								[13]
Kokubo's solution	37	??? 200ml per sample, replaced 2 day interval	7.4					[14]
Hanks	37 C	NaOH	7.4 initial					[15]
Hanks	37	??? Adjst with NaOH and HCl	7.4					[16]
Hanks	28-32 C	none	7.4					[17]

Corrosion Solution	Cor Soln Temp	Corrosion Soln Buffer	Corr Soln pH	Solution Refreshed	mass loss max time	Mass loss coat	mass loss control	Ref
Hanks	37C	None		0.4 mL /mm2 or 40mL per cm2	31 Days (1,3,5,7,15, 31)	0.3	0.35	[18]
Hanks	310 K	none, CO3 in solution						[19]
Hanks	37 C	none/carbonate present	???	not stated				[20]
DMEM	37	not said, think CO2	7.4	48 hours				[21]
Hanks	37	refreshed every 2 days	7.4		18 days	1.01mmpy	3.7mmpy	[22]
								[23]
								[24]
8g/L NaCl								[25]
not relevant to bio								[26]
								[27]
0.93 g/l H_3BO_4 and 9.86 g/l $Na_2B_4O_7$	room		9.2					[28]
SBF Kokubo		none?	7.4 initial	nope	3 days			[29]
Hanks		???	7.4			none	none	[30]
Hanks		???	7.4			none	none	[30]
mod SBF	37	HEPES	7.4 up to 8.2	no				[31]
SBF like hanks	37	HEPES 17.8 g/L	7.4		5 days			[32]
Hanks		none	7.4		3 days	??	??	[33]
SBF (hanksish)	37	TRIS + HCL	7.4 start up to 7.7 at 128h	no				[34]
								[35]
								[36]
mSBF (reported elsewhere, human plasma)	37	HEPES	7.4	200 mL/cm2	250 hrs	maintained for 8 days then degraded	none	[37]
DMEM +10% FCS	37	CO2 5%	7.36		1-12 hrs	survived after 12 hours	didn't survive after 12 hours	[38]
SBF like hanks		TRIS + HCL	4					[39]
SBF Kokubo	37							[40]

Corrosion Solution	Cor Soln Temp	Corrosion Soln Buffer	Corr Soln pH	Solution Refreshed	mass loss max time	Mass loss coat	mass loss control	Ref
								[41]
Hanks	???	???	???	???				[42]
Kokubo's solution	37C	????	7.4					[43]
3.5 wt% NaCl	24+-3C	none	nont stated					[44]
3.5% NaCl	room	???	NR					[45]
Hanks	37	???	???			none		[46]
MEM	37	co2 5% incubator	7.4 I think		48 hours	0.03	2 mg/cm2/day	[47]
cell culture and in vivo		CO2 in cell culture	7.4			none	none	[48]
3.5 wt% NaCl		none	??			none	none	[49]
3.5% NaCl	room	none	???	no				[49]
mHanks Cl down to blood	310 K	none?	8	rotated 120 rpm for flow				[50]
SBF: 8.035 g/L NaCl, 0.355 g/L NaHCO3, 0.225 g/L KCl, 0.231 g/LK2HPO4·3H2O, 0.311 g/L MgCl2·6H2O, and 0.292 g/L CaCl2		TRIS and HCl	7.4 initially, up to 7.56 at 147h					[51]
none						none	none	[52]
none						none	none	[53]
3.5 wt% NaCl (shore simulation)						none	none	[54]
Hanks, PBS, saline	37		7.4 initial		26 days max			[55]
3.5 NaCl	room							[56]

Corrosion Values Continuted

H2 evo coat	H2 Evo Control	H2 time	PDP timepoint	PDP icorr coat (µA/cm2)	PDP icor control(µA/cm2)	EIS timepoint	EIS Rp Coat (ohms)	EIS Rp Uncoat (ohms)	Mg ion Coat	Mg ion control	Ref
			48hr immersion 3h pure mg in NaCl	2.70E-05	3.00E-04	2h pure mg 2hr	1037	109			[1]
			48hr immersion 2h pure mg in NaCl	2.70E-05	3.00E-04	20min pure mg 2hr NaCl	2000	363			[1]
			48hr immersion 3h AZ91D in NaCl	6.25E-08	3.04E-05	10h Az91D 3hr	1198	1100			[1]
			48hr immersion 2h AZ91D in NaCl	8.51E-07	3.04E-05	1h Az91D 3hr NaCl	2029	1500			[1]
											[2]
			not mentioned	1.05E-07	1.76E-05						[3]
			40 min	1.73E-07	1.35E-05						[4]
				1.25E-05	4.00E-04	12h to 15 days	4000	800			[5]
				4.00E-09	3.00E-07	5 and 48 hrs	see doc				[6]
			3 days? Unclear								[7]
											[8]
											[9]
											[10]
						24 h I think	500	350			[11]
			24 hrs	1.09E-05	6.26E-05	24 hrs	3657	885			[12]
			10 min	2.6	70	10 min	4210	331			[13]
.004 MAOED, .006 MAO only?	0.07 mL/cm2/day H2	5 days									[14]
			???	1.00E-07	1.00E-06						[15]
						0 and 4 weeks	120000	1500	200-600	2400 - 1000	[16]
13.1, 9.7, 4 mL	43 mL	16 days	immediate								[17]
											[18]
			steady state ocp	1.45E-05	1.35E-04						[19]
						10 min	15000	2000			[20]

H2 evo coat	H2 Evo Control	H2 time	PDP timepoint	PDP icorr coat (µA/cm2)	PDP icor control(µA/cm2)	EIS timepoint	EIS Rp Coat (ohms)	EIS Rp Uncoat (ohms)	Mg ion Coat	Mg ion control	Ref
						1,7,11 Days	380,28,19 kOhms	6.8,7.8,8.7 kOhms			[21]
			10 - 15 min, cathodic shift				5200	180			[22]
											[23]
											[24]
						1 hr	250-2000 ohms	no control?			[25]
											[26]
											[27]
				2							[28]
									100 at 70 hrs	350	[29]
145	248	70 h	immediate	6.27	556	none	none	none			[30]
6	28	240 h	immediate	2.75E-06	2.74E-04	none	none	none			[30]
.5,1.25,1.5 ml/cm2	3	up to 500 hrs									[31]
											[32]
				7.46E-06	5.90E-04						[33]
			??? Less than 5 days	2.50E-06	1.27E-04						[34]
											[35]
											[36]
			Right away	1.29E-05	2.03E-04						[37]
			not said, think the fig is wrong.	1.43E-03	1.43E-03						[38]
1.95mmpy	4.13mmpy	10 days	120 S				none	none			[39]
			not sure	4.70E-06	3.89E-04						[40]
											[41]
			???	1.26E-07	3.16E-05						[42]
			5 min - measure in A	1.59E-	3.33E-02						[43]

H2 evo coat	H2 Evo Control	H2 time	PDP timepoint	PDP icorr coat (µA/cm2)	PDP icor control(µA/cm2)	EIS timepoint	EIS Rp Coat (ohms)	EIS Rp Uncoat (ohms)	Mg ion Coat	Mg ion control	Ref
				05							
			168 hrs (1hrs different)	26.1	84.4						[44]
			600 s	2.00E-06	1.00E-04				2 and 5	25	[45]
none			???	2.34E-06	2.93E-06	?	8399	1494			[46]
			48 hrs		2 orders of mag different				none		[47]
none											[48]
none	none	none	360 s	1E-07	0.0001	none	none	none			[49]
			360 s	5.00E-07	1.00E-03						[49]
						0 to 6 hrs	1.00E+05	4.00E+03	2.75 ave, 4 days	3.25	[50]
1	9	137 h	?	?	?						[51]
none	none	none	none	none	none						[52]
none	none	none	none	none	none						[53]
none	none	none	1 hour	1.00E-06	1.00E-03						[54]
			???	1.18E-06	2.93E-04						[55]
			360s	1.00E-07	2.00E-04						[56]

1. Xue, D., Y. Yun, M.J. Schulz, and V. Shanov, *Corrosion protection of biodegradable magnesium implants using anodization.* Materials Science and Engineering: C, 2010. **31**(2): p. 215-223.

2. Shi, Z., G. Song, and A. Atrens, *The corrosion performance of anodised magnesium alloys.* Corrosion Science, 2006. **48**(11): p. 3531-3546.

3. Yao, Z.P., L.L. Li, X.R. Liu, and Z.H. Jiang, *Preparation of ceramic conversion layers containing Ca and P on AZ91D Mg alloys by plasma electrolytic oxidation.* Surface Engineering, 2010. **26**(5): p. 317-320.

4. Zhao, L., C. Cui, Q. Wang, and S. Bu, *Growth characteristics and corrosion resistance of micro-arc oxidation coating on pure magnesium for biomedical applications.* Corrosion Science, 2010. **52**(7): p. 2228-2234.

5. Shi, P., W.F. Ng, M.H. Wong, and F.T. Cheng, *Improvement of corrosion resistance of pure magnesium in Hanks' solution by microarc oxidation with sol-gel TiO2 sealing.* Journal of Alloys and Compounds, 2009. **469**(1-2): p. 286-292.

6. Han, X.G., X.P. Zhu, and M.K. Lei, *Electrochemical properties of microarc oxidation films on a magnesium alloy modified by high-intensity pulsed ion beam.* 2011.

7. Lei, T., C. Ouyang, W. Tang, L.-F. Li, and L.-S. Zhou, *Enhanced corrosion protection of MgO coatings on magnesium alloy deposited by an anodic electrodeposition process.* Corrosion Science. **52**(10): p. 3504-3508.

8. Lei, T., C. Ouyang, W. Tang, L.-F. Li, and L.-S. Zhou, *Preparation of MgO coatings on magnesium alloys for corrosion protection.* Surface and Coatings Technology, 2010. **204**(23): p. 3798-3803.

9. Hiromoto, S., T. Shishido, A. Yamamoto, N. Maruyama, H. Somekawa, and T. Mukai, *Precipitation control of calcium phosphate on pure magnesium by anodization.* Corrosion Science, 2008. **50**(10): p. 2906-2913.

10. Peixoto Barbosa, D. and G. Knörnschild, *Anodization of Mg-alloy AZ91 in NaOH solutions.* Surface and Coatings Technology, 2009. **203**(12): p. 1629-1636.

11. Keim, S., J.G. Brunner, B. Fabry, and S. Virtanen, *Control of magnesium corrosion and biocompatibility with biomimetic coatings.* Journal of Biomedical Materials Research - Part B Applied Biomaterials, 2011. **96 B**(1): p. 84-90.

12. Waterman, J., A. Pietak, N. Birbilis, T. Woodfield, G. Dias, and M.P. Staiger, *Corrosion resistance of biomimetic calcium phosphate coatings on magnesium due to varying pretreatment time.* Materials Science and Engineering: B, 2011. **176**(20): p. 1756-1760.

13. Hu, J., C. Wang, W.C. Ren, S. Zhang, and F. Liu, *Microstructure evolution and corrosion mechanism of dicalcium phosphate dihydrate coating on magnesium alloy in simulated body fluid.* Materials Chemistry and Physics, 2010. **119**(1-2): p. 294-298.

14. Shi, Y., M. Qi, Y. Chen, and P. Shi, *MAO-DCPD composite coating on Mg alloy for degradable implant applications.* 2011. **65**(14): p. 2201-2204.

15. Ping, L., L. Yin, G. Meiqing, F. Haidong, and X. Xinhua, *Corrosion and drug release properties of EN-plating/PLGA composite coating on MAO film.* Materials Science & Engineering: C (Materials for Biological Applications), 2011. **31**(7): p. 1285-9.

16. Lu, P., L. Cao, Y. Liu, X. Xu, and X. Wu, *Evaluation of magnesium ions release, biocorrosion, and hemocompatibility of MAO/PLLA-modified magnesium alloy WE42.* Journal of Biomedical Materials Research - Part B Applied Biomaterials, 2011. **96 B**(1): p. 101-109.

17. Zhang, C.Y., J.C. Gao, and C.L. Liu. *Effect of fluoride treatment on corrosion property of AZ31 magnesium alloy in Hank's solution*. 2011. Changsha, China: Trans Tech Publications.

18. Zhu, Y., G. Wu, Y.-H. Zhang, and Q. Zhao, *Growth and characterization of Mg(OH)2 film on magnesium alloy AZ31.* Applied Surface Science, 2011.

19. Wei, Z., H. Du, and E. Zhang, *The formation mechanism and biocorrosion property of CaSiO3/CaHPO4 · 2H2O composite conversion coating on the extruded Mg-Zn-Ca alloy for bone implant application·.* Surface and Interface Analysis, 2011. **43**: p. 791-794.

20. Cui, X., Y. Yang, E. Liu, G. Jin, J. Zhong, and Q. Li, *Corrosion behaviors in physiological solution of cerium conversion coatings on AZ31 magnesium alloy.* Applied Surface Science, 2011. **257**(23): p. 9703-9709.

21. Carboneras, M., M.C. GarcÃ-a-Alonso, and M.L. Escudero, *Biodegradation kinetics of modified magnesium-based materials in cell culture medium.* Corrosion Science, 2011. **53**(4): p. 1433-1439.

22. Chiu, K.Y., M.H. Wong, F.T. Cheng, and H.C. Man, *Characterization and corrosion studies of fluoride conversion coating on degradable Mg implants.* Surface & Coatings Technology, 2007(202): p. 590-598.

23. da Conceicao, T.F., N. Scharnagl, C. Blawert, W. Dietzel, and K.U. Kainer, *Surface modification of magnesium alloy AZ31 by hydrofluoric acid treatment and its effect on the corrosion behaviour.* Thin Solid Films, 2010. **518**(18): p. 5209-5218.

24. Jianrui, L., G. Yina, and H. Weidong, *Study on the corrosion resistance of phytic acid conversion coating for magnesium alloys.* Surface and Coatings Technology, 2006. **201**(3-4): p. 1536-1541.

25. Pereda, M.D., C. Alonso, M. Gamero, J.A. del Valle, and M. Fernandez Lorenzo de Mele, *Comparative study of fluoride conversion coatings formed on biodegradable powder metallurgy Mg: the effect of chlorides at physiological level.* Materials Science & Engineering: C (Materials for Biological Applications), 2011. **31**(5): p. 858-65.

26. Li, J.-z., J.-g. Huang, Y.-w. Tian, and C.-s. Liu, *Corrosion action and passivation mechanism of magnesium alloy in fluoride solution.* TRANSACTIONS OF NONFERROUS METALS SOCIETY OF CHINA, 2009. **19**(1): p. 50-54.

27. Shengxue, Y., L. Qiaoyan, H. Jing, Z. Zhanwei, and Z. Qianyun, *Preparation and Performance of Rare Earths Chemical Conversion Film on Magnesium Alloy.* Journal of Rare Earths, 2006. **24**(1, Supplement 1): p. 397-400.

28. Yong, Z., J. Zhu, C. Qiu, and Y. Liu, *Molybdate/phosphate composite conversion coating on magnesium alloy surface for corrosion protection.* Applied Surface Science, 2008. **255**(5, Part 1): p. 1672-1680.

29. Jo, J.-H., B.-G. Kang, K.-S. Shin, H.-E. Kim, B.-D. Hahn, D.-S. Park, and Y.-H. Koh, *Hydroxyapatite coating on magnesium with MgF2 interlayer for enhanced corrosion resistance and biocompatibility.* Journal of Materials Science: Materials in Medicine, 2011. **22**: p. 2437-2447.

30. Chun-Yan, Z., Z. Rong-Chang, L. Cheng-Long, and G. Jia-Cheng, *Comparison of calcium phosphate coatings on Mg-Al and Mg-Ca alloys and their corrosion behavior in Hank's solution.* Surface and Coatings Technology, 2008. **204**(21-22): p. 3636-3640.

31. Song, Y., S. Zhang, J. Li, C. Zhao, and X. Zhang, *Electrodeposition of Ca-P coatings on biodegradable Mg alloy: In vitro biomineralization behavior.* Acta Biomaterialia, 2010. **6**(5): p. 1736-1742.

32. Kannan, M.B. and L. Orr, *In Vitro mechanical integrity of hydroxyapatite coated magnesium alloy.* Biomedical Materials, 2011. **6**(4): p. 045003 (11 pp.)-045003 (11 pp.).

33. Zhang, C.-y., R.-c. Zeng, R.-s. Chen, C.-l. Liu, and J.-c. Gao, *Preparation of calcium phosphate coatings on Mg-1.0Ca alloy.* TRANSACTIONS OF NONFERROUS METALS SOCIETY OF CHINA, 2010. **20, Supplement 2**(0): p. s655-s659-s655-s659.

34. Meng, E.C., S.K. Guan, H.X. Wang, L.G. Wang, S.J. Zhu, J.H. Hu, C.X. Ren, J.H. Gao, and Y.S. Feng, *Effect of electrodeposition modes on surface characteristics and corrosion properties of fluorine-doped hydroxyapatite coatings on Mg-Zn-Ca alloy.* Applied Surface Science, 2011. **257**(11): p. 4811-4816.

35. Wu, C., Z. Wen, C. Dai, Y. Lu, and F. Yang, *Fabrication of calcium phosphate/chitosan coatings on AZ91D magnesium alloy with a novel method.* Surface and Coatings Technology, 2010. **204**(20): p. 3336-3347.

36. Bakkar, A. and V. Neubert, *Electrodeposition onto magnesium in air and water stable ionic liquids: From corrosion to successful plating.* Electrochemistry Communications, 2007. **9**(9): p. 2428-2435.

37. Chen, Y., Y. Song, S. Zhang, J. Li, C. Zhao, and X. Zhang, *Interaction between a high purity magnesium surface and PCL and PLA coatings during dynamic degradation.* Biomedical Materials, 2011. **6**: p. 025005-025005.

38. Salunke, P., V. Shanov, and F. Witte, *High purity biodegradable magnesium coating for implant application.* Materials Science and Engineering: B, 2011. **176**(20): p. 1711-1717.

39. Chen, S., S. Guan, B. Chen, W. Li, J. Wang, L. Wang, S. Zhu, and J. Hu, *Corrosion behavior of TiO2 films on Mg–Zn alloy in simulated body fluid.* Applied Surface Science, 2011. **257**(9): p. 4464-4467.

40. Hahn, B.-D., D.-S. Park, J.-J. Choi, J. Ryu, W.-H. Yoon, J.-H. Choi, H.-E. Kim, and S.-G. Kim, *Aerosol deposition of hydroxyapatiteâ€“chitosan composite coatings on biodegradable magnesium alloy.* Surface and Coatings Technology, 2011. **205**(8-9): p. 3112-3118.

41. Yang, J.X., Y.P. Jiao, F.Z. Cui, I.-S. Lee, Q.S. Yin, and Y. Zhang, *Modification of degradation behavior of magnesium alloy by IBAD coating of calcium phosphate.* Surface and Coatings Technology, 2008. **202**(22-23): p. 5733-5736.

42. Hu, J., C. Zhang, B. Cui, K. Bai, S. Guan, L. Wang, and S. Zhu, *In vitro degradation of AZ31 magnesium alloy coated with nano TiO 2 film by sol-gel method.* Applied Surface Science, 2011. **257**(21): p. 8772-8777.

43. Meiheng, L., C. Qian, Z. Wenjin, H. Wangyu, and S. Yong, *Corrosion behavior in SBF for titania coatings on Mg-Ca alloy.* Journal of Materials Science, 2011. **46**(7): p. 2365-9.

44. Lopez, A.J., E. Otero, and J. Rams, *Sol-gel silica coatings on ZE41 magnesium alloy for corrosion protection.* Surface & Coatings Technology, 2010. **205**(7): p. 2375-85.

45. Hiromoto, S. and M. Tomozawa, *Hydroxyapatite coating of AZ31 magnesium alloy by a solution treatment and its corrosion behavior in NaCl solution.* Surface and Coatings Technology, 2011. **205**(19): p. 4711-4719.

46. Li-li, T., W. Qiang, G. Fang, X. Xiao-song, Q. Jian-hong, and Y. Ke, *Preparation and characterization of Ca-P coating on AZ31 magnesium alloy.* TRANSACTIONS OF NONFERROUS METALS SOCIETY OF CHINA, 2010. **20**(Suppl. 2): p. S648-S654-S648-S654.

47. Chen, X.B., N. Birbilis, and T.B. Abbott, *A simple route towards a hydroxyapatite-Mg(OH)2 conversion coating for magnesium.* Corrosion Science, 2011. **53**(6): p. 2263-2268.

48. Xu, L., F. Pan, G. Yu, L. Yang, E. Zhang, and K. Yang, *In vitro and in vivo evaluation of the surface bioactivity of a calcium phosphate coated magnesium alloy.* Biomaterials, 2009. **30**(8): p. 1512-1523.

49. Tomozawa, M. and S. Hiromoto, *Microstructure of hydroxyapatite- and octacalcium phosphate-coatings formed on magnesium by a hydrothermal treatment at various pH values.* Acta Materialia, 2011. **59**(1): p. 355-363.

50. Hiromoto, S. and M. Tomozawa, *Corrosion behavior of magnesium with hydroxyapatite coatings formed by hydrothermal treatment.* Materials Transactions, 2010. **51**(11): p. 2080-2087.

51. Liu, G.Y., J. Hu, Z.K. Ding, and C. Wang, *Bioactive calcium phosphate coating formed on micro-arc oxidized magnesium by chemical deposition.* Applied Surface Science, 2011. **257**(6): p. 2051-7.

52. Gray-Munro, J.E. and M. Strong, *The mechanism of deposition of calcium phosphate coatings from solution onto magnesium alloy AZ31.* Journal of Biomedical Materials Research Part A, 2009. **90A**(2): p. 339-350.

53. Tomozawa, M., S. Hiromoto, and Y. Harada, *Microstructure of hydroxyapatite-coated magnesium prepared in aqueous solution.* Surface and Coatings Technology. **204**(20): p. 3243-3247.

54. Hiromoto, S. and A. Yamamoto, *High corrosion resistance of magnesium coated with hydroxyapatite directly synthesized in an aqueous solution.* Electrochimica Acta, 2009. **54**(27): p. 7085-7093.

55. Wang, Q., L. Tan, W. Xu, B. Zhang, and K. Yang, *Dynamic behaviors of a CaP coated AZ31B magnesium alloy during in vitro and in vivo degradations.* Materials Science and Engineering: B, 2011. **176**(20): p. 1718-1726.

56. Tomozawa, M. and S. Hiromoto, *Growth mechanism of hydroxyapatite-coatings formed on pure magnesium and corrosion behavior of the coated magnesium.* Applied Surface Science, 2011. **257**(19): p. 8253-8257.

End app a

APPENDIX B : Biomimetic Coating Methodology

- Ultrasonically clean all glassware and apparatus in ethanoic acid and distilled water to remove all CaP from the surface. Rinse with distilled water and allow to dry

- Prepare Mg samples for coating by applying the correct polish, surface treatments, and cleaning processes.

- Set hot water bath at 37^{o}C

- Prepare solution 1 in 1 L of distilled H_2O at 37^{o}C (this step 1 is to form amorphous calcium phosphate or ACP, **no** NaCl used to avoid corrosion of samples (literature method uses 40 g/L), Na+ bumped up by adding more NaHCO3 so that more Na+ ions present for ensuring ACP forms and no crystalline HA forms, ACP is a necessary precursor layer to nucleate crystalline HA in second step). The solution can nucleate CaP phases when mixed that will not be soluble again. Therefore, the salts should be mixed only directly before the coating process is to be started.

Solution Step 1	
Salt:	**g/L**
CaCl2	1.65
KH2PO4	0.3
MgSO47H20	1.8
Na2HPO42H20	0.4
NaHCO3	2.27

Literature value = 0.55

- Attach aeration stone to tube, to CO_2 tank via rubber stopper. Gently bubble CO_2 through solution for 15 minutes. Measure pH of solution, should be ~5-6.

- Place samples on a nonconductive mesh holder. Do not use metal apparatus, or allow the individual samples to come into contact with each other, as this can lead to galvanic corrosion in the solution. When the samples into 1L beaker, pour solution 1 into beaker. Place beaker + samples + solution into hot water bath.

- Attach aeration stone to air pump. Diffuse air through solution (Air gets rid of precipitation and CO2 encourages precipitation of HA crystals)

- Cover and let incubate for 24 hours, in hot water bath with air diffusion.

- Measure pH of solution after incubation. Should be ~8. Pour off liquid through funnel with Whatman filter paper to collect precipitate. Precipitate should primarily consist of $CaCO_3$.

- Wash samples very well with distilled water, clean apparatus as directed above

- Prepare solution 2 (aim of this step is to form OCP/HA crystals, need to minimise Mg and HCO3 as these inhibit OCP/HA formation, note low amount of NaCl compared to literature):

Solution Step 2	
Salt:	g/L
NaCl	7
CaCl2	1.65
KH2PO4	0.3
Na2HPO42H20	0.4
NaHCO3	0.35

- Set hot water bath at 37^{o}C

- Repeat procedure above with CO_2 diffusion, incubation of samples in basket with air diffusion for 24 hours. After CO_2 diffusion, initial solution pH ~5 (solution should be crystal clear at this point). Final solution pH ~6.5. Wash samples very well in distilled water.